27 August 2010 | $10

Science

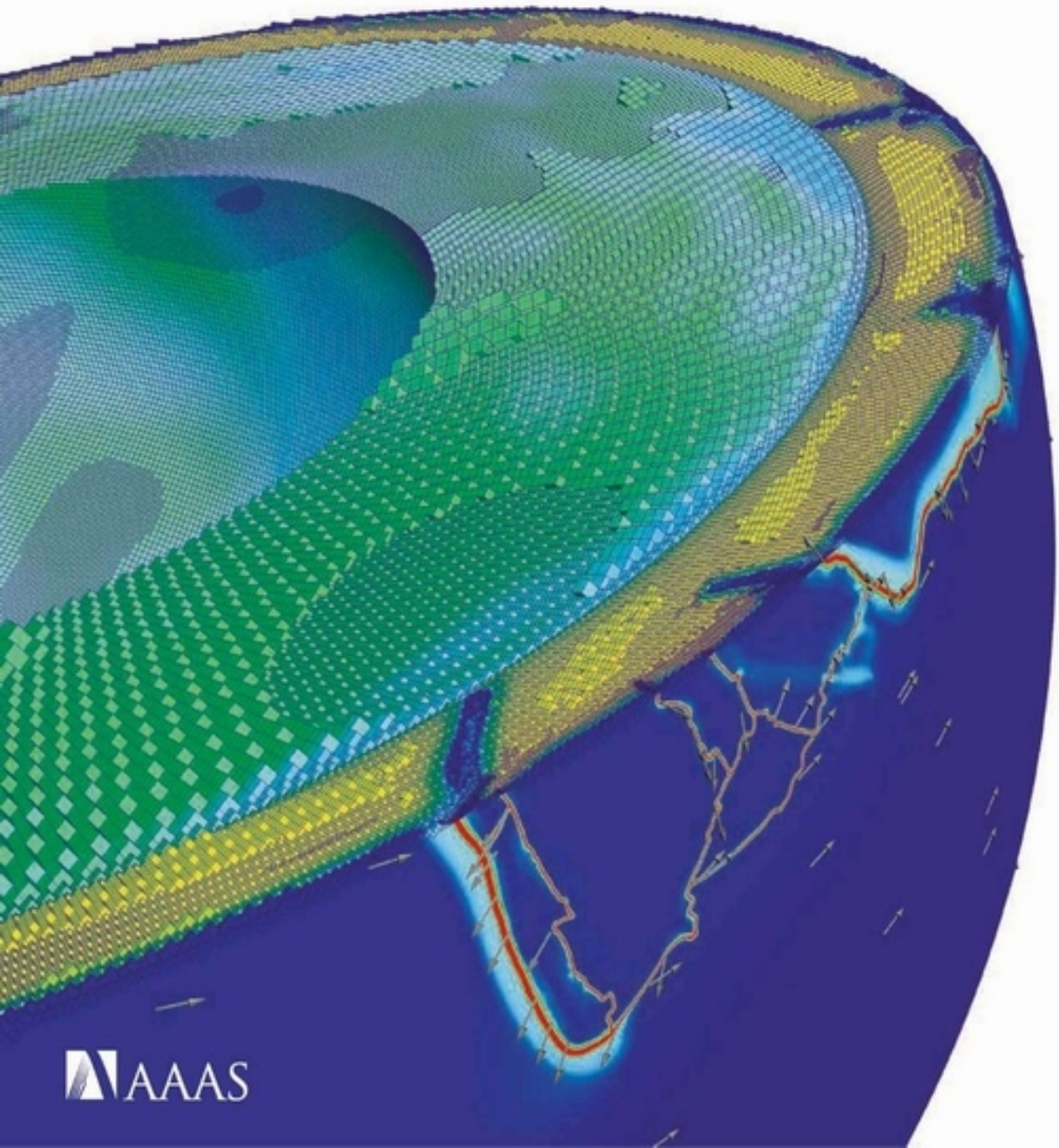

AAAS

EDITORIAL

996 What Is STEM Education?
Rodger W. Bybee

NEWS OF THE WEEK

1000 New XMRV Paper Looks Good, Skeptics Admit—Yet Doubts Linger
1001 Hard Summer for Corals Kindles Fears for Survival of Reefs
1002 Astronomers Hope Their Prize Telescope Isn't Blinded by the Light
1003 U.S. Physicists Eye Australia for New Site of Gravitational-Wave Detector
1004 To Scientists' Dismay, Mixed-Up Cell Lines Strike Again
1005 From *Science*'s Online Daily News Site
1006 Organizers Panned for Omitting Israelis From Meeting in Jordan
1006 NSF Turns Math Earmark on Its Ear to Fund New Institute
1007 From the *Science* Policy Blog

NEWS FOCUS

1008 Google Earth Shows Clandestine Worlds
>> Science *Podcast*
1010 From Pigs to People: The Emergence of a New Superbug

LETTERS

1012 Dietary Restriction: Standing Up for Sirtuins
J. A. Baur et al.
Response
L. Fontana and L. Partridge
Response
V. D. Longo
Dietary Restriction: Theory Fails to Satiate
L. Hayflick
Response
L. Fontana et al.
1013 TECHNICAL COMMENT ABSTRACTS

BOOKS *ET AL.*

1016 Teaching Children Science
S. G. Kohlstedt, reviewed by M. V. Barrow Jr.
1017 The Invisible Gorilla
C. Chabris and D. Simons, reviewed by A. Oliva

POLICY FORUM

1018 Scenario-Building for the Deepwater Horizon Oil Spill
G. E. Machlis and M. K. McNutt

PERSPECTIVES

1020 Fine-Scale Modeling of Global Plate Tectonics
T. Becker
>> *Research Article p. 1033*
1021 Prime, Boost, and Broaden
R. W. Doms
>> *Report p. 1060*
1022 Decisions Made Better
M. O. Ernst
>> *Report p. 1081*
1024 Microenvironment Mimicry
M. Bhatia
>> *Report p. 1078*
1025 Opening the Door to Peptide-Based Porous Solids
P. A. Wright
>> *Report p. 1053*
1026 Looking Inside Adenovirus
S. C. Harrison
>> *Research Article p. 1038; Report p. 1071*

SCIENCE PRIZE ESSAY

1028 The Universe Online
M. J. Raddick and A. S. Szalay

BREVIA

1032 CoRoT Reveals a Magnetic Activity Cycle in a Sun-Like Star
R. A. García et al.
Observations of a distant star reveal a magnetic activity cycle similar to that of the Sun.

CONTENTS continued >>

page 1001

page 1016

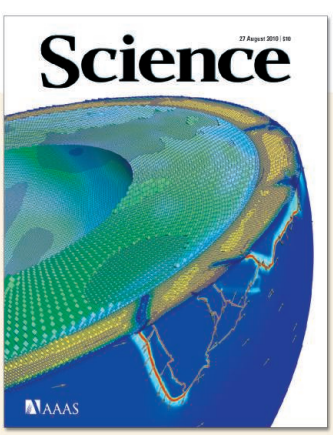

COVER

Dynamic interaction of tectonic plates in the southwest Pacific Ocean computed from a flow model of Earth's interior (arrows show predicted velocity). The computational mesh, for which color represents viscosity (yellow, softer; blue, stiffer), is refined to resolve the forces in the deep mantle that are coupled directly into the edges of plates through narrow slabs. Red lines indicate low-viscosity zones corresponding to plate boundaries. See page 1033.

Image: Georg Stadler, The University of Texas at Austin

DEPARTMENTS

995 This Week in *Science*
997 Editors' Choice
998 *Science* Staff
999 Random Samples
1030 AAAS News & Notes
1089 New Products
1090 *Science* Careers

Published by AAAS

RESEARCH ARTICLES

1033 The Dynamics of Plate Tectonics and Mantle Flow: From Local to Global Scales
G. Stadler et al.
Computational advances enable the modeling of global geophysical processes to the scale of a kilometer.
>> *Perspective p. 1020*

1038 Atomic Structure of Human Adenovirus by Cryo-EM Reveals Interactions Among Protein Networks
H. Liu et al.
High-resolution structures provide a basis for optimizing adenovirus as a vaccine and gene-therapy vector.
>> *Perspective p. 1026; Report p. 1071*

REPORTS

1043 Strange Metal Transport Realized by Gauge/Gravity Duality
T. Faulkner et al.
Black hole theory is used to develop a mathematical description of a class of metals with unusual electronic properties.

1047 Dynamical Instability Produces Transform Faults at Mid-Ocean Ridges
T. Gerya
Transform faults on the sea floor are rotated and stretched sections of the mid-ocean ridge.

1050 The Chlorine Isotope Composition of the Moon and Implications for an Anhydrous Mantle
Z. D. Sharp et al.
The range of chlorine isotope values of the Moon is distinct from those of Earth and meteorites, indicating that the Moon is dry.

1053 An Adaptable Peptide-Based Porous Material
J. Rabone et al.
Conformational changes in a porous material during the sorption of small molecules lead to a dynamic increase in porosity.
>> *Perspective p. 1025*

1057 Trapping a Diradical Transition State by Mechanochemical Polymer Extension
J. M. Lenhardt et al.
Strained carbon rings in the backbone of a polymer can be opened by external application of shear forces.

1060 Induction of Broadly Neutralizing H1N1 Influenza Antibodies by Vaccination
C.-J. Wei et al.
An influenza virus vaccine elicits a broadly neutralizing, cross-protective antibody response in mice, ferrets, and nonhuman primates.
>> *Perspective p. 1021*

1065 Secreted Peptide Signals Required for Maintenance of Root Stem Cell Niche in *Arabidopsis*
Y. Matsuzaki et al.
Short-range signaling by sulfated peptides maintains root stem cells.

1068 Genomic Comparison of the Ants *Camponotus floridanus* and *Harpegnathos saltator*
R. Bonasio et al.
Comparison reveals the epigenetic controls on caste development in ants.
>> Science *Podcast*

1071 Crystal Structure of Human Adenovirus at 3.5 Å Resolution
V. S. Reddy et al.
High-resolution structures provide a basis for optimizing adenovirus as a vaccine and gene-therapy vector.
>> *Perspective p. 1026; Research Article p. 1038*

1075 Insects Betray Themselves in Nature to Predators by Rapid Isomerization of Green Leaf Volatiles
S. Allmann and I. T. Baldwin
Damage caused by a caterpillar releases compounds that are transformed by the pest's saliva into a predator attractant.

1078 Substrate Elasticity Regulates Skeletal Muscle Stem Cell Self-Renewal in Culture
P. M. Gilbert et al.
Muscle stem cells prefer a soft substrate.
>> *Perspective p. 1024*

1081 Optimally Interacting Minds
B. Bahrami et al.
Sharing choices and confidence in those choices can be an empowering experience.
>> *Perspective p. 1022*

1085 Phosphatidic Acid Is a pH Biosensor That Links Membrane Biogenesis to Metabolism
B. P. Young et al.
Lipid signaling in yeast is regulated by intracellular pH.

CONTENTS continued >>

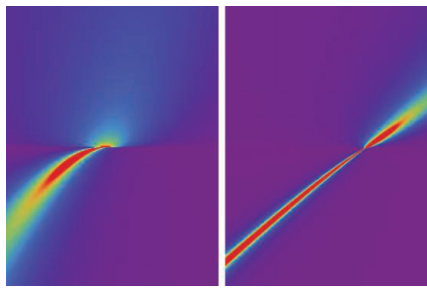

page 1043

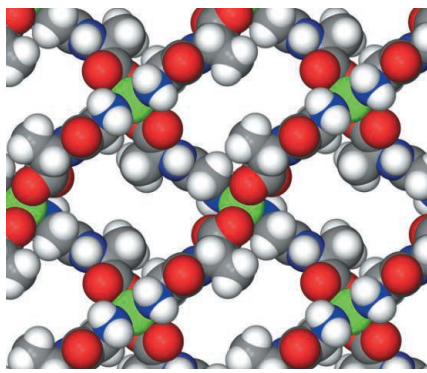

pages 1025 & 1053

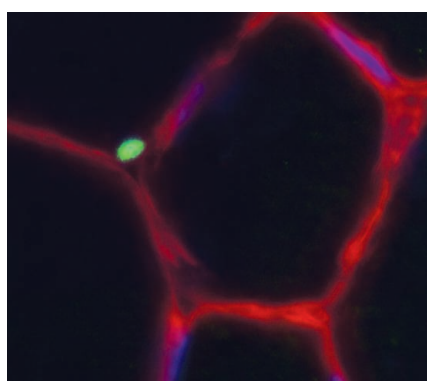

pages 1024 & 1078

SCIENCEONLINE

SCIENCEXPRESS
www.sciencexpress.org

Mitotic Recombination in Patients with Ichthyosis Causes Reversion of Dominant Mutations in *KRT10*
K. A. Choate et al.
Patches of normal skin in patients with a rare skin disorder are due to cells that have lost the disease-causing mutation.
10.1126/science.1192280

Freezing Tolerance in Plants Requires Lipid Remodeling at the Outer Chloroplast Membrane
E. R. Moellering et al.
An enzyme that remodels galactolipids protects chloroplasts against freeze damage in *Arabidopsis thaliana*.
10.1126/science.1191803

α-Synuclein Promotes SNARE-Complex Assembly in Vivo and in Vitro
J. Burré et al.
A protein implicated in neurodegeneration promotes the assembly of membrane fusion complexes.
10.1126/science.1195227

Kepler-9: A System of Multiple Planets Transiting a Sun-Like Star, Confirmed by Timing Variations
M. J. Holman et al.
Two Saturn-sized planets show variations in the times they take to transit their star due to gravitational interaction.
10.1126/science.1195778
>> Science *Podcast*

Deep-Sea Oil Plume Enriches Indigenous Oil-Degrading Bacteria
T. C. Hazen et al.
Cold-loving bacteria biodegrade hydrocarbons in the oil plume faster than expected.
10.1126/science.1195979

TECHNICALCOMMENTS

Comment on "A Southern Tyrant Reptile"
M. C. Herne et al.
Full text at www.sciencemag.org/cgi/content/full/329/5995/1013-c

Response to Comment on "A Southern Tyrant Reptile"
R. B. J. Benson et al.
Full text at www.sciencemag.org/cgi/content/full/329/5995/1013-d

SCIENCENOW
www.sciencenow.org
Highlights From Our Daily News Coverage

Hair Follicles Track the Body's Clock
Researchers follow sleep-wake cycles by plucking hairs from scalps and beards.

Tapping Tesla to Save Trapped Miners
Century-old technology uses magnetic waves to communicate through rock.

You Are Now Free to Move About the Insect
Researchers discover how flies settle on a comfortable cruising altitude.

CREDIT: YANA HAMMOND/AAAS

SCIENCESIGNALING
www.sciencesignaling.org
The Signal Transduction Knowledge Environment

RESEARCH ARTICLE: Self-Induced Patched Receptor Down-Regulation Modulates Cell Sensitivity to the Hedgehog Morphogen Gradient
A. Casali
A self-regulating receptor allows cells to maintain the appropriate balance of ligand-bound and unbound receptors.

RESEARCH ARTICLE: Akt-RSK-S6-Kinase Signaling Networks Activated by Oncogenic Receptor Tyrosine Kinases
A. Moritz et al.

PODCAST
M. J. Comb and A. M. VanHook
A phosphoproteomic analysis of signaling pathways downstream of oncogenic receptor tyrosine kinases identifies potential therapeutic targets.

RESEARCH ARTICLE: A Direct and Functional Interaction Between G_o and Rab5 During G Protein–Coupled Receptor Signaling
V. Purvanov et al.
Regulation of a small GTPase by a heterotrimeric G protein determines the outcome of signaling from the receptor Frizzled.

PERSPECTIVE: Bridging the Synaptic Cleft—Lessons from Orphan Glutamate Receptors
S. M. Schmid and M. Hollmann
Three proteins act as a transsynaptic bridge at a major type of cerebellar synapse.

SCIENCECAREERS
www.sciencecareers.org/career_magazine
Free Career Resources for Scientists

Making Team Science Work: Advice From a Team
K. Hede
A long-term commitment and an ego-free workplace allow the Yale Melanoma Research Group to excel.

Experimental Error: All That Glitters Is All We Remember
A. Ruben
Why are we most fascinated by the irrelevant aspects of science?

SCIENCETRANSLATIONAL MEDICINE
www.sciencetranslationalmedicine.org
Integrating Medicine and Science

EDITORIAL: Advancing Science, Promoting Peace
P. C. Agre and V. Turekian
Despite political differences, scientific diplomacy can help to bridge disparate cultures.

PERSPECTIVE: Recommendations for Biomarker Identification and Qualification in Clinical Proteomics
H. Mischak et al.
Recommendations about structuring proteomic biomarker studies should increase the probability that such markers will be clinically useful.

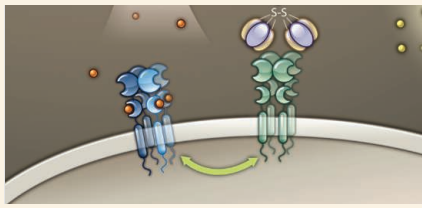

SCIENCESIGNALING
Bridging the synaptic cleft.

RESEARCH ARTICLE: A Biosynthetic Alternative to Human Donor Tissue for Inducing Corneal Regeneration: 24-Month Follow-Up of a Phase 1 Clinical Study
P. Fagerholm et al.
A biosynthetic cornea is stably integrated with host tissues for 2 years after implantation and produces nerve regeneration and vision improvement.

RESEARCH ARTICLE: Drug Reaction with Eosinophilia and Systemic Symptoms (DRESS): A Multiorgan Antiviral T Cell Response
D. Picard et al.
A dangerous drug reaction may be caused by a severe immune response to reactivated resident herpes viruses.

SCIENCEPODCAST
www.sciencemag.org/multimedia/podcast
Free Weekly Show
Download the 27 August *Science* Podcast to hear about modeling the epigenetics of aging and behavior, multiple planets discovered around a Sun-like star, using satellite images for archaeological research, and more.

SCIENCEINSIDER
news.sciencemag.org/scienceinsider
Science Policy News and Analysis

SCIENCE (ISSN 0036-8075) is published weekly on Friday, except the last week in December, by the American Association for the Advancement of Science, 1200 New York Avenue, NW, Washington, DC 20005. Periodicals Mail postage (publication No. 484460) paid at Washington, DC, and additional mailing offices. Copyright © 2010 by the American Association for the Advancement of Science. The title SCIENCE is a registered trademark of the AAAS. Domestic individual membership and subscription (51 issues): $146 ($74 allocated to subscription). Domestic institutional subscription (51 issues): $910; Foreign postage extra: Mexico, Caribbean (surface mail) $55; other countries (air assist delivery) $85. First class, airmail, student, and emeritus rates on request. Canadian rates with GST available upon request, GST #1254 88122. Publications Mail Agreement Number 1069624. **Printed in the U.S.A.**

Change of address: Allow 4 weeks, giving old and new addresses and 8-digit account number. **Postmaster:** Send change of address to AAAS, P.O. Box 96178, Washington, DC 20090–6178. **Single-copy sales:** $10.00 current issue, $15.00 back issue prepaid includes surface postage; bulk rates on request. **Authorization to photocopy** material for internal or personal use under circumstances not falling within the fair use provisions of the Copyright Act is granted by AAAS to libraries and other users registered with the Copyright Clearance Center (CCC) Transactional Reporting Service, provided that $20.00 per article is paid directly to CCC, 222 Rosewood Drive, Danvers, MA 01923. The identification code for *Science* is 0036-8075. *Science* is indexed in the *Reader's Guide to Periodical Literature* and in several specialized indexes.

AAAS
ADVANCING SCIENCE, SERVING SOCIETY

What Is STEM Education?

Rodger W. Bybee is retired executive director of the Biological Sciences Curriculum Study and was chair of the Science Expert Group for the Programme for International Student Assessment 2006. E-mail: RBybee@bscs.org

THE UNITED STATES NEEDS A BROADER, MORE COORDINATED STRATEGY FOR PRECOLLEGE EDUCATION in science, technology, engineering, and mathematics (STEM). That strategy should include all the STEM disciplines and address the need for greater diversity in the STEM professions, for a workforce with deep technical and personal skills, and for a STEM-literate citizenry prepared to address the grand challenges of the 21st century. There have been repeated efforts to produce major improvements in such education, including the production of voluntary national education standards for science and for mathematics in the 1990s. But as a battle-scarred veteran of those efforts, I view the next decade as the time when real progress might finally be made.

The term "STEM education" is now widely used, but what does it mean and how might it influence American education?

For most, it means only science and mathematics, even though the products of technology and engineering have so greatly influenced everyday life. A true STEM education should increase students' understanding of how things work and improve their use of technologies. STEM education should also introduce more engineering during precollege education. Engineering is directly involved in problem solving and innovation, two themes with high priorities on every nation's agenda. Given its economic importance to society, students should learn about engineering and develop some of the skills and abilities associated with the design process. The good news is that the National Assessment Governing Board has recognized the importance of this issue and recently approved the evaluation of technology and engineering education through examinations that will be given to U.S. students in 2014. Likewise, the draft Framework for Science Education released last month by the U.S. National Academies includes technology and engineering among four targeted disciplines.

To succeed in this new round of education reforms, the United States will need equal treatment for science—broadly defined to include technology and engineering—in the reauthorization of the Elementary and Secondary Education Act (currently referred to as No Child Left Behind). For the past 8 years, this legislation has had the unintentional result of reducing or eliminating science from school programs, especially at the elementary level, by not including science test scores as a significant part of the calculation for measuring Adequate Yearly Progress. The current blueprint of the U.S. Department of Education for the reauthorization fails to remedy this situation; the final legislation could and should.

As stressed in the National Academies report *Rising Above the Gathering Storm*, students must acquire such skills as adaptability, complex communication, social skills, nonroutine problem solving, self-management, and systems thinking to compete in the modern economy. To the degree that STEM curricula incorporate group activities, laboratory investigations, and projects, they afford the opportunity for students to develop these essential 21st-century skills and prepare them to become citizens who are better able to make decisions about personal health, energy efficiency, environmental quality, resource use, and national security. Indeed, the competencies that citizens need to understand and address such issues, from the personal to global perspectives, are as clearly linked to knowledge in the STEM disciplines as they are to economics, politics, and cultural values.

The STEM community responded vigorously to produce the Sputnik-spurred education reforms of the 1960s. Likewise, the United States needs a bold new federal strategy for improving education that includes the creation of high-quality, integrated instruction and materials, as well as the placement of problems associated with grand challenges of society at the center of study. It is time to move beyond slogans and make STEM literacy a reality for all students.

– Rodger W. Bybee

10.1126/science.1194998

Published by AAAS

Downloaded from www.sciencemag.org on August 27, 2010

CREDITS: (TOP) SUSAN RUST; (LEFT) PETER VOGEL, PHYSICS BALSA BRIDGE BUILDING CONTEST, NOTRE DAME REGIONAL SECONDARY SCHOOL, VANCOUVER BC (WWW.BALSABRIDGE.COM)

www.sciencemag.org

Science

1200 New York Avenue, NW
Washington, DC 20005
Editorial: 202-326-6550, FAX 202-289-7562
News: 202-326-6581, FAX 202-371-9227
Bateman House, 82-88 Hills Road
Cambridge, UK CB2 1LQ
+44 (0) 1223 326500, FAX +44 (0) 1223 326501

Subscription Services For change of address, missing issues, new orders and renewals, and payment questions: 866-434-AAAS (2227) or 202-326-6417, FAX 202-842-1065. Mailing addresses: AAAS, P.O. Box 96178, Washington, DC 20090-6178 or AAAS Member Services, 1200 New York Avenue, NW, Washington, DC 20005

Institutional Site Licenses please call 202-326-6755 for any questions or information

Reprints: Author Inquiries 800-635-7181
Commercial Inquiries 803-359-4578

Permissions 202-326-7074, FAX 202-682-0816

Member Benefits AAAS/Barnes&Noble.com bookstore www.aaas.org/bn; AAAS Online Store www.apisource.com/aaas/ code MKB6; AAAS Travels: Betchart Expeditions 800-252-4910; Apple Store www.apple.com/eppstore/aaas; Bank of America MasterCard 1-800-833-6262 priority code FAA3YU; Cold Spring Harbor Laboratory Press Publications www.cshlpress.com/affiliates/aaas.htm; GEICO Auto Insurance www.geico.com/landingpage/go51.htm?logo=17624; Hertz 800-654-2200 CDP#343457; Office Depot https://bsd.officedepot.com/portalLogin.do; Seabury & Smith Life Insurance 800-424-9883; Subaru VIP Program 202-326-6417; VIP Moving Services www.vipmayflower.com/domestic/index.html; Other Benefits: AAAS Member Services 202-326-6417 or www.aaasmember.org.

science_editors@aaas.org	(for general editorial queries)
science_letters@aaas.org	(for queries about letters)
science_reviews@aaas.org	(for returning manuscript reviews)
science_bookrevs@aaas.org	(for book review queries)

Published by the American Association for the Advancement of Science (AAAS), *Science* serves its readers as a forum for the presentation and discussion of important issues related to the advancement of science, including the presentation of minority or conflicting points of view, rather than by publishing only material on which a consensus has been reached. Accordingly, all articles published in *Science*—including editorials, news and comment, and book reviews—are signed and reflect the individual views of the authors and not official points of view adopted by AAAS or the institutions with which the authors are affiliated.

AAAS was founded in 1848 and incorporated in 1874. Its mission is to advance science, engineering, and innovation throughout the world for the benefit of all people. The goals of the association are to: enhance communication among scientists, engineers, and the public; promote and defend the integrity of science and its use; strengthen support for the science and technology enterprise; provide a voice for science on societal issues; promote the responsible use of science in public policy; strengthen and diversify the science and technology workforce; foster education in science and technology for everyone; increase public engagement with science and technology; and advance international cooperation in science.

Information for Authors
See pages 352 and 353 of the 15 January 2010 issue or access www.sciencemag.org/about/authors

EDITOR-IN-CHIEF **Bruce Alberts**
EXECUTIVE EDITOR **Monica M. Bradford** NEWS EDITOR **Colin Norman**
MANAGING EDITOR, RESEARCH JOURNALS **Katrina L. Kelner**
DEPUTY EDITORS **R. Brooks Hanson, Barbara R. Jasny, Andrew M. Sugden**

Editorial senior editors/commentary Lisa D. Chong, Brad Wible; **senior editors** Gilbert J. Chin, Pamela J. Hines, Paula A. Kiberstis (Boston), Marc S. Lavine (Toronto), Beverly A. Purnell, L. Bryan Ray, Guy Riddihough, H. Jesse Smith, Phillip D. Szuromi (Tennessee), Valda Vinson, Jake S. Yeston; **associate editors** Kristen L. Mueller, Jelena Stajic, Nicholas S. Wigginton, Laura M. Zahn; **research associate** Alexis Wynne Mogul; **book review editor** Sherman J. Suter; **associate letters editor** Jennifer Sills; **editorial manager** Cara Tate; **senior copy editors** Jeffrey E. Cook, Cynthia Howe, Harry Jach, Lauren Kmec, Barbara P. Ordway, Trista Wagoner; **copy editor** Chris Filiatreau; **editorial coordinators** Carolyn Kyle, Beverly Shields; **publications assistants** Ramatoulaye Diop, Joi S. Granger, Emily Guise, Jeffrey Hearn, Michael Hicks, Lisa Johnson, Scott Miller, Jerry Richardson, Jennifer A. Seibert, Brian White, Anita Wynn; **editorial assistants** Emily C. Horton, Patricia M. Moore, Miriam Weinberg; **executive assistant** Alison Crawford; **administrative support** Maryrose Madrid; **editorial fellow** Melissa R. McCartney

Editorial director, web and new media Stewart Wills; **senior web editor** Tara S. Marathe; **web editor** Robert Frederick; **web development manager** Martyn Green; **web developer** Andrew Whitesell; **intern** Sophia Cai

News deputy news editors Robert Coontz, David Grimm, Eliot Marshall, Jeffrey Mervis, Leslie Roberts; **contributing editors** Elizabeth Culotta, Polly Shulman; **news writers** Yudhijit Bhattacharjee, Adrian Cho, Jennifer Couzin, Jocelyn Kaiser, Richard A. Kerr, Eli Kintisch, Greg Miller, Elizabeth Pennisi, Lauren Schenkman, Robert F. Service (Pacific NW), Erik Stokstad (Online); **web developer** Daniel Berger; **intern** Kristen Minogue; **contributing correspondents** Jon Cohen (San Diego, CA), Daniel Ferber, Ann Gibbons, Sam Kean, Robert Koenig, Andrew Lawler, Mitch Leslie, Charles C. Mann, Virginia Morell, Gary Taubes; **copy editors** Linda B. Felaco, Melvin Gatling, Melissa Raimondi; **administrative support** Scherraine Mack; **bureaus** San Diego, CA: 760-942-3252, FAX 760-942-4979; Pacific Northwest: 503-963-1940

Production director James Landry; **senior manager** Wendy K. Shank; **assistant manager** Rebecca Doshi; **senior specialists** Steve Forrester, Chris Redwood, Anthony Rosen; **Preflight director** David M. Tompkins; **manager** Marcus Spiegler; **specialist** Jason Hillman

Art director Yael Fitzpatrick; **associate art director** Laura Creveling; **senior illustrators** Chris Bickel, Katharine Sutliff; **illustrator** Yana Hammond; **senior art associates** Holly Bishop, Preston Huey, Nayomi Kevitiyagala; **art associates** Kay Engman, Matthew Twombly; **photo editor** Leslie Blizard

***Science* International**

Europe (science@science-int.co.uk) **editorial: international managing editor** Andrew M. Sugden; **senior editor/commentary** Julia Fahrenkamp-Uppenbrink; **senior editors** Caroline Ash, Stella M. Hurtley, Ian S. Osborne, Peter Stern; **associate editor** Maria Cruz; **locum editor** Helen Pickersgill; **editorial support** Rachel Roberts, Alice Whaley; **administrative support** John Cannell, Janet Clements, Louise Hartwell; **news: europe news editor** John Travis; **deputy news editor** Daniel Clery; **contributing correspondents** Michael Balter (Paris), John Bohannon (Vienna), Martin Enserink (Amsterdam and Paris), Gretchen Vogel (Berlin); **intern** Sarah Reed

Latin America contributing correspondent Antonio Regalado

Asia Japan Office: Asca Corporation, Tomoko Furusawa, Rustic Bldg. 7F, 77 Tenjin-cho, Shinjuku-ku, Tokyo 162-0808, Japan; +81 3 6802 4616, FAX +81 3 6802 4615, inquiry@sciencemag.jp; **asia news editor** Richard Stone (Beijing: rstone@aaas.org); **contributing correspondents** Dennis Normile [Japan: +81 (0) 3 3391 0630, FAX +81 (0) 3 5936 3531; dnormile@gol.com]; Hao Xin [China: cindyhao@gmail.com]; Pallava Bagla [South Asia: +91 (0) 11 2271 2896; pbagla@vsnl.com]

EXECUTIVE PUBLISHER **Alan I. Leshner**
PUBLISHER **Beth Rosner**

Fulfillment Systems and Operations (membership@aaas.org); **director** Waylon Butler; **customer service supervisor** Pat Butler; **specialists** Latoya Casteel, LaVonda Crawford, Vicki Linton, April Marshall; **data entry supervisor** Cynthia Johnson; **specialists** Shirlene Hall, Tarrika Hill, William Jones

Business Operations and Administration director Deborah Rivera-Wienhold; **business systems and financial analysis director** Randy Yi; **manager, business analysis** Eric Knott; **manager, business operations** Jessica Tierney; **financial analysts** Priti Pamnani, Celeste Troxler; **rights and permissions: administrator** Emilie David; **associate** Elizabeth Sandler; **marketing director** Ian King; **marketing managers** Allison Pritchard, Alison Chandler, Julianne Wielga; **marketing associates** Aimee Aponte, Mary Ellen Crowley, Wendy Wise; **senior marketing executive** Jennifer Reeves; **director, site licensing** Tom Ryan; **director, corporate relations** Eileen Bernadette Moran; **publisher relations, eresources specialist** Kiki Forsythe; **senior publisher relations specialist** Catherine Holland; **publisher relations, east coast** Phillip Smith; **publisher relations, west coast** Philip Tsolakidis; **fulfillment supervisor** Iquo Edim; **fulfillment coordinator** Carrie MacDonald; **marketing manager** Christina Schlecht; **marketing associate** Laura Tutino; **electronic media: manager** Lizabeth Harman; **project manager** Trista Snyder; **assistant manager** Lisa Stanford; **senior production specialists** Ryan Atkins, Christopher Coleman, **computer specialist** Walter Jones, Kai Zhang; **production specialists** Angela Forest, Nichele Johnston, Kimberly Oster; **director, web and new media** Will Collins

advertising director, worldwide ad sales Bill Moran
commercial editor Sean Sanders: 202-326-6430
assistant commercial editor Tianna Hicklin 202-326-6463
project director, outreach Brianna Blaser

Product (science_advertising@aaas.org); **midwest** Rick Bongiovanni: 330-405-7080, FAX 330-405-7081; **east coast/e. canada** Laurie Faraday: 508-747-9395, FAX 617-507-8189; **west coast/w. canada** Lynne Stickrod: 415-931-9782, FAX 415-520-6940; **uk/europe/asia** Roger Goncalves: TEL/FAX +41 43 243 1358; **japan** ASCA Corporation, Nanako Ide +81 (0) 3 6802 4616, FAX +81 (0) 3 6802 4615; ads@sciencemag.jp; **senior traffic associate** Deiandra Simms

worldwide associate director of *Science* Careers Tracy Holmes: +44 (0) 1223 326525, FAX +44 (0) 1223 326532

Classified (advertise@sciencecareers.org); **u.s.: midwest/west coast/south central/canada** Tina Burks: 202-326-6577; **east coast/industry** Elizabeth Early: 202-326-6578; **advertising operations manager** Kate Panganiban **sales coordinators** Rohan Edmonson, Shirley Young; **europe/row sales:** Susanne Kharraz, Dan Pennington, Alex Palmer; **sales assistant** Lisa Patterson; **japan** ASCA Corporation, Jie Chin +81 (0) 3 6802 4616, FAX +81 (0) 3 6802 4615; careerads@sciencemag.jp; **advertising support manager** Karen Foote: 202-326-6740; **advertising production operations manager** Deborah Tompkins; **senior production specialist/graphic designer** Amy Hardcastle; **production specialist** Yuse Lajiminmuhip; **senior traffic associate** Christine Hall

AAAS Board of Directors retiring president, chair Peter C. Agre; **president** Alice Huang; **president-elect** Nina Fedoroff; **treasurer** David E. Shaw; **chief executive officer** Alan I. Leshner; **board** Linda P. B. Katehi, Nancy Knowlton, Stephen Mayo, Cherry A. Murray, Julia M. Phillips, Sue V. Rosser, David D. Sabatini, Thomas A. Woolsey

AAAS
ADVANCING SCIENCE, SERVING SOCIETY

SENIOR EDITORIAL BOARD

John I. Brauman, *Chair, Stanford Univ.*
Richard Losick, *Harvard Univ.*
Linda Partridge, *Univ. College London*
Michael S. Turner, *University of Chicago*

BOARD OF REVIEWING EDITORS

Adriano Aguzzi, *Univ. Hospital Zürich*
Takuzo Aida, *Univ. of Tokyo.*
Sonia Altizer, *Univ. of Georgia*
David Altshuler, *Broad Institute*
Arturo Alvarez-Buylla, *Univ. of California, San Francisco*
Richard Amasino, *Univ. of Wisconsin, Madison*
Angelika Amon, *MIT*
Kathryn Anderson, *Memorial Sloan-Kettering Cancer Center*
Siv G. E. Andersson, *Uppsala Univ.*
Peter Andolfatto, *Princeton Univ.*
Meinrat O. Andreae, *Max Planck Inst., Mainz*
John A. Bargh, *Yale Univ.*
Ben Barres, *Stanford Medical School*
Marisa Bartolomei, *Univ. of Penn. School of Med.*
Jordi Bascompte, *Estación Biológica de Doñana, CSIC*
Facundo Batista, *London Research Inst.*
Ray H. Baughman, *Univ. of Texas, Dallas*
Yasmine Belkaid, *NIAID, NIH*
Stephen J. Benkovic, *Penn State Univ.*
Gregory C. Beroza, *Stanford Univ.*
Ton Bisseling, *Wageningen Univ.*
Mina Bissell, *Lawrence Berkeley National Lab*
Peer Bork, *EMBL*
Robert W. Boyd, *Univ. of Rochester*
Paul M. Brakefield, *Leiden Univ.*
Christian Büchel, *Universitätsklinikum Hamburg-Eppendorf*
Joseph A. Burns, *Cornell Univ.*
William P. Butz, *Population Reference Bureau*
Mats Carlsson, *Univ. of Oslo*
Mildred Cho, *Stanford Univ.*
David Clapham, *Children's Hospital, Boston*
David Clary, *Oxford University*
J. M. Claverie, *CNRS, Marseille*
Jonathan D. Cohen, *Princeton Univ.*
Andrew Cossins, *Univ. of Liverpool*
Robert H. Crabtree, *Yale Univ.*
Wolfgang Cramer, *Potsdam Inst. for Climate Impact Research*
F. Fleming Crim, *Univ. of Wisconsin*
Jeff L. Dangl, *Univ. of North Carolina*
Stanislas Dehaene, *Collège de France*
Edward DeLong, *MIT*
Emmanouil T. Dermitzakis, *Univ. of Geneva Medical School*
Robert Desimone, *MIT*
Claude Desplan, *New York Univ.*
Dennis Discher, *Univ. of Pennsylvania*
Scott C. Doney, *Woods Hole Oceanographic Inst.*
Jennifer A. Doudna, *Univ. of California, Berkeley*
Julian Downward, *Cancer Research UK*
Bruce Dunn, *Univ. of California, Los Angeles*
Christopher Dye, *WHO*
Michael B. Elowitz, *Calif. Inst. of Technology*
Gerhard Ertl, *Fritz-Haber-Institut, Berlin*
Mark Estelle, *Indiana Univ.*
Barry Everitt, *Univ. of Cambridge*
Paul G. Falkowski, *Rutgers Univ.*
Ernst Fehr, *Univ. of Zurich*
Tom Fenchel, *Univ. of Copenhagen*
Alain Fischer, *INSERM*
Wulfram Gerstner, *EPFL Lausanne*
Charles Godfray, *Univ. of Oxford*
Diane Griffin, *Johns Hopkins Bloomberg School of Public Health*
Christian Haass, *Ludwig Maximilians Univ.*
Steven Hahn, *Fred Hutchinson Cancer Research Center*
Gregory J. Hannon, *Cold Spring Harbor Lab.*
Niels Hansen, *Technical Univ. of Denmark*
Dennis L. Hartmann, *Univ. of Washington*
Chris Hawkesworth, *Univ. of St Andrews*
Martin Heimann, *Max Planck Inst., Jena*
James A. Hendler, *Rensselaer Polytechnic Inst.*
Janet G. Hering, *Swiss Fed. Inst. of Aquatic Science & Technology*
Ray Hilborn, *Univ. of Washington*
Michael E. Himmel, *National Renewable Energy Lab.*
Kei Hirose, *Tokyo Inst. of Technology*
Ove Hoegh-Guldberg, *Univ. of Queensland*
Lora Hooper, *UT Southwestern Medical Ctr at Dallas*
Ronald R. Hoy, *Cornell Univ.*
Jeffrey A. Hubbell, *EPFL Lausanne*
Steven Jacobsen, *Univ. of California, Los Angeles*
Peter Jonas, *Universität Freiburg*
Barbara B. Kahn, *Harvard Medical School*
Daniel Kahne, *Harvard Univ.*
Bernhard Keimer, *Max Planck Inst., Stuttgart*
Robert Kingston, *Harvard Medical School*
Hanna Kokko, *Univ. of Helsinki*
Alberto R. Kornblihtt, *Univ. of Buenos Aires*
Leonid Kruglyak, *Princeton Univ.*
Lee Kump, *Penn State Univ.*
Mitchell A. Lazar, *Univ. of Pennsylvania*
David Lazer, *Harvard Univ.*
Virginia Lee, *Univ. of Pennsylvania*
Julian Lewis, *Cancer Research UK*
Olle Lindvall, *Univ. Hospital, Lund*
Marcia C. Linn, *Univ. of California, Berkeley*
John Lis, *Cornell Univ.*
Richard Losick, *Harvard Univ.*
Ke Lu, *Chinese Acad. of Sciences*
Laura Machesky, *CRUK Beatson Inst. for Cancer Research*
Andrew P. MacKenzie, *Univ. of St Andrews*
Anne Magurran, *Univ. of St Andrews*
Oscar Marin, *CSIC & Univ. Miguel Hernández*
Charles Marshall, *Univ. of California, Berkeley*
Martin M. Matzuk, *Baylor College of Medicine*
Grahma Medley, *Univ. of Warwick*
Virginia Miller, *Washington Univ.*
Yasushi Miyashita, *Univ. of Tokyo*
Richard Morris, *Univ. of Edinburgh*
Edvard Moser, *Norwegian Univ. of Science and Technology*
Sean Munro, *MRC Lab. of Molecular Biology*
Naoto Nagaosa, *Univ. of Tokyo*
James Nelson, *Stanford Univ. School of Med.*
Timothy W. Nilsen, *Case Western Reserve Univ.*
Pär Nordlund, *Karolinska Inst.*
Helga Nowotny, *European Research Advisory Board*
Stuart H. Orkin, *Dana-Farber Cancer Inst.*
Christine Ortiz, *MIT*
Elinor Ostrom, *Indiana Univ.*
Andrew Oswald, *Univ. of Warwick*
Jonathan T. Overpeck, *Univ. of Arizona*
P. David Pearson, *Univ. of California, Berkeley*
John Pendry, *Imperial College*
Reginald M. Penner, *Univ. of California, Irvine*
John H. J. Petrini, *Memorial Sloan-Kettering Cancer Center*
Simon Phillpot, *Univ. of Florida*
Philippe Poulin, *CNRS*
Colin Renfrew, *Univ. of Cambridge*
Trevor Robbins, *Univ. of Cambridge*
Barbara A. Romanowicz, *Univ. of California, Berkeley*
Jens Rostrup-Nielsen, *Haldor Topsoe*
Edward M. Rubin, *Lawrence Berkeley National Lab*
Shimon Sakaguchi, *Kyoto Univ.*
Michael J. Sanderson, *Univ. of Arizona*
Jürgen Sandkühler, *Medical Univ. of Vienna*
Randy Seeley, *Univ. of Cincinnati*
Christine Seidman, *Harvard Medical School*
David Sibley, *Washington Univ*
Joseph Silk, *Univ. of Oxford*
Montgomery Slatkin, *Univ. of California, Berkeley*
Davor Solter, *Inst. of Medical Biology, Singapore*
Allan C. Spradling, *Carnegie Institution of Washington*
Jonathan Sprent, *Garvan Inst. of Medical Research*
Elsbeth Stern, *ETH Zürich*
Yoshiko Takahashi, *Nara Inst. of Science and Technology*
Jurg Tschopp, *Univ. of Lausanne*
Herbert Virgin, *Washington Univ.*
Bert Vogelstein, *Johns Hopkins Univ.*
Bruce D. Walker, *Harvard Medical School*
Christopher A. Walsh, *Harvard Medical School*
David A. Wardle, *Swedish Univ. of Agric Sciences*
Colin Watts, *Univ. of Dundee*
Detlef Weigel, *Max Planck Inst., Tübingen*
Jonathan Weissman, *Univ. of California, San Francisco*
Sue Wessler, *Univ. of Georgia*
Ian A. Wilson, *The Scripps Res. Inst.*
Timothy D. Wilson, *Univ. of Virginia*
Xiaoliang Sunney Xie, *Harvard Univ.*
John R. Yates III, *The Scripps Res. Inst.*
Jan Zaanen, *Leiden Univ.*
Mayana Zatz, *University of Sao Paolo*
Huda Zoghbi, *Baylor College of Medicine*
Maria Zuber, *MIT*

BOOK REVIEW BOARD

John Aldrich, *Duke Univ.*
David Bloom, *Harvard Univ.*
Angela Creager, *Princeton Univ.*
Richard Shweder, *Univ. of Chicago*
Ed Wasserman, *DuPont*
Lewis Wolpert, *Univ. College London*

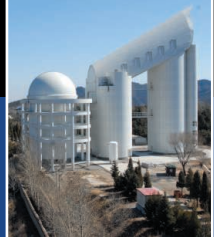

Blinded by the light? 1002

Better resolution for LIGO 1003

CHRONIC FATIGUE SYNDROME

New XMRV Paper Looks Good, Skeptics Admit—Yet Doubts Linger

The plot thickens. This week, a long-awaited paper by U.S. government labs about the link between a virus and chronic fatigue syndrome (CFS) finally saw the light of day. The study confirms a controversial 2009 paper that reported CFS patients are often infected with the virus, called XMRV. Since then, four other studies have failed to duplicate those findings. Even skeptics are impressed by how much care the authors of the new study took to ensure accuracy. But that makes it even more baffling why some labs easily detect the virus while others can't find a trace of it in any patient.

The new paper, published on Monday by the *Proceedings of the National Academy of Sciences* (*PNAS*), also adds a confusing twist: Rather than XMRV itself, the team found a broader and more diverse group of closely related viruses. That leads some critics to say the paper is a new finding, not confirmation of the first one. "Let's be clear. This is another virus," says retrovirologist Myra McClure of Imperial College London, a co-author of one of the four negative studies.

The controversy began in October 2009, when a team led by Judy Mikovits of the Whittemore Peterson Institute (WPI) in Reno, Nevada, reported in *Science* (23 October 2009, p. 585) that 67% of CFS patients were infected with XMRV, compared to just 3.4% of healthy controls. The study caused huge excitement among patients and raised hopes of a cure. But when four other groups were unable to repeat the results, some suspected that WPI, a privately funded lab many researchers had never even heard of, might be wrong.

U.S. government labs soon found themselves on opposite sides of the debate. Researchers at the Centers for Disease Control and Prevention (CDC) failed to find the virus, whereas the new study—by scientists at the Food and Drug Administration (FDA), the National Institutes of Health (NIH), and Harvard Medical School—says that Mikovits was right. Both groups temporarily put their papers on hold to check their results and try to understand what was going on (*Science*, 2 July, p. 18). Both eventually felt confident enough to publish, and the negative CDC paper appeared in *Retrovirology* in July.

No doubt. NIH's Harvey Alter says he's sure the findings are not the result of mistakes or contamination.

For the *PNAS* paper, researchers looked for traces of XMRV's so-called *gag* gene in samples taken from 37 CFS patients collected in the mid-1990s. They found evidence for the virus in 32 (87%) of the patients, but in only 3 out of 44 healthy controls (6.8%). The group went to great lengths to avoid errors, says senior author Harvey Alter of the NIH Clinical Center. XMRV is closely related to an endogenous mouse retrovirus, so the team tested every sample positive for XMRV for traces of mouse mitochondrial DNA, which would have been a telltale sign of lab contamination. They found none. They also took fresh samples from eight of the patients and found that, 15 years on, they were still infected, and that the virus had evolved, "just as we would expect from a retrovirus," says Alter.

The data do seem solid, admits Steve Monroe, director of CDC's Division of High-Consequence Pathogens and Pathology. "It's simply a good paper," adds virologist Reinhard Kurth, former director of the Robert Koch Institute in Berlin. Alter, a widely respected virologist and winner of the Albert Lasker Award for Clinical Medical Research, "clearly knows what he is doing." But Kurth nonetheless remains skeptical. So does Robin Weiss of Imperial College London, who says he's seen too many instances of proposed new human retroviruses that fell apart on closer inspection—including one he reported in 1999. "You can have a very good reputation and be very careful, and still get it wrong," Weiss says.

Part of the problem, skeptics say, is that the researchers didn't exactly replicate the *Science* paper. XMRV is a so-called xenotropic murine virus, which means it can no longer enter mouse cells but can infect cells of other species. The *PNAS* authors say the viral sequences they find are quite diverse and more closely resemble the so-called polytropic mouse viruses, which is why they adopted the term MLV-related virus, for murine leukemia virus. But Alter says that XMRV is a subset of MLVs, and that his work does support the earlier study. Mikovits—who is "delighted" by the results—says that in the meantime, her group has found more diversity in the virus as well.

A working group coordinated by the National Heart, Lung, and Blood Institute (NHLBI) is already trying to find out why careful studies by veteran scientists can have such opposing results. Patient selection could play a role: Different studies have used different diagnostic and recruitment criteria. But even so, it's hard to explain why four studies wouldn't have included a single infected patient.

Subtle differences in sample collection and handling, or in the way tests are performed, could also have led the four labs to miss the virus. But CDC's Monroe says he's confident that his lab can identify XMRV correctly. As part of the NHLBI program, researchers at FDA, CDC, WPI, and other labs have all blindly tested a panel of samples, some of them "spiked" with different amounts of the virus; all of them performed well. Further exchange of samples and reagents is now under way. "They should be able to clear this up by Christmas," says Kurth.

–MARTIN ENSERINK

CREDIT: NIH

Downloaded from www.sciencemag.org on August 26, 2010

Published by AAAS

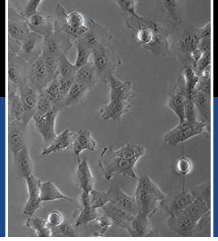

Cases of mistaken identity
1004

Research with Google Earth
1008

MARINE ECOLOGY

Hard Summer for Corals Kindles Fears for Survival of Reefs

Coral reefs are reeling from extensive bleaching in the Indian Ocean and throughout Southeast Asia. "It rivals 1998," when massive bleaching associated with high ocean temperatures destroyed 16% of the world's coral reefs, says Clive Wilkinson, a coral reef ecologist at Australia's Reef and Rainforest Research Centre in Townsville. And although some hard-hit areas have cooled—offering hope that some reefs may rebound—other regions are just now heating up. Based on current sea surface temperatures, the U.S. National Oceanic and Atmospheric Administration (NOAA) has issued an alert for the Western Pacific and the Caribbean. "We're looking at the potential for very warm temperatures causing significant coral bleaching over the next couple of months," says C. Mark Eakin, a NOAA coral reef ecologist in charge of the agency's Coral Reef Watch.

The blight is expected to harm a host of sea creatures. When the "rainforests of the oceans" are degraded or die, a wide variety of marine life that depend on reefs suffer. And humans too feel the pain: Any decrease in fisheries productivity and loss of tourism affects coastal communities.

Many reefs will be hard pressed to recover from this year's bleaching. According to Eakin, global warming appears to be increasing the frequency of bleaching events. That can spell doom for reefs. "If you get too many repetitive lethal events, the corals will not recover," Wilkinson says.

Corals harbor symbiotic algae called zooxanthellae that use photosynthesis to produce nutrients for themselves and their hosts. Sustained above-average water temperatures and intense sunlight can upset the delicate symbiotic balance, prompting corals to expel zooxanthellae. The corals turn white, or bleach. If weather conditions ease quickly enough, the algae repopulate coral. Prolonged bleaching is lethal.

The most recent massive worldwide bleaching incident occurred in 1998, when El Niño conditions in the South Pacific caused sea surface temperatures to soar across the globe. This year, too, the hand of El Niño was at work. According to Coral Reef Watch, warming started in early summer in the Indian Ocean and persisted until cooling monsoon rains arrived. High temperatures later hit Southeast Asia and the Coral Triangle, which stretches from central Indonesia east to the Solomon Islands and north through the Philippines. In recent weeks, sea surface temperatures have risen in the Western Pacific in a band from Micronesia to Guam and the Northern Mariana Islands, and in the southern Caribbean. In some areas, says Eakin, temperatures "are worse than in '98."

Scientists are still surveying the damage. Early data are grim. Reefs on both sides of the Thai Peninsula were hit, with up to 100% of some coral species bleached, says James True, a coral biologist at Prince of Songkla University in Hat Yai, Thailand. He expects at least 80% of the most sensitive species to die. "A few inshore reefs got so badly damaged they probably won't ever come back to the way they were," he says. Among surviving corals, "disease is rampant," True says, with two to three times the usual incidence of necrotic lesions and growth anomalies. Similar reports of "quite extensive bleaching" have come from Vietnam and through the heart of the Coral Triangle in Indonesia and the Philippines, says Wilkinson, who coordinates the Global Coral Reef Monitoring Network, which tracks reef status and promotes conservation.

Whiter shade of pale. A bleached coral on a Thai reef will likely crumble and litter the sea floor.

CREDIT: JAMES GUEST

Some ailing reefs had just begun to recover from the 1998 bleaching. "We've got examples of reefs that were bouncing back quite rapidly 10 years after a 90% die off," Wilkinson says. But they were still at least a decade away from full health, and it would take decades longer for slower growing corals to recover. Eakin says that is a particular worry in the Caribbean, where localized bleaching caused extensive coral death 5 years ago and reefs have yet to bounce back.

This year's bleaching event has some disturbing new wrinkles. In some regions, it seems to be hammering normally resistant species while sparing *Acropora*, a fast-growing coral that is usually the first to succumb. "We don't know why, but it's tempting to suggest it is adaptation," says James Guest, a marine biologist at the National University of Singapore. *Acropora* that survived in 1998 and repopulated reefs may have had some resistance to bleaching, he says, or perhaps they have taken in zooxanthellae that are less sensitive to higher temperatures. Even if further studies demonstrate some degree of adaptation among corals, Guest warns that future reefs will look quite different from those of today.

Researchers can only watch as the nightmare unfolds. While bleaching is occurring, "there's literally nothing you can do," Wilkinson says. Reefs that were recovering from the 1998 event were far from inhabited coasts or managed in a way to minimize stress from damaging fishing practices and sedimentation from runoff. This year, much of the bleaching is occurring on reefs already under siege.

The long-term prognosis is bleak. Global warming is pushing baseline sea temperatures upward, says Eakin, causing localized bleaching even in years without an El Niño. "Unless there is concerted action to reduce greenhouse gases," he warns, "bleaching will become increasingly common and not just during extraordinary weather events."

–DENNIS NORMILE

Downloaded from www.sciencemag.org on August 26, 2010

Published by AAAS

LAMOST lite? Rising light pollution may undermine LAMOST's ambitious science program.

CREDIT: R. STONE/*SCIENCE*

CHINA

Astronomers Hope Their Prize Telescope Isn't Blinded by the Light

BEIJING—Chinese astronomers thought they had their hands full, fine-tuning their complicated new survey telescope into next year. Now they have a more urgent problem: Light pollution could jeopardize its ambitious science program.

Concerns are growing over light from a planned astronomy education center to be built near the $40 million Large Sky Area Multi-Object Fiber Spectroscopic Telescope (LAMOST) in Xinglong, 170 kilometers northeast of Beijing. "The local sky is already bright. Even a little more light will ruin the project," warns Deng Licai, an astronomer with the National Astronomical Observatories of the Chinese Academy of Sciences (NAOC) here who is rallying opposition to the center. If authorities follow through with their plan to put the center just south of LAMOST, Deng says, "I will do anything to stop it."

Senior NAOC officials are aware of the threat. The education center, they say, would reduce light pollution because it could dampen light from dwellings—villagers will be relocated—and astronomers will regulate the center's operations and lighting. Villagers may also learn to value a dark sky and voluntarily reduce light emissions. "We want a win-win solution," says senior engineer Liu Xiaoqun, an NAOC deputy director-general. NAOC is also helping draft a national regulation that would curtail light pollution in the vicinity of observatories across the country.

For China's astronomy community, the stakes are high. "This is the most important instrument of our generation," says Deng. LAMOST, now also called the Guoshoujing Telescope, after a Ming Dynasty astronomer, should be able to peer twice as deep into space and time as its predecessor, the Sloan Digital Sky Survey. Astronomers plan to acquire spectra from 14 million celestial sources to shed light on the structure of the universe and on a long-standing puzzle: how galaxies form (*Science*, 4 April 2008, p. 34).

Astronomers realized China's growth would bring increasing light pollution. For LAMOST, the main culprits are Beijing and the telescope's home in Xinglong, a county of 50,000. "But it's worse than we expected," Deng says. For months, NAOC leaders have been discussing with local officials how to safeguard observing conditions. In response, the Xinglong government has closed 18 factories, removed 50 dust-spewing boilers and furnaces, shuttered five searchlights, and fit more than 200 streetlights with covers, says Liu. Further steps could include replacing incandescent streetlights with low-pressure sodium lamps and turning off some streetlights after most people go to sleep, says Jiang Xiaojun, chief engineer of Xinglong Station. However, he warns, "if light pollution around the observatory is uncontrolled and keeps increasing, the observatory will have to be closed down or moved away."

The education center is a new source of angst. In 2007, the governments of Xinglong County and Chengde, a major city with authority over Xinglong, began drafting plans to build the center on the south-facing slope of the hill on which LAMOST is perched. Local authorities see the telescope as a tourist draw that could boost their economy. "Nobody, including us, has the privilege … to impose limits on their development," Liu says. The challenge is to minimize the impact on the observatory, he says. That could mean, for example, keeping any night activities indoors and behind thick curtains. Another possible remedy is to build the center farther from the observatory, says LAMOST chief engineer Cui Xiangqun of the Nanjing Institute of Astronomical Optics and Technology.

Some Chinese astronomers chafe at the fact that they were not aware of ongoing discussions about the education center. Deng says he learned about the plan from a news report on the Internet several weeks ago. "I could not believe it," he says. LAMOST is pointed southward, at a patch of sky near the meridian. Any light from a facility would further brighten LAMOST's viewing area—from 20 degrees north of overhead to 50 degrees south of overhead—"and be extremely harmful to the site," says Deng. "The closer a light source is to the telescope, the higher in the sky the plume of light is visible," adds Heidi Newberg, an astronomer at Rensselaer Polytechnic Institute in Troy, New York, and a member of LAMOST's survey planning working group.

Meanwhile, engineers are racing to commission the complex telescope, which has an innovative active optics system that deforms the correcting mirror's 24 plates individually. At the focal surface, 4000 optical fibers will feed starlight into a battalion of spectrographs. Data gathered in recent weeks have revealed more than a dozen uncharted quasars and scores of planetary nebulae in the Andromeda Galaxy, two teams report in the latest issue of *Research in Astronomy and Astrophysics*. As promising as the early data are, Deng says, it will take several months to get the telescope performing up to its design specifications. Then the survey proper would get under way.

"For the sake of astronomical productivity," says Newberg, "I hope that development in the region can be kept to a minimum, particularly to the south of the telescope, and particularly in the next 5 to 10 years." Deng, for one, is not optimistic. "Anytime a scientific or environmental project is in conflict with development in China," he says, "development always wins." Now, with the education center likely to go ahead, Deng says LAMOST astronomers are even mulling whether to "adjust our science plan to carry out less important research."

–RICHARD STONE

Downloaded from www.sciencemag.org on August 27, 2010

Published by AAAS

RESEARCH FACILITIES

U.S. Physicists Eye Australia for New Site of Gravitational-Wave Detector

U.S. physicists hope that the offer is too good for Australia to refuse.

They want to take parts from their massive twin gravitational-wave detectors and use them to build a third detector near Perth in western Australia. Adding a detector down under would greatly enhance the ability of the Laser Interferometer Gravitational-Wave Observatory (LIGO) to pinpoint sources of gravitational waves, should such waves ever be spotted. The cost to Australia would be $170 million, the price tag for building and maintaining the new site. In return, Australian physicists would gain full participation in the half-billion-dollar experiment.

"It's absolutely a win-win situation," says David Blair, a physicist at the University of Western Australia (UWA) in Crawley. But the Australian government must decide in the next year. "We're asking a lot of Australia," says Stanley Whitcomb, a physicist at the California Institute of Technology (Caltech) in Pasadena and LIGO's chief scientist. "I don't think there's anybody who thinks there's better than a 50-50 chance of this happening."

LIGO Executive Director Jay Marx hatched the idea last October after a workshop in Shanghai, China, as a way to greatly enhance LIGO's performance as a gravitational-wave telescope as well as a detector. Built for $294 million by the U.S. National Science Foundation (NSF), LIGO aims to detect tiny ripples in the fabric of space and time set off when, for example, two massive neutron stars spiral into each other. To sense those ripples, LIGO uses huge optical motion sensors called interferometers in Hanford, Washington, and Livingston, Louisiana.

LIGO already works in concert with a European detector, called VIRGO, in Cascina, Italy, near Pisa. By comparing the times at which the three detectors sense a pulse of gravitational waves, scientists should be able to locate the waves' source to within a couple of degrees in some parts of the sky. But LIGO and VIRGO cannot pin down sources that lie in the plane defined by the locations of the three detectors. Adding a fourth station in Australia would create other planes and enable researchers to locate a source to within a degree or so across the entire sky (see figure.)

In fact, a third LIGO detector is already running in the background at the Hanford site. Each LIGO station consists of two 4-kilometer-long vacuum chambers arranged in a gigantic L. Light from a high-power laser bounces between the mirrors at either end of each tube, or "arm," and by comparing the two streams of light scientists can detect changes in the relative lengths of the arms as small as 0.001 times the width of a proton. At Hanford, a second set of mirrors and equipment in the same building forms a 2-kilometer interferometer that serves as a crosscheck for the bigger device.

But there's now a chance to move that third detector somewhere else, says Albert Lazzarini, a physicist at Caltech and deputy director of LIGO. Two years ago, LIGO scientists began a $205 million upgrade to all the detectors that, when it's completed in 2015, should make them 10 times more sensitive. The original plan for Advanced LIGO was to stretch the smaller Hanford detector to a full-size one at its current site. But it does not have to sit atop the first detector to serve as a crosscheck, Lazzarini says.

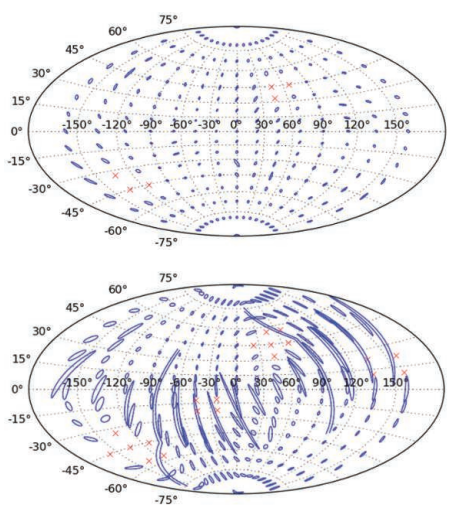

Clearly better. These sky maps—smaller ellipses denote higher precision—show that the addition of another detector in Australia (*top*) would greatly improve physicists' ability to pinpoint gravitational-wave sources under the current plan (*above*). LIGO's Louisiana site is pictured.

So in the new scheme, parts for that detector would be shipped to Australia to build a new detector in Gingin, 80 kilometers north of Perth. "We would basically be asking the NSF to deliver one set of hardware to another continent," Lazzarini says.

That's a radical change of plans, and it would have to happen fast: Researchers plan to start taking apart the current LIGO detectors in October and installing the new equipment next year. But NSF likes the idea of putting a detector in Australia so much that it's willing to rock the boat, says Beverly Berger, program director for gravitational physics at the agency. "It's project management 101 that you don't change a major project once it's under way unless you've got a compelling reason to do so," she says. This week, NSF officials pitched the plan to the agency's governing National Science Board.

NSF officials are not willing to pay more for Advanced LIGO, however, so the burden will fall on the Australian government. Building the site would cost about $125 million, says Robyn Owens, vice president for research at UWA, and running it for 10 years would cost another $45 million. If all goes well, the Australian detector could start taking data in 2017.

Australian physicists have been trying for decades to persuade their government to build a similar detector. "We really think that this collaboration could make all the difference," Blair says. Whitcomb notes that Australia has by far the most robust gravitational-wave community in the Southern Hemisphere.

The road to approval may be tricky, however. It will begin with a proposal to Australia's National Research Infrastructure Committee, but beyond that there is no protocol for getting such an expensive project approved, Owens says. Instead, researchers must simply convince politicians that the idea is worth funding. And that may have just gotten a bit harder. Australia's Labor Party lost its parliamentary majority in national elections last weekend, while the more-conservative Liberal/National coalition, which has promised to cut spending, gained seats. One party or the other will likely form a coalition government.

Still, Owens and colleagues are hopeful that politicians in both parties will recognize the opportunity. "This project has the ability to capture people's imagination," she says. Time is short: The Australians have only a year or so to claim their prize before LIGO researchers start installing the hardware at Hanford.

–ADRIAN CHO

CREDITS (TOP TO BOTTOM): *REPORT OF THE COMMITTEE TO COMPARE THE SCIENTIFIC CASES FOR AHLV AND HHLV*, R. WEISS ET AL.; (PHOTO) NSF/LIGO

Downloaded from www.sciencemag.org on August 26, 2010

Published by AAAS

CELL BIOLOGY

To Scientists' Dismay, Mixed-Up Cell Lines Strike Again

Call it the case of the cells that grew too much. Over the past 5 years, a handful of research teams have raised concerns about ongoing attempts to transplant mesenchymal stem cells (MSCs), stem cells found in bone marrow and muscle, into people with heart disease and other conditions. The groups had found that MSCs could become cancerlike after growing for months in the lab. But three of these research teams have now discovered that the cancerlike cells they spotted are unrelated to the original MSCs. In each case, tumor cells that the researchers were using for other projects had contaminated the MSCs and, because they grow faster than the stem cells, ultimately took over the cell culture.

The discovery of these contaminations prompted the retraction this month of one paper and the correction of another. "It's not a good feeling," says Rolf Bjerkvig, a cell biologist at the University of Bergen in Norway who led one of the teams deceived by stray cancer cells. "First you are in shock. Then you have to cope with it."

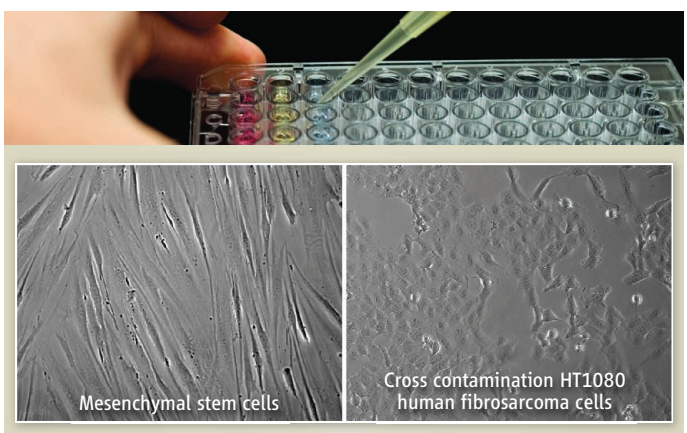

Suspicious scene. Researchers in Norway thought that mesenchymal stem cells (*bottom left*) in their lab had turned cancerous. Months after publishing a paper, they discovered that the tumor cells (*bottom right*) were the result of contamination.

The news has left stem cell scientists uncertain about whether MSC therapy poses a cancer risk. It's also reinvigorated calls for scientists to take safeguards against cell line contamination—an issue that has vexed biologists for decades (*Science*, 16 February 2007, p. 928)—and for journals to require that cell lines be validated as a condition of publication.

The problem of misidentified cells, say cell banking experts and researchers who have learned the hard way, has a simple solution: DNA fingerprinting. The same technology that can help solve murder or rape cases can easily and cheaply prevent months or even years of wasted work, says Wilhelm Dirks of the German Collection of Microorganisms and Cell Cultures (DSMZ) in Braunschweig, Germany.

Yet journals and funding agencies have resisted pleas by many scientists to require DNA fingerprinting of cell lines. Dirks is now part of a panel that is in the final stages of writing standards to guide researchers in using a type of DNA fingerprinting called short tandem repeat (STR) profiling to identify human cell lines. He and his colleagues hope the standards, which were commissioned by the cell repository ATCC in Manassas, Virginia, will raise awareness of cell misidentification and help make it standard practice for labs to check their cell lines regularly for cross-contamination.

Like many of the previous cases of spurious cells, the new MSC examples involve tumor cells. In 2005, J. García-Castro, now at the Instituto de Salud Carlos III in Madrid, and his colleagues reported in *Cancer Research* that MSCs growing in their lab spontaneously turned tumorlike. But during several years of attempting to determine what triggered the transformation, the researchers never saw a similar event. Finally, the group used STR analysis to characterize the transformed cells and the MSC. They didn't match. Instead, the transformed cells are very similar to a sarcoma tumor cell line called HT1080, García-Castro and his co-authors reported in May. They retracted the original paper on 15 August.

Bjerkvig and his colleagues had a remarkably similar experience. Several years ago, they thought they observed the spontaneous transformation of MSCs into cancerlike cells. When Bjerkvig learned that German scientists had seen the same thing in their lab, the two groups cooperated on a paper, published last year in *Cancer Research*.

But a few months after the publication, Bjerkvig says, his lab subjected all their cell lines to DNA fingerprinting and found that the transformed cells failed to match the MSCs. Instead, they fit the DNA profile of HT1080 as well as a cell line called U-2 OS. They alerted their German colleagues, whose "transformed" cells turned out to be glioma cell lines called U251 and U373. The teams reported their discovery online 14 July in *Cancer Research*.

Bjerkvig and García-Castro now both urge research groups to test their cell lines' identities early and often. Unfortunately, says Dirks, despite 50 years of warnings about cell line contamination, very few groups do so, and the problem is still widespread. For example, he says, there have been more than 1000 papers published using a cell line called ECV304, which was originally thought to be normal endothelial cells that had spontaneously immortalized in lab culture. But in 1999, Dirks and several colleagues showed that the cells were in fact another cell line derived from a human bladder carcinoma. And yet, nearly 80 papers published in 2008 still referred to ECV304 as normal endothelial cells, Dirks and his colleague Roderick MacLeod found.

They and two dozen colleagues on ATCC's panel hope that their newly developed standards will be "the beginning of the end" of cell line misidentification. The document and an accompanying database will provide validated DNA profiles for known cell lines as well as guidelines for interpreting STR assays. "It should be the bible for DNA fingerprinting," says Liz Kerrigan of ATCC. The database, hosted by the National Center for Biotechnology Information in Bethesda, Maryland, will also allow scientists to add STR profiles from new lines derived in their labs, Kerrigan says. Expense is no excuse, Dirks says; a full STR analysis costs less than $200. Already, several online databases make it possible for scientists to compare the DNA fingerprints of cells in their labs with those of cell lines in cell banks around the world. Dirks says use of DSMZ's database has been growing steadily since it went online last year.

As for scientists using MSCs, the question of whether transplants of the cells pose a cancer risk remains unsettled. Bjerkvig notes that a handful of other groups have published evidence that the stem cells can turn cancerous, but their papers also lack STR profiling to rule out contamination. **–GRETCHEN VOGEL**

CREDITS (TOP TO BOTTOM): © ISTOCKPHOTO.COM/RON KLOBERDANZ; ANJA TORSVIK AND ANDERS MOLVEN/UNIVERSITY OF BERGEN, NORWAY

Downloaded from www.sciencemag.org on August 26, 2010

Published by AAAS

ScienceNOW

From *Science*'s Online Daily News Site

Martian Volcano Mud May Have Hosted Life

They're not exactly prime real estate, but Martians may have called them home. The craterlike features in this image, taken by NASA's Mars Reconnaissance Orbiter, are not from comet or asteroid impacts. They're small volcanic cones about 250 meters wide, thousands of which dot a northern lowlands region of the Red Planet called Acidalia Planitia.

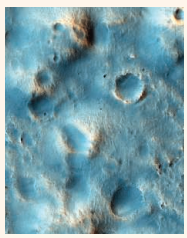

Scientists analyzing the cones have concluded that their centers are filled with sediments that once harbored water. The muddy layers were ejected from deep under the surface possibly billions of years ago. If so, the team reports in this month's issue of the journal *Icarus*, the mud could have contained enough organic materials to support primitive forms of life. Even if the sediments turn out to be lifeless, they could reveal more about the planet's chemical and geological history. http://bit.ly/mars-mud

Zombies Thrived on Ancient Earth

Zombies have roamed Earth for at least 48 million years. Zombie ants, that is. Today, *Ophiocordyceps* **fungi** are well known for taking over the minds of ants such as the *Camponotus leonardi* worker pictured above. Once infected, an ant wanders away from its colony, bites down on a leaf vein near the forest floor, and dies—creating ideal conditions for the fungal fruiting body that sprouts from its corpse. Only parasitized ants perform this routine, and the bite marks they leave are so distinctive that they're recognizable even in fossil foliage, researchers report in *Biology Letters.* The ancient leaf pictured bears 29 scars that represent the last acts of up to seven ants, probably close relatives of the modern *Camponotus zombies.* That makes the leaf the first known fossil evidence of zombie behavior in any animal. http://bit.ly/zombie-ant

Hair Follicles Track the Body's Clock

Those red-eye flights and all nighters may be leaving their mark in your hair. Researchers have found that hair follicles contain a signature of the 24-hour circadian clock that sets our sleeping habits. The finding could provide a painless way to monitor patients with sleep disorders or study health problems in shift workers.

Makoto Akashi of Yamaguchi University in Japan and his colleagues disrupted the sleep-wake cycle of healthy volunteers until, after 3 weeks, they were waking up about 4 hours later than normal. Then they checked how the disruption affected the activity of the volunteers' circadian clock genes. Rather than draw blood or take skin samples several times a day, the team examined RNA from the cell-rich follicles of hairs plucked from scalps or beards. The activity of the hair follicles' circadian genes had shifted along with the sleep patterns—but only by about 2½ hours, the team reports in the *Proceedings of the National Academy of Sciences*.

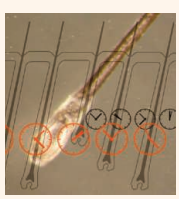

Akashi's group saw a similar lag of about 5 hours in shift workers who switched from the morning shift to the evening shift and back over 3 weeks, indicating that that wasn't enough time for their body clocks to adjust to the new schedules. http://bit.ly/hair-sleep

Bacteria Are Gobbling Gulf Oil

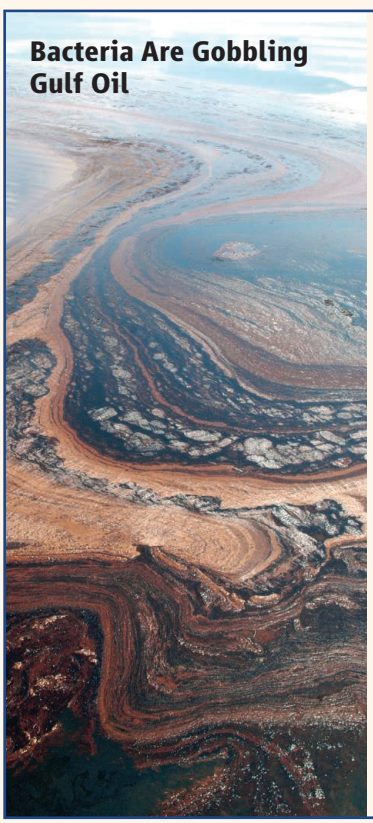

Last week, oceanographer Richard Camilli and colleagues at the Woods Hole Oceanographic Institution in Massachusetts sounded a cautionary note on the gulf oil spill: They reported in *Science* that measurements of oxygen dissolved in seawater indicated that microbes had not appreciably degraded the oil during its first 5 days out of BP's blown well (http://bit.ly/camilli). Now a new study offers some reassurance: The bugs are flocking to the remaining crude in droves, though it's not clear how quickly they're digesting it.

Microbiologist Terry Hazen of the University of California, Berkeley, and colleagues pulled samples of seawater from a plume 1100 meters beneath the surface and the uncontaminated area surrounding it. Microbes were more than twice as dense inside the plume as outside it; what's more, genes specifically geared to degrade hydrocarbons were more common in the plume, the team reports online in *Science*. The team estimates that the bugs could cut concentrations of one type of hydrocarbon, alkanes, in half within a week.

But oil is made up of dozens of other hydrocarbons as well, other researchers point out, and it's unclear how long they'll remain. http://bit.ly/t-hazen

Read the full postings, comments, and more at **news.sciencemag.org/sciencenow**.

CREDITS: (TOP, LEFT TO RIGHT) NASA/JPL/UNIVERSITY OF ARIZONA; TORSTEN WAPPLER; DAVID HUGHES; (BOTTOM, LEFT TO RIGHT) ARNE-R. DIERCKS/NIUST/NOAA; NATSUKI KIMURA

Downloaded from www.sciencemag.org on August 26, 2010

Published by AAAS

CHEMISTRY

Organizers Panned for Omitting Israelis From Meeting in Jordan

Political tensions between Israel and the Arab world are threatening to overshadow an upcoming chemistry conference in Jordan. The verbal sparring has already created plenty of raw feelings and led to much finger-pointing.

Local organizers for the 11th Eurasia Conference on Chemical Sciences aren't saying why they didn't invite any speakers from Israel, which borders Jordan and has the region's largest chemical research enterprise. But one Israeli scientist calls the snub "intentional," and few, if any, have registered for the conference. Roald Hoffmann, a chemistry Nobel laureate at Cornell University who was among the more than 100 chemists invited to speak at the meeting, is outraged at what he views as an encroachment of politics into science. He's asked fellow invited speakers to boycott the meeting unless the organizers invite Israelis. Conference organizers, in turn, say it is Hoffmann who's playing politics and that they won't be bullied into revising their plans.

Begun in 1988, the conference gives young scientists in developing countries a chance to rub elbows with world-class researchers. Israeli scientists have been speakers and participants at previous meetings, which are held every 2 years in developing countries throughout Asia and the Middle East. The 2008 meeting in the Philippines, for example, featured a plenary talk by Aaron Ciechanover, a Nobel laureate at the Israel Institute of Technology in Haifa.

Not this year. After accepting an invitation to speak at the meeting, Hoffmann was asked to help organize a workshop to run concurrent with the 6 to 10 October conference. He and fellow chemistry Nobelist and workshop organizer Dudley Herschbach discovered that none of the workshop participants was from Israel and asked conference organizers to reach out to Israeli students. Then they learned that the workshop had been canceled.

"That's when I became suspicious," says Hoffmann, who calls the absence of Israeli invited speakers at the main conference "preposterous." He tried a back-channel effort, which failed. That's when he called for a boycott.

Other chemists from Israel and elsewhere agree that the absence of Israelis on the list of invited speakers is glaring, given their regional prominence. "To ignore Israel is something very visible," says Ehud Keinan, president of the Israel Chemical Society and a chemist at the Israel Institute of Technology.

In response to Hoffmann's concerns, the chair of the conference's national organizing committee, Musa Nazer, e-mailed the invited speakers to explain that they were chosen not by nationality but "based on nominations and consultations with eminent chemists, topics of the conference, available slots in the program," and other criteria. It was too late to make changes in the lineup, he added. "We wish to emphasize that inviting speakers at the present stage under pressure and threat does not enhance a positive atmosphere for this conference or any conference of this caliber," the letter concludes.

Hoffmann isn't just urging a speaker boycott. He also wants the International Union of Pure and Applied Chemistry (IUPAC) to withdraw its support. Joshua Jortner, former president of the Israel Academy of Sciences and Humanities, has asked IUPAC to investi-

U.S. SCIENCE POLICY

NSF Turns Math Earmark on Its Ear to Fund New Institute

When Congress tells a federal agency to spend money on a particular project not in its budget request—a process called earmarking—the agency generally has little choice but to comply (*Science*, 20 August, p. 892). The National Science Foundation (NSF), however, has quietly folded one recent earmark into a competitive grants program, eliminating what seemed to be one state's advantage. Even more surprisingly, NSF apparently has done it without incurring the wrath of that state's senior legislator: Majority Leader Harry Reid (D–NV), the most powerful member of the U.S. Senate.

Counted out. Majority Leader Harry Reid fell short in his attempt to obtain a new math institute for Nevada.

CREDIT: U.S. SENATE

In March 2009, Reid inserted language into a spending bill that gave NSF $3 million "to establish a mathematical institute devoted to the identification and development of mathematical talent and to advance mathematical topics critical to the national interest" (*Science*, 20 March 2009, p. 1548). Reid wanted to build upon the work of the Davidson Academy, a one-of-a-kind public school for exceptionally gifted middle- and high school–aged students on the campus of the University of Nevada, Reno.

Coincidentally, NSF's Division of Mathematical Sciences (DMS) had just put out a solicitation for a new round of funding for its biggest single program, a network of seven mathematics institutes at universities around the country (mathinstitutes.org). Rather than simply complying with Reid's directive, it added his earmark to the $20 million set aside for the new competition.

The solicitation attracted proposals from the four existing institutes—at the University of California, Berkeley, UCLA, University of Minnesota, and Ohio State University—whose funding was about to expire, along with various newcomers. Among the latter was a team of educational psychologists from the University of Iowa, Johns Hopkins University, and the Davidson Institute for Talent Development in Reno. The group proposed an institute to serve the tiny population of "profoundly gifted" precollege students that Reid had in mind.

This month, NSF announced the results of the competition: The four incumbents won a new round of funding, and a fifth institute, the Institute for Computational

Downloaded from www.sciencemag.org on August 26, 2010

Published by AAAS

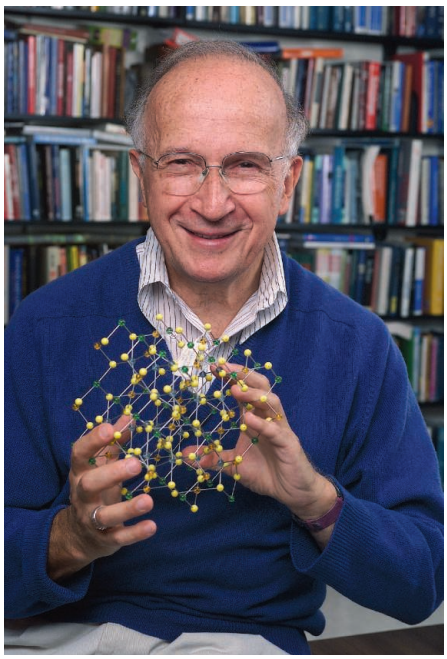

No-show. Roald Hoffmann says the lack of Israeli speakers is "preposterous."

gate the issue and to push for the inclusion of Israelis among the featured speakers.

That's not going to happen, according to IUPAC President Nicole Moreau. In a letter to Hoffmann, Moreau says she is not considering withdrawing IUPAC sponsorship for the conference. The choice of invited speakers is not among the list of criteria for IUPAC's sponsorship of a conference, she says, and withdrawing support based on the exclusion of speakers from a particular country would set an unwelcome precedent.

Jortner, also a former president of IUPAC, says he's disappointed by the response. He notes that the United Nations Educational, Scientific and Cultural Organization pulled its sponsorship from a 2008 geological sciences meeting in Jordan following similar complaints. "I strongly feel the same attitude must be applied right now," Jortner says.

Others are looking for a way to defuse the tension. "I don't want to inflate this episode to levels where [the damage] would be irreversible," Keinan says. In fact, last week Keinan sent a letter to the approximately 1000 chemical society members encouraging them to consider attending the meeting.

"It's extremely frustrating for everybody," says Bernd Rode, one of the conference's founders and a chemist at the University of Innsbruck, Austria. Even if nothing changes before the meeting, Rode says, conference organizers will hold a panel discussion to allow participants to discuss the issue thoroughly.

–ROBERT F. SERVICE

and Experimental Research in Mathematics (ICERM), will be created at Brown University. ICERM's director, mathematician Jill Pipher, says the 5-year, $15.5 million award will allow researchers to "integrate math and computation" by fostering collaborations aimed at developing advanced search tools that tackle problems in fields such as health care and national security.

What happened to Reid's idea of an institute for math prodigies? Although many of the existing institutes work with elementary and secondary school students and teachers, those activities generally are not supported by their grant. Nor will they be the focus of the Brown institute. "DMS wants to fund mathematical research, starting at the undergraduate level, and that's the core mission for us," says Pipher, an expert in cryptography. "At the same time, the interaction of mathematics and computers has the potential to attract young people."

Although the Brown institute will cater to professional scientists and mathematicians, NSF officials believe that they have fully addressed the second part of Reid's request to create a math institute that addresses critical national interests. "We feel that the Brown proposal satisfies that language," says the division's deputy director, Deborah Lockhart.

NSF's decision appears to be okay with Reid. "Although Sen. Reid included language in the 2009 Appropriations bill encouraging the NSF to provide more opportunities for gifted students," his Nevada press secretary, Tom Brede, e-mailed *Science* after the Brown institute was announced on 5 August, "the decision to award grants was made by a peer-review panel. He is pleased that the NSF was able to expand the number of mathematics research institutes."

Iowa's Susan Assouline is disappointed but not surprised by NSF's decision. "They weren't interested in thinking outside the box," she says about NSF's reviewers. "We were a university-based project that would be serving K-12 students. That was a hard concept to get across." Assouline says her team has obtained other funding to continue its work with this special population and has no plans to approach NSF again.

–JEFFREY MERVIS

CREDIT: GARY HODGES

*Science*Insider

From the *Science* Policy Blog

As this issue of *Science* went to press, a court decision earlier this week **temporarily blocking federal funding** for work with human embryonic stem cells (hESCs) has left some researchers working with the cells facing a cutoff of funding.

U.S. District Judge Royce Lamberth issued a temporary injunction on 23 August blocking the National Institutes of Health (NIH) from implementing its hESC guidelines. In his 15-page ruling, Lamberth said that hESC research "necessarily depends upon the destruction of a human embryo." He cited a law called the Dickey-Wicker Amendment that bars federal funding for research that destroys human embryos, saying the government cannot fund work with hESCs. The ruling came as part of a lawsuit filed by Christian groups and two doctors opposed to embryo research.

NIH Director Francis Collins said that researchers who had already received grant money this year to study hESCs could continue their 200 or so projects. But more than 60 grants in review have been pulled aside, and 22 funded investigators awaiting their annual payment in September may not receive it. http://bit.ly/StemBan

Harvard University confirmed last week that cognitive scientist Marc Hauser is on leave after having been found guilty of **eight counts of scientific misconduct**. A number of papers will have to be retracted or corrected, including one published in *Science* (7 September 2007, p. 1402) that is being reviewed. Two federal research agencies that have funded his work have launched their own investigations, as has the Department of Justice. http://bit.ly/Hauserletter

The U.S. biomedical research community is reacting with concern to a proposal from the National Institutes of Health to clamp down on **financial conflicts of interest**. In more than 170 comments, many universities, groups, and individual scientists urge NIH to limit the information requested in a proposed regulation. They also think the government should create a central public database for disclosing conflicts. http://bit.ly/conflictsNIH

For more science policy news, visit **news.sciencemag.org/scienceinsider**.

Downloaded from www.sciencemag.org on August 26, 2010

Published by AAAS

Secret no more. A new study charts Gitmo's growth from April 2003 (*inset*) to November 2004.

Google Earth Shows Clandestine Worlds

Archaeologists are using Google's eye in the sky to bring covert activities to light, from prison building at Guantánamo Bay to looting in the Middle East

THE PRISON CAMP AT THE U.S. NAVAL station in Guantánamo Bay, Cuba, has been a secretive proposition from the start. The U.S. government has never released official information on the size of the camp or the layout of its buildings. The 176 detainees still there are not permitted to speak directly to journalists.

For human-rights advocates, Gitmo is terra incognita, a place of many unknowns, and its clandestine nature and location on foreign soil have helped fuel suspicions about the treatment of detainees there. In a new study published in *World Archaeology* this week, archaeology Ph.D. student Adrian Myers of Stanford University in Palo Alto, California, strips away part of the secrecy. By analyzing a series of satellite images easily accessible on Google Earth, Myers has drawn the first independent map of Gitmo and charted its explosive growth over the past 7 years. "He has taken the archaeological eye and turned it on Google Earth images of a heavily clouded political prison," says cultural anthropologist David Price of St. Martin's University in Lacey, Washington. "And this is telling us something about what's going on at Gitmo."

Myers's analysis of the prison is one of an eclectic array of archaeological studies that use Google Earth—an inexpensive online service combining satellite images and maps—to explore concealed activities and to push the boundaries of archaeological research. Researchers are using the software to track looting on an unprecedented scale, for example, scrutinizing sites scattered across Jordan. And in war-torn Afghanistan, where ground surveys are too dangerous, Google Earth's images allow archaeologists to virtually field-walk huge swaths of terrain and survey for new sites.

Archaeologists have used satellite images since the 1980s, but the current projects would be unthinkable with expensive commercial satellite imagery, which also requires remote-sensing expertise. Google Earth doesn't work well everywhere, but in some places it is spurring archaeologists to venture into entirely new fields. The looting studies, for example, are "a great first step in raising public awareness of the problem," says archaeologist Morag Kersel of DePaul University in Chicago, Illinois, "and it shows that Google Earth can be used for a lot more than identifying your own backyard."

Online
sciencemag.org
Podcast interview with author Heather Pringle.

Concrete expansion. Gitmo exploded in size.

Myers began studying Google Earth images of Guantánamo Bay in April 2009 while gathering data for his dissertation on the archaeology of internment camps. At first, he wondered whether he would be able to see the prison, given that Google Earth gets images from private companies that are subject to laws restricting the release of images of military installations and other sensitive places. Myers expected Gitmo to be blurred out. But it wasn't. "When I navigated there," he says, "I remember saying, 'Holy crap, you can see it.' "

Myers downloaded Google Earth's high-resolution images of Gitmo taken on three dates between April 2003 and February 2008. He then loaded them into a geographical information system and identified features such as roads, guard towers, and barbed wire fences. To better interpret what he was seeing, he compared the satellite images with official ground photos of the prison and with plans he found in a leaked government report. "That was key," says Susan Wolfinbarger, a remote-sensing expert at the American Association for the Advancement of Science (which publishes *Science*). "That extra contextual information helps you to interpret it."

By comparing the dated satellite images, Myers traced the prison's evolution. Initially, the government built temporary plywood barracks surrounded by chain-link

CREDITS (TOP TO BOTTOM): GOOGLE EARTH 2010; (INSET) GOOGLE EARTH/DIGITALGLOBE/EUROPA TECHNOLOGIES 2010; U.S. DEPARTMENT OF DEFENSE 2006

Downloaded from www.sciencemag.org on August 26, 2010

Published by AAAS

fences. But as the war dragged on, it built a more permanent facility, Camp Delta, that contained structures closely resembling concrete supermaximum-security prisons. It also significantly expanded Gitmo. Over a 5-year period beginning in April 2003, the number of prison structures soared by nearly 40%; floor space expanded from 42,920 to 61,558 square meters, an increase of about 40%.

Myers thinks the makeshift prison in 2003 reveals how the U.S. military was caught off-guard by the war on terror, capturing suspects before it had prepared a prison, and that the later building boom signaled an intention to hold prisoners for a long period. Given the many questions that human-rights groups have raised about the covert prison over the years, adds Wolfinbarger, it's somewhat surprising that an archaeologist was the first to map it: "I can't believe that someone in geography didn't think to do this." (A Pentagon spokesperson declined to comment on Myers's study and said she could not confirm that the images were of Gitmo.)

Myers argues that his study serves the public interest by creating an independent record that cannot be erased later. "These kinds of prison camps disappear really quickly when their use is up," he says. "After the Second World War, the American government tried to strip away and bulldoze the Japanese-American internment camps."

He notes, however, that using Google Earth images raises ethical issues. Google Inc. does not ask landowners for permission to post online satellite images of their property, including military bases. That policy could potentially violate privacy rights or jeopardize national security.

Google says it isn't revealing anything that it shouldn't. By law, the United States government can exert shutter control over all commercial remote sensing carried out by U.S. companies, including the ones that supply images to Google. "The government could block or alter the images if it wanted to, but it chooses not to," says Google spokesperson Kate Hurowitz.

While Myers uses Google Earth to examine a secretive prison, others are using the technology to peer into another covert world: the illegal trade in antiquities. Archaeologists have long lacked hard data on the extent and intensity of looting worldwide, which they say makes it more difficult to persuade policymakers to take action. And in the past, attention has often focused on the plundering of single artifacts such as the Euphronios Krater, a finely painted bowl looted from an Etruscan tomb.

Noting an abundance of Jordanian antiquities in British shops, archaeologist Daniel Contreras of Stanford University and independent archaeologist Neil Brodie wanted to quantify the extent of looting in Jordan. They calculated that using commercial satellite imagery would require between $0.9 million and $2.5 million, plus considerable remote-sensing expertise. They lacked both, so they settled on Google Earth, which has imagery only in visible wavelengths but is cheap and comes with map coordinates. They found that much of Jordan was covered by high-resolution images, representing less than 1 meter per pixel.

Looting's big picture. Google Earth images revealed the extent of looters' pits (outlined in red) in Jordan.

The pair located known sites on the images by importing a digital archaeological atlas into the $400 Google Earth Pro software. Then they looked at ancient cemeteries and sites near roads for telltale traces of pitting. They found 25 heavily looted sites, calculated their area, and ground-truthed the results by visiting 16 sites.

In all, they determined that 51 hectares of Jordan's known archaeological sites had been destroyed by looters as of 2007. Their report this year in the *Journal of Field Archaeology* is the first "really graphic, quantitative data on the scale of looting there," says Brodie. Since then, Contreras has used Google Earth images to measure 47 hectares of looting in one valley in Peru, as he reported in the June issue of *Antiquity*.

Contreras believes that Google Earth will help focus attention on the broader picture of looting. The new studies reveal the scale of the problem "that goes far beyond the loss of individual contexts," he says. He's now looking into the feasibility of a Google Earth crowdsourcing project, recruiting citizens to examine online images for surges in looting.

While Contreras and others scan for looters, others are using Google Earth to search for new archaeological sites. La Trobe University Ph.D. student David Thomas put in his last field season in Afghanistan in 2005; after that, security concerns and bureaucracy prevented fieldwork. But Afghanistan has a rich past, with large areas virtually unknown to archaeologists. So Thomas decided to survey the countryside with Google Earth.

He and his small team started off by analyzing imagery of 45 known medieval sites. While they were mapping a massive fortress known as Qal'a-i Hauz—the only recorded site in Afghanistan's Registan Desert—they decided to prospect for new sites to the north. Poring over images encompassing 1367 square kilometers, the team identified 451 possible new sites in the harsh desert, ranging from small burial mounds and single-family dwellings to deserted villages, reservoirs, and subterranean canals. The images were so clear and detailed, says Thomas, that "you could even tell the buildings that were mosques because they had a *mihrab* [a bulge in the western wall that contains a prayer niche] pointing toward Mecca." Their work was published in the *Aerial Archaeology Research Group News* in 2008.

Thomas's team now needs to ground-truth and date the sites. But already, he says, the project has demonstrated the importance of surveying deserts and other inhospitable regions. Although Google Earth images can't be used everywhere—the image resolution varies from place to place, and some images just show thick cloud cover—he considers them a cheap and effective way to search for sites in Afghanistan. "I think the potential is huge," he concludes. "There are 46,000 square kilometers of high-resolution Google Earth images for Afghanistan, and all we've done is look at less than 1% of that."

–HEATHER PRINGLE

Heather Pringle is a contributing editor at *Archaeology* magazine.

CREDIT: DANIEL CONTRERAS/GOOGLE EARTH 2008

Downloaded from www.sciencemag.org on August 26, 2010

Published by AAAS

INFECTIOUS DISEASE

From Pigs to People: The Emergence of a New Superbug

The discovery of a novel strain of MRSA able to jump from livestock to humans has sparked a multicountry effort to see how dangerous it might be

The first infection was puzzling, almost inexplicable. In July 2004, Andreas Voss of Radboud University Nijmegen Medical Center in the Netherlands admitted a 6-month-old girl for surgery to repair a congenital heart defect.

Because an infection with the common bacterium *Staphylococcus aureus* would pose a grave risk following heart surgery, Voss and his colleagues screened the baby girl for the microbe. They found not just *S. aureus* but also a menacing drug-resistant form known as methicillin-resistant *S. aureus* (MRSA). The physicians were flummoxed. Although MRSA has reached epidemic proportions in much of the developed world, MRSA infections are rare in the Netherlands, thanks to an aggressive "search and destroy" policy the country launched in the mid-1990s to screen for the superbug in health-care settings, where it most frequently spreads. In the Netherlands now, the biggest risk for MRSA infection is a stay in a germ-ridden foreign hospital.

But this baby girl had never left the country. "We couldn't find a single source" of exposure, Voss recalls. But there was one clue: Her parents were pig farmers.

Within weeks, a second MRSA-colonized patient appeared at the hospital: another pig farmer. Then a third: the child of a veterinarian who worked only with pigs. "It was dumb luck I would say," Voss recalls. "We had within a short time three unexpected cases that all had pig written on them."

Pigs and other livestock commonly, and generally harmlessly, harbor *S. aureus*. But except for a single report buried in the scientific literature, no one had realized that pigs or other livestock harbored MRSA, and no MRSA strain had ever been known to jump from livestock to humans. If the Dutch doctors' fears were correct, a novel strain had just gained that ability, opening up a new route for a potentially dangerous superbug to spread among humans. "Initially, we were very much afraid that this would be a major problem that could spread to the entire population," says Jan Kluytmans, a microbiologist at VU University Medical Center in Amsterdam whom Voss recruited early on to help investigate.

Index case. MRSA from pigs on Eric and Ine van den Heuvel's farm was detected in their daughter, Eveline, when she was an infant.

In recent months, the dangers of livestock-associated MRSA have been played up in controversial media reports, including a special series by *CBS Evening News*, as a consequence of the livestock industry's indiscriminate use of medically important antibiotics to fatten livestock. Such uses can lead *S. aureus* and other bacteria to swap whole sets of resistance genes, potentially transferring resistance to antibiotics like methicillin that haven't even been used in agriculture.

Such awareness has fueled a push to restrict this long-debated use of antibiotics; this summer, the U.S. Food and Drug Administration has proposed to phase it out. Industry is opposed, saying the risk is negligible. Both sides are using the emergence of this new superbug to bolster their cases.

So far, the worst fears about the strain have not been realized. It did jump from pigs to people, scientists determined through gumshoe detective work. And it has caused serious disease—although rarely—among farmers and veterinarians who work with pigs and other livestock, and their families, although most of them carry the microbe harmlessly in their noses. But it doesn't appear to be readily transmissible between humans, so the chance of a broad community epidemic seems low.

However, MRSA readily mixes and matches genes with other bacteria that make it more virulent, more transmissible, and harder to treat—and this newly emerged strain could take that route too. "Is it something to worry about? Absolutely," says infectious-disease specialist Vance Fowler of Duke University Medical Center in Durham, North Carolina.

At risk. Pigs in confinement barns can harbor MRSA. A few farm families have contracted dangerous infections.

A growing menace

MRSA appeared first in hospitals, where medical procedures can ferry bugs into the unprotected interior of the body and patients are particularly vulnerable to infection. Until the 1990s, it posed only a mild threat, and the vast majority of *S. aureus* infections remained sensitive to methicillin. But since then, MRSA strains have increasingly displaced sensitive *S. aureus* strains and acquired resistance to other antibiotics, making hospital infections far more dangerous (*Science*, 18 July 2008, p. 356). Today, *S. aureus* accounts for about 20% of all hospital bloodstream infections in the United States, and 65% of the *S. aureus* infections in intensive-care units resist methicillin, among other antibiotics. MRSA killed approximately 18,650 Americans in 2005, researchers from the U.S. Centers for Disease Control and Prevention (CDC) reported in *The Journal of the American Medical Association* in 2007, a higher death toll than that of HIV/AIDS.

For years, the most dangerous strain of MRSA remained inside hospitals. Some strains began to circulate in the wider com-

Downloaded from www.sciencemag.org on August 26, 2010

CREDITS (TOP TO BOTTOM): MARIEKE VAN DEN HEUVEL; GLEN STUBBE/LANDOV

Published by AAAS

munity, mostly among people in tight spaces such as prisons, and those with a lot of skin contact, such as family members and participants in contact sports. They were largely considered a nuisance, far less dangerous than hospital-acquired infections, mostly because they infected healthy people whose skin and immune defenses kept them from infiltrating the body, and they were easier to stop with antibiotics.

Since the 1990s, however, community-acquired MRSA has grown more menacing, picking up genes that make it more virulent and resistant to an increasing variety of antibiotics. Most life-threatening infections still occur in hospitalized patients or those who have undergone outpatient treatments such as dialysis or surgery. But each year in the United States, community-acquired MRSA causes about 13,000 infections serious enough to require hospitalization and more than 1400 deaths, according to the 2007 CDC report. What's more, the lines between hospital-associated and community-associated strains are blurring, as strains formerly limited to the hospital have begun colonizing healthy people, and strains once limited to the community now sicken many patients in hospitals.

So when the livestock-associated strain showed up in people, public experts had no idea how risky it might be or become.

A peculiar strain

The three isolates from the Nijmegen hospital turned out to be from a single strain, which researchers now call ST398.

With permission from the young patient's father, Voss's team cultured bacteria from pigs on his farm and did a quick and dirty test on him and 25 of his pig-farming colleagues. Within 2 months of the girl's admission, they'd learned that one in four was asymptomatically carrying MRSA, compared with just 0.03% of the general Dutch population. Although crude, the analysis provided pretty strong evidence that the bug had come from pigs.

To confirm that route of transmission, Kluytmans and Voss did a case-control study that examined years' worth of MRSA infection data housed at the Dutch national microbial reference center. In 2007, they reported in *Emerging Infectious Diseases* that those who carried ST398 were 12 times more likely to be pig farmers than nonfarmers and that almost all the MRSA from farmers belonged to strain ST398. Cattle farmers were also 20 times more likely to carry the strain. The strain has since turned up in chickens, horses, dogs, and cats, posing a potential but poorly understood threat to humans.

Soon scientists in two other European pig-farming hot spots, Denmark and Germany, began finding the strain in their backyards. And in 2008, medical microbiologist Robert Skov of the Statens Serum Institut in Copenhagen reported a case-control study in *Emerging Infectious Diseases* that showed that the strain had spread in Denmark and was clearly linked to pig farming there as well.

No one knew then how virulent the strain was, but some of the data were and remain concerning. Case reports continue to appear of MRSA strain ST398 causing minor skin and soft tissue infections as well as mastitis, severe wound infections, pneumonia, and even some flesh-eating disease in countries throughout Europe. To date, Voss has seen about 10 cases of severe bloodstream infections of ST398 and two ST398 infections following hip-replacement surgery.

More recently, researchers have tested how readily ST398 can spread among humans and have learned, somewhat reassuringly, that it does not spread easily beyond farms. Medical microbiologist Wolfgang Witte's team at the Robert Koch Institute in Wernigerode, Germany, tested at a school in North-Rhine Westphalia, an area of Germany where pigs are farmed intensively, figuring that if the strain spread among healthy people, it would likely show up among schoolchildren who spend each day together. The team reported last year in *PLoS ONE* that while 250 of 462 students at the school were positive for some sort of *S. aureus*, only three carried ST398 MRSA in their noses, and all three lived on pig farms.

ST398 is also spreading on farms in North America, according to a handful of recent studies. For example, last year Tara Smith of Iowa State University in Ames and colleagues reported in *PLoS ONE* that nearly half the hogs and 45% of the workers on a Midwestern hog farm were colonized with ST398. But the strain seems less menacing in North America than it is in Europe. Only one farm worker in Smith's study became ill. And microbiologist Michael Mulvey's team from Canada's National Microbiology Laboratory in Winnipeg reported in *Emerging Infectious Diseases* in April that only 0.25% of the 3687 MRSA isolates from people infected in Manitoba and Saskatchewan were strain ST398. Researchers speculate that the transatlantic difference may simply be due to the fact that ST398 got a head start in Europe, or it may face more competition in the United States and Canada from other human-adapted MRSA strains.

For New MRSA Strain, a New Distribution

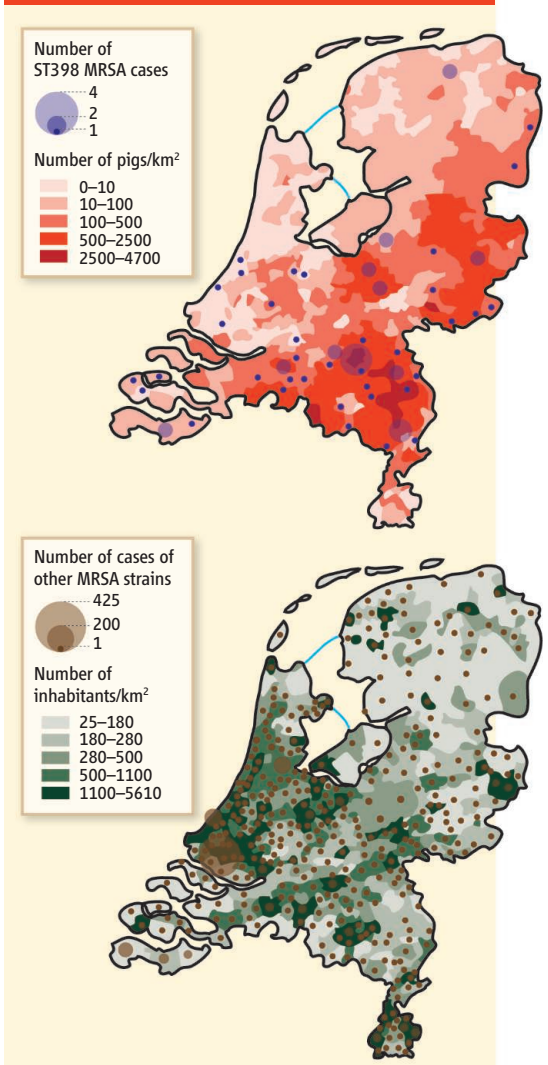

Follow the pork. In the Netherlands, rates of human infections with MRSA strain ST398 tracked with pig populations (*top*), while rates of other MRSA strains tracked with human populations (*bottom*).

Opinion is divided on whether ST398's behavior so far provides reassurance about its future conduct. Brandi Limbago of CDC, who tracks infection-causing MRSA strains in the United States, says that "for now I think it's a nonissue in this country." But others, such as Fowler of Duke, warn that it is too soon to sound the all clear. Half the swine herd in the Iowa study was carrying ST398, he points out. That's a lot of pig noses. And the strain could yet adapt and become more dangerous, just as community-acquired MRSA has done. That's why ST398 needs to be carefully monitored, says veterinary microbiologist Gail Hansen of the Pew Health Group in Washington, D.C. "Sometimes these things don't become a problem, but you don't want to take your eye off the ball." **–DAN FERBER**

CREDIT: ADAPTED FROM I. VAN LOO *ET AL.*, *EMERGING INFECTIOUS DISEASES* **13**, (DECEMBER 2007)

Downloaded from www.sciencemag.org on August 26, 2010

Published by AAAS

Illusions of the mind 1017

Modeling mantle dynamics 1020

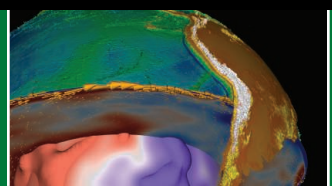

LETTERS

edited by Jennifer Sills

Dietary Restriction: Standing Up for Sirtuins

WE BELIEVE THAT L. FONTANA, L. PARTRIDGE, AND V. D. LONGO SHOULD HAVE INCLUDED A DISCUSSION of sirtuins in their Review "Extending healthy life span—From yeast to humans" (16 April, p. 321). We also believe that some of the references used are misleading.

The authors state that the purpose of their Review is to "consider the role of nutrient-sensing signaling pathways in mediating the beneficial effects of dietary restriction." Yet there was no mention of the sirtuins, a family of critically important nutrient-sensing proteins that promote health span from yeast to mammals, as shown by more than 1000 peer-reviewed publications from labs around the world. The authors state that "[i]t is unlikely that a single, linear pathway mediates the effects of dietary restriction in any organism," and we agree. Indeed, the aging field now recognizes that healthy life span is under the influence of several nutrient-sensing pathways, and there is at least as much evidence for the involvement of sirtuins in the dietary restriction response as for any of the pathways discussed in the Review (*1*).

Numerous independent studies show that dietary restriction does not extend life span when sirtuins are deleted. This result has been shown in multiple organisms, from yeast to flies and even in mice (*2*). Moreover, deleting SIRT1, SIRT3, SIRT4, or SIRT5 abrogates various physiological aspects of dietary restriction and fasting, including longevity (*3*). SIRT1 activity in mice increases during dietary restriction, and enforced SIRT1 activity results in a dietary restriction–like physiology and protection from many of the same degenerative diseases that are protected by dietary restriction in mice, including cancer, neurodegeneration, inflammatory disorders, metabolic syndrome and type 2 diabetes, and cardiovascular disease (*4*). In humans, there is also evidence that sirtuins may be involved in mediating the response to dietary restriction and increasing health span. For example, SIRT1 levels increase in humans practicing dietary restriction (*5*), and there are strong associations between alleles that increase SIRT1 expression and increased metabolic rate, as well as protection from type 2 diabetes (*6*).

Collectively, these studies provide strong support for a central role of sirtuins, as well as other nutrient-sensing proteins, as mediators of the effects of dietary restriction and the extension of healthy life span.

We also believe that the Review fails to assign due credit for major discoveries in the aging field, and not just from the sirtuin field. In some cases, credit is incorrectly attributed. For instance, the ablation of *Drosophila* germ line as it affects insulin-like peptides (dlps) and life span was performed by Flatt *et al*. (*7*). In another instance, data is selectively used to support the view that insulin signaling plays a role in dietary restriction, which is the opposite of what the original paper shows (*8*).

The Review shows dietary restriction working through insulin signaling in nematodes and flies, both of which are controversial. Studies indicate that daf-16/FoxO is not required for life-span extension by dietary restriction in nematodes (*9*) or in flies (*8*). Published data further demonstrate that dietary restriction robustly extends fly life span even when RNAi has suppressed diet-associated changes in insulin-like peptides.

JOSEPH A. BAUR,[1] DANICA CHEN,[2] EDUARDO N. CHINI,[3] KATRIN CHUA,[4] HAIM Y. COHEN,[5] RAFAEL DE CABO,[6] CHUXIA DENG,[7] STEFANIE DIMMELER,[8] DAVID GIUS,[9] LEONARD P. GUARENTE,[10]* STEPHEN L. HELFAND,[11] SHIN-ICHIRO IMAI,[12] HIROSHI ITOH,[13] TAKASHI KADOWAKI,[14] DAISUKE KOYA,[15] CHRISTIAAN LEEUWENBURGH,[16] MICHAEL MCBURNEY,[17] YO-ICHI NABESHIMA,[18] CHRISTIAN NERI,[19] PHILIPP OBERDOERFFER,[20] RICHARD G. PESTELL,[21] BLANKA ROGINA,[22] JUNICHI SADOSHIMA,[23] VITTORIO SARTORELLI,[24] MANUEL SERRANO,[25] DAVID A. SINCLAIR,[26] CLEMENS STEEGBORN,[27] MARC TATAR,[28]* HEIDI A. TISSENBAUM,[29] QIANG TONG,[30] KAZUO TSUBOTA,[31] ALEJANDRO VAQUERO,[32] ERIC VERDIN[33]

[1]Department of Physiology, University of Pennsylvania School of Medicine, Philadelphia, PA 19104, USA. [2]Department of Nutritional Science and Toxicology, University of California, Berkeley, CA 94720–3104, USA. [3]Anesthesia Research, St. Mary's Hospital, Mayo Clinic, Rochester, MN 55905, USA. [4]Department of Medicine, Stanford University, Palo Alto, CA 94305, USA. [5]The Mina and Everard Goodman Faculty of Life Sciences, Bar-Ilan University, Ramat-Gan 52900, Israel. [6]Laboratory of Experimental Gerontology, National Institute on Aging, National Institutes of Health, Baltimore, MD 21224, USA. [7]Genetics of Development and Disease Branch, National Institute of Diabetes and Digestive and Kidney Diseases/National Institutes of Health, Bethesda, MD 20892, USA. [8]Molecular Cardiology, Department of Internal Medicine III, J. W. Goethe University, 60325 Frankfurt, Germany. [9]Department of Radiation Oncology and Pediatrics, Vanderbilt University Medical Center, Nashville, TN 37232, USA. [10]Department of Biology, Massachusetts Institute of Technology, Cambridge, MA 02139, USA. [11]Department of Molecular Biology, Cell Biology and Biochemistry, Brown University, Providence, RI 02912, USA. [12]Department of Developmental Biology, Washington University School of Medicine, St. Louis, MO 63110, USA. [13]Division of Endocrinology, Metabolism and Nephrology, Keio University School of Medicine, Tokyo, Japan. [14]Department of Diabetes and Metabolic Diseases, The University of Tokyo, 160-8582 Tokyo, Japan. [15]Diabetes and Endocrinology, Kanazawa Medical University, Uchinada, Ishikawa 920-0293, Japan. [16]Department of Aging and Geriatrics, University of Florida, Gainesville, FL 32611, USA. [17]Department of Medicine and Biochemistry, Ottawa Health Research Institute, Ottawa, ON K1H 8L6, Canada. [18]Institute of Biomedical Research

Letters to the Editor

Letters (~300 words) discuss material published in *Science* in the previous 3 months or issues of general interest. They can be submitted through the Web (www.submit2science.org) or by regular mail (1200 New York Ave., NW, Washington, DC 20005, USA). Letters are not acknowledged upon receipt, nor are authors generally consulted before publication. Whether published in full or in part, letters are subject to editing for clarity and space.

CREDIT: ISTOCKPHOTO.COM

Downloaded from www.sciencemag.org on August 26, 2010

Published by AAAS

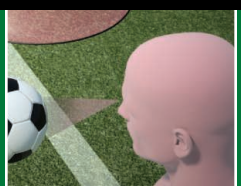

Joint decisions
1022

SPORE prize essay
1028

and Innovation Foundation for Biomedical Research and Innovation, 2-2 Minatojima-Minamimachi Chuo-ku Kobe 650-0047 Japan. [19]INSERM, Unit 894, Laboratory of Neuronal Cell Biology and Pathology, 75014 Paris, France. [20]Mouse Cancer Genetics Program, National Cancer Institute/National Institutes of Health, Frederick, MD 21702, USA. [21]Department of Cancer Biology and Medical Oncology, Kimmel Cancer Center, Thomas Jefferson University, Philadelphia, PA 19107, USA. [22]Department of Genetics and Developmental Biology, University of Connecticut Health Center, Farmington, CT 06030, USA. [23]Cardiovascular Research Institute, University of Medicine and Dentistry of New Jersey, Newark, NJ 07103, USA. [24]Laboratory of Muscle Stem Cells and Gene Regulation, National Institute of Arthritis and Musculoskeletal and Skin Diseases, National Institutes of Health, Bethesda, MD 20892, USA. [25]Spanish National Cancer Research Center (CNIO), Madrid, Spain. [26]Department of Pathology, Harvard Medical School, Boston, MA 02115, USA. [27]Department of Biochemistry, University of Bayreuth, Germany. [28]Department of Ecology and Evolutionary Biology, Brown University, Providence, RI 02912, USA. [29]Program in Gene Function and Expression, University of Massachusetts Medical School, Worcester, MA 01605, USA. [30]Baylor College of Medicine, Houston, TX 77030, USA. [31]Department of Ophthalmology, Keio University School of Medicine, Tokyo, Japan. [32]Cancer Epigenetics and Biology Program (PEBC), ICREA, and IDIBELL, L´Hospitalet de Llobregat, Barcelona, 08907, Spain. [33]Gladstone Institute of Virology and Immunology, University of California, San Francisco, San Francisco, CA 94158, USA.
*To whom correspondence should be addressed. E-mail: leng@mit.edu (L.P.G.); marc_tatar@brown.edu (M.T.)

References

1. T. Finkel *et al.*, *Nature* **460**, 587 (2009).
2. G. Boily *et al.*, *PLoS ONE* **3**, e1759 (2008).
3. S. Imai, L. Guarente, *Trends Pharmacol. Sci.* **31**, 212 (2010).
4. M. C. Haigis, D. A. Sinclair, *Annu. Rev. Pathol.* **5**, 253 (2010).
5. A. E. Civitarese *et al.*, *PLoS Med.* **4**, e76 (2007).
6. M. Lagouge *et al.*, *Cell* **127**, 1109 (2006).
7. T. Flatt *et al.*, *Proc. Natl. Acad. Sci. U.S.A.* **105**, 6368 (2008).
8. K. J. Min *et al.*, *Aging Cell* **7**, 199 (2008).
9. B. Lakowski, S. Hekimi, *Proc. Natl. Acad. Sci. U.S.A.* **95**, 13091 (1998).
10. L.P.G. and D.A.S. are co-chairs, and S.I. and E.V. are members of the scientific advisory board for Sirtris, a GSK company. D.A.S. owns shares in GSK. E.N.C. has a sponsored research agreement with Sirtris/GSK. R.d.C. has a cooperative research and development agreement with Sirtris/GSK. All other authors declare that they have no conflicts of interest.

Response

BAUR *ET AL.* QUOTE OUR STATEMENT THAT our Review aimed to "consider the role of nutrient-sensing signaling pathways in mediating the beneficial effects of dietary restriction." However, they failed to quote the next sentence: "We focus on processes that are evolutionarily conserved in multiple organisms and discuss the evidence for their potentially protective, and detrimental, effects in humans." Although much work has been published on sirtuins, and they undoubtedly play an important role in health and disease (*1*, *2*), no publications have experimentally demonstrated that altered sirtuin activity can increase mammalian life span. An extension in both median and maximum life span (defined as the mean life span of the longest-lived 10% within a cohort) in conjunction with a deceleration of many age-dependent physiological and structural changes in multiple organs and tissues is required to demonstrate that an intervention slows aging and promotes mammalian longevity (*3*). We considered it inappropriate to discuss the role of sirtuins, given that at present, their potential relevance to human aging is not proven.

We chose to cite mainly reviews or very recent work. We acknowledge authors whose relevant publications were therefore not directly cited.

LUIGI FONTANA[1,2]* AND LINDA PARTRIDGE[3]*
[1]Division of Geriatrics and Nutritional Science, Washington University School of Medicine, St. Louis, MO 63110, USA. [2]Division of Nutrition and Aging, Istituto Superiore di Sanità, 00161 Rome, Italy. [3]Institute of Healthy Aging, and Department of Genetics, Evolution, and Environment, University College London, London WC1E 6BT, UK.
*To whom correspondence should be addressed. E-mail: lfontana@dom.wustl.edu (L.F.); l.partridge@ucl.ac.uk (L.P.).

References

1. D. A. Sinclair, *Mech. Ageing Dev.* **126**, 987 (2005).
2. L. Guarente, *Cold Spring Harb. Symp. Quant. Biol.* **72**, 483 (2007).
3. K. Flurkey, J. M. Currer, D. E. Harrison, in *The Mouse in Biomedical Research Vol. III: Normative Biology, Husbandry, and Models*, J. G. Fox *et al.*, Eds. (American College of Laboratory Animal Medicine, Elsevier, Burlington, MA, ed. 2, 2007), pp. 637–672.

Response

I AGREE WITH BAUR *ET AL.* THAT DISCUSSION of sirtuins would have enhanced our Review. However, I also agree with my coauthors that it would have been difficult to integrate sirtuins sections with those on the GH/IGF-I, Tor/S6K, and AC/PKA signaling pathways, given that a straightforward and conserved functional connection between them has not been demonstrated.

The goal of the Review was not to cover all the pathways that mediate the effects of dietary restriction, but to discuss the link between dietary restriction and the pathways established to extend longevity in simple organisms and mammals. Notably, dietary restriction includes calorie restriction but also protein restriction or complete starvation. At this point, the link between sirtuins, dietary restriction, and longevity extension is far from straightforward, given that these deacetylases can play different roles depending on the type of dietary restriction. For example, *SIR2* is required for replicative life-span extension by dietary restriction in yeast, but this finding has been challenged, and *SIR2* has the opposite effect on the yeast chronological life span under starvation conditions (*1*–*4*). In worms, the role of sirtuins is also complex, given that they were shown to be required for dietary restriction–induced life-span extension (*5*) but not for the effects of starvation on longevity (*6*). In *Drosophila*, Sir2 also extends life span (*7*) but overexpression of its ortholog Sirt1 in mice improves healthy aging but does not extend longevity (*8*), and animals lacking Sirt1 have reduced GH and IGF-I levels

TECHNICAL COMMENT ABSTRACTS

Comment on "A Southern Tyrant Reptile"

Matthew C. Herne, Jay P. Nair, Steven W. Salisbury

Benson *et al*. (Brevia, 26 March 2010, p. 1613) reported on an Australian tyrannosauroid, represented by a pubis from the late Early Cretaceous of Victoria. However, our examination of this specimen reveals that the critical character used for this referral is not present. We contend that the bone likely belongs to a currently recognized group of Australian theropod or another group not currently known.

Full text at www.sciencemag.org/cgi/content/full/329/5995/1013-c

Response to Comment on "A Southern Tyrant Reptile"

Roger B. J. Benson, Paul M. Barrett, Tom H. Rich, Patricia Vickers-Rich, David Pickering, Timothy Holland

Herne *et al*. doubt our identification of tyrannosauroid pubes from the Lower Cretaceous of Australia. They suggest that the fossil is broken and can only be identified as an indeterminate neotetanuran (representing the wider clade that includes coelurosaurs such as birds and tyrannosauroids, and also more primitive large theropods, the allosauroids). However, we maintain that unique tyrannosauroid features are clearly preserved or interpretable.

Full text at www.sciencemag.org/cgi/content/full/329/5995/1013-d

Downloaded from www.sciencemag.org on August 26, 2010

Published by AAAS

(associated with life-span extension) (*9*), yet they are short-lived under both standard and dietary restriction conditions. Clearly, this is a very important and conserved enzyme that alters the level and/or activity of many proteins, including growth factors and transcription factors with the potential to affect multiple diseases of aging. The hypothesis that it is a conserved anti-aging gene and a central mediator of the effects of dietary restriction on life span independently of diseases remains valid, but further studies are required to determine whether this is true and whether the mechanisms responsible for this effect are conserved from yeast to mammals.

Regarding the role of insulin signaling in the effects of dietary restriction, I agree that it is controversial, given that continuous dietary restriction can extend life span independently of DAF-16, but DAF-2 and/or DAF-16 are implicated in the effects of several types of dietary restriction on aging. For example, some forms of dietary restriction require DAF-16 for full life-span extension (*10*) and one form (intermittent fasting) does not extend further the survival of daf-2 mutants (*11*). This is in agreement with the effect of dietary restriction in reducing IGF-I, with the inability of dietary restriction to further extend the life span of the long-lived GHR deficient mice (*9*) and with the findings that neither the deletion of transcription factors Msn2 and Msn4 (regulated by Ras/AC/PKA) nor that of Gis1 (regulated by Tor/Sch9) prevent dietary restriction from extending chronological life span in yeast, yet deletion of all three abolishes most of its anti-aging effects (see the Review). Thus, certain forms of dietary restriction may extend longevity in worms by modulating multiple pathways including DAF-2 and/or DAF-16, as proposed in Fig. 3, whereas other forms may not. Clearly, additional studies are necessary to understand the link between insulin/IGF-I signaling, different types of dietary restriction, and aging.

VALTER D. LONGO
Division of Biogerontology, Andrus Gerontology Center, University of Southern California at Los Angeles, Los Angeles, CA 90089–0191, USA. E-mail: vlongo@usc.edu

References
1. S. J. Lin, P. A. Defossez, L. Guarente, *Science* **289**, 2126 (2000).
2. M. Kaeberlein *et al.*, *PLoS Biol*. **2**, E296 (2004).
3. D. W. Lamming *et al.*, *Science* **309**, 1861 (2005).
4. P. Fabrizio *et al.*, *Cell* **123**, 655 (2005).
5. Y. Wang, H. A. Tissenbaum, *Mech. Ageing Dev*. **127**, 48 (2006).
6. G. D. Lee *et al.*, *Aging Cell* **5**, 515 (2006).
7. B. Rogina, S. L. Helfand, S. Frankel, *Science* **298**, 1745 (2002).
8. D. Herranz *et al.*, *Nat. Comm*. **2010**, 1 (2010).
9. M. S. Bonkowski, J. S. Rocha, M. M. Masternak, K. A. Al Regaiey, A. Bartke, *Proc. Natl. Acad. Sci. U.S.A.* **103**, 7901 (2006).
10. E. L. Greer, A. Brunet, *Aging Cell* **8**, 113 (2009).
11. S. Honjoh, T. Yamamoto, M. Uno, E. Nishida, *Nature* **457**, 726 (2009).

Dietary Restriction: Theory Fails to Satiate

IN THE REVIEW "EXTENDING HEALTHY LIFE span—From yeast to humans" (16 April, p. 321), L. Fontana *et al.* discuss the positive effects of dietary restriction—or to be more precise, caloric restriction—on longevity. However, these results are far from a universal phenomenon. For years, studies of many taxa have failed to observe an increase in longevity (*1*, *2*). One recent report even revealed that in 41 recombinant inbred strains of mice, caloric restriction "shortened life span in more strains than those in which it lengthened life" (*3*).

Fontana *et al.* also overlooked an alternative explanation for the alleged increase in longevity by caloric restriction. In these

FOCUS ON CAREERS

ANNUAL POSTDOC SURVEY

The Postdoc Experience

Make the most of your postdoc in today's competitive job market.

turn to page 1091

or view online at sciencecareers.org/career_magazine/business_office_features

Downloaded from www.sciencemag.org on August 26, 2010

studies, control animals are either fed as much as they want or some arbitrary lesser amount. The more accurate interpretation of caloric restriction results may be that overfeeding reduces longevity. The lifestyle of feral animals—alternating periods of feasting and famine—mimics a caloric restriction–fed animal more closely than it does an overfed animal. Consequently, caloric restriction studies have simply revealed the average greater longevity for the species under feral conditions, explained in part by the absence of pathology brought on by overeating and obesity.

LEONARD HAYFLICK
Department of Anatomy, University of California, San Francisco, The Sea Ranch, CA 95497, USA. E-mail: lenh38@aol.com

References
1. J. R. Carey *et al.*, *Aging Cell* **1**, 140 (2002).
2. T. M. Cooper *et al.*, *FASEB J.* **18**, 1591 (2004).
3. C.-Y. Liao *et al.*, *Aging Cell* **9**, 92 (2010).

Response

WE DISAGREE WITH THE HYPOTHESIS THAT dietary restriction extends life span simply by preventing diseases caused by overfeeding and obesity. First, the effect of dietary restriction on life-span extension is observed in a number of organisms that are not affected by overfeeding and cardiovascular diseases, including yeast and worms. Second, in a number of studies performed on mice, in which pathologies do affect life span, the dietary restriction group has been compared to control groups fed a limited level of calories (e.g., 85 to 95% of the calories of mice fed an unlimited amount) to avoid comparison with metabolically abnormal overweight and obese animals (*1*). Third, in many model organisms, a monotonic relationship exists between dietary restriction and longevity response (*2*, *3*). Moreover, a similar monotonic relationship between dietary restriction and cancer prevention has been observed in rodents (i.e., 15 to 53% dietary restriction caused a proportionate linear 20 to 62% reduction in tumor incidence) (*4*).

Nonetheless, the effects of dietary restriction are not homogeneous. As Hayflick pointed out, in some mouse strains a 40% dietary restriction reduces life span, and the growth of cancer cells with constitutive activation of the PI3K pathway was shown to be unaffected by dietary restriction (*5*–*7*). Thus, it will be important to identify additional mutations and polymorphisms that can mimic or block the beneficial effects of dietary restriction, because they will shed light on the mechanisms of protection induced by limited nutrients. Naturally, it would not be surprising if, as pointed out by Hayflick, many feral animals in fact consume a calorie-restricted diet which already optimizes longevity.

LUIGI FONTANA,[1,2]* LINDA PARTRIDGE,[3]* VALTER D. LONGO[4]*
[1]Division of Geriatrics and Nutritional Science, Washington University in St. Louis, MO 63110, USA. [2]Division of Nutrition and Aging, Istituto Superiore di Sanità, 00161 Rome, Italy. [3]Institute of Healthy Aging, and G.E.E., University College London, London WC1E 6BT, UK. [4]Division of Biogerontology, Andrus Gerontology Center, University of Southern California at Los Angeles, Los Angeles, CA 90089–0191, USA.
*To whom correspondence should be addressed. E-mail: lfontana@dom.wustl.edu (L.F.); l.partridge@ucl.ac.uk (L.P.); vlongo@usc.edu (V.D.L)

References
1. T. D. Pugh, R. G. Klopp, R. Weindruch, *Neurobiol. Aging* **20**, 157 (1999).
2. R. Weindruch, R. L. Walford, *The Retardation of Aging and Disease by Dietary Restriction* (Thomas, Springfield, IL, 1988).
3. E. J. Masoro, *Caloric Restriction: A Key to Understanding and Modulating Aging* (Elsevier, Amsterdam, 2002).
4. D. Albanes, *Cancer Res.* **47**, 1987 (1987).
5. C.-Y. Liao *et al.*, *Aging Cell* **9**, 92 (2010).
6. M. Ferguson *et al.*, *Exp. Gerontol.* **43**, 757 (2008).
7. N. Y. Kalaany, D. M. Sabatini, *Nature* **458**, 725 (2009).

Call for Papers

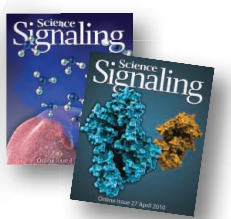

Science Signaling

Science Signaling, from the publisher of *Science*, features top-notch, peer reviewed, original research weekly. The journal is indexed in MEDLINE/PubMed.

- Biochemistry
- Bioinformatics
- Cell Biology
- Development
- Immunology
- Molecular Biology
- Neuroscience
- Pharmacology
- Physiology and Medicine

Submit your research at: www.sciencesignaling.org/about/help/research.dtl

Subscribing to ***Science Signaling*** ensures that you and your lab have the latest cell signaling resources. For more information visit **ScienceSignaling.org**

Science Signaling
AAAS

Downloaded from www.sciencemag.org on August 26, 2010

Comment on "A Southern Tyrant Reptile"

Matthew C. Herne,[1]* Jay P. Nair,[1] Steven W. Salisbury[1,2]

Benson *et al*. (Brevia, 26 March 2010, p. 1613) reported on an Australian tyrannosauroid, represented by a pubis from the late Early Cretaceous of Victoria. However, our examination of this specimen reveals that the critical character used for this referral is not present. We contend that the bone likely belongs to a currently recognized group of Australian theropod or another group not currently known.

Benson *et al*. (*1*) reported the presence of "a southern tyrant reptile"—the first tyrannosauroid theropod dinosaur from Gondwana. This finding, based on an isolated pair of fused pubic bones [National Museum of Victoria (NMV) P186046] from the Early Cretaceous of Victoria, southeastern Australia, has profound implications for tyrannosauroid evolution and paleobiogeography. According to Benson *et al*., a combination of character states of the right pubis (*2*) indicates not only placement within Tyrannosauroidea but also a close relationship with Tyrannosauridae specifically. This family of large, hypercarnivorous theropods includes such taxa as *Tyrannosaurus* and *Albertosaurus* and is otherwise known only from the Late Cretaceous of the northern hemisphere.

Central to Benson *et al*.'s (*1*) assignment of NMV P186046 is their identification of a tubercle, which, although they claim to be broken, they say once formed a "prominent, anterolaterally curving, flangelike morphology" on the proximal extremity of the pubis (i.e., the iliac peduncle) (Fig. 1A). Benson *et al*. (*1*) consider this morphology diagnostic of tyrannosaurids and dromaeosaurids following previous studies (*3*, *4*). According to Benson *et al*. [figure 1B in (*1*)], a shadowed groove on NMV P186046 represents the broken base of the pubic tubercle. When present in theropods, the pubic tubercle forms a discrete structure that projects anteriorly to anterolaterally from the iliac peduncle (*3*, *4*). This is exemplified in tyrannosaurids and dromaeosaurids, where the tubercle forms a prominent rugose anterolateral projection (*3*–*5*). The tubercle is therefore distinct from the anteriorly directed expansion of the iliac peduncle, which, typically in tetanurans, extends between the proximal pubic shaft and the iliac facet [figure S1 in (*1*)] (*6*, *7*).

Benson *et al*. [figure S1F in (*1*)] further used "flangelike" to differentiate the tubercle morphology of tyrannosaurids from the "moundlike" morphology of non-tyrannosaurids. Additionally, according to Benson *et al*., rugosity on the lateral surface of the iliac peduncle in tyrannosaurids is also coincident with the presence of a pubic tubercle. Benson *et al*. claim that the presence of such rugosity on NMV P186046 confirms the possession of a prominent tubercle before breakage [figures 1B and S1E in (*1*)]. However, neither the presence of this rugosity nor a "flangelike" to "moundlike" tubercle morphology have been used as character states in any cladistic analysis of which we are aware.

Three character states of the pubic boot were identified by Benson *et al*. (*1*) in NMV P186046: a narrowly transverse, parallel-sided pubic boot; an anteroposteriorly large pubic boot; and a lengthy anterior expansion of the pubic boot. A narrowly transverse, parallel-sided pubic boot is considered a coelurosaurian synapomorphy (*8*), as Benson *et al*. (*1*) indicate. A large pubic boot is widely distributed among neotetanurans, as is alluded to by Benson *et al*. From their estimate of boot-to-shaft ratio in NMV P186046, Benson *et al*. (*1*) indicate comparable proportions to that of tyrannosauroids, some basal coelurosaurs, and some non-coelurosaurian neotetanurans, such as *Aerosteon*. Within Tyrannosauroidea, the lengthy anterior expansion of the pubic boot in NMV P186046 is considered by Benson *et al*. (*1*) to be uniquely shared with tyrannosaurids. Outside Tyrannosauroidea, the trait also occurs in some ornithomimosaurs and oviraptorosaurs. Benson *et al*. (*1*) consider the purportedly tyrannosaurid-like pubic tubercle, lack of specific dromaeosaurid pubic characters, and unique combination of pubic character states possessed by NMV P186046 as clearly indicative of close tyrannosaurid affinities within Tyrannosauroidea.

Our firsthand examination of NMV P186046 indicates that the anteroproximal portion of the iliac peduncle is incomplete, as indicated by the exposure of internal trabecular bone (Fig. 1). We provide a reconstructed outline of the complete iliac peduncle (Fig. 1A) based on typical tetanuran morphology [figure S1, F to P, in (*1*)]. The preserved anterolateral edge of the iliac peduncle in NMV P186046 is linear, and there is no indication of a tubercle projecting anteriorly to this edge or laterally from the essentially planar lateral surface of the peduncle. Thus, contrary to Benson *et al*. (*1*), we find no conclusive evidence of discrete tubercle development in NMV P186046. Fractured surface bone is evident posterior to the anterolateral edge (Fig. 1, A and B). Reconstruction of these broken fragments to form an anterolaterally prominent tubercle, as suggested by Benson *et al*. (*1*), is speculative. Additionally, we failed to identify any rugosity on NMV P186046 in the region identified by Benson *et al*. [figures 1B and S1E in (*1*)]. To the contrary, this area consists of smooth surface bone and further proximally, partially exposed trabecular bone (Fig. 1A).

The lack of a prominent anterolaterally curving pubic tubercle on NMV P186046 undermines Benson *et al*.'s (*1*) argument that the specimen

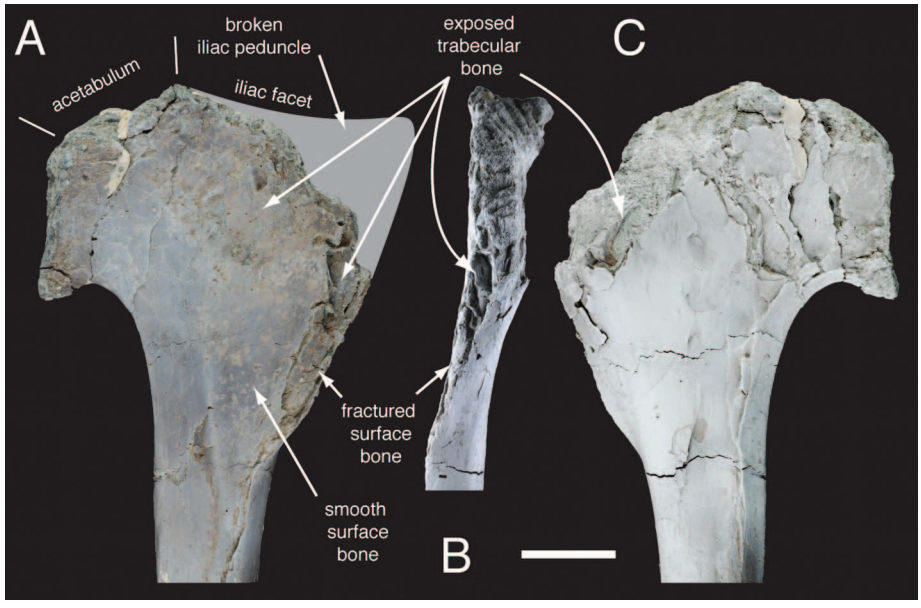

Fig. 1. Neotetanurae indet. (NMV P186046), proximal portion of the right pubis in lateral (**A**), anterior (**B**), and medial (**C**) views. The shaded area in (A) shows the reconstructed outline of the complete iliac peduncle based on typical tetanuran morphology. Scale bar, 10 mm. Images courtesy of Museum Victoria.

[1]School of Biological Sciences, University of Queensland, Brisbane, QLD 4072, Australia. [2]Vertebrate Paleontology Section, Carnegie Museum of Natural History, 4400 Forbes Avenue, Pittsburgh, PA 15213, USA.

*To whom correspondence should be addressed. E-mail: m.herne@uq.edu.au

Downloaded from www.sciencemag.org on August 26, 2010

belongs to a taxon that is closely related to tyrannosaurids. Given the presence of a transversely narrow pubic boot (*8*), we accept the possibility that NMV P186046 is referable to Coelurosauria (*1*); however, as we are uncertain of the degree of bone loss from the ventral pubic boot [in agreement with Benson *et al*. (*1*) that the pubic boot is broken], we only tentatively acknowledge this referral. Furthermore, the broader distribution among neotetanurans of the other pubic boot traits identified in NMV P186046 (*1*) indicates that a more inclusive neotetanuran placement would be more parsimonious.

Despite more than 100 years of collecting, there is no record of tyrannosauroids on any of the other southern continents. Recent reassessments of Australia's nonavian Cretaceous dinosaurs indicate affinities with faunas from other Gondwanan landmasses (*9*, *10*). Currently recognized Australian Cretaceous theropods include carcharodontosaurians (*9*, *11*) and paravian coelurosaurians (*9*), with both clades occurring in the Aptian-Albian assemblages of southern Victoria from which NMV P186046 derives. Rather than representing an aberrant occurrence of an otherwise exclusively Laurasian theropod clade, we believe it is more likely that NMV P186046 belongs to one of the aforementioned, typically Gondwanan, theropod clades, or another as yet unrecognized neotetanuran taxon. Although the occurrence of tyrannosauroids on the southern continents during the Early Cretaceous would not be incompatible with their evolutionary history (*12*), we consider the referral of NMV P186046 to Neotetanurae indet. to be more consistent with its preserved anatomy.

References and Notes

1. R. B. J. Benson, P. M. Barrett, T. H. Rich, P. Vickers-Rich, *Science* **327**, 1613 (2010).
2. NMV P186046 is preserved in three parts: an almost complete right pubic body and shaft, a partial left pubis, and a fused pubic boot. NMV P186046 is incorrectly labeled in figure 1A of (*1*) as "NMV P186069" (an ornithopod tooth).
3. M. A. Norell, P. J. Makovicky, *Am. Mus. Novit.* **3215**, 1 (1997).
4. J. R. Hutchinson, *Zool. J. Linn. Soc.* **131**, 123 (2001).
5. C. A. Brochu, *J. Vertebr. Palaeontol. Mem.* **7**, 1 (2003).
6. Z. Dong, Z. Tang, *Vertebr. Palasiat.* **23**, 77 (1985).
7. P. J. Currie, X.-C. Zhao, *Can. J. Earth Sci.* **30**, 2037 (1993).
8. O. W. M. Rauhut, *Spec. Pap. Palaeontol.* **69**, 1 (2003).
9. F. Agnolin, M. Ezcurra, D. Pais, S. W. Salisbury, *J. Syst. Paleontol.* **8**, 257 (2010).
10. N. D. Smith *et al*., *Proc. Biol. Sci.* **275**, 2085 (2008).
11. R. B. J. Benson, M. T. Carrano, S. L. Brusatte, *Naturwissenschaften* **97**, 71 (2010).
12. O. W. M. Rauhut, A. C. Milner, S. C. Moore-Fay, *Zool. J. Linn. Soc.* **158**, 155 (2010).

13. We thank K. Geddes, D. Herne, and anonymous referees for their comments. We thank the preparatory and collections staff of Museum Victoria for specimen access. Financial support was provided by the Australian Research Council (LP0776851), the University of Queensland, Carnegie Museum of Natural History and Longreach Regional Council.

26 March 2010; accepted 28 July 2010
10.1126/science.1190100

Downloaded from www.sciencemag.org on August 26, 2010

Response to Comment on "A Southern Tyrant Reptile"

Roger B. J. Benson,[1]* Paul M. Barrett,[2] Tom H. Rich,[3,4] Patricia Vickers-Rich,[3,4] David Pickering,[3] Timothy Holland[3,4]

Herne *et al*. doubt our identification of tyrannosauroid pubes from the Lower Cretaceous of Australia. They suggest that the fossil is broken and can be identified only as an indeterminate neotetanuran (representing the wider clade that includes coelurosaurs such as birds and tyrannosauroids, and also more primitive large theropods, the allosauroids). However, we maintain that unique tyrannosauroid features are clearly preserved or interpretable.

We reported an Australian tyrannosauroid, represented by a pubis from the late Early Cretaceous [National Museum of Victoria (NMV) P186046] (*1*). Herne *et al*. (*2*), however, argue that the pubic tubercle is broken and cannot provide evidence for tyrannosauroid affinities. We described the base of the broken pubic tubercle as indicative of an anterolaterally curving morphology, similar to that of tyrannosaurids (*3*) [figure 1D in (*1*)]. In NMV P186046, the broken surface of the tubercle faces laterally, and the bone surfaces on either side of the break curve anterolaterally (Fig. 1). Furthermore, the distal portion of the tubercle is preserved and projects laterally (Fig. 1). Thus, an anterolaterally directed, "flangelike" pubic tubercle was present. Although this has not been included in published phylogenetic analyses, it is absent in all non-tyrannosauroid theropods with pubes similar to NMV P186046 [figure S1 in (*1*)] and thus indicates tyrannosauroid affinities. A well-defined depression is located posterior to the pubic tubercle (Fig. 1A). Herne *et al*. (*2*) state that this depression is smooth, unlike in tyrannosaurids in which it is rugose [figure 1D in (*1*)] (*3*). However, rugosity is present proximally (Fig. 1) and is independent of irregular patches of superficial damage. A well-defined, rugose depression adjacent to the tubercle is also present in tyrannosaurids but is absent in other theropods [figure S1 in (*1*), (*3*)].

The transversely narrow pubic boot of NMV P186046 indicates placement within Coelurosauria [e.g., (*4*, *5*)], the wider clade including Tyrannosauroidea. Even the largest coelurosaur, *Tyrannosaurus*, has a narrow pubic boot, with a length-to-width ratio of 5.3 (*3*). This is similar to the ratio of 6.6 in NMV P186046, which is narrow compared with ~2.4 in non-coelurosaurian neotetanurans (allosauroids) with boots of comparable size (*6*). Herne *et al*. (*2*) suggest that NMV P186046 is incomplete distally and may have been wide before breakage. However, to be proportionally broad, as in allosauroids, NMV P186046 must have been 58 mm wide, almost three times the preserved width of 21 mm. This requires an eccentric morphology not documented in any other theropod and is therefore unlikely. Furthermore, in basal neotetanurans, the entire pubis is transversely broad [e.g., (*6*, *7*) and figure S1 in (*1*)], not just the pubic boot. NMV P186046 is slender [figure 1C in (*1*)], as in other coelurosaurs (1, *3*–*5*). Among coelurosaurs, only tyrannosaurids have a large and anteriorly expanded pubic boot similar to that of NMV P186046 [e.g., (*1*, *3*, *8*, *9*)]. Based on this observation and the morphology of the pubic tubercle, we maintain that NMV P186046 can be identified as a tyrannosauroid.

Finally, Herne *et al*. (*2*) state that because a long history of collecting has not uncovered any Gondwanan tyrannosauroids, their presence is unlikely. There are three problems with this claim. First, any hypothesis of tyrannosauroid absence should be based on evidence, not expectation. We have made the case, here and previously (*1*), that the anatomical evidence for an Australian tyrannosauroid is clear. Second, the Gondwanan dinosaur record is poorly sampled in comparison with that from Laurasia. New discoveries and more critical paleobiogeographic analyses have shown that the hypothesis of distinct "Laurasian" and "Gondwanan" dinosaur faunas during the Early Cretaceous (*10*) is too simplistic. Many "endemic" clades are now known from both hemispheres [e.g., "Gondwanan" abelisauroids (*11*) in Europe and "Laurasian" dromaeosaurids in South America (e.g., *12*)]. Third, of the Australian theropod clades cited by Herne *et al*. (*2*), only the carcharodontosaurian *Australovenator* is represented by substantially complete remains (*13*). These are of similar age to NMV P186046 and indicate that it is the sister taxon of *Fukuiraptor* from Japan (*14*). This demonstrates that closely related theropod taxa can be present in both Laurasian and Gondwanan faunas during the middle Cretaceous. Thus, the presence of Australian tyrannosauroids is not implausible and should not be rejected a priori.

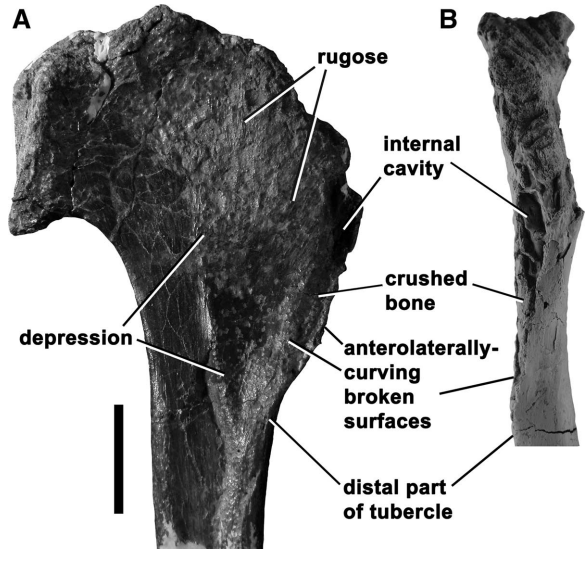

Fig. 1. Proximal end of the right pubis of NMV P186046 in lateral (**A**) and anterior (**B**) views. Scale bar, 20 mm.

References and Notes

1. R. B. J. Benson, P. M. Barrett, T. H. Rich, P. Vickers-Rich, *Science* **327**, 1613 (2010).
2. M. C. Herne, J. P. Nair, S. W. Salisbury, *Science* **329**, 1013 (2010); www.sciencemag.org/cgi/content/full/329/5995/1013-c.
3. C. A. Brochu, *Soc. Vertebr. Paleontol. Mem.* **7**, 1 (2002).
4. O. W. M. Rauhut, *Spec. Pap. Palaeontol.* **69**, 1 (2003).
5. R. B. J. Benson, *Zool. J. Linn. Soc.* **158**, 882 (2010).
6. P. C. Sereno *et al*., *PLoS ONE* **3**, e3303 (2008).
7. J. H. Madsen Jr., *Utah Geol. Min. Surv. Bull.* **109**, 3 (1976).
8. D. B. Weishampel, P. Dodson, H. Osmólska, *The Dinosauria* (Univ. of California Press, Berkeley, CA, ed. 2, 2004).
9. X. Xu *et al*., *Nature* **439**, 715 (2006).
10. J. F. Bonaparte, S. Kielan-Jaworowska, in *Fourth Symposium on Mesozoic Terrestrial Ecosystems*, P. J. Currie, E. H. Koster, Eds. (Tyrrell Museum of Palaeontology, Drumheller, AB, Canada, 1987), pp. 24–29.
11. M. T. Carrano, S. D. Sampson, *J. Syst. Palaeontol.* **6**, 183 (2008).
12. P. J. Makovicky, S. Apesteguía, F. L. Agnolín, *Nature* **437**, 1007 (2005).
13. S. A. Hocknull *et al*., *PLoS ONE* **4**, e6190 (2009).
14. R. B. J. Benson, M. T. Carrano, S. L. Brusatte, *Naturwissenschaften* **97**, 71 (2010).

12 April 2010; accepted 4 August 2010
10.1126/science.1190195

[1]Department of Earth Sciences, University of Cambridge, Cambridge CB2 3EQ, UK. [2]Department of Palaeontology, Natural History Museum, London SW7 5BD, UK. [3]Palaeontology Department, Museum Victoria, Melbourne, Victoria 3000, Australia. [4]School of Geosciences, Monash University, Clayton, Victoria 3800, Australia.

*To whom correspondence should be addressed. E-mail: rbb27@cam.ac.uk

Downloaded from www.sciencemag.org on August 26, 2010

EDUCATION

Learning from the Natural World

Mark V. Barrow Jr.

In a testy op-ed piece published in *Science* more than a century ago (*1*), the American botanist and museum curator William J. Beal asked, "What is nature study?" Beal posed the question at a time when educators across much of the United States had embraced the movement to provide elementary school students with regular firsthand exposure to the natural world. But even as millions of young schoolchildren were learning to identify local birds, observe the life cycles of insects, and cultivate school gardens, debates raged about the goals, methods, and even the very definition of the educational innovation that had come to be widely known as nature study. Was this new approach primarily an effort to introduce the rudiments of science or to cultivate a broad sympathy for the natural world? Like many of his colleagues, Beal acknowledged that the burgeoning nature study movement had accomplished much good, but he also worried that the educational activities carried out under that name relied too much on imagination and sentiment rather than reason and cold, hard scientific facts.

Sampling nature. Elementary school students collecting caterpillars to study (Louisville, Kentucky, circa 1910).

Teaching Children Science
Hands-On Nature Study in North America, 1890–1930

by Sally Gregory Kohlstedt
University of Chicago Press, Chicago, 2010. 379 pp. $45, £29. ISBN 9780226449906.

In *Teaching Children Science*, historian of science Sally Gregory Kohlstedt (University of Minnesota) offers a meticulously researched, engagingly presented, and wonderfully perceptive history of the multifaceted nature study movement. Prior to the end of the 19th century, a handful of widely scattered American educators had introduced natural history into their classrooms, but they failed to gain a lasting foothold for their curricular innovations. By the 1890s, however, progressive educational reformers increasingly challenged the hidebound curriculum that had long dominated American primary schools, a curriculum that used rote memorization and recitation to teach the venerable triumvirate of reading, writing, and arithmetic. Resonating with these calls for reform, nature study advocates called for a more hands-on, child-centered approach to primary education, one that relied on extensive interaction with the natural world to enliven a mind-numbing curriculum that tended to squelch rather than encourage children's inherent curiosity. But beyond a commitment to placing local natural objects at the center of the learning experience, the professors, teachers, and educational administrators who promoted nature study shared little else in common. Even so—or as Kohlstedt argues, perhaps because of this very diversity—nature study rapidly gained entry into America's public schools during the century's final decade.

More-or-less distinct visions for the enterprise radiated from at least three geographic centers. In Chicago, Wilbur Jackman introduced his particular approach with a pioneering text (*2*). Through this, subsequent publications, and prominent positions at the Cook County Normal School and the University of Chicago's Laboratory School, Jackman promoted a "rolling year" curriculum in which students experienced regular field trips during the warmer months of the year and completed indoor observations and experiments when cold weather made venturing outdoors less appealing and less productive. In New York City, the newly opened Teachers College of Columbia University and several normal schools in the region joined forces with the American Museum of Natural History, the New York Botanical Garden, and other local natural history institutions to promote the wide adoption of an urban-focused nature study. Maurice Bigelow, a Harvard-trained biologist and Teachers College faculty member, launched the first professional journal specifically devoted to the topic, *Nature-Study Review*, in 1905 and the American Nature-Study Society two years later. According to Kohlstedt, these events perhaps marked the "high point of the nature study movement."

At Cornell, the botanist, horticulturalist, and educator Liberty Hyde Bailey, whom Kohlstedt describes as "perhaps the most publicly recognized name in nature study," focused on rural contexts. He hoped that fostering a stronger sense of place in rural children, along with a sense of wonder about the rich natural bounty that surrounded them, would help stem a troubling out-migration from America's hinterlands. In a widely cited and frequently reprinted book (*3*), Bailey argued that "Nature study is not a science. It is not knowledge. It is not facts. It is spirit. It is concerned with the child's outlook on the world." Numerous Cornell faculty shared Bailey's vision, including Anna Botsford Comstock, who authored a leading text in the field (*4*) that remains in print to this day.

In the years following the Great War, science and technology gained in cultural authority, progressive optimism waned, and standardization and testing increasingly infiltrated America's larger school systems. In this new cultural and educational milieu, "elementary science," which included not just beginning biology but also basic chemistry and physics, triumphed over nature study. Behind the name change, however, Kohlstedt sees much continuity: "A legacy of window boxes, school gardens, nature walks, classroom terrariums, and hamster cages—whether designated 'nature study' or not—remained as evidence of the significant classroom innovation that had occurred in just one generation." At the same time, nature study continued to infuse the informal educational experiences offered through scouting programs, Audubon societies, summer camps, and state and national parks.

A definitive history of the American nature study movement, *Teaching Children Science* will appeal not only to historians of science, education, and the environment but also to environmental educators of all persuasions, who continue to struggle with the tension inherent in trying to inculcate students with both a sympathy for and a scientifically

The reviewer is at the Department of History, Virginia Tech, Blacksburg, VA 24061, USA. E-mail: barrow@vt.edu

CREDIT: *NATURE-STUDY REVIEW* 6, 220 (1910)

Downloaded from www.sciencemag.org on August 27, 2010

Published by AAAS

informed understanding of the natural world. In the current era of increasing environmental peril, it is more imperative than ever that we strike the right balance here.

References

1. W. J. Beal, *Science* **15**, 991 (1902).
2. W. S. Jackman, *Nature Study for the Common Schools* (Holt, New York, 1891).
3. L. H. Bailey, *The Nature-Study Idea: Being an Interpretation of the New School-Movement to Put the Child in Sympathy with Nature* (Doubleday, Page, New York, 1903).
4. A. B. Comstock, *Handbook of Nature-Study for Teachers and Parents, Based on the Cornell Nature-Study Leaflets, with Much Additional Material and Many New Illustrations* (Comstock, Ithaca, NY, 1911).

10.1126/science.1192566

PSYCHOLOGY

Seeing and Thinking in the Mist

Aude Oliva

In a scene reminiscent of "Candid Camera," a disoriented "journalist" holding a map asks a pedestrian for directions while events are captured on video. As the pedestrian diligently points along the map, two "workers" carrying a large door rudely walk between the interlocutors, disrupting the face-to-face conversation. Behind the door, out of the sight of the pedestrian, one worker changes places with the journalist and proceeds to continue the conversation. Amazingly, more than half of the pedestrians who had unknowingly walked into this experiment failed to notice that they were now talking to someone new.

In *The Invisible Gorilla*, cognitive psychologists Christopher Chabris (Union College, New York) and Daniel Simons (University of Illinois) describe psychology experiments, historical facts, and interesting anecdotes that reveal the fallibility of our intuitions about what we see, remember, know, think, predict, and believe. The book explores illusions of attention, memory, confidence, knowledge, cause, and potential, which in essence work in concert and construct the mind. With each chapter, the reader's self-awareness grows as previously neglected dimensions of our everyday experience are witnessed.

The reviewer is at the Department of Brain and Cognitive Sciences, Massachusetts Institute of Technology, Cambridge, MA 02139, USA. E-mail: oliva@mit.edu

The Invisible Gorilla
And Other Ways Our Intuitions Deceive Us

by Christopher Chabris and Daniel Simons
Crown, New York, 2010. 320 pp. $27, C$32. ISBN 9780307459657.

Dating back to Ronald Rensink's 1997 demonstration of "change blindness" (*1*), many of the visual illusions described in the book have become popular teaching tools featured in countless lectures and videos. The authors' infamous gorilla experiment (*2*), now a staple in vision sciences studies, asks the participant to count the number of times a basketball passes between members of one of two distinct teams while a "gorilla" walks through the scene. Surprisingly enough, most participants miss the imposing gorilla, even though it stops to bang its chest, as they are too focused on the assigned task. I have probably ruined the effect for you, but try it on a friend.

Frequently missed. A frame from the gorilla experiment.

The gorilla illusion is an elegant demonstration of inattentional blindness, a phenomenon describing how people can miss unexpected objects that appear right where they are looking. The belief that we can see and remember more than we actually do creates an illusion of control, one that can be dangerous when talking on the phone while driving or texting while crossing a street. We are never completely in charge when we are multitasking. We have limited mental resources and the more demanding a task is, the less resources are available to catch the wandering gorillas. Our mind is faithful to one thing at a time.

Take the illusion of memory: Because the world is consistent and predictable most of the time, we rely on our past experiences to fill in the proverbial blanks of what was actually seen with what we think we saw. Failure to recall exact details can lead to continuity errors. The authors discuss the job of the script supervisor, who is supposed to ensure consistency between scenes by tracking all of their details. Do script supervisors have a superior memory? Perhaps not, but critically important details are better remembered when we have feedback about what was missed, such as a script supervisor's notes. Real life, for better or for worse, does not often provide such feedback.

Chabris and Simons explain the illusion of confidence (the tendencies to overestimate our own abilities and to confuse other people's confidence levels with their real capabilities) through tightly reasoned descriptions of tournament games, competitive reality shows, and other group decision processes. The authors describe ingenious experiments on the "confidence inflation phenomenon": individuals who all independently register low levels of confidence about an option will regardless choose that option with high confidence by simply deliberating among themselves. In addition, groups such as juries who must reach a collective decision are susceptible to arriving at the wrong conclusion because it was argued for by someone extremely confident in their logic, despite its flaws. Inflated confidence can defeat the purpose of a group meeting (to combine knowledge to arrive at the best possible decision).

The illusion of potential leads people to believe that there are mental exercises that can make them smarter, faster, prettier, or stronger. That conviction is even more inflated when merged with the illusion of knowledge, where people confuse the mere familiarity they acquired from repeated exposures to a concept with a true understanding of the process. Add the other illusions to the false beliefs and you can picture how the mind functions: the six illusions work together, one for all and all for one. Altogether, I applaud Chabris and Simons's articulate communication of the many ways our minds fail us.

What have we learned? Vision can be blind, memory egocentric, knowledge sparse, reasoning false, and thoughts doubtful. So, are our minds hoaxes? No, these illusions are the consequences of how our brains work. Most of these failures are shortcuts that our minds use to deal with the overflow of information. The danger is not that our minds work this way but that we often wrongly estimate our capabilities and limitations. By making us aware of the realm of everyday illusions, *The Invisible Gorilla* teaches us a lesson of cognitive modesty: think before you leap.

References

1. R. A. Rensink, J. K. O'Regan, J. J. Clark, *Psychol. Sci.* **8**, 368 (1997).
2. D. J. Simons, C. F. Chabris, *Perception* **28**, 1059 (1999).

10.1126/science.1192289

CREDIT: © DANIEL SIMONS/UNIVERSITY OF ILLINOIS

Downloaded from www.sciencemag.org on August 27, 2010

Published by AAAS

DISASTERS

Scenario-Building for the Deepwater Horizon Oil Spill

Interdisciplinary science-based scenarios can assist responses to the Gulf oil spill and similar environmental crises.

Gary E. Machlis[1]* and Marcia K. McNutt[2]

In May 2010, the U.S. Department of the Interior (DOI) established a Strategic Sciences Working Group (SSWG) to assess how the Deepwater Horizon (DH) oil spill may impact the ecology, economy, and people of the Gulf of Mexico (GOM). It included scientists from diverse disciplines and federal, academic, and nongovernmental organizations. The SSWG was not to conduct a scientific investigation, but to provide rapid scientific assessment of potential consequences of the spill that could provide usable knowledge to decision-makers.

Such teams are not common to formal government response efforts. Most scientific activity at early stages of the spill was tactical, e.g., documenting preimpact conditions, monitoring oil transport, assessing resource damage, and supporting technical decisions associated with oil containment. Interdisciplinary and comprehensive analyses of consequences were not integral to these tactical efforts. The SSWG was a strategic and experimental response initiated by DOI, novel to the DH spill for its combination of (i) independence from standard response structures [e.g., the Incident Command System (ICS) and Natural Resource Damage Assessment (NRDA)]; (ii) collaborative engagement of federal and nonfederal scientists; (iii) rapid scenario-building within a interdisciplinary framework; (iv) assignment of scientific uncertainties; and (v) potential application to mid- and long-term recovery. The SSWG assembled in Mobile, Alabama, within 36 hours of establishment and developed initial scenarios 23 to 28 May 2010. A full description of the methodology and scenario results is available in the group's first technical report (*1*).

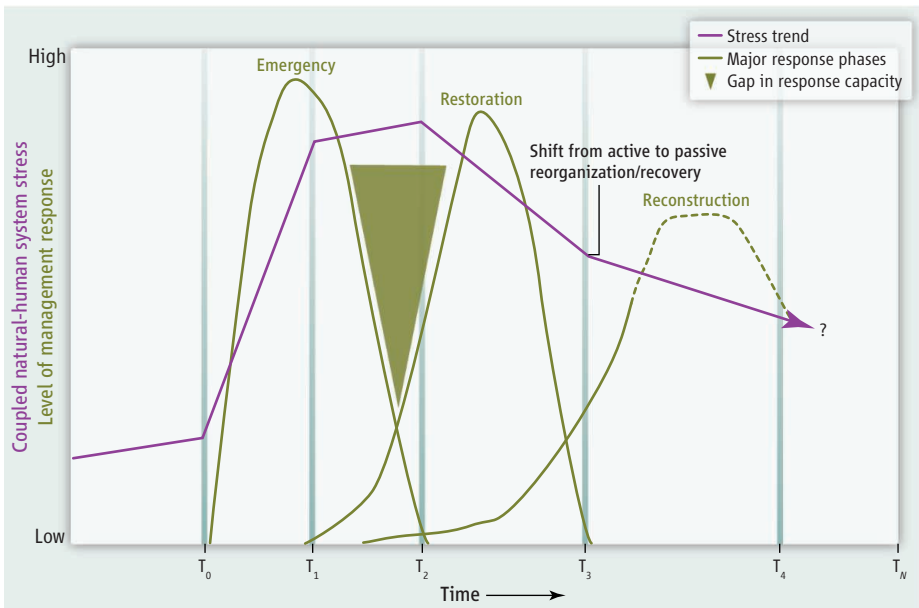

Conceptual scenario framework. This shows system stress, time horizons, major management response phases, and the potential gap in response capacity. [Adapted from (*1*)]

Organizing Framework

During major incidents such as the DH oil spill, response time is critical, conditions change rapidly, quantitative models and/or their requisite data may be unavailable, and many key factors are unknown. Scenario-building, originally developed for the military (*2*) and adapted by large-scale firms and others, offers several advantages, particularly its capacity to systematically examine possible futures and cascading consequences that are complex and uncertain (*3*, *4*). Unlike quantitative modeling or risk assessment, scenarios identify alternative futures rather than predict new-state conditions. Limitations include constraints due to available expert opinion and lack of theory (*4*).

There are numerous approaches to constructing science-based scenarios (*3*). For the oil spill, the SSWG adapted and applied a specific, coupled natural-human systems model to identify key variables (*5*) and developed a conceptual framework adapted from the natural hazards literature to reflect the DH oil spill (*6*, *7*). Scenarios were not limited to discrete physical, chemical, biological, economic, and/or sociocultural consequences but included how these consequences interact in shaping possible trajectories of the overall system.

The scenario framework (see the figure) incorporates system stress over key time horizons through recovery. Baseline stress in the GOM was treated as increasing before the DH oil spill, due to nutrient loading, expansion of the seasonal hypoxic area, wetland loss, land subsidence, invasive species, climate change, fishing pressures, effects of past hurricane damage, and national and regional economic recession (*8*–*11*). At the time of the DH explosion (T_0; 20 April 2010), system stress began to rapidly accumulate. After oil flow containment (T_1; well shut-in occurred 15 July 2010) system stress may continue to rise due to lagged effects, e.g., landfall of previously released oil and/or chronic toxicity to sensitive ecosystem components. At T_2, system stress begins to decline because of a combination of reduced inputs of stressors, resilience in the coupled natural-human system, and emergency and recovery responses. Long-term recovery (T_3, T_4, to T_N) involves some reorganization of the system rather than full return to preexisting states (*12*); future baseline stress is largely unknown. Natural variability is overlaid on general stress trends (*13*).

Building the Scenarios

The SSWG rapid assessment involved establishing a matrix of alternative scenario param-

[1]Lead scientist, Strategic Sciences Working Group, U.S. Department of the Interior, and science advisor to the director, U.S. National Park Service, Washington, DC 20024, USA. [2]Science advisor to secretary of interior and director, U.S. Geological Survey, Washington, DC 20024, USA.

*Author for correspondence. E-mail: gary_machlis@nps.gov

Downloaded from www.sciencemag.org on August 27, 2010

Published by AAAS

eters, using parameter subsets to develop a detailed "chain of consequences," and assigning a level of uncertainty to each element in each chain. The SSWG developed four key parameters, based on expert opinion and data from ICS briefings: (i) estimated flow rate for DH oil release [5000; 12,000 to 19,000; 40,000; or 100,000 barrels (bbl)/day]; (ii) estimated time to containment of the oil release (40, 100, or 160 days); (iii) time horizons (T_1 to T_4, and T_N); and (iv) geographic and spatial units of interest (vertical life zones, major ecosystem types, sociopolitical and administrative units, and GOM biodiversity quadrants) (*14*–*17*). This approach allowed for adaptation to new information, such as revised flow-rate estimates or oil landfall data. Beginning with specific scenario parameters, group members examined variables in the coupled natural-human system model, developed chains of consequences, and integrated these into an overall scenario. Online literature searches and input from additional subject-matter experts were also used. The SSWG applied a scale of informal scientific certainty (*18*), well-suited to scenario-building, that allows for rapid refinement as new information becomes available. The SSWG established uncertainty levels for each cascading consequence. Where opinions diverged, the precautionary principle dictated assignment of the lower level of certainty.

A Recovery Scenario

Scenario S3, constructed 27 May 2010, was requested by the DOI Mobile Incident Command. It employed estimates by the ICS Flow Rate Technical Group released that morning (other scenarios used higher flow estimates), and oil landfall patterns reported for the previous 48 hours. S3 examined time horizons for short-term and long-term recovery (T_2 to T_4), assumed 12,000 to 19,000 bbl/day oil release, and 100 days to containment. Geographic focus was the littoral zone in the northwest biodiversity quadrant of the GOM, including Louisiana and Texas. Several highlights emerged, for example: (i) Delayed mortality of wetland flora is probable and could impair fisheries recovery and resistance to hurricane damage, with cascading consequences from rerelease of sequestered oil; (ii) rerelease of sequestered oil triggered by storms and hurricanes is reasonably certain to lead to a resumption of stress in the coupled natural-human system; (iii) recovery by oysters may be slow and is likely to result in long-term displacement of some oyster harvesters; (iv) delayed stress on cultural communities, e.g., Isleños, Acadians, and United Houma [Indian] Nation, is reasonably certain; (v) institutional adjustments related to regulation and reorganization of government systems are reasonably certain.

Applications to the DH Oil Spill

The SSWG scenarios provide decision-makers with possible intervention points (e.g., when mid-water contamination reaches critical levels and/or tax revenues begin to decline). Decision-makers can focus attention on key interventions likely to reduce negative impacts (e.g., rerelease of sequestered oil) and/or increase resilience and positive recovery responses (e.g., improved monitoring or targeted income support). The scenarios reveal potential surprises that might be initially overlooked by decision-makers (e.g., fishing closures leading to rebound of previously stressed fish populations or the impact of re-introducing compromised birds into migratory bird populations). The scenarios can identify potential new monitoring needs (e.g., advanced monitoring technologies for mid-water pollution, new protocols for monitoring rerelease of sequestered oil, and/or long-term monitoring for occupational exposure or financial stress). Such advances can support ongoing inventory and monitoring programs, inform modeling efforts, help develop future NRDA protocols, and contribute to incident command training. Chains of consequences with their approximate levels of scientific uncertainty can help prioritize research and policy needs by identifying important, but not yet well understood, relations (e.g., the relation between landfall hurricanes, oiling of marshland, and ecosystem stress).

A Strategic Sciences Approach

Science is only one of many inputs into policy during a complex event such as the DH oil spill. Beyond technical problem analyses (e.g., evaluating "kill" methods for shutting the DH well), the influence of a particular scientific assessment upon policy is partial, given the range of inputs, interests, and institutions involved.

Comparison of the DH spill with other regional disruptive events may be insightful. Three response phases following Hurricane Katrina were (i) emergency, (ii) restoration, and (iii) reconstruction (*19*). Although Hurricane Katrina and the DH oil spill differ in substantial ways (e.g., high loss of life and severe infrastructure damage), overlaying generalized response phases onto the scenario framework (see the figure) reveals a potential gap in capacity between emergency and recovery phases, which, for the DH oil spill, is likely a period of continued increase in system stress. Elements of the restoration phase should be initiated concurrently with the standing down of the emergency, so as to more quickly and effectively achieve recovery of the coupled natural-human system. Timely development and implementation of restoration plans are essential. Further SSWG scenario-building focused on recovery is currently under way [another SSWG session is scheduled 20 to 24 September in New Orleans, with updates available at (*20*)] and includes additional subject matter experts, decision-support tools, and refined scenario techniques. We believe there is a valuable role for this strategic approach to science and policy interaction as the federal government learns from the DH oil spill, plans and implements GOM recovery, and prepares for future environmental crises.

References and Notes

1. Department of the Interior, "Strategic Sciences Working Group Progress Report, 9 June 2010" (Department of the Interior, Washington, DC, 2010); www.usgs.gov/deepwater_horizon/.
2. H. Khan, *Thinking About the Unthinkable* (Horizon Press, New York, 1965).
3. T. J. Chermack, S. A. Lynham, W. E. A. Ruona, *Futures Res. Q.* **7**, 7 (2001).
4. G. D. Peterson, G. S. Cumming, S. R. Carpenter, *Conserv. Biol.* **17**, 358 (2003).
5. G. E. Machlis, J. E. Force, W. R. Burch Jr., *Soc. Nat. Resour.* **10**, 347 (1997).
6. J. E. Haas, R. W. Kates, M. J. Bowden, *Reconstruction Following Disaster* (MIT Press, Cambridge, MA, 1977).
7. R. W. Kates, C. E. Colten, S. Laska, S. P. Leatherman, *Proc. Natl. Acad. Sci. U.S.A.* **103**, 14653 (2006).
8. J. Tibbetts, *Environ. Health Perspect.* **112**, A282 (2004).
9. N. N. Rabalais, R. E. Turner, W. J. Wiseman Jr., *J. Environ. Qual.* **30**, 320 (2001).
10. D. Burley, P. Jenkins, S. Laska, T. Davis, *Organ. Environ.* **20**, 347 (2007).
11. S. A. Castillo, P. Moreno-Casasola, *J. Coast. Conserv.* **2**, 13 (1996).
12. C. S. Holling, *Annu. Rev. Ecol. Syst.* **4**, 1 (1973).
13. D. Wang, N. D. Weaver, M. Kesarwani, X. Dong, J. Rockstrom, *Science* **308**, 1036 (2005).
14. B. H. Robison, *Conserv. Biol.* **23**, 847 (2009).
15. J. J. Maguire, Fisheries topics: Ecosystems: Types of ecosystems [online] (Fisheries and Aquaculture Department, FAO, Rome, 2005); www.fao.org/fishery/topic/3320/en
16. E. S. Sheppard, R. McMaster, *Scale and Geographic Inquiry: Nature, Society, and Method* (Blackwell, Malden, MA, 2004)
17. D. L. Felder, D. K. Camp, Eds., *Gulf of Mexico Origin, Waters, and Biota: Volume I, Biodiversity* (Texas A&M Univ. Press, College Station, TX, 2009).
18. C. Weiss, *Law Probab. Risk* **2**, 25 (2003).
19. C. E. Colten, R. W. Kates, S. Laska, *Community Resilience: Lessons from New Orleans and Hurricane Katrina* (Community and Regional Resilience Institute, Oak Ridge, TN, 2008).
20. U.S. DOI, Deepwater Horizon Response, www.doi.gov/deepwaterhorizon/index.cfm.

21. The authors thank members of the DOI SSWG: C. Colten, S. Dalton, J. Grace, J. Eitel, J. Hay, G. Plumb, E. Widder, and R. Woita. Additional assistance, advice, and review were provided by A. Castle, J. Cross, J. Jarvis, J. McKendry, S. Kimball, B. Werkheiser, colleagues of SSWG members, and anonymous reviewers.

10.1126/science.1195382

Downloaded from www.sciencemag.org on August 27, 2010

Published by AAAS

GEOPHYSICS

Fine-Scale Modeling of Global Plate Tectonics

Powerful numerical methods are enabling the creation of fine-grained models of Earth's dynamic geology.

Thorsten Becker

The tectonic motions on the surface of Earth and much of its geological activity can be explained as a part of mantle convection. Relatively rigid lithospheric plates form the top, cold boundary layer of the convecting mantle, and the potential energy released during the cooling of the planet is balanced by viscous dissipation during deformation of mantle rocks (*1*, *2*). A theory of plate tectonics has to account for compositional and rock strength variations, both of which are affected by the dynamics of convective flow. Such behavior can lead to nonlinear feedback and result in heterogeneity, possibly down to sub-meter scale. On page 1033 of this issue, Stadler *et al*. (*3*) present a groundbreaking numerical model for plate tectonics that should help to resolve questions relating to how the strongly deforming and narrow plate boundaries form and evolve.

Stadler *et al*. use an adaptive mesh refinement (AMR) finite element method with variable resolution. Such techniques are widely used in fields such as engineering and physics, but have not been previously used for global mantle dynamics with such sophistication. What makes AMR valuable for studying the challenging continuum mechanics problems presented by plate tectonics lies in the details. Stadler *et al*. show how to best apply AMR methods on massively parallel supercomputers, in particular minimizing the additional overhead that arises from the mesh refinement stage of the solution process (see the figure). The newly afforded resolution allows the role of nonlinear rock creep laws for plate motions to be explored in detail. They focus on the important role of subduction zones where the oceanic slabs plunge back into the mantle, as reflected in the formation of steep trenches in the ocean floor and deep seismicity.

AMR allows inclusion of more realistic geometries for the subducting lithosphere alongside narrow plate boundaries, and on top of large lateral variations in strength in the mantle underneath the plates, such as those expected as a result of volatile release and melting below volcanic arcs.

The role of plate strength at subduction zones, where the lithosphere dives down into the mantle as slabs, is one example where previous models lead to opposite conclusions. Slabs appear to be the dominant control on plate speeds (*4*), but how slabs pull the plates and transmit deformation to the surface in detail is still unclear. On the basis of global, lower-resolution models, the asymmetry between fast moving oceanic and slow continental plates has been interpreted such that a one-sided slab pull is transmitted through a stiff slab (*5*). Alternatively, the mantle underneath oceanic plates may be weaker than beneath continents, which may explain plate motions and other aspects of plate tectonics with relatively weak slabs (*6*). How slabs pull the plates and move the trench that forms at sites of plate convergence with respect to the lower mantle appears to hinge on how the work done by bending the plate at the surface, and throughout the upper mantle, compares to the total viscous dissipation. If slab bending is important, then Earth's thermal evolution may be strongly controlled by the details of the temperature-dependent structure of the oceanic crust and lithosphere (*7*). Regional modeling can address slab dynamics and

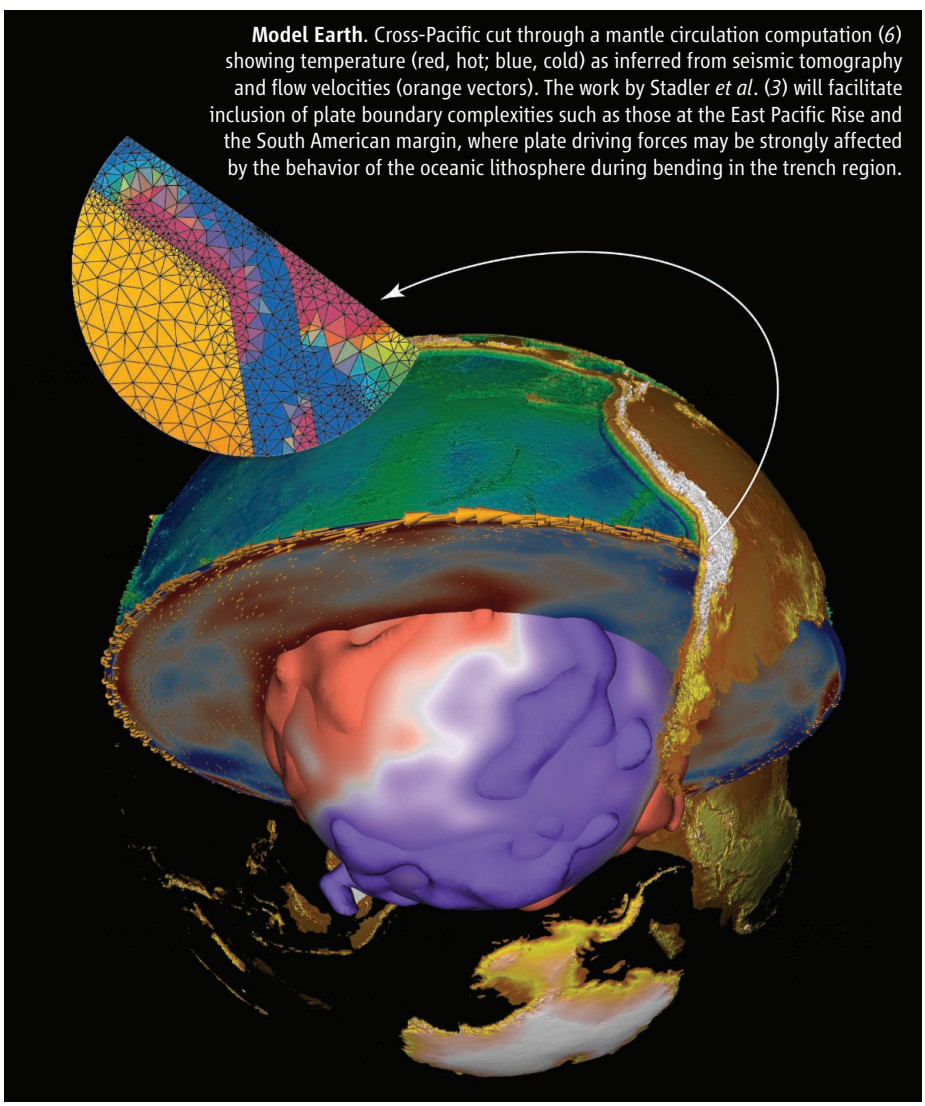

Model Earth. Cross-Pacific cut through a mantle circulation computation (*6*) showing temperature (red, hot; blue, cold) as inferred from seismic tomography and flow velocities (orange vectors). The work by Stadler *et al*. (*3*) will facilitate inclusion of plate boundary complexities such as those at the East Pacific Rise and the South American margin, where plate driving forces may be strongly affected by the behavior of the oceanic lithosphere during bending in the trench region.

CREDIT: (INSET OF MESH) MÉLANIE GÉRAULT

Department of Earth Sciences, University of Southern California, Los Angeles, CA 90089–0740, USA. E-mail: thorstinski@gmail.com

Downloaded from www.sciencemag.org on August 27, 2010

Published by AAAS

trench motions at high resolution but has also led to contrasting interpretations of the role of slab bending (*8*, *9*). One reason for the disagreement between studies may be that large-scale flow effects and the lower mantle were not fully included in the regional models. The now more complete AMR models can test all of the important ingredients at both local and global scales. The initial results from Stadler *et al*. suggest relatively high viscous dissipation in a weak subduction margin, but a relatively small contribution of slab deformation to the total mantle dissipation budget.

In the AMR models, plate speeds can be explained well when only upper-mantle slabs are included as driving density anomalies. More surprisingly, Stadler *et al*. found that the model fit degrades when additional density anomalies in the lower mantle, as inferred from seismic tomography, are incorporated. Why the new computations show this behavior, which contrasts with findings from previous, lower-resolution models, is somewhat unclear. How slab strength may have coupled to plate tectonic motions now and in the early Earth (*10*) remains to be fully explored. Evaluating the distribution of viscous dissipation and the slab force transmission from the faulted margin at the trench down into the deep mantle with further, high-resolution modeling should help to improve our understanding of the causes and consequences of reorganizations of plate motions and heat transport over geological time scales.

Models that can track dynamic properties of Earth's evolution are the next challenge for AMR methods. These could be used to tackle challenging problems such as the formation of plate boundaries during which strain localization processes may require locally very high resolution. There are some potential issues with applying AMR to dynamically evolving thermochemical convection problems that are related to nonlinear coupling between the equations governing mantle flow and temperature. However, if those are overcome and the method proves to be robust and widely available, global computational geodynamics might never look back.

References

1. D. Bercovici, Y. Ricard, M. Richards, in *The History and Dynamics of Global Plate Motions*, M. Richards, R. Gordon, R. D. van der Hilst, Eds., Geophys. Monograph 121 (American Geophysical Union, Washington, DC, 2000), pp. 5–46.
2. P. J. Tackley, in *The History and Dynamics of Global Plate Motions*, M. Richards, R. Gordon, R. D. van der Hilst, Eds., Geophys. Monograph 121 (American Geophysical Union, Washington, DC, 2000), pp. 47–72.
3. G. Stadler *et al*., *Science* **329**, 1033 (2010).
4. D. W. Forsyth, S. Uyeda, *Geophys. J. R. Astron. Soc.* **43**, 163 (1975).
5. C. P. Conrad, C. Lithgow-Bertelloni, *Science* **298**, 207 (2002).
6. T. W. Becker, *Geophys. J. Int.* **167**, 943 (2006).
7. C. P. Conrad, B. H. Hager, *Geophys. Res. Lett.* **26**, 3041 (1999).
8. F. A. Capitanio, G. Morra, S. Goes, *Geochem. Geophys. Geosyst.* **10**, Q04002 (2009).
9. E. Di Giuseppe, C. Faccenna, F. Funiciello, J. van Hunen, D. Giardini, *Lithosphere* **1**, 121 (2009).
10. J. van Hunen, A. P. van den Berg, *Lithos* **103**, 217 (2008).

10.1126/science.1194858

IMMUNOLOGY

Prime, Boost, and Broaden

A combined immunization approach represents a possible strategy for developing a "universal" flu vaccine.

Robert W. Doms

The need to produce an effective seasonal flu vaccine every year, coupled with the recent H1N1 influenza virus pandemic, underscores the importance of developing a universal flu vaccine. However, a major obstacle is the ability of the virus to evade the immune system, accumulating mutations that allow it to avoid recognition by neutralizing antibodies. The continual evolution of such mutations results in an ever-changing variety of circulating virus strains that ultimately render a vaccine ineffective. Each year, components of the seasonal flu vaccine are altered in the hope of matching these to virus strains that will evolve and circulate in humans in the months to come (*1*). This results in vaccines with variable efficacy—as recently as the 2007/2008 flu season, the seasonal vaccine was a poor match for circulating strains and afforded little protection from infection. In addition to mutations, entirely new viral proteins can be introduced into human viruses from the large reservoir of avian influenza strains. Thus, it is evident that a vaccine capable of eliciting antibodies that neutralize a much broader array of virus strains is needed. On page 1060 of this issue, Wei *et al*. (*2*) suggest that changing the way in which influenza virus vaccines are delivered, rather than the vaccine components themselves, may elicit antibodies that could confer protection from diverse viruses for years.

Immunization with the seasonal influenza virus vaccine evokes antibodies that bind to discrete sites in the globular head domain of the viral HA protein (see the figure). Influenza virus strains are grouped into subtypes that are numbered sequentially after the HA molecule they express (H1, H2, H3, etc.). The viral neuraminidase protein (the "N" in "H1N1") plays a negligible role in virus neutralization. In recent years, H1 and H3 virus strains have circulated in humans, with occasional localized outbreaks of H5 and H7 viruses from avian sources. The most commonly used seasonal vaccine contains representative, inactivated H1 and H3 viruses, which give rise to subtype-specific antibodies that neutralize H1 and H3 viruses. These are genetically similar

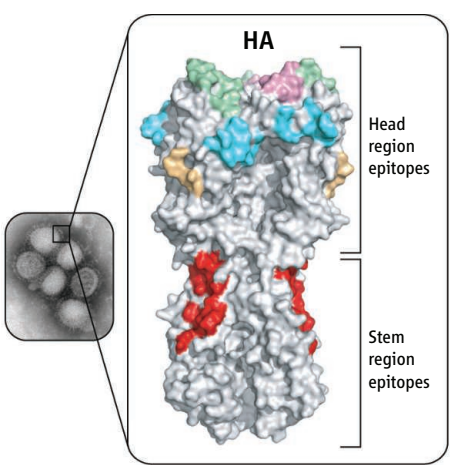

Antibody recognition. Most antibodies against influenza A virus (inset shows the 2009 H1N1 strain) bind to the highly variable part of the hemagglutinin (HA) glycoprotein at the surface of the virus particle (head region). In the H1 subtype, these antibodies recognize four major sites (Sa, Sb, Ca, and Cb are shown in green, pink, cyan, and yellow, respectively). The HA structure of the 2009 H1N1 virus is shown (PDB code 3LZG). Antibodies that neutralize multiple strains both within a virus subtype and from different subtypes bind to a highly conserved region (red) in the stem region of HA.

Department of Microbiology, University of Pennsylvania, Philadelphia, PA 19104, USA. E-mail: doms@mail.med.upenn.edu

CREDIT: CDC (INSET); D. EKIERT, I. WILSON

Downloaded from www.sciencemag.org on August 27, 2010

Published by AAAS

to the inactivated viruses, but not more distantly related H1 or H3 viruses, much less viruses from other subtypes. When a new virus strain is introduced into humans, such as the H1N1 virus in 2009, an entirely new vaccine or vaccine component is required. This continual game of catch-up is a dangerous one because it takes time to produce a vaccine to a new circulating strain, and a particularly virulent strain might reach pandemic status before the process is complete. This has spurred the search for antibodies that can neutralize not only multiple strains within an influenza virus subtype, but viruses from different subtypes as well. Recently, a number of antibodies that fulfill these properties have been identified (*3*–*6*). Two of these have been crystallized while bound to HA, showing that these antibodies, unlike the vast majority of neutralizing antibodies elicited by infection or vaccination, bind to a highly conserved region in the stem region of HA rather than to epitopes in the globular head domain (*5*, *6*). By binding to HA in this position, stem-targeting antibodies prevent HA from undergoing the conformational changes needed to catalyze the membrane fusion reaction needed for virus infection.

Identifying broadly cross-reactive, neutralizing antibodies to influenza virus reveals the potential for a more effective vaccine, but stimulating the production of such antibodies presents a challenge. A growing number of broadly neutralizing antibodies to HIV have been identified, for example, but no vaccination strategy to date has elicited such antibodies efficiently (*7*–*9*). Strategies to achieve broad neutralization include generating novel immunogens that elicit broadly neutralizing antibodies, or using immunization procedures coupled with existing vaccine components to achieve the same end. Wei *et al*. took the second approach, using a prime-boost strategy in which mice, ferrets, and monkeys were primed with a DNA vaccine expressing an HA protein based on an existing seasonal flu vaccine. They were then boosted with the inactivated seasonal flu vaccine itself. Thus, the innovation was not the immunogen per se, but rather the DNA vaccine priming step. Strikingly, when HA from the 1999 seasonal H1 flu vaccine was used in this manner, the resulting sera efficiently neutralized H1 viruses dating as far back as 1934, as well as H1 viruses that emerged in 2006 and 2007—a span of more than 70 years. Some cross-neutralization of H3 and H5 viruses was also achieved, and animals were protected from a lethal challenge with virus. Neither the DNA vaccine nor the seasonal vaccine alone achieved these results. Viruses bearing mutations in the conserved stem epitope escaped neutralization elicited by this vaccination strategy. Therefore, DNA priming before the use of a standard seasonal flu vaccine broadened the humoral immune response to include antibodies to the stem of HA, perhaps by facilitating the T cell help needed to stimulate the development of antibody-producing B cells.

The findings of Wei *et al*. provide proof of concept that broadly neutralizing antibodies to influenza virus can be elicited through immunization, although similar prime-boost approaches have failed to produce broadly neutralizing antibodies to HIV (*9*). An important practical consideration is that the prime-boost technique used by Wei *et al*. will require at least two or more injections at different times, necessitating multiple visits to a care-giver. By contrast, the most commonly used seasonal flu vaccine requires only a single intramuscular injection. On the other hand, the broad neutralization seen in the prime-boost method may diminish the need for annual immunizations. Further work is needed to elucidate whether all influenza subtypes and strains will lend themselves to this immunization approach. The results of Wei *et al*. call for a renewed focus on vaccine development, with emphasis on immunization strategies as well as the immunogens themselves.

References

1. S. Salzberg, *Nature* **454**, 160 (2008).
2. C.-J. Wei *et al*., *Science* **329**, 1060 (2010); published online 15 July 2010 (10.1126/science.1192517).
3. A. K. Kashyap *et al*., *Proc. Natl. Acad. Sci. U.S.A.* **105**, 5986 (2008).
4. T. T. Wang *et al*., *PLoS Pathog.* **6**, e1000796 (2010).
5. D. C. Ekiert *et al*., *Science* **324**, 246 (2009).
6. J. Sui *et al*., *Nat. Struct. Mol. Biol.* **16**, 265 (2009).
7. T. Zhou *et al*., *Science* **329**, 811 (2010); published online 8 July 2010 (10.1126/science.1192819).
8. L. M. Walker *et al*., *Science* **326**, 285 (2009).
9. P. D. Kwong, I. A. Wilson, *Nat. Immunol.* **10**, 573 (2009).

10.1126/science.1195116

BEHAVIOR

Decisions Made Better

Marc O. Ernst

Under certain circumstances, joint decisions of a group can be better than those of the individuals.

We constantly make decisions based on perceptual experiences. For example, a referee at a soccer match trusts his eyes to judge whether the ball crossed the goal line. Sometimes, the resulting decisions are false, with devastating consequences for one team. If two referees watching the same match made joint decisions, would the result overall be more precise? On page 1081 of this issue, Bahrami *et al*. (*1*) find that joint decisions are better than those made individually, but only under certain conditions.

Max Planck Institute for Biological Cybernetics. Spemannstr. 41, 72076 Tübingen, Germany. E-mail: marc.ernst@tuebingen.mpg.de

For most joint decisions, the referees will not need to confer with one another about their observations, as their individual perceptions will agree—the ball crossed the goal line or it did not. No benefit in joint decision-making can result from such concurring observations. If during negotiation, however, it becomes apparent that their observations differ, what strategy can be used to resolve this conflict and come up with the best joint answer? That is, what decision strategy would result in a benefit for the group?

If the referees disagree in their individual judgments, the simplest way to resolve the conflict is to flip a coin. This strategy is less than optimal because it would be wrong half of the time, such that joint decision performance, taking all decisions together, will be in-between that of the two referees and not better than either one alone. To improve on this outcome, more information is needed. For example, if we knew from previous experience that Referee 1 usually makes more accurate decisions, we would ask that person to always make the final call. However, decision performance is just as good as having one referee present at the match, and there is still no improvement. So what is the best strategy to resolve the conflict and lead to a group benefit? The answer is simple. Every decision has a right and a wrong answer, so when there is a conflict, only one referee is correct. Which referee is correct, however, will differ from decision to decision. If in every case the

Downloaded from www.sciencemag.org on August 27, 2010

Published by AAAS

referee who currently has the correct answer would make the joint decision, group performance (considering all decisions) would be better than that of each individual alone. The problem is, how do the referees know who currently made the correct decision?

Decisions based on individual perceptions are inevitably uncertain because they rely on sensory evidence that is corrupted by noise. Such noise is always introduced when sensory information from the eyes, ears, or hands is processed by the nervous system (*2*). The amount of noise depends on the particular perceptual situation (viewing distance, lighting conditions, etc.) so that decisional uncertainty will vary from moment to moment. More noise implies more uncertainty and a greater chance to get the answer wrong. Thus, an indication of who got the right answer can be the level of certainty with which a decision can be made. If so, an individual would need to communicate this certainty level to the other group members. If the more certain referee always provides the joint answer, because she or he is more likely to be correct, an overall group benefit can be achieved.

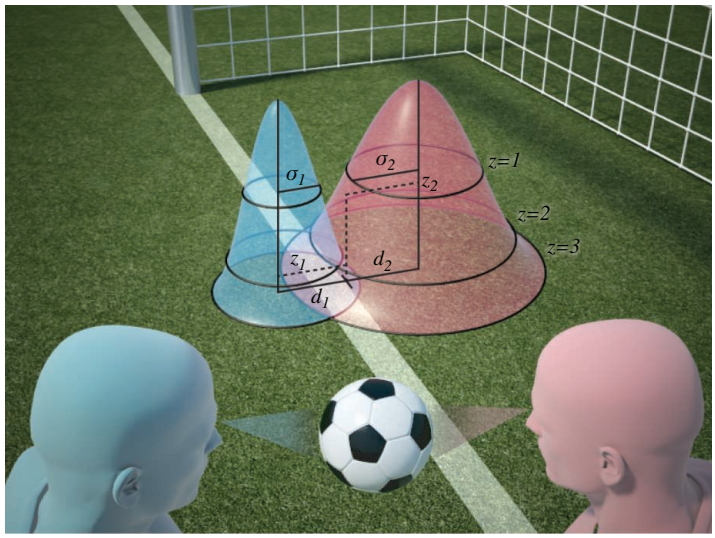

Joint decisions. Noisy estimates of the landing position of the ball for Referee 1 (blue) and Referee 2 (red). See the text for a description on how referees might make the best possible decision on where the ball landed.

Bahrami *et al*. show that humans do indeed communicate some measure of certainty in their decision when they are free to discuss their perceptual experiences. This allowed pairs of individuals in their study to improve joint performance substantially under most of the conditions tested. To understand why performance on joint decisions did not always improve, the authors looked at the certainty measure that participants communicated to each other. To illustrate the decision process, consider the perceptual experiences of the two referees (see the figure). The peaks of the two normal distributions specify the percept where the ball apparently landed; the spread of the distributions indicates the noise associated with the individual perceptual estimates. According to Bahrami *et al*., the certainty with which each referee decides whether the ball crossed the goal line is the distance (d_i) between the percept (peak) and decision-line (i.e., goal line), divided by the spread of the distribution (σ_i). This ratio, a *z*-score ($z_i = d_i/\sigma_i$), is the level of certainty that humans apparently communicate to each other when making a joint decision, as this model best fits the data of Bahrami *et al*. Given this certainty measure, there is a simple strategy for resolving disagreement over decisions: The referee who is currently more certain—that is, the one who has the higher *z*-score—gets to make the joint decision. Expressed as an equation, this decision rule is given by: $d_1/\sigma_1 + d_2/\sigma_2 = 0$. When this sum is positive, Referee 1 will make the joint decision; otherwise, Referee 2 will.

However, this is not the best possible way to combine information and come to a joint decision. Examples of how to combine information in the most optimal way, thereby guaranteeing the most precise final judgement, are provided by studies on the integration of information across the senses (*3*–*6*). For example, when judging the size of an object, visual and tactile information is integrated to improve the overall size estimation (*5*). These studies show that the best possible way to integrate information is to form a weighted average of the different information sources (*7*). Applied to the situation of judging whether the ball crossed the goal line, this weighted average is given by $d = (d_1/\sigma_1^2 + d_2/\sigma_2^2)/N$ with $N = 1/\sigma_1^2 + 1/\sigma_2^2$. According to this equation, the distance d is the optimal joint estimate of where the ball has landed. The sign of d, therefore, determines whether the ball apparently went over the goal line. Thus, the optimal decision rule can then easily be derived as $d_1/\sigma_1^2 + d_2/\sigma_2^2 = 0$. Comparing this optimal decision rule to the earlier one, it is clear that the referees (and humans generally) should use d_i/σ_i^2, instead of the z-score d_i/σ_i, for communicating the level of certainty in their perceptual estimates. Such optimal joint decision-making would guarantee the group a benefit over its individuals, similar to the way in which multisensory integration incurs a benefit for sensory estimation.

Joint decision-making is generally worse when using d_i/σ_i instead of d_i/σ_i^2. However, the difference in performance based on these measures vanishes when the noises are equal ($\sigma_1 = \sigma_2$), because then the two decision rules become equal ($d_1 + d_2 = 0$). When the noises are equal, the maximal benefit of joint decision-making can be achieved, which is an improvement of roughly 40% (factor of $\sqrt{2}$) over its individuals. As the difference between σ_1 and σ_2 increases, joint decision-making using a certainty measure based on the *z*-scores will become increasingly less beneficial, up to a point where joint decision-making even incurs a cost instead of providing a benefit. This switch occurs when the difference between the noises of the individual judgments falls below $\sigma_1 \approx 0.4\sigma_2$ (*1*). Thus, referees using *z*-scores as their certainty measure can benefit from joint decision-making only if the noise levels of their perceptual estimates are similar; otherwise, they risk incurring a cost when deciding jointly.

Humans use d_i/σ_i instead of d_i/σ_i^2 when communicating their level of certainty and by doing so they risk a cost, but it is unclear why. One reason may be that the optimal certainty measure, other than the *z*-score, is not unit-free. This may cause problems when trying to communicate such measures, because all group members have to use the same units. Imagine an American and a European referee making joint decisions—one using inches, the other meters. It would be interesting to see whether, by providing feedback, people could be trained to use the better of the two certainty measures, so that joint decisions would always be better than that of individuals. Whether it is feasible to have two referees negotiating each decision during a soccer match is another matter entirely.

References and Notes

1. B. Bahrami *et al*., *Science* **329**, 1081 (2010).
2. A. A. Faisal *et al*., *Nat. Rev. Neurosci.* **9**, 292 (2008).
3. M. S. Landy *et al*., *Vision Res.* **35**, 389 (1995).
4. Z. Ghahramani *et al*., in *Self-Organization, Computational Maps and Motor Control*, P. G. Morasso, V. Sanguineti, Eds. (Elsevier, Amsterdam, 1997), pp. 117–147.
5. M. O. Ernst, M. S. Banks, *Nature* **415**, 429 (2002).
6. D. Alais, D. Burr, *Curr. Biol.* **14**, 257 (2004).
7. W. G. Cochran, *J.R. Stat. Soc.* **4** (suppl.), 102 (1937).
8. I thank M. Breidt for help with the figure design and the European Union [grant *THE* (IST-2009-248587)] and Bernstein Centre for Computational Neuroscience, Tübingen (BMBF; FKZ: 01GQ1002) for support.

10.1126/science.1194920

CREDIT: MARTIN BREIDT/MAX PLANCK INSTITUTE FOR BIOLOGICAL CYBERNETICS

Downloaded from www.sciencemag.org on August 27, 2010

Published by AAAS

DEVELOPMENTAL BIOLOGY

Microenvironment Mimicry

Mickie Bhatia

Muscle stem cells cultured in vitro retain regenerative ability when conditions reflect the physical nature of their in vivo environment.

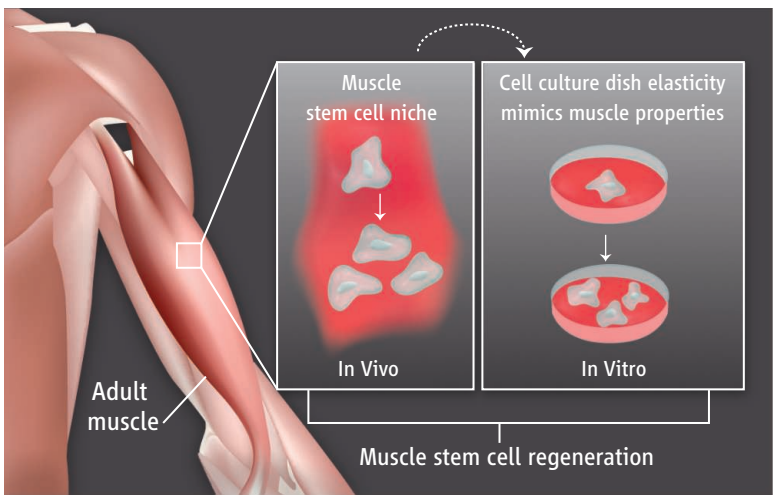

Just like home. The physiological niche for muscle stem cells resides in specific locations within a muscle bundle. They self-renew to give rise to more stem cells and differentiate into mature myoblasts that regenerate muscle fiber upon injury or disease-based degeneration. Outside of this homeostatic environment, muscle stem cells may be cultured in microenvironments in the presence of optimized predefined growth factors and on a flexible substrate that mimics the flexibility of muscle tissue.

Stem cells define their physiological homes, or niches, as the place of residence where they self-renew and differentiate (*1*), supporting growth, homeostasis, and tissue-regenerative response upon injury and disease (*2*). On page 1078 of this issue, Gilbert *et al*. (*3*) remind us that home is not merely a location, but also a specialized physical environment that modulates cell behavior. The authors show that muscle stem cells derived from mice retain their regenerative properties in cell culture as long as the elastic comforts of their physiological niche are duplicated. Thus, mimicking the biophysical properties of a niche may be equally important to other stem cell types.

The immense tissue-regenerative ability of adult stem cells is lost when they are placed in a cell culture microenvironment, even when the appropriate biochemical signals (such as growth factors) are supplied (*2*, *4*). This presents a formidable challenge to the study and manipulation of stem cells in culture for experimental or therapeutic purposes. Gilbert *et al*. focused on the biophysical aspects of the in vitro environment through the use of hydrogels, a substrate with elastic properties that may reflect those of muscle bundles. The authors determined that with the appropriate biochemical factors present, muscle stem cells survive and display a simultaneous balance of self-renewal and differentiation [a hallmark of the stem cell regenerative phenotype (*5*)] when cultured in vitro on a flexible, elastic surface (see the figure). Moreover, muscle stem cells cultured in this manner could sustain regenerative properties when transplanted into recipient mice that were depleted of muscle stem cells or had damaged muscle tissue. By using muscle cells engineered to express a luciferase enzyme (and thus emit bioluminescence), the authors could visually track individual stem cells (and their lineages) in vivo by whole-animal bioluminescence imaging that allowed a quantitative measurement of regenerative capacity. This effect was most potent at the initial point of cell division of individual stem cells in culture, when the two resulting daughter cell progeny of a single stem cell cultured under these conditions shared a putative muscle stem cell marker (Pax7) (*6*). Thus, recapitulation of the biophysical flexibility of the muscle tissue niche made muscle stem cells far less "homesick," such that they behaved more like what would be expected in their native environment.

Despite the beneficial effects demonstrated by Gilbert *et al*., muscle stem cells still "miss home" even under optimized conditions of reduced substrate rigidity. Those cultured on an elastic substrate still had lower in vivo muscle regenerative capacity relative to those freshly isolated from muscle tissue. This indicates that additional biochemical and biophysical elements of the stem cell niche still need to be identified. In the end, this in vitro system may provide an ideal experimental foundation to further tweak the environment through the addition or removal of biochemical factors (agonists and antagonists of signaling pathways) and to explore the role of other biophysical elements.

The findings of Gilbert *et al*. also remind us that not all individuals live alone or in a vacuum. Accordingly, an in vitro niche may provide a good house, but it is still inert and devoid of the ability to respond to macro- and microenvironmental influences arising from physiological processes (hormonal changes, inflammation, and nervous system function, for example) that make the entire residence operable. Emerging evidence suggests that the stem cell niche governs stem cell fate (*4*, *5*), but clearly the niche must react to the needs of the organism and facilitate appropriate signals to stem cells for growth and repair. In addition, individual stem cells may be unique and heterogeneous in their cell division cycle regulation, and can constitute both quiescent and active populations that coexist in the same niche (*7*). This may indicate that part of the microenvironment is, in fact, other stem cell or progenitor populations that are not examined when testing single stem cells deposited in engineered niche environments (*8*). And in some cases, the in vitro biophysical niche may prevent stem cells from regenerating and instead promote tumor growth, as is the case for germ stem cells of the fly *Drosophila melanogaster* (*9*). By contrast, human pluripotent stem cells (*10*) create their own niche microenvironment by producing niche cells to support self-renewal.

As the study of Gilbert *et al*. was performed in mice, it remains to be determined whether similar biophysical properties are relevant to the regeneration of human stem cells. It would thus be prudent to revisit several human stem cell culture techniques. The majority of these practices rely on biochemical features alone, and the physical substratum is largely ignored. In human blood and intestinal tissue, resident stem cells have fairly well-defined niche environments (*4*,

Stem Cell and Cancer Research Institute, McMaster University, Hamilton, Ontario L8N 3Z5, Canada. E-mail: mbhatia@mcmaster.ca

CREDIT: N. KEVITTYAGALA/*SCIENCE*

Downloaded from www.sciencemag.org on August 27, 2010

Published by AAAS

11), and the element of biophysical rigidity that nonetheless enables movement of stem cells could be explored in detail to improve stem cell expansion. As clinical applications normally target damaged tissue that has succumbed to physical injury or disease degeneration, it's unclear whether the damaged tissue in which stem cells would be transplanted after in vitro culture would be as hospitable as the in vitro culture microenvironment. Mimicking a "damaged tissue" microenvironment in vitro may allow improved stem cell expansion during real-life cases of regeneration, or may increase the preparedness of stem cells to improve regenerative processes once transplanted. Such in vitro microenvironments that reflect physiological damage may be ideal tools to examine biophysical parameters that induce adult stem cell regeneration (*12*) without the need for ex vivo culture and/or retransplanting of stem cells at all.

References

1. D. J. Rossi, C. H. Jamieson, I. L. Weissman, *Cell* **132**, 681 (2008).
2. D. T. Scadden, *Nature* **441**, 1075 (2006).
3. P. M. Gilbert *et al.*, *Science* **329**, 1078 (2010); published online 15 July 2010 (10.1126/science.1191035).
4. M. H. Stewart, S. C. Bendall, M. Bhatia, *J. Mol. Med.* **86**, 875 (2008).
5. T. Schroeder, *Cell Stem Cell* **6**, 203 (2010).
6. S. Kuang, M. A. Gillespie, M. A. Rudnicki, *Cell Stem Cell* **2**, 22 (2008).
7. L. Li, H. Clevers, *Science* **327**, 542 (2010).
8. M. P. Lutolf, P. M. Gilbert, H. M. Blau, *Nature* **462**, 433 (2009).
9. L. A. Johnston, *Science* **324**, 1679 (2009).
10. S. C. Bendall *et al.*, *Nature* **448**, 1015 (2007).
11. A. Haegebarth, H. Clevers, *Am. J. Pathol.* **174**, 715 (2009).
12. D. Hess *et al.*, *Nat. Biotechnol.* **21**, 763 (2003).

10.1126/science.1194919

CHEMISTRY

Opening the Door to Peptide-Based Porous Solids

The twisting motion of a dipeptide linker group acts as a pressure-sensitive gate for the adsorption of gases within a crystalline solid.

Paul A. Wright

Enzymes and ion channels often undergo structural transitions that accommodate the binding of small molecules or ions, whereas porous solids that adsorb and store gases tend to have rigid structures that are unaffected by molecular binding. On page 1053 of this issue, Rabone *et al*. (*1*) describe a metal-organic framework, or MOF, made up of zinc ions bridged by flexible dipeptide linkers (glycylalanine), that changes the geometry and connectivity of its pore structure when it takes up small molecules. Unlike most porous solids, in which gas uptake increases steadily with increasing gas pressure, the gas pressure must exceed a critical "gate opening" pressure before the micropores of their material open to allow gas adsorption (see the figure, panel A). Although gating phenomena have been reported (*2*, *3*), Rabone *et al*. have used an unprecedented array of experimental and computational techniques to reveal the underlying mechanism, and show that pore opening results from torsional motion and displacements of the dipeptide linkers.

Until the mid-1990s, most synthetic porous solids were either activated carbons or inorganic zeolites and their analogs. With a few exceptions, such porous solids have rigid frameworks that undergo only slight structural changes upon adsorption of molecules into their channels and cages. Their adsorption behavior is mainly determined by interaction of the small-molecule adsorbate with the framework and with other adsorbate molecules.

The discovery of porous coordination polymers and MOFs (*4*–*6*) led to the observation of a much wider range of adsorption behavior commensurate with their near-limitless structural and chemical diversity (*7*). Some of these frameworks are rigid, or show only slight distortions in framework structure caused by tilting or rotation of linkers. Others show more dramatic changes—for example, solvent molecules coordinated to metal cations can be removed to leave open binding sites, or there can be changes in

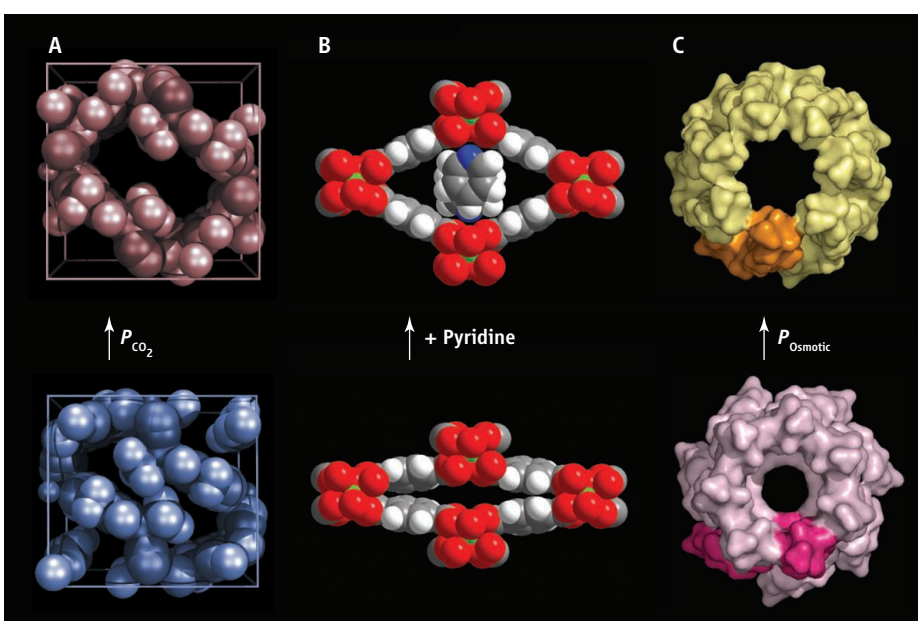

Open-and-shut cases. (**A**) Rabone *et al*. synthesized a metal-organic framework compound from zinc ions and glycylalanine dipeptides. At a critical pressure of CO_2, the pores in the framework open to allow the gas molecules (not shown) to adsorb. This opening is the result of torsional motion of the dipeptide linkers. The behavior is intermediate between that observed in (**B**) the adsorbate-induced breathing of the flexible metal-organic framework compound MIL-53(Fe), which contains rigid 1,4-benzenedicarboxylate linkers, and (**C**) the gate opening of the bacterial mechanosensitive channel of small conductance (MscS) in response to osmotic pressure. [Credits: (A) Rabone *et al.*; (B) Millange *et al*. (*9*); (C) Cabrita *et al*. (*12*)]

School of Chemistry, University of St. Andrews, Purdie Building, North Haugh, St. Andrews, Fife, KY16 9ST, UK. E-mail: paw2@st-andrews.ac.uk

Downloaded from www.sciencemag.org on August 27, 2010

Published by AAAS

linker coordination or in conformation (*8*). In addition, there are examples of flexible solids that demonstrate a high degree of expansion and contraction ("breathing") upon adsorbate uptake and loss. In the MIL-53 solids (*7*, *9*), chains of MO_6 octahedra (where the metal can be aluminum, iron, and others) that share corner oxygen atoms are linked by rigid 1,4-benzenedicarboxylate units. The three-dimensional trellis-like structures that form "breathe"—they undergo a scissoring motion when gas adsorbs or desorbs (see the figure, panel B).

Like the zinc-dipeptide compounds of Rabone *et al*., many of these flexible porous solids exhibit a gate-opening pressure, where the free-energy cost of structural rearrangements necessary to open the structure is paid by the energy associated with making bonds when molecules adsorb. They also exhibit hysteresis—plots of the amounts of gas adsorbed as a function of pressure are different for adsorption and desorption cycles. In the zinc dipeptide the hysteresis arises because there are different structural arrangements accessed along adsorption and desorption pathways, and the barriers to transport between pores depend on whether the pores are filled or empty. Rabone *et al*. resolved details of the gate-opening of their zinc dipeptide for carbon dioxide (CO_2) through high-resolution structural studies. Torsional motion of the dipeptide linker blocks or unblocks the pore opening. The disordered arrangement of the peptide without CO_2 present becomes more ordered as the CO_2 adsorbs and creates a random distribution of closed and open pores.

The use of amino acids and peptides as linkers within MOFs has received considerable attention because of their ready availability and inherent chirality (*10*). Such materials can find application in chiral adsorption and catalysis. Rabone *et al*. emphasized the relation of the metal dipeptide to structural biology by modeling the structural changes with molecular mechanics and molecular dynamics methods and by constructing Ramachandran plots of dihedral angles between peptides. Recent crystallographic studies of bacterial membrane proteins (*11*, *12*) provide perhaps the most striking structural-biology analogy to the gate-opening behavior reported by Rabone *et al*. Mechanosensitive membrane proteins can regulate the diffusion of hydrated ions out of cells as a response to osmotic pressure. In the closed form of the mechanosensitive channel of small conductance, MscS (see the figure, panel C), the 5 Å–diameter pore is too small to permit the egress of hydrated ions, but increasing the osmotic pressure to a critical gate-opening pressure opens the pore diameter to 13 Å, allowing hydrated ions to pass. The structural rearrangement occurs by a rotational rearrangement of the three different helices present in the structure via torsional motions of amino acid residues. The channel opens in a way reminiscent of the mechanism of a camera iris. Changing amino acid substituents by site-selective mutagenesis revealed how the gate-opening pressure is controlled. In the open form, the amino acid side chains withdraw from the central pore, in a manner reminiscent of the pore opening that Rabone *et al*. observed to occur in their solid as a result of the dipeptide twist.

The study of Rabone *et al*. helps improve our understanding of biological processes such as the opening and closing of ion channels. The relative simplicity and crystalline nature of the zinc dipeptide structure means that the transition, which is based on torsional motion within amino acid residues, can be followed by experiment and modeling to a higher resolution than is possible for biological molecules. Such details will be relevant to other critical issues, such as protein folding and unfolding (*13*), particularly when considering free-energy landscapes and metastable states. Furthermore, the adoption of concepts of flexible frameworks based on naturally occurring molecules should open the field to the preparation of complex crystalline biohybrid frameworks incorporating functionality as well as flexible porosity.

References

1. J. Rabone *et al*., *Science* **329**, 1053 (2010).
2. R. Kitaura, K. Seki, G. Akiyama, S. Kitagawa, *Angew. Chem. Int. Ed.* **42**, 428 (2003).
3. P. Llewellyn, S. Bourelly, C. Serre, Y. Filinchuk, G. Férey, *Angew. Chem. Int. Ed.* **45**, 7751 (2006).
4. O. M. Yaghi *et al*., *Nature* **423**, 705 (2003).
5. S. Kitagawa, R. Kitaura, S.-I. Noro, *Angew. Chem. Int. Ed.* **43**, 2334 (2004).
6. G. Férey, C. Mellot-Draznieks, C. Serre, F. Millange, *Acc. Chem. Res.* **38**, 217 (2005).
7. G. Férey, C. Serre, *Chem. Soc. Rev.* **38**, 1380 (2009).
8. S. R. Miller *et al*., *J. Am. Chem. Soc.* **130**, 15967 (2008).
9. F. Millange, C. Serre, N. Guillou, G. Férey, R. I. Walton, *Angew. Chem. Int. Ed.* **47**, 4100 (2008).
10. R. Vaidhyanathan *et al*., *Angew. Chem. Int. Ed.* **45**, 6495 (2006).
11. R. B. Bass, P. Strop, M. Barclay, D. C. Rees, *Science* **298**, 1582 (2002).
12. W. Wang *et al*., *Science* **321**, 1179 (2008).
13. L. D. Cabrita, C. M. Dobson, J. Christodoulou, *Curr. Opin. Struct. Biol.* **20**, 33 (2010).

10.1126/science.1195176

VIROLOGY

Looking Inside Adenovirus

Vaccines and gene therapy vectors could benefit from new insights into structure.

Stephen C. Harrison

Adenoviruses are a large group of DNA viruses with a distinguished experimental history, including contributions to the discovery of RNA splicing and the elucidation of central pathways in cell transformation (*1*). Some adenoviruses are human pathogens. They are also very much in vogue as potential vaccine and gene therapy vectors. Structure-based redesign of their cell-targeting and antigenic properties is therefore a desirable goal. Although the striking icosahedral shape of an adenovirus particle has made its image an icon in virology (see the figure), the complexity of its molecular organization has required that a picture of an intact virion be assembled by fitting high-resolution structures of the "major" components (the "hexon," "penton base," and "penton fiber") into lower-resolution images from cryoelectron microscopy (cryo-EM) (*2*). Two papers in this issue will help to eliminate that requirement. On page 1071, Reddy *et al*. (*3*) report the crystal structure of a modified adenovirus type 5 (Ad5), in which short penton fibers from another serotype replace those of the wild-type Ad5. On page 1038, Zhou and colleagues (*4*) report a cryo-EM reconstruction of Ad5 with sufficient resolution to trace polypeptide chains in three of the "minor" proteins that hold hexons and pentons together, giving a more detailed view than hitherto possible of interactions that determine particle assembly.

The most abundant protein in an adenovirus particle—and the principal determinant of its antigenic properties—is the hexon (*5*). Despite its name, this protein is a trimer, but

Howard Hughes Medical Institute and Jack and Eileen Connors Laboratory of Structural Biology, Harvard Medical School, 250 Longwood Avenue, Boston, MA 02115, USA, and Children's Hospital, 3 Blackfan Circle, Boston, MA 02115, USA. E-mail: harrison@crystal.harvard.edu

Downloaded from www.sciencemag.org on August 27, 2010

Published by AAAS

each subunit has two rather similar parts, giving the trimeric oligomer a pseudo-hexagonal character. Each of these two modules is a "β–jelly roll" domain, with elaborate outward-projecting loops between its strands. The loops are the most variable regions of the protein; their variation is the basis of serotype diversity. The subunit of the penton base resembles one half of the bipartite hexon subunit, with less elaborate projecting loops (*6*). Thus, the entire outer shell comprises 25 × 60 such modules, of three different kinds. Although inserted into the fivefold symmetric penton base, the penton fiber is a trimer (*7*). Its precise adaptation to the base is not yet evident, even in the present structures. At its tip is a knob that determines receptor specificity (*8*).

The hexon trimers form planar, sheet-like structures within each face, and gentle disruption of the particle yields so-called "groups of nine" (GONs), as marked in the figure (*9*). Under other circumstances, the pentons and the five surrounding "peripentonal hexons" dissociate from an otherwise intact virion, suggesting that these elements form a second subassembly, which Liu *et al*. (*4*) have called a "group of six" (although it is really a "group of five plus one"). The most important new information from the structures presented here concerns how three different minor proteins (designated IIIa, VIII, and IX) serve as "cement" to hold together each subassembly and to link them to each other.

The fundamental structural module of the adenovirus hexon and penton is present in many other icosahedral viruses, of both eukaryotes and prokaryotes (*10*). In simpler structures, such as those of the picornaviruses (e.g., polioviruses and rhinoviruses) or polyoma- and papillomaviruses, the geometry of the overall assembly is determined by interactions of N- and C-terminal "arms," extensions at the termini of the β–jelly roll domain that link with each other and with neighboring subunits. In the adenovirus particle, these arms are no longer covalent extensions of the β–jelly roll module, but rather independent polypeptides. Their function is nonetheless very similar. The interactions of protein IX, which winds into the crevices between hexons on the outer surface of the virion, gather the nine hexons of the GON into a pinwheel-like assembly and dictate that further hexons do not add onto its rim. One might thus imagine a different and larger "protein IX" that generates a larger hexon pinwheel, thereby creating a larger particle from otherwise similar structural elements. The C-terminal segment of protein IX also participates in a bundle of α helices connecting neighboring GONs. In a similar manner, protein IIIA links the penton base and peripentonal hexons into a cluster (the "GOS"). Protein VIII, like protein IX, helps cement the GON while also participating in contacts that tie the GON to the GOS (particularly through interaction with protein IIIA) and adjacent GONs to each other. Both protein IIIA and protein VIII contact inward-facing surfaces of the hexon and penton.

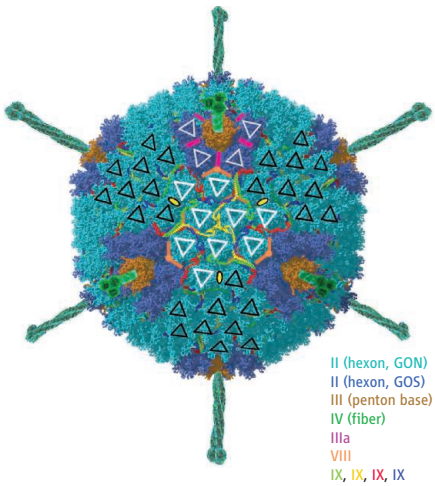

A new view. An adenovirus particle, with structural components highlighted. The overall diameter of the particle (not including the spikes) is about 900 Å. Superposed on a medium-resolution image of the virion surface are triangles showing four groups of nine (GONs)—one in the center, in white, and three surrounding it, in black. The triangles are in orientations that join the tips of the three hexon subunits. One set of peripentonal hexons is designated by gray triangles. The hexons in the GONs are in light blue; the peripentonal hexons, in dark blue; the penton bases, in brown; the penton fibers, in green. The network of protein IX subunits, snaking between the hexons on the outside of the particle, is in yellow, bright green, blue, and red; the positions of some copies of two internal minor proteins, which would not be visible from the outside, are shown by colored lines (proteins IIIa and VIII, in orange and magenta, respectively). The view is directly along a threefold symmetry axis of the particle and hence onto the central GON. The yellow ovals show positions of twofold axes of symmetry.

The antigenic, hypervariable loops of the hexon are largely disordered in crystals of isolated hexons. In the intact virions, some of these segments have contacts, either between hexons or with protein IX, that appear to stabilize them. Because a majority of adults, in both developed and developing countries, have circulating antibodies against Ad5, "loop swaps" between Ad5 and other, rarer serotypes have been attempted in efforts to generate Ad5-based vaccine vectors that escape neutralization (*11*). This "immunogen design" has depended on a definition of loop boundaries from positions at which loops become invisible in the hexon crystallographic density map. The new information defines these loops more precisely, and it should therefore facilitate new work on "rationally" designed adenovirus vectors with altered antigenic structure.

Substantial technical achievement underlies both of these papers. The x-ray crystallographic approach required creating a virus with Ad35 penton fibers—much shorter than those of wild-type Ad5. Moreover, the fibers appear to have receded into the penton base, leaving only the knobs projecting (*3*). Reddy *et al*. suggest that this recession represents an entry intermediate, but it could also be a consequence of mixing proteins in the recombinant virion. The cryo-EM structure is a tour de force of contemporary electron microscopy. It is not the first in which a polypeptide chain could be traced de novo, but it is a particularly complex and elaborate one. Indeed, the cryo-EM density map of Liu *et al*. appears to be substantially clearer and more interpretable than the x-ray density map of Reddy *et al*. Several other icosahedral virus structures have shown that cryo-EM single-particle analysis now rivals x-ray crystallography when applied to large, homogeneous, highly symmetric objects (*12*–*14*). It can be argued that only conquerable computational barriers now prevent extension to less symmetric structures, although rigidity and conformational homogeneity (qualities experimentally selected when growing crystals) will continue to be important (*14*). The new results thus use frontier technologies of structural biology to advance basic and applied virology.

References

1. A. J. Berk, in *Fields Virology*, D. M. Knipe, P. M. Howley, Eds. (Lippincott Williams & Wilkins, Philadelphia, 2007), pp. 2356–2395.
2. S. D. Saban, M. Silvestry, G. R. Nemerow, P. L. Stewart, *J. Virol.* **80**, 12049 (2006).
3. V. S. Reddy, S. K. Natchiar, P. L. Stewart, G. R. Nemerow, *Science* **329**, 1071 (2010).
4. H. Liu *et al., Science* **329**, 1038 (2010).
5. J. J. Rux, P. R. Kuser, R. M. Burnett, *J. Virol.* **77**, 9553 (2003).
6. C. Zubieta, G. Schoehn, J. Chroboczek, S. Cusack, *Mol. Cell* **17**, 121 (2005).
7. M. J. van Raaij, A. Mitraki, G. Lavigne, S. Cusack, *Nature* **401**, 935 (1999).
8. D. Xia, L. J. Henry, R. D. Gerard, J. Deisenhofer, *Structure* **2**, 1259 (1994).
9. R. A. Crowther, R. M. Franklin, *J. Mol. Biol.* **68**, 181 (1972).
10. S. C. Harrison, in *Fields Virology*, D. M. Knipe, P. M. Howley, Eds. (Lippincott Williams & Wilkins, Philadelphia, 2007), pp. 59–98.
11. D. M. Roberts *et al*., *Nature* **441**, 239 (2006).
12. X. Zhang *et al*., *Proc. Natl. Acad. Sci. U.S.A.* **105**, 1867 (2008).
13. X. Yu, L. Jin, H. Zhou, *Nature* **453**, 415 (2008).
14. M. Wolf, R. L. Garcea, N. Grigorieff, S. C. Harrison, *Proc. Natl. Acad. Sci. U.S.A.* **107**, 6298 (2010).

10.1126/science.1194922

BACKGROUND IMAGE COURTESY OF HONG ZHOU/UNIVERSITY OF CALIFORNIA, LOS ANGELES

Downloaded from www.sciencemag.org on August 27, 2010

Published by AAAS

SPORE* SERIES WINNER

The Universe Online

Data from the Sloan Digital Sky Survey can be used by students, teachers, and the public to contribute to scientific research.

M. Jordan Raddick† and Alexander S. Szalay

Modern science is advancing at an unprecedented rate, and the amount of scientific data is doubling every year (*1*). These data have sparked a revolution in the way astronomy is practiced. No longer are scientists forced to wait months for access to a telescope to learn about the night sky; instead, entire research projects can be accomplished with online data sources. Representing modern astronomy, the Sloan Digital Sky Survey (SDSS) has made its entire data set available through an online portal for public use as an educational resource and to invite volunteer contributions to scientific research.

The SDSS (*2*, *3*) has worked since 1991 to create a map of the universe and is the astronomy equivalent of the Human Genome Project. The dedicated 2.5-m-diameter telescope in New Mexico used a 120-megapixel camera to image more than one-quarter of the entire night sky, 1.5 square degrees of sky at a time, about eight times the area of the full Moon, both inside and outside of the Milky Way, and has created a three-dimensional (3D) map of the brightest one million galaxies and quasars. A pair of spectrographs fed by optical fibers measured spectra of, and hence distances to, more than 600 galaxies and quasars in a single observation. A custom-designed set of software pipelines kept pace with the enormous data flow from the telescope (see the first figure).

The SDSS's Web site (www.sdss.org) provides the main access portal to all the information about the project. It contains an introduction to the science enabled by the survey, such as the discovery of the most distant quasars and the creation of the most detailed map of the galaxy distribution, as well as a series of press releases describing key new results.

The SDSS has been successful in generating new scientific discoveries, including measurements of thousands of asteroids (*4*), maps of the complicated merger history of the outer Milky Way (*5*), and the first detection of the baryon acoustic peak; a measurement of how structure formed in the early universe (*6*). A search of the Astrophysics Data System (http://adsabs.harvard.edu) shows over 3000 papers with "Sloan Digital Sky Survey" in the title or abstract, resulting in more than 100,000 citations. The series of discoveries resulting from the SDSS will continue for many years to come as an extension of the survey has been implemented.

All data used to make these discoveries, describing more than 350 million stars and galaxies, are available to students, teachers, and the public through the SDSS's SkyServer database and its Web-based interface (http://skyserver.sdss.org). The site includes many different tools for visually exploring and searching the data. The Navigate tool allows users to navigate through the sky in a Mapquest-like interface. Users can pan through the sky, zoom in and out, and click on stars and galaxies for more information, such as that star's or galaxy's position in the sky and its magnitude (brightness). Links to the "Quick Look" and "Explore" tools from the Navigate tool allow users to examine complete SDSS data on any object. The images used by these tools were built from the 2.5 trillion pixels of original raw data.

The Search Form tool has a more traditional approach; users select from a series of menus to search the database. For example, users can search for stars at a given position in the sky, or they can search for galaxies brighter than a certain limit. Users can also enter queries to the database in Structured Query Language directly, which allows more flexible and sophisticated searches.

SkyServer also has a multiuser collaborative environment, called CasJobs (http://casjobs.sdss.org/casjobs), which enables users to launch extensive analyses. Users can store and share their (sometimes very large) intermediate results on the SDSS server and also form efficient collaborations. CasJobs also makes automatic notes on the ad hoc analysis steps the users performed, which can later be recalled. Much of the technical descriptions and facts about the SDSS and the data presented are closely linked to the data itself by an extensive automated documentation framework that describes the details of the data, the units, and the links between different data items. This documentation can be found on both SkyServer and on the SDSS's main Web site.

The data and access that SkyServer offers present an opportunity for students, teachers, and the public to learn about astronomy and other sciences. This has implications for the way students learn about science, as education research studies show that engagement with the authentic process of science is a key component of science learning (*7*, *8*). Because of the expense and paucity of access to the large

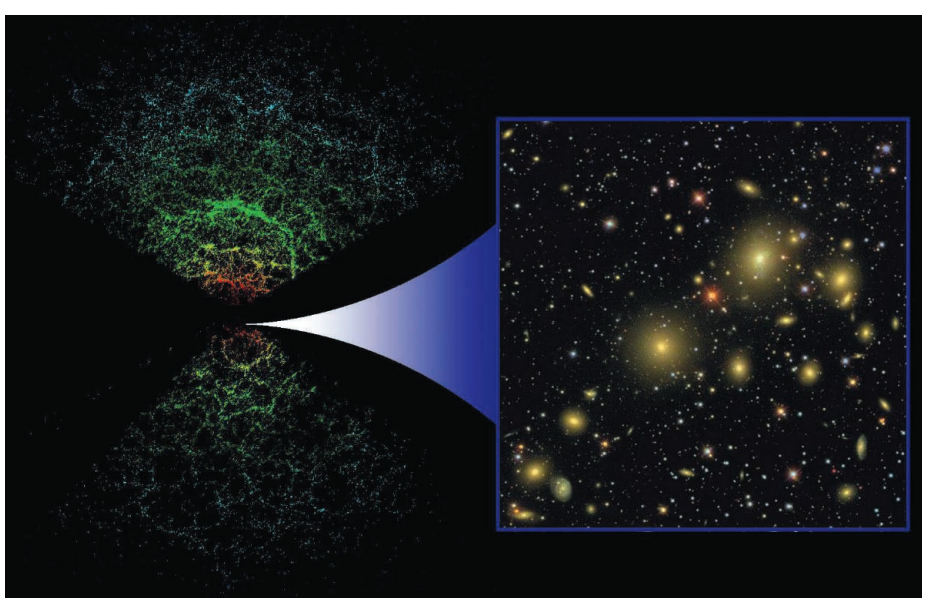

The SDSS is two separate surveys in one. Galaxies are identified in 2D images (right), then have their distances determined from their spectra to create a 2 billion light-years-deep 3D map (left) where each galaxy is shown as a single point, its color representing its luminosity.

CREDIT: BILL KEEL

Department of Physics and Astronomy, The Johns Hopkins University, Baltimore, MD 21218, USA.

*SPORE, *Science* Prize for Online Resources in Education; www.sciencemag.org/special/spore/. †Author for correspondence. E-mail: raddick@jhu.edu

Downloaded from www.sciencemag.org on August 27, 2010

Published by AAAS

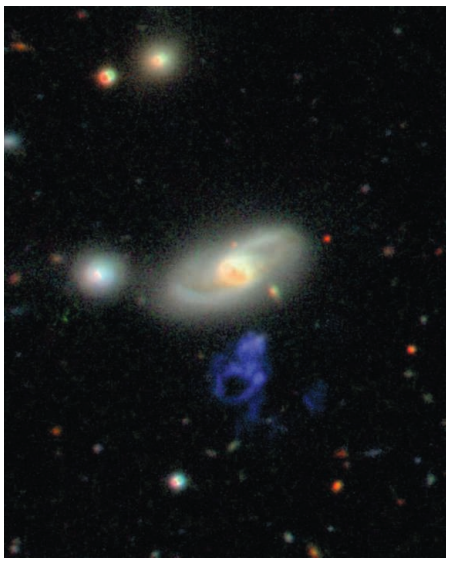

Hanny's Voorwerp. The mass (shown here in purple) is a new class of cosmic object discovered by a Dutch schoolteacher, an astronomy novice, while using Galaxy Zoo.

telescopes, telescope time has usually been reserved for leading scientists, and learners have largely been excluded from direct and active engagement with astronomy. But now, with access to the visual data that SkyServer offers, anyone with Internet access can interact with the data just as the scientists do.

To help enable the use of scientific data in the classroom, SkyServer also features a series of science projects for middle school, high school, and college students (*9*). With these projects, students can re-create major discoveries from the history of astronomy: They can understand why stars have different colors, can classify stellar spectra, or can create a Hubble diagram to show that the universe is expanding. Most projects include Excel spreadsheet templates so that students can analyze the data they find with tools they already know how to use.

The projects were designed by the science writer who developed the rest of the Web site, in collaboration with middle and high school science teachers, in order for the projects to have the same look and feel as the rest of the site. Each project took 2 to 4 months to create. Projects were developed iteratively; the design cycle began with discussions between the teachers and the science writer, and then they would trade drafts of the lesson plans. Web developers also worked to improve online tools using feedback from teachers. The projects require extensive use of the SDSS and various tools for analysis. All projects are linked to Project 2061 *Benchmarks for Science Literacy* (*10*).

SDSS science projects have been used by high schools, colleges, and self-paced learners throughout the world. As of 2006, the projects had registered 297,000 Web sessions, defined as a continuous stream of mouse clicks for more than 30 s, equivalent to providing 47,000 hours of instruction (*11*). As of June 2010, the projects have more than 25 million Web hits and more than a million different individual devices (Internet Protocol addresses) were accessing the data.

Access to SDSS data is not limited to the SDSS and SkyServer Web sites, however. The Web service that the Navigate tool is based on, ImgCutout (*12*), delivers SDSS data to a variety of other tools, including Microsoft's World Wide Telescope (www.worldwidetelescope.org) and Google Sky (www.google.com/sky). Both tools allow users to start with a view of the entire night sky and zoom in to a specified object, such as the Eagle Nebula, and include many other data sources besides the SDSS.

Another project that SDSS data access has enabled is a "citizen science" Web site, Galaxy Zoo (www.galaxyzoo.org), where Internet volunteers have classified galaxies on the basis of their SDSS images (*13*). Galaxy Zoo now uses data from the Hubble Space Telescope. Galaxy Zoo discoveries based on SDSS data have included a determination of the relation between the morphology of galaxies and their environment (*14*) and the observation that galaxies close to one another tend to have aligned spin directions (*15*). None of these discoveries would have been possible without the participation of thousands of Galaxy Zoo volunteers, who have visually classified over 40 million galaxies, a task too large for a small number of individuals. Galaxy Zoo volunteers are also using SDSS data to conduct their own creative scientific research. A comment on the Galaxy Zoo forum by a Dutch schoolteacher led to the identification of a unique object, Hanny's Voorwerp, which proved to be an astronomical object of unknown nature and remains the object of active astrophysical research (*16*) (see the second figure). Further investigation on SkyServer by volunteers led to the discovery of a new class of star-forming galaxies (*17*).

SkyServer tools allow students, teachers, and the public to view astronomy data. SkyServer projects allow learners to use these data to recreate famous discoveries in modern astronomy, such as detecting the expansion of the universe. Other interfaces, such as Google Sky and World Wide Telescope, permit the public to view SDSS data in relation to other astronomical data sets. Galaxy Zoo allows online volunteers to contribute to the advancement of science. Together, these sites are tapping into the hunger and enthusiasm of members of the general public to engage with scientific research, and are helping to make science more democratic.

About the Authors

M. Jordan Raddick is an education and public outreach specialist in the Department of Physics and Astronomy of the Johns Hopkins University. He also maintains the SkyServer Web site of the Sloan Digital Sky Survey and the virtualobservatory.org Web site of the National Virtual Observatory.

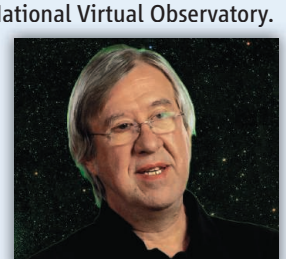

Alexander S. Szalay is a professor of Physics and Astronomy of the John Hopkins University with an interest in theoretical astrophysics and galaxy formation.

CREDITS: (TOP) MIKE EVANS (BOTTOM) LEFT, M. JORDAN RADDICK; RIGHT, JOHN PATZER

References and Notes

1. J. Gray *et al.*, *SIGMOD Rec.* **34**, 34 (2005).
2. M. Lemonick, *Discover* (March 2009); http://discovermagazine.com/2009/mar/06-world.s-hardest-working-telescope/.
3. D. York *et al.*, *Astron. J.* **120**, 1579 (2000).
4. Z. Ivezi *et al.*, *Astron. J.* **122**, 2749 (2001).
5. V. Belokurov *et al.*, *Astrophys. J.* **642**, L137 (2006).
6. D. J. Eisenstein *et al.*, *Astrophys. J.* **633**, 560 (2005).
7. J. D. Bransford, A. L. Brown, R. R. Cocking, *How People Learn: Brain, Mind, Experience, and School* (*Expanded Edition*) (National Academies Press, Washington, DC. 2000).
8. S. Michaels, A. W. Shouse, H. A. Schweingruber, *Ready, Set, Science!: Putting Research to Work in K–12 Classrooms* (National Academies Press, Washington, DC, 2008).
9. R. Sparks, C. Stoughton, M. J. Raddick, *Astronom. Soc. Pacific Conf. Ser.* **319**, 394 (2004).
10. American Association for the Advancement of Science, *Benchmarks for Science Literacy: Project 2061* (Oxford Univ. Press, New York, 1993).
11. J. Gray *et al.*, *SIGMOD Rec.* **34**, 34 (2005).
12. M. Nieto-Santisteban, A. Szalay, J. Gray, *ADASS XIII Astronom. Soc. Pacific Conf. Ser.* **314**, 666 (2004).
13. C. J. Lintott *et al.*, *Mon. Not. R. Astron. Soc.* **389**, 1179 (2008).
14. S. P. Bamford *et al.*, *Mon. Not. R. Astron. Soc.* **393**, 1324 (2009).
15. A. Slosar *et al.*, *Mon. Not. R. Astron. Soc.* **392**, 1225 (2009).
16. C. J. Lintott *et al.*, *Mon. Not. R. Astron. Soc.* **399**, 129 (2009).
17. C. Cardamone *et al.*, *Mon. Not. R. Astron. Soc.* **399**, 1191 (2009).

10.1126/science.1186936

Downloaded from www.sciencemag.org on August 27, 2010

Published by AAAS

SCIENCE DIPLOMACY

Scientists, Educators Chart Course For Haiti's Future Prosperity

SAN JUAN, PUERTO RICO—As Haiti struggles to recover from a shattering January earthquake, a grassroots, multinational team of scientists, educators, and business leaders is developing a plan that sets science and education as a foundation for rebuilding and future growth.

Under a framework that emerged from a workshop organized by the AAAS Caribbean Division, Haiti's science and technology capacity would be systematically built through Haitian policy, new investment, and international collaboration. While specific recommendations are still taking shape, they will range from rebuilding laboratories and improving school materials to ensuring that Haitian development policy is informed by the latest environmental science.

"These recommendations are being shaped by Haitians who have a ground-level view of current conditions and future needs," said Caribbean Division President Jorge Colón. "It's important that they lead the effort, since any role that science and science education will play in the reconstruction of Haiti should be based on Haiti's development goals. But it is clear that support from the science community in the Caribbean and beyond will be important for success."

"The shortcomings of science education and the science culture in Haiti help explain the extraordinary scope of damage caused by the earthquake," said Fritz Deshommes, vice rector of research at l'Université d'État d'Haiti. "Now we desperately need to integrate science into the process of reconstruction and renewal. For that reason, the workshop was very important—it will help build the scientific community in Haiti and strengthen bonds with the regional and global scientific community."

Workshop organizers and participants already have shared preliminary recommendations with key science and education leaders in Haiti, Puerto Rico, and the United States. A final report is expected in late summer or early fall.

The workshop—held 10 to 12 July in Puerto Rico and 15 to 18 July in Haiti—appears to have been the first meeting of its kind since 12 January, when the impoverished nation was rocked by a 7.0 magnitude earthquake. The quake killed more than 300,000 Haitians and injured 300,000 more; some 1.5 million people were left homeless.

The AAAS Center for Science Diplomacy joined the Caribbean Division in sponsoring the workshop. Additional support was provided by the University of Puerto Rico (UPR), the College of Natural Resources at the University of Idaho, and the Association of American Geographers (AAG).

The Puerto Rico portion of the workshop convened 10 scientists, educators, business executives, and policy experts from Haiti and the Haitian diaspora, along with 12 colleagues from Puerto Rico, the United States, Canada, and Rwanda.

Haitian speakers set the context, describing the science-related challenges facing their country, the destruction of laboratories and education facilities, and the potential for rebuilding and expanding science capacity. U.S. and Puerto Rican scholars discussed such issues as earthquake recovery, land use, and reforestation.

Thus far, participants said, the Haitian government's recovery plans have not set science and science education as priorities. In subsequent sessions, they developed more than 30 preliminary goals and recommendations.

The most overarching goal: build Haitian science capacity to address specific Haitian challenges. New investment would be needed in science education, research, and information technology to further Haiti's sustainable development and prosperity.

Other initiatives could establish an association of Haitian scientists, build understanding of science among the Haitian public and political leaders, and develop international research collaborations aligned with Haiti's sustainable development goals.

Jean McKendry, a senior researcher at AAG, and Gary Machlis, a professor of conservation at the University of Idaho, joined Colón in presenting the preliminary results as the workshop reconvened in Port-au-Prince.

They met with the Haitian presidential commissions on education and technology, information, and communication, and with groups of working scientists and school principals. At each meeting, they gathered suggestions for refining the preliminary recommendations.

"The challenges of rebuilding Haiti are extraordinary—and so are the Haitian scientists, science teachers, and university leaders," Machlis said. "If the science and education communities in the Caribbean, the United States and other areas can match their commitment, the partnerships emerging from this workshop can produce great progress."

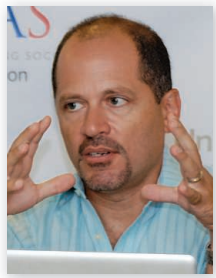

Rebuilding and renewal. Among those at the workshop on Haitian science were (clockwise from top left): Nadine Francis, a Haitian chemist who works in water purification; AAAS Caribbean Division President Jorge Colón; Evens Emmanuel, dean of science and engineering at Quisqueya University in Haiti; and Gary Machlis, a professor of conservation at the University of Idaho.

2009 Annual Report

Download the report at www.aaas.org/publications/annual_report/.

Downloaded from www.sciencemag.org on August 27, 2010

AAAS AWARDS

Nominations Needed for Public Engagement Award

The need for effective science communicators is clear, as science-based issues such as climate change, stem cell research, synthetic biology, neuroscience, and evolution become social and political flashpoints. Yet, traditional reward systems such as tenure and grants typically have not recognized efforts to build constructive public engagement with science and technology.

In response, a new AAAS Early Career Award for Public Engagement with Science has been established to recognize such efforts and to "send a powerful message about the value of science communication activities," said AAAS CEO and *Science* Executive Publisher Alan I. Leshner.

The award, intended to encourage a lifelong commitment to science communication, was initiated by Bob and Margee Hazen and quickly garnered support from other donors, including Leshner and his wife Agnes, *Science* Editor-in-Chief Bruce Alberts and wife Betty, and the Gordon and Betty Moore Foundation. The Noyce Foundation has contributed support for a special video featuring the award winner.

Bob Hazen, a mineralogist and science-literacy champion, said that promoting public engagement can be "a balancing act" for many researchers who must fit communication efforts into a lengthy list of priorities dominated by research, publication, and teaching.

Yet, communicating research results and engaging with nonscientists are keys to building a broad base of support for science. "Our research funding often depends on public support," noted Hazen, who has published an array of popular science books, many in collaboration with his spouse Margee, a writer and historian of science. "Our ability to make ourselves relevant and have society listen to us on issues related to the environment, the economy, health, defense, and safety depends on our effectiveness as communicators."

Identifying additional reward systems for early career scientists is essential, Alberts said. Those researchers "are often especially effective as ambassadors of science"—leveraging their energy and enthusiasm to make technical information accessible to nonscientists.

Nominations for the award will be accepted through 15 October, reported AAAS Public Engagement Manager Tiffany Lohwater. "The award will recognize outstanding efforts to promote interactive dialogue between scientists and nonscientific, public audiences," she explained. "Eligible efforts might include, for instance, informal science education, public outreach, mass media communication, science cafés, exhibits, effective use of social media, or a host of other activities."

Including a $5000 prize and support to attend the 2011 AAAS Annual Meeting, the award is open to individual early career scientists and engineers who have been working in their current field for less than 7 years (at a pre-tenure or equivalent level).

Science communicators. Bob Hazen, a researcher and author, and his wife Margee Hazen, a writer and science historian, initiated the new AAAS Early Career Award for Public Engagement with Science, with other donors.

Nominations will be independently reviewed by a selection committee including Bob Hazen of the Carnegie Institution for Science's Geophysical Laboratory and George Mason University; May R. Berenbaum of the University of Illinois at Urbana-Champaign; Robert Fri of Resources for the Future; Juan Gilbert of Clemson University; Bruce Lewenstein of Cornell University; Nalini Nadkarni of Evergreen State College; and past AAAS President James J. McCarthy of Harvard University.

See www.aaas.org/go/PESaward for details regarding award eligibility and nominations. To support the award endowment, go to www.aaas.org/makeagift, or contact AAAS Development Director Juli Staiano at jstaiano@aaas.org, (202) 326-7028.

—Ginger Pinholster

PROJECT 2061

Classroom Innovation Planned in Chemistry, Biochemistry

Learning about chemical reactions is essential for advanced chemistry studies and, increasingly, to understand the chemistry of life itself. But test scores and other evidence show that many U.S. middle and high school students struggle to understand even basic chemical reactions such as oxidation or photosynthesis.

Now, with a $2.4 million grant from the U.S. Department of Education, AAAS's Project 2061 and the Biological Sciences Curriculum Study (BSCS) are embarking on a project to develop chemistry and biochemistry materials for middle school students and teachers, based on the latest research in learning.

Jo Ellen Roseman, director of the long-term science literacy project, said improved ways of teaching how atoms and molecules behave in chemical reactions will prepare students for more advanced classes in high school and college. At the same time, she said, it will give them a foundation for understanding climate change, alternative energy sources, the uses of nanotechnology, and other science topics that are already the focus of policy debate.

Each unit "will organize the scientific ideas into a coherent story for teachers and students," said Roseman. "The scientific ideas will be more likely to be…tied together and linked to carefully chosen phenomena and representations."

The materials will be designed and tested over the next 3 years at schools in Colorado, Maryland, Massachusetts, and Washington, D.C., in classrooms involving 18 teachers and nearly 2000 students.

The grant was issued by the National Center for Education Research in the Department of Education's Institute of Education Sciences.

CREDIT: PHOTO COURTESY OF BOB AND MARGEE HAZEN

Downloaded from www.sciencemag.org on August 27, 2010

Published by AAAS

CoRoT Reveals a Magnetic Activity Cycle in a Sun-Like Star

Rafael A. García,[1]* Savita Mathur,[2] David Salabert,[3,4] Jérôme Ballot,[5] Clara Régulo,[3,4] Travis S. Metcalfe,[2] Annie Baglin[6]

Our understanding of and capability to predict the 11-year activity cycle of the Sun (*1*), which is driven by a dynamo process seated at the bottom of the convective zone, is far from being complete, as suggested by the recent unusually long solar minimum of cycle 23 (*2*, *3*). Observations of magnetic activity cycles in other stars can potentially improve our knowledge of dynamo processes because they allow us to sample different physical conditions distinct from those in the Sun. Although many stars exhibit activity cycles and some empirical relations have been found (*4*), a detailed knowledge of the internal structure and dynamics of the star—in particular, the depth of the convective envelope and the degree of differential rotation—is required to improve the constraints on theory. Here, we show how asteroseismology has revealed the signature of a magnetic activity cycle in a Sun-like star.

Helio- and asteroseismology are the only tools available that can probe the structure and dynamics of the Sun and stars through the study of acoustic oscillations (*5*). The oscillation modes are sensitive to variations in the magnetic field, and their characteristics change throughout the activity cycle. In the Sun, for instance, the oscillation frequencies are shifted higher during solar maximum while the amplitudes decrease, showing anticorrelated temporal variations (*6*–*9*).

The Convection Rotation and Planetary Transits (CoRoT) mission has so far observed six main-sequence stars exhibiting solarlike oscillations during more than 130 days each as part of its asteroseismic program (*10*). One of these stars is HD49933, an F5V star 20% more massive and 34% larger than the Sun. It has been observed twice, for 60 days in 2007 and 137 days in 2008, spanning a total of 400 days. More than 50 individual acoustic modes have been identified (*11*, *12*) and then used to model the stellar interior [for example, (*13*)]. Its rotation period is 3.4 days (8 to 9 times faster than the Sun).

To search for the effects of magnetic activity in this star, we measured the variation of the mode amplitude and the frequency shift of the acoustic-mode envelope (*7*). As observed in the Sun, there is an anticorrelated temporal variation between both parameters (Fig. 1), revealing a modulation in the second epoch that seems to indicate a period of at least 120 days related to the internal magnetic activity of HD49933. The observations agree with the scaling proposed by (*8*), which predicts larger-than-solar frequency shifts for stars that are hotter and more evolved, in contradiction to the scaling suggested by (*9*). The long-period variations detected in the luminosity of the star, interpreted as fluctuations in the positions and sizes of starspots, allow us to also study the surface activity (*7*). Indeed, the starspot signature changes with time, showing a quiet period during the first part of the second set of observations (Fig. 1). This confirms the existence of an activity cycle, which seems to be shifted in time compared with the seismic indicators. Lastly, medium resolution spectra of the calcium H and K lines obtained on 13 April 2010 confirm that HD49933 is an active star with a Mount Wilson S index of 0.3 (*7*). Asteroseismology has thus revealed a stellar activity cycle analogous to that of the Sun.

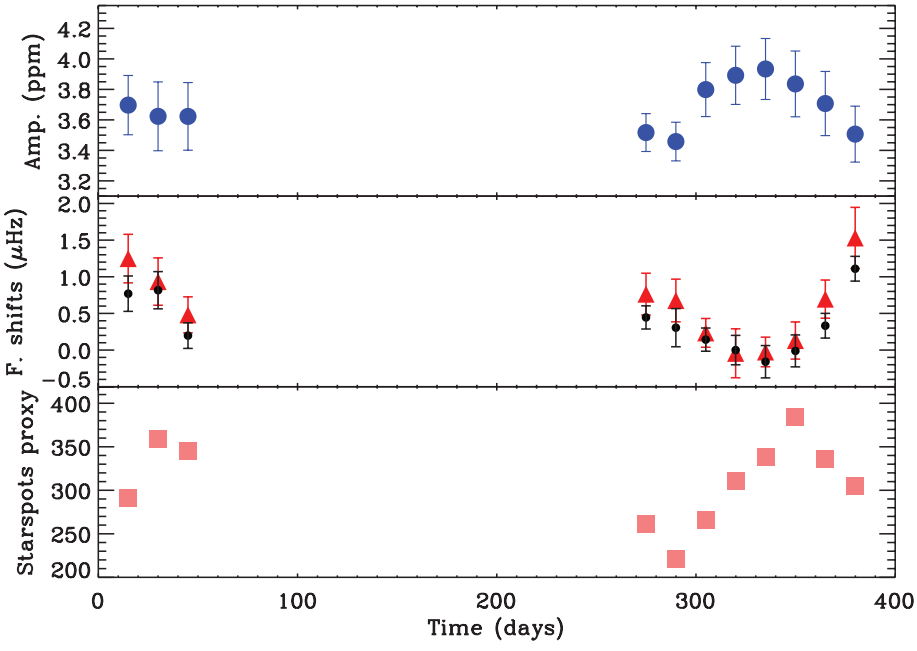

Fig. 1. Time evolution beginning 6 February 2007 of the mode amplitude (**top**); the frequency shifts using two different methods (**middle**), cross correlations (red triangles) and individual frequency shifts (black circles); and a starspot proxy (**bottom**) built by computing the standard deviation of the light curve (*7*). All of them were computed by using 30-day-long subseries shifted every 15 days (50% overlapping). The corresponding 1σ error bars are shown.

References and Notes

1. P. Charbonneau, *Living Rev. Solar Phys.* **2**, 2 (2005).
2. D. Salabert, R. A. García, P. L. Pallé, S. J. Jiménez-Reyes, *Astron. Astrophys.* **504**, L1 (2009).
3. S. C. Tripathy, K. Jain, F. Hill, J. W. Leibacher, *Astrophys. J.* **711**, L84 (2010).
4. S. L. Baliunas *et al.*, *Astrophys. J.* **438**, 269 (1995).
5. D. O. Gough *et al.*, *Science* **272**, 1296 (1996).
6. S. J. Jiménez-Reyes, W. J. Chaplin, Y. Elsworth, R. A. Garcia, *Astrophys. J.* **604**, 969 (2004).
7. Materials and methods are available as supporting material on *Science* Online.
8. T. S. Metcalfe, W. A. Dziembowski, P. G. Judge, M. Snow, *Mon. Not. R. Astron. Soc.* **379**, L16 (2007).
9. W. J. Chaplin, Y. Elsworth, G. Houdek, R. New, *Mon. Not. R. Astron. Soc.* **377**, 17 (2007).
10. E. Michel *et al.*, *Science* **322**, 558 (2008).
11. T. Appourchaux *et al.*, *Astron. Astrophys.* **488**, 705 (2008).
12. O. Benomar *et al.*, *Astron. Astrophys.* **507**, L13 (2009).
13. L. Piau, S. Turck-Chièze, V. Duez, R. F. Stein, *Astron. Astrophys.* **506**, 175 (2009).

14. The CoRoT space mission has been developed and is operated by CNES, with contributions from Austria, Belgium, Brazil, European Space Agency (Research Science Support Department and Science Program), Germany, and Spain. This work has been partially supported by the Spanish National Research Plan (grant PNAyA2007-62650) and by the "Programme National de Physique Stellaire" at CEA/Saclay. NCAR is supported by NSF.

Supporting Online Material

www.sciencemag.org/cgi/content/full/329/5995/1032/DC1
Materials and Methods
Figs. S1 to S4
References

19 April 2010; accepted 15 July 2010
10.1126/science.1191064

[1]Laboratoire Astrophysique, Instrumentation, et Modélisation, CEA/Direction des Sciences de la Matière–CNRS, Université Paris 7 Diderot, Institut de Recherche sur les Lois Fondamentales de l'Univers/Service d'Astrophysique, Centre de Saclay, 91191 Gif-sur-Yvette, France. [2]High Altitude Observatory, National Center for Atmospheric Research (NCAR), Post Office Box 3000, Boulder, CO 80307, USA. [3]Instituto de Astrofísica de Canarias, 38200 La Laguna, Tenerife, Spain. [4]Departmento de Astrofísica, Universidad de La Laguna, 38206 La Laguna, Tenerife, Spain. [5]Laboratoire d'Astrophysique de Toulouse-Tarbes, Université de Toulouse, CNRS, 31400 Toulouse, France. [6]Laboratoire d'études spatiales et d'instrumentation en astrophysique, UMR8109, Université Pierre et Marie Curie, Université Denis Diderot, Observatoire de Paris, 92195 Meudon Cedex, France.

*To whom correspondence should be addressed. E-mail: Rafael.Garcia@cea.fr

Downloaded from www.sciencemag.org on August 27, 2010

The Dynamics of Plate Tectonics and Mantle Flow: From Local to Global Scales

Georg Stadler,[1] Michael Gurnis,[2]* Carsten Burstedde,[1] Lucas C. Wilcox,[1]†
Laura Alisic,[2] Omar Ghattas[1,3,4]

Plate tectonics is regulated by driving and resisting forces concentrated at plate boundaries, but observationally constrained high-resolution models of global mantle flow remain a computational challenge. We capitalized on advances in adaptive mesh refinement algorithms on parallel computers to simulate global mantle flow by incorporating plate motions, with individual plate margins resolved down to a scale of 1 kilometer. Back-arc extension and slab rollback are emergent consequences of slab descent in the upper mantle. Cold thermal anomalies within the lower mantle couple into oceanic plates through narrow high-viscosity slabs, altering the velocity of oceanic plates. Viscous dissipation within the bending lithosphere at trenches amounts to ~5 to 20% of the total dissipation through the entire lithosphere and mantle.

Mantle convection and associated plate tectonics are principal controls on the thermal and geological evolution of the Earth. These processes are central to our understanding of the origin and evolution of tectonic deformation, the evolution of the thermal and compositional states of the mantle, and ultimately the evolution of Earth as a whole. Plate creation and motion largely govern the loss of heat from the solid earth (*1*), and the strength of plates may control the energy dissipation and hence heat loss over geological time (*2*). However, despite the central importance of plate dynamics, there are fundamental uncertainties on the forces resisting and driving plate motions.

Although there is consensus that the 1- to 10-cm-per-year motion of plates is driven largely by the thermal buoyancy within subducted slabs (*3*) and perturbed by upper-mantle solid-solid phase transitions (*4*) and cooling of oceanic lithosphere from ridge to trench, the importance of the aseismic extension of slabs within the lower mantle (*5*) remains unresolved. The strength of subducted slabs probably regulates the velocity of plate tectonics. The vast majority of available negative buoyancy driving plates is within the transition zone and lower mantle, and if slabs are strong, then this force can be coupled directly into the edges of oceanic plates at trenches (*6*). However, if the oceanic lithosphere is strong during initial subduction as it bends below the trench, then the dissipation within the narrow high-viscosity slab could limit plate velocity (*7*). Although the importance of plate margin and slab strength has been studied in two- and three-dimensional Cartesian models aimed at understanding the physics of subduction (*4*, *8*–*11*) and in limited regional models that assimilate observed structure (*12*, *13*), the incorporation of realistic rheologies into models with narrow slabs and plate boundaries has remained an elusive goal of global geodynamics. Whether slabs are weak or strong remains unresolved (*4*).

With the incorporation of strong slabs and realistic treatment of plate margins, the ability to observationally constrain models would increase substantially. Observations constrain the deformation of slabs and will prove useful in global models: Examples include the strain rate and state of stress within slabs from deep focus earthquakes (*14*) and the kinematics of slab rollback in subduction zones with present-day back-arc extension (*15*). Large fractions of Earth's surface (~15% globally) do not follow a rigid plate tectonic model but undergo deformation close to trenches and farther from plate margins (*16*). Some oceanic plates are deforming diffusively within their interiors, especially the Indo-Australian plates (*17*). The rich array of geodetic, topographic, gravitational, and seismic observations from local to regional scales constrains these deformations and could validate global

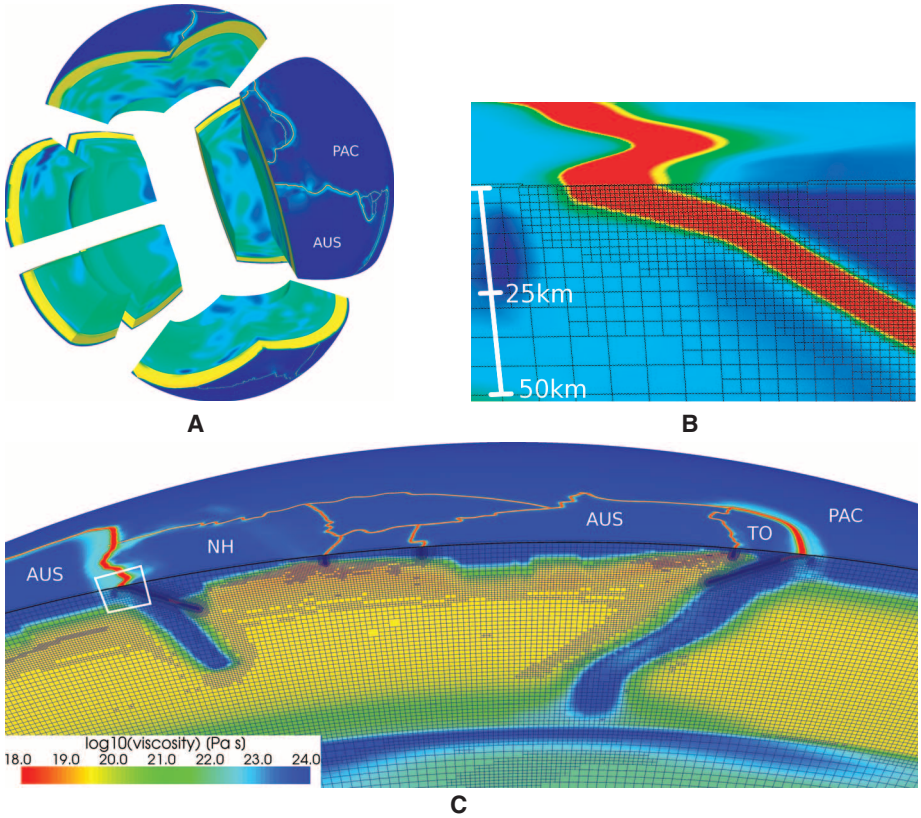

Fig. 1. (**A**) Splitting of Earth's mantle into 24 warped cubes. The effective viscosity field is shown; the narrow low-viscosity zones corresponding to plate boundaries are seen as red lines on Earth's surface. (**B**) Zoom into the hinge zone of the Australian plate [as indicated by the box in (**C**)] showing the adaptively refined mesh with a finest resolution of about 1 km. (C) Cross section showing the refinement that occurs both around plate boundaries and dynamically in response to the nonlinear viscosity, with plastic failure in the region from the New Hebrides to Tonga in the SW Pacific. Plates are labeled Australian, AUS; New Hebrides, NH; Tonga, TO; and Pacific, PAC.

[1]Institute for Computational Engineering and Sciences, The University of Texas at Austin, Austin, TX 78712, USA. [2]Seismological Laboratory, California Institute of Technology, Pasadena, CA 91125, USA. [3]Jackson School of Geosciences, The University of Texas at Austin, Austin, TX 78713, USA. [4]Department of Mechanical Engineering, The University of Texas at Austin, Austin, TX 78712, USA.

*To whom correspondence should be addressed. E-mail: gurnis@caltech.edu

†Present address: HyPerComp, Westlake Village, CA 91361, USA.

Downloaded from www.sciencemag.org on August 27, 2010

dynamics if we are able to capture the commensurate scales in models with realistic rheologies.

Arguably, the biggest limitation on current progress is not observational, but computational: Solution through models that incorporate realistic rheologies and local geological structure has historically been prohibitive because of limitations in numerical methods and computational resources. Taken as a whole, the current generation of models poorly exploits the observational constraints on present-day deformation. For example, models of plate motion do not use observations of deformation at plate margins and interiors because numerical simulation of global mantle convection down to the scale of faulted plate boundaries has been intractable because of the wide range of time and length scales involved. Using adaptive mesh refinement (AMR) on highly parallel computers has allowed us to incorporate realistic rheologies and fine-scale observations in global mantle convection simulations and in turn reach fundamental conclusions about the forces driving the plates and the energy dissipation throughout the solid earth by intimately linking these models to observations.

Parallel adaptive mesh refinement. Capturing the large viscosity variations occurring at plate boundaries requires a mesh with about 1-km local resolution. A globally uniform mesh with 1-km mesh size would require ~10^{12} mesh elements, beyond both the capacity of contemporary supercomputers and the reach of numerical solution methods. With AMR, we achieve 1-km resolution near plate boundaries while using a coarser 5-km resolution within thermal boundary layers (including the oceanic lithosphere) and 15- to 50-km resolution for the rest of the mantle, saving a factor of over 10^3 as compared with a uniform mesh. The resulting reduction in problem size to a few hundred million elements is critical to making the simulations tractable on petascale supercomputers.

However, scaling AMR to thousands of processors is a challenge (*18*). Adaptively refined meshes entail irregular and dynamically changing topological mesh relations, whereas solution on parallel computers makes it necessary to store just a small part of the mesh on each processor. These mesh partitions must be changed after each refinement and coarsening step to ensure that the computational load on individual processors is balanced. We have developed scalable algorithms for these mesh operations as well as numerical solution of the mantle flow equations in our AMR finite element framework (*19*–*21*). Our parallel AMR algorithms are based on a forest of adaptive octrees, in which multiple warped cubes are joined to represent general geometries. The spherical shell used to represent the mantle is composed of 24 cubes (Fig. 1). Each cube is adaptively subdivided by using an octree data structure, which allows for fast algorithms to manage the mesh adaptivity and to construct the mesh connectivity information required in numerical simulations (*22*). These algorithms, which have scaled to over 200,000 processor cores, are applicable to a broad spectrum of multiscale scientific and engineering problems that require high resolution in localized (possibly dynamically evolving) regions, such as near fronts, discontinuities, material interfaces, reentrant corners, and boundary and interior layers.

Rheology and assimilated constraints. We solved for present-day, instantaneous mantle flow

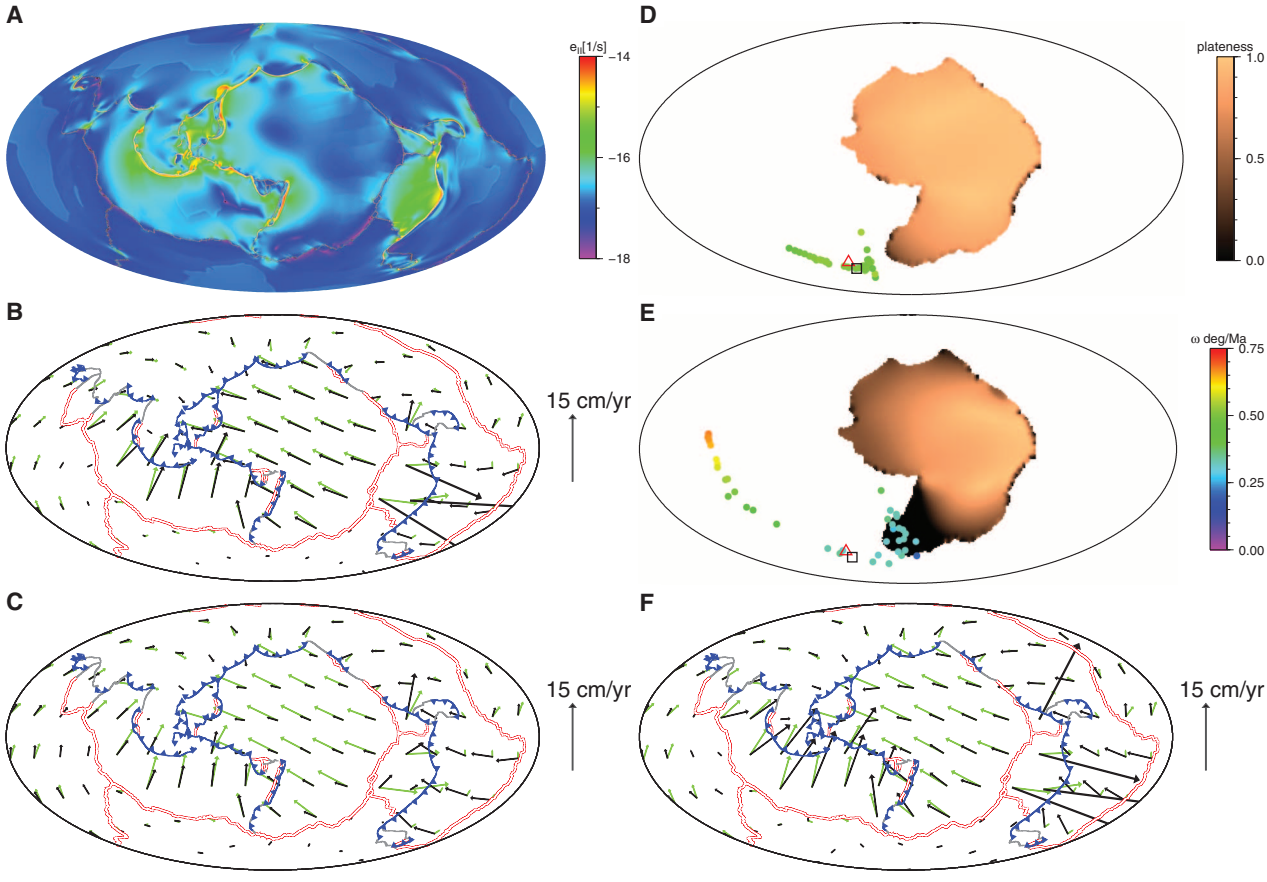

Fig. 2. Strain rate, plate velocities, and plateness for three cases centered at 180°W. (**A**, **B** and **D**) Case 1, with only plate cooling and upper mantle slabs. (**C**) Case 2, identical to case 1 except for lower-mantle lateral structure. (**E** and **F**) Case 4, similar to case 2, except that $n = 3.5$. (A) Second invariant of strain rate. (B), (C), and (F) Plate motions in a NNR from (*27*) as green arrows and predicted velocities as black arrows; actual plate margins are shown as red, gray, and blue symbols. (D) and (E) Plateness for PAC shown in two ways: vector difference between computed velocity and velocity from best-fitting Euler pole, P_2 (*22*), as a raster field with color palette shown to the right of (D); and individually inferred Euler poles within spherical caps (radius 20°) with magnitude of rotation (ω) denoted with color of pole [palette shown to the right of (E)]. The Nuvel1-NNR pole position is shown as a red triangle and best-fitting pole for all computed velocities within PAC as a black square.

Downloaded from www.sciencemag.org on August 27, 2010

as a balance of mass and momentum (Stokes flow), in which flow velocities, strain rate, and state of stress are determined while a distribution of temperature (density) throughout the solid earth is assumed. Diffusion- and dislocation-creep and plastic-yielding govern lithosphere and mantle viscosity. Experimental constraints provide us with the form of the constitutive relation (*22*) and the ranges for uncertain parameters, over which we then vary. With these relations, dislocation-creep dominates in the upper mantle, whereas diffusion-creep is present throughout the whole mantle but dominates deformation in the lower mantle. Plastic-yielding is incorporated and defines a maximum strength of a material.

We incorporated plate margins as narrow zones with reduced viscosity through a spatially dependent prefactor to the constitutive relation, not unlike the approach used by others (*4*). Ridge and transform boundaries are treated as shallow vertical planes with locations from published compilations (*23*). For subduction zones, we used a global synthesis of seismic focal mechanisms for interplate thrust events, constraining a surface that continuously changes shape while following the strike of the plate boundary (*22*). The depth of these zones can extend below the depth of seismic coupling into the mantle wedge because water release from subducting slabs may result in a dipping low-viscosity zone above the slab within the mantle wedge (*24*).

The global models are driven entirely by temperature variations with three components, one based on the thermal age of the surface, a second based on seismicity-defined slabs, and a third on seismic tomography (*22*), which is similar to the input used in recent, lower-resolution models (*25*, *26*). We created upper-mantle structure with seismicity and not with tomography so as to maximize the sharpness of features in the upper mantle. Globally, slabs are too poorly resolved in current tomography models because mantle wedges and slabs often blur together. Resolving the slabs as high-viscosity stress guides is critical for correctly resolving plate motions (*8*).

Plate motions and plateness. Even when the rheology is laboratory-based and mantle structure is seismically constrained, rigid plates are not guaranteed with nonlinear and plastic rheologies. Consequently, besides the traditional use of a single Euler pole for each plate we assessed how closely surface velocities matched that of rigid blocks—that is, the plateness (*22*). However, to fit plate motions we found it necessary to substantially reduce the yield stress (to ~100 MPa) from experimental values, which is not surprising given prior results (*8*). A nominal case with only buoyancy associated with upper-mantle slabs and plate-cooling had plate motions generally matching those in a no-net rotation (NNR) frame of reference (*27*). However, we found large variations in surface viscosity and strain rate on small and large scales, especially near subducting plate boundaries with strain rates varying regionally from ~10^{-14} to ~10^{-17} s^{-1} (Fig. 2A). Bands of high strain rate bound the subducting plate boundary adjacent to a band of low strain rate on the overriding plate. Although globally small (Fig. 2A), these variations are much longer in wavelength than the surface expression of faults between plates. In models in which these dipping zones are comparable in dimension with plate thickness, the subducting plate can flux through the weak zone, which is a common artifact of low-resolution models. Instead, the lithosphere slides by the fault so that viscosity and strain rate of the slab are determined dynamically. Consequently, the nature of coupling between slabs and plates is qualitatively different from previous models. These larger-scale variations in strain rate and viscosity are generated by bending, with the width of the deformation region being dependent on the nonlinear rheology and degree of coupling between subducting slab and deeper mantle (Figs. 3D and 4D).

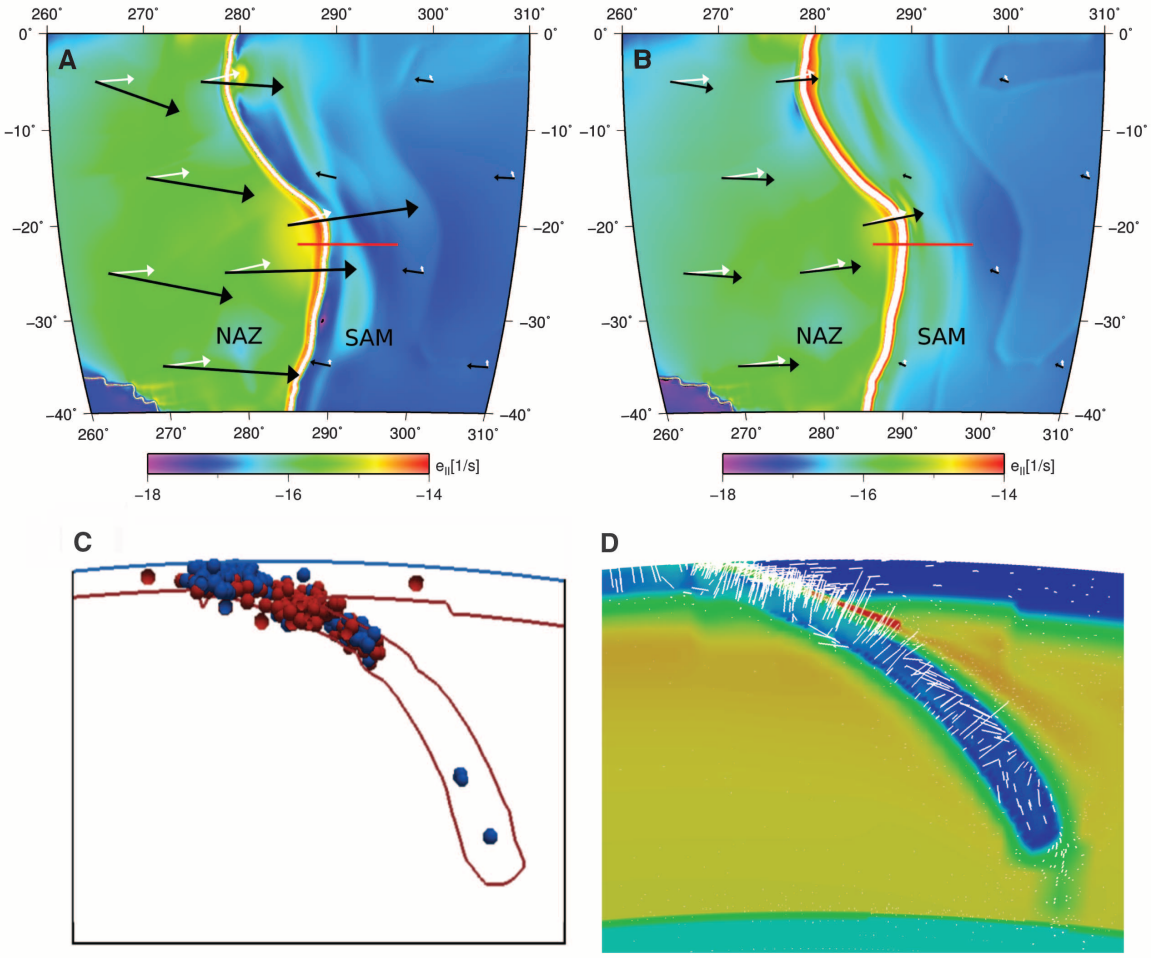

Fig. 3. Velocity vectors and surface strain rate for case 1 in (**A**) and case 6 in (**B**) that show the effect of increasing viscosity in the weak zone within the Columbia, Peru, and Chile trenches. White arrows are from Nuvel1-NNR (*27*), and black arrows are from predictions. Position of cross sections in (**C**) and (**D**) is indicated with red line. (C) Down-dip compression (blue) and down-dip tension (red) from CMT solutions (*22*). (D) Predicted compressional axes for case 6. Plates are labeled Nazca, NAZ, and South America, SAM.

Downloaded from www.sciencemag.org on August 27, 2010

Plate velocities for the nominal case (Fig. 2B) better match observed plate motions as compared with those of linear models (*5*, *28*). The major oceanic plates move faster than the overriding plates so that convergence is asymmetric, unlike symmetric convergence in linear models (*5*, *28*). The complex rheology of slabs allows upper-mantle slabs to pull oceanic plates toward trenches. Although the end result is similar to parametrizations used in linear models (*29*), the pull results from the self-consistent balance between buoyancy and the nonlinear resisting forces in the bending plate and, hence, gives greater insight into the forces driving and resisting plate motion.

When strong slabs embed into the lower mantle, plate motions can change substantially, as evident with the addition of temperature variations in the transition zone and lower mantle inferred from seismic tomography. This addition causes overall mantle flow velocities and most oceanic plate velocities to decrease (Fig. 2, B and C) (*22*), which is a behavior opposite to that expected from a linear system (*5*). In addition, the range in surface strain rate decreases while the plate margins become narrower but higher in viscosity. A combination of slabs penetrating the transition zone and temperature-dependent viscosity within the lower mantle (*22*) are likely causes for these results. A cross section through the Chilean subducting boundary (Fig. 3D) shows a gap in the continuity of high viscosity between slab and lower mantle. When temperature variations in the transition zone and lower mantle are present, the high-viscosity slab embeds into the high-viscosity lower mantle so that the much higher viscosities at depth resist surface tectonic motion (*22*). The presence of lower-mantle structure leads to a breakdown in asymmetric convergence at trenches (Fig. 2C). The inclusion of high-viscosity narrow slabs causes oceanic plates to either speed up or slow down through a much greater coupling with the high-viscosity lower mantle and occurs despite the nonlinearity of slab rheology. This suggests a close balance between plate motions and deep mantle processes.

Conducting searches over the ranges of uncertain parameters in the constitutive relation [activation energy in upper and lower mantle, grain-size, yield stress, and the nonlinear exponent n (*22*)], we were able to achieve rigid plate motions (Fig. 2D). Nearly perfect plate motions with little intraplate strain for the Pacific plate (PAC) can be found, with only the region south of New Zealand experiencing substantial strain. The rigidity of PAC is a sensitive function of the nonlinear rheology; if the nonlinearity is too strong, the plateness of PAC degrades to unacceptable levels. For example, if we combine n = 3.5 and larger activation volumes with lower mantle buoyancy, substantial strain occurs within PAC, resulting in deformation extending >10^3 km from convergent boundaries and widely separated Euler poles for the northern and southern parts of PAC (Fig. 2E). Even though values closer to n = 3.5 are more consistent with experimental work (*30*), we find that intraplate strain increased rapidly for $n > 3$ with platenesses apparently inconsistent with observations. Plateness also improves with smaller viscosities in the upper mantle, which is consistent with generic models (*8*). The Indo-Australian plate separates into two zones with a broad area of deformation (Fig. 2A), which is consistent with observations (*17*); however, the range of platenesses was less sensitive to the nonlinear viscosity than it was for PAC.

Slab deformation and interplate coupling. The nominal model substantially over-predicts the velocity of the Nazca (NAZ) plate toward the east and South America (SAM) toward the west (Fig. 2B). Linear models also predict unrealistic symmetric convergence toward the Peru-Chile trench (*5*, *28*), which is inconsistent with plate kinematics in an NNR frame of reference that shows SAM to be approximately stationary. The addition of the lower-mantle structure as described above degrades the fit as both plates slow down, creating symmetric convergence toward the trench (Fig. 2C). Cross sections through the Nazca slab beneath SAM show that the state of stress is inconsistent with deep focus earthquakes, which indicate that the deepest events are strongly in down-dip compression, whereas events in 200 to 300 km in depth are in tension (Fig. 3C). In the lithosphere, although the subducting plate is in strong tension near the trench, SAM is only in mild compression with the axis of principal compression approximately orientated north-south. Great earthquakes along the Chile trench suggest that this is amongst the most coupled plate boundaries (*31*). By increasing the viscosity of the weak zone between NAZ and SAM (*22*), we simultaneously change the broad-scale plate kinematics and the state of stress in upper-mantle slabs and the overriding plate. Compared with the nominal case, with only plate cooling and slabs, increasing the interplate coupling slows NAZ toward the east, stops the westward motion of SAM, and reorients compression within the

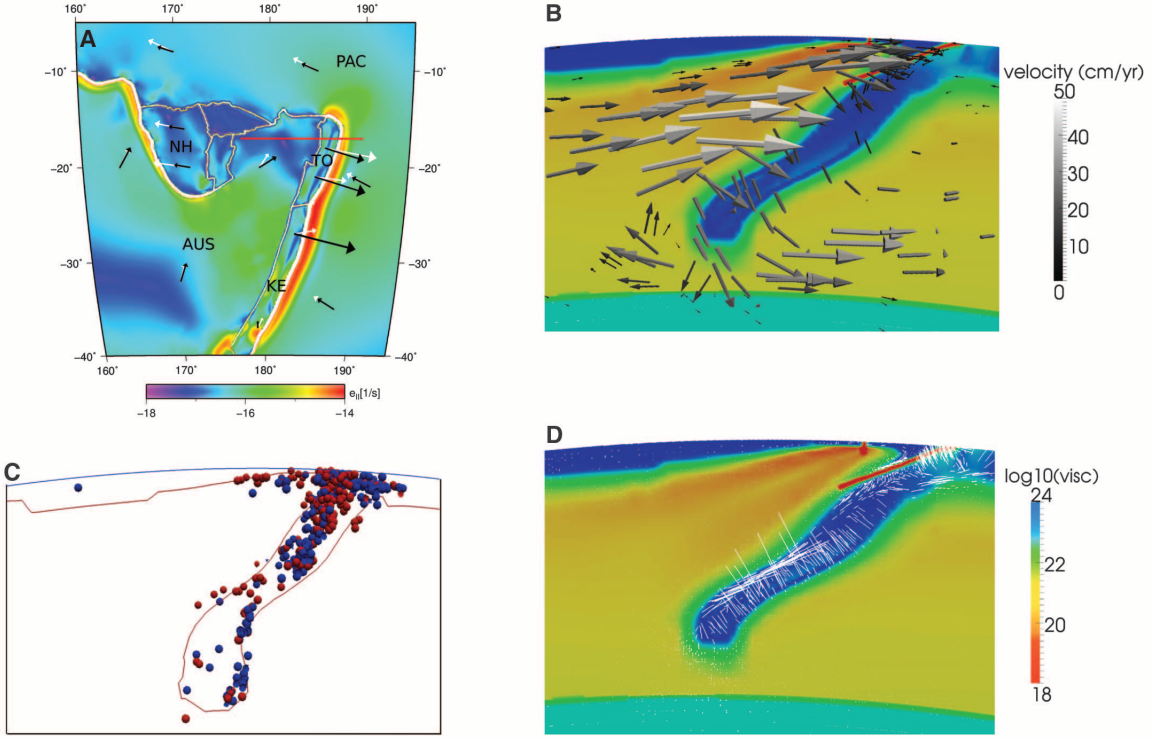

Fig. 4. (**A**) Map of surface strain rate with plate velocities for plates in a NNR frame of reference for the New Hebrides-Tonga region. Predictions are in black and white arrows from Nuvel1-NNR (*27*), with micro-plate motions from (*23*). Plates are labeled Australian, AUS; New Hebrides, NH; Tonga, TO; Kermadec, KE; and Pacific, PAC. Cross-sections in (**B**), (**C**), and (**D**) denoted by red line in (A). (B) Predicted velocity and viscosity. (C) Down-dip compression (blue) and down-dip tension (red) from CMT solutions (*22*). (D) Predicted compressional axes for case 6.

Downloaded from www.sciencemag.org on August 27, 2010

Andes to be strongly east-west (Fig. 3), but otherwise global plate motions remain unchanged.

Besides fitting deformation of ocean-continent boundaries, we find models consistent with deformation, rapid trench rollback, and back-arc extension that characterize some ocean-ocean subduction zones. Predicting such deformation has remained elusive for global and regional models. Although most generic models of trench rollback remove the overriding plate so that hot mantle extends to the surface enveloping the subducting slab (*10*, *11*), our approach includes the overriding plate. We find that the New Hebrides slab with the attendant New Hebrides (NH) plate nearly always rolls back (without penetration into the transition zone, the slab descends vertically into the mantle, pulling the coupled Australian plate). The slab is always in a state of down-dip tension, as observed seismically.

The better known rapid rollback of Tonga-Kermadec with its distinctive down-dip compression within the Benioff zone emerges in some models and may be a sensitive function of the rheological structure within the overriding plate. During the analysis of early simulations, we found that two data sets used to create input conditions—namely, the position of plate boundaries (*23*) and plate age (*32*)—were inconsistent with the ridges not overlapping and that the zone of youngest lithosphere within the Lau Basin and Hauvre Trough was less extensive than thought (*22*). We found that the Kermadec (KE) and Tonga (TO) micro-plates became locked to the Australian (AUS), and the Tonga trench did not roll back even for different n, yield stresses, and upper- and lower-mantle viscosities. However, by aligning the ridges and decreasing the age of the overriding plate to be consistent with regional geology (*22*), KE and TO became decoupled from AUS, allowing the TO-KE trench to rapidly roll back, as indicated by rapid eastward motion of the two micro-plates (Fig. 4A). In detail, KE pivots to the east around an Euler pole near the North Island of New Zealand, as observed.

In addition, the state of stress for models with rapid trench rollback also fits the state of stress from seismic focal mechanisms. The modeled slabs are in down-dip compression in the transition zone, strongly in compression between the transition zone and upper mantle along the top of the slab, but in tension within the hinge zone, all of which is consistent with seismic focal mechanisms (Fig. 4, C to D). Viscosity near the hinge zone is reduced by ~10 times over ~100 km (Fig. 4D) and even more so along the axis of the trench and is consistent with the extreme local reduction in plate rigidity in the Kermadec trench and outer trench wall (*33*). With the low viscosities in the wedge and large pressure gradients near slabs, flow velocities within the mantle wedge are ~5 times higher than that of the slab, which is consistent with a recent regional study (*13*).

Energy dissipation in global models. The location of energy dissipation within the solid earth remains unresolved; some analyses place nearly all dissipation within the hinge zone (*7*, *34*), whereas others do not (*35*, *36*). However, previous models made a priori assumptions about plate motions and hinge zone viscosity. By using seismic focal mechanisms and trench rollback, the state of stress and strain rate can be observationally constrained independently of plate motions.

We find high dissipation (*22*) within slabs, the mantle wedge, and slab regions within the lower mantle (Fig. 5). Within slabs, the highest values of dissipation occur in the hinge zones, but dissipation is high through the entire slab; another local maximum occurs within the transition zone, which is consistent with a peak in energy release from seismicity (*37*). The low-viscosity zone between plates is also a zone of high dissipation. Surprisingly, even though the viscosity is probably very low (*12*), the mantle wedge is a zone of high dissipation (Fig. 5C) because strain rates are high (Fig. 4B) (*13*).

We found a smaller proportion of the dissipation within the hinge zones as compared with the entire mantle and lithosphere. Even when assuming no buoyancy within the lower mantle, the dissipation within the hinge zone is generally less than 20% of the total viscous dissipation within the mantle (*22*). The lower mantle could be a source of substantial dissipation (Fig. 5) (*22*), reaching as high as 70% of the total, depending on the viscosity of the lower mantle and the lateral variations driven by temperature-dependent viscosity. If that is the case, then the dissipation in the hinge zone could be <5%. By considering the whole mantle and lithosphere, in which the hinge zone is one of several components in a tightly coupled system, these estimates are smaller than previous estimates (*7*, *34*) but consistent with recent energetic arguments (*38*).

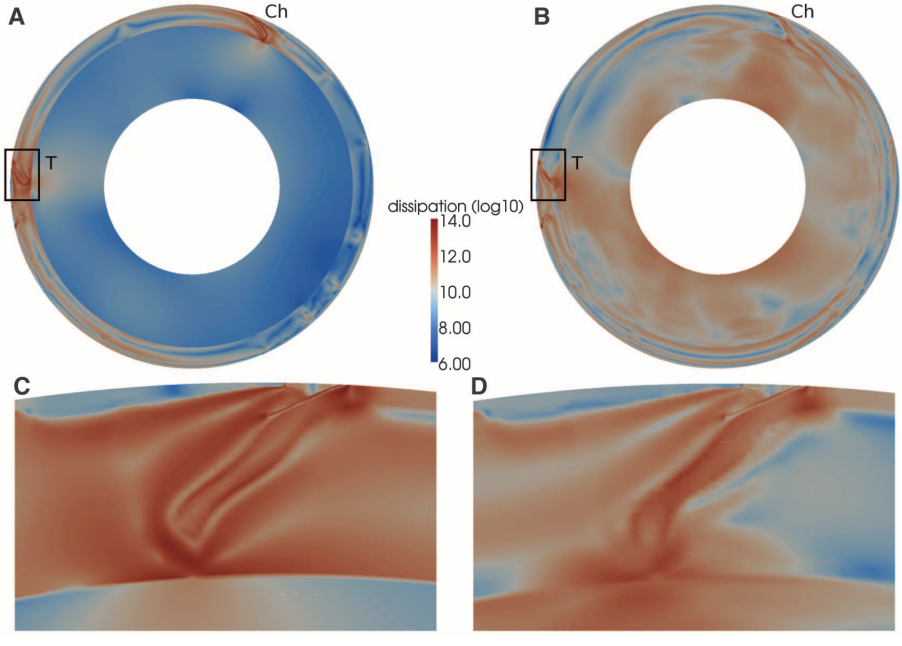

Fig. 5. Pointwise dissipation for models in cross section through small-circle at 17°S for case 6 (without lower-mantle structure) in (**A**) and through Case 8 (with lower-mantle structure) in (**B**). The Tonga area is denoted with the letter T, and the Northern Chile area with letters Ch. (**C**) Zoom-in on the Tonga area for case 6. (**D**) Same zoom-in for case 8.

References and Notes

1. G. F. Davies, *Dynamic Earth: Plates Plumes and Mantle Convection* (Cambridge Univ. Press, Cambridge, 1999).
2. C. P. Conrad, B. H. Hager, *Geophys. Res. Lett.* **26**, 3041 (1999).
3. B. H. Hager, R. J. O'Connell, *J. Geophys. Res.* **86** (B6), 4843 (1981).
4. M. I. Billen, *Annu. Rev. Earth Planet. Sci.* **36**, 325 (2008).
5. M. A. Lithgow-Bertelloni, C. Richards, *Rev. Geophys.* **26**, 27 (1998).
6. S. Zhong, M. Gurnis, *Science* **267**, 838 (1995).
7. C. P. Conrad, B. H. Hager, *J. Geophys. Res.* **104** (B8), 17551 (1999).
8. S. Zhong, M. Gurnis, L. Moresi, *J. Geophys. Res.* **103** (B7), 15255 (1998).
9. H. Cizkova, J. van Hunen, A. P. van den Berg, N. J. Vlaar, *Earth Planet. Sci. Lett.* **199**, 447 (2002).
10. W. P. Schellart, *J. Geophys. Res.* **109** (B7), B07401 (2004).
11. C. Faccenna, A. Heuret, F. Funiciello, S. Lallemand, T. W. Becker, *Earth Planet. Sci. Lett.* **257**, 29 (2007).
12. M. I. Billen, M. Gurnis, M. Simons, *Geophys. J. Int.* **153**, 359 (2003).
13. M. A. Jadamec, M. I. Billen, *Nature* **465**, 338 (2010).
14. B. Isacks, P. Molnar, *Rev. Geophys. Space Phys.* **9**, 103 (1971).
15. J. F. Dewey, *The Continental Crust and Its Mineral Deposits*, D. W. Strangway, Ed. (Geological Association of Canada, Toronto, 1980), pp. 553–573.
16. R. G. Gordon, S. Stein, *Science* **256**, 333 (1992).
17. R. G. Gordon, C. DeMets, J.-Y. Royer, *Nature* **395**, 370 (1998).
18. L. F. Diachin, R. Hornung, P. Plassmann, A. Wissink, *Software, Environments, and Tools: Parallel Processing for Scientific Computing*, M. A. Heroux, P. Raghavan, H. D. Simon, Eds. (SIAM, Philadelphia, 2006), pp. 143–162.
19. C. Burstedde *et al.*, *SC '08: Proceedings of the 2008 ACM/IEEE Conference on Supercomputing* (IEEE Press, Piscataway, NJ, 2008), pp. 1–15.

Downloaded from www.sciencemag.org on August 27, 2010

20. C. Burstedde *et al.*, *J. Phys. Conf. Ser.* **180**, 012009 (2009).
21. C. Burstedde, O. Ghattas, G. Stadler, T. Tu, L. C. Wilcox, *Comput. Methods Appl. Mech. Eng.* **198**, 1691 (2009).
22. Materials and methods are available as supporting material on *Science* Online.
23. P. Bird, *Geochem. Geophys. Geosyst.* **4**, 1027 (2003).
24. L. B. Hebert, P. Antoshechkina, P. Asimow, M. Gurnis, *Earth Planet. Sci. Lett.* **278**, 243 (2009).
25. A. Ghosh, T. W. Becker, S. Zhong, *Geophys. Res. Lett.* **37**, L01301 (2010).
26. M. Yoshida, T. Nakakuki, *Phys. Earth Planet. Inter.* **172**, 278 (2009).
27. D. F. Argus, R. G. Gordon, *Geophys. Res. Lett.* **18**, 2039 (1991).
28. T. W. Becker, R. J. O'Connell, *Geochem. Geophys. Geosyst.* **2**, 1060 (2001).
29. C. P. Conrad, C. Lithgow-Bertelloni, *Science* **298**, 207 (2002).
30. G. Hirth, D. Kohlstedt, *Geophys. Monogr.* **138**, 83 (2003).
31. S. Uyeda, H. Kanamori, *J. Geophys. Res.* **84** (B3), 1049 (1979).
32. R. D. Muller, M. Sdrolias, C. Gaina, W. R. Roest, *Geochem. Geophys. Geosyst.* **9**, Q04006 (2008).
33. M. I. Billen, M. Gurnis, *J. Geophys. Res.* **110** (B5), B05407 (2005).
34. B. A. Buffett, D. B. Rowley, *Earth Planet. Sci. Lett.* **245**, 359 (2006).
35. B. Wu, C. P. Conrad, A. Heuret, C. Lithgow-Bertelloni, S. Lallemand, *Earth Planet. Sci. Lett.* **272**, 412 (2008).
36. G. Davies, *Earth Planet. Sci. Lett.* **287**, 513 (2009).
37. K. Abe, H. Kanamori, *J. Geophys. Res.* **84** (B7), 3589 (1979).
38. W. Leng, S. Zhong, *Earth Planet. Sci. Lett.* 10.1016/j.espl.2010.06.016 (2010).
39. We thank W. Leng, T. Becker, and J.-P. Avouac for helpful comments on the manuscript. This work was partially supported by NSF's PetaApps program (OCI-0749334 and OCI-0748898), NSF Earth Sciences (EAR-0426271 and EAR-0810303), U.S. Department of Energy Office of Science's SciDAC program (DE-FC02-06ER25782 and DE-SC0002710), NSF grants CCF-0427985 and DMS-072474, and the Caltech Tectonics Observatory (by the Gordon and Betty Moore Foundation). Computing resources on Texas Advanced Computing Center's Ranger and Spur systems were provided through the NSF TeraGrid under grant TG-MCA04N026.

Supporting Online Material
www.sciencemag.org/cgi/content/full/329/5995/1033/DC1
Materials and Methods
SOM Text
Figs. S1 to S6
Tables S1 to S5
References

21 April 2010; accepted 14 July 2010
10.1126/science.1191223

Atomic Structure of Human Adenovirus by Cryo-EM Reveals Interactions Among Protein Networks

Hongrong Liu,[1,2,3] Lei Jin,[1,2] Sok Boon S. Koh,[4] Ivo Atanasov,[2] Stan Schein,[2,5,6] Lily Wu,[2,4] Z. Hong Zhou[1,2*]

Construction of a complex virus may involve a hierarchy of assembly elements. Here, we report the structure of the whole human adenovirus virion at 3.6 angstroms resolution by cryo–electron microscopy (cryo-EM), revealing in situ atomic models of three minor capsid proteins (IIIa, VIII, and IX), extensions of the (penton base and hexon) major capsid proteins, and interactions within three protein-protein networks. One network is mediated by protein IIIa at the vertices, within group-of-six (GOS) tiles—a penton base and its five surrounding hexons. Another is mediated by ropes (protein IX) that lash hexons together to form group-of-nine (GON) tiles and bind GONs to GONs. The third, mediated by IIIa and VIII, binds each GOS to five surrounding GONs. Optimization of adenovirus for cancer and gene therapy could target these networks.

Human adenovirus (Ad) causes acute respiratory, gastrointestinal, and ocular infections, as well as fulminant infections among children and immunocompromised individuals, and engineered versions are used for gene therapy and vaccines against cancer and other diseases (*1*–*4*). It is among the largest (~920 Å diameter) and most complex (~150 megadaltons) of the nonenveloped double-stranded DNA (dsDNA) viruses (*5*). Its icosahedral capsid shell (Fig. 1) is composed of three major proteins: 240 hexon trimers ("hexons"), each in the shape of a hexagon; 12 penton-base pentamers ("penton base"), each in the shape of a pentagon; 12 penton base–associated fiber trimers ("fibers"); and four minor proteins (IIIa, VI, VIII, and IX) (table S1) (*5*–*7*). The genome core inside the capsid is composed of the DNA; five additional proteins (V, VII, μ, IVa2, and terminal protein); and viral protease (*8*). We sought to characterize the logic and details of the interactions responsible for assembly and stabilization of the virion.

Crystal structures (~3 Å) are available for the isolated hexon (*9*, *10*), penton base (*11*), and fiber (*12*). Cryo–electron microscopy (cryo-EM) structures are available for the intact virion (*7*, *13*–*17*)—including the minor proteins VIII and IIIa on the inner surface of the capsid and IX on the outer surface—but at a resolution (6 Å) (*15*) that does not permit characterization of interactions among the proteins. Here, we report a 3.6 Å resolution structure of human adenovirus type 5 (Ad5) by cryo-EM single-particle analysis, that enabled us to construct atomic models for these three minor proteins and to resolve critical regions of the hexon and penton base not seen by x-ray crystallography. These models reveal networks of interactions mediated by minor proteins IIIa, VIII, and IX that stabilize two large systems of tiles—on each facet a group of nine (GON) capsomers (*6*, *18*–*20*) and at each vertex a group of six (GOS) capsomers—and hold those tiles together.

Overall structure of the virion. We reconstructed the three-dimensional structure (density map) of Ad5 (Fig. 1A and movies S1 and S2) from 31,815 individual particle images in 1350 films using the IMIRS software package (*21*, *22*). The effective resolution of our structure, 3.6 Å, is estimated by the reference-based Fourier shell correlation coefficient (*23*) (fig. S1). Representative α-helix density map (Fig. 1C and movie S3) and β-strand density maps (fig. S2 and movie S4) from the hexon protein (movie S5) are consistent with this estimate.

The 240 quasi-equivalent hexons are classified as H1, H2, H3, and H4, according to their location within each facet of the pseudo T = 25 icosahedral capsid (*6*) (Fig. 1B). The 12 penton bases are centered on the 12 vertices of the icosahedron (Fig. 1, A and B), and each of the 12 fiber trimers associates with a penton base. The densities of hexons, penton bases, fibers, and the four minor proteins (IIIa, VIII, VI, and IX) are individually colored in Fig. 1B and movie S2. Minor protein IX is inlaid into the outer surface (Fig. 1B, top) of the capsid—not on the outer surface itself but halfway down the hexon (*15*, *16*) (side view in the top left inset of Fig. 1B). By contrast, minor proteins IIIa and VIII sit on the inner surface (Fig. 1B, bottom) underneath the inner boundaries of penton bases and hexons (side view in the bottom right inset of Fig. 1B) (*15*). Protein VI is also located beneath hexons, as indicated by previous cryo-EM structures, in a cavity on the inner surface of each hexon (*15*, *24*). Our result is consistent with this observation, but perhaps due to random occupancy (~360 copies among 720 hexon monomers), the cryo-EM density is weak. The copy numbers and resolved amino acids of these capsid proteins are summarized in table S1.

Protein IIIa. Monomers of protein IIIa (red in Fig. 2A), underneath the penton base and peripentonal (H1) hexons, are arranged around the fivefold axis (Fig. 2A). We resolve the structure of amino acids 7 to 300 of protein IIIa.

[1]Department of Microbiology, Immunology, and Molecular Genetics, University of California, Los Angeles (UCLA), Los Angeles, CA 90095–7364, USA. [2]California NanoSystems Institute, UCLA, Los Angeles, CA 90095–7151, USA. [3]Institute of Modern Physics, Xiangtan University, Xiangtan, Hunan 411105, China. [4]Department of Molecular and Medical Pharmacology, Institute of Molecular Medicine (IMED), UCLA School of Medicine, Los Angeles, CA 90095–1735, USA. [5]Department of Psychology, UCLA, Los Angeles, CA 90095–1563, USA. [6]Brain Research Institute, UCLA, Los Angeles, CA 90095–1761, USA.

*To whom correspondence should be addressed. E-mail: Hong.Zhou@ucla.edu

Downloaded from www.sciencemag.org on August 27, 2010

The remainder of the protein (amino acids 301 to 585) is not visible, which implies flexibility. The resolved structure is predominantly helical (Fig. 2B), with only one three-stranded β sheet (fig. S3). It has the shape of a seahorse (Fig. 2B and movie S6) and can be divided into four domains according to their interactions with other proteins (Fig. 2B). We can visualize densities associated with the side chains of ~85% of the amino acids (fig. S3), but not all of these densities are sufficiently distinctive for us to identify amino acids. Therefore, we use amino acids that are large and distinctive (table S2) as "landmarks" to obtain accurate registration of amino acids in our atomic model. Construction of the protein IIIa atomic model allows us to describe interactions with other proteins by identifying amino acids with a visible density at the site of side-chain contacts [(*22*); proposed details of nine sites of interactions in table S3A]. For example, the GOS-glue domain, the tail of the seahorse, interacts with a penton-base monomer (Fig. 2A, right, bottom inset), an adjacent protein IIIa (same inset), and two peripentonal hexons, thus binding the penton base to neighboring peripentonal hexons. The VIII-binding domain, the neck of the seahorse, interacts with protein VIII (Fig. 2A, right, top inset) to bind peripentonal hexons to hexons farther away.

Protein VIII. Monomers of protein VIII, also located on the inner capsid surface, are arranged around both fivefold and threefold axes (Fig. 2A). Each monomer is organized into an extended conformation with three domains: head, neck, and body (Fig. 2C). Our density map and the resulting model of the head domain are in good agreement with previous mass spectrometry data showing that protein VIII is cleaved at two positions during viral maturation, G110 and R159 (*25*), (Fig. 2C, inset), which causes the middle segment (amino acids 111 to 158) to be shed from the mature capsid (*26*). As with protein IIIa, we can visualize densities associated with the side chains of ~85% of the amino acids (fig. S4), and we use bulky amino acids (table S2) as landmarks to build our atomic model (fig. S4 and movie S7). Similarly, we identify 13 sites of interactions—each characterized by visible densities at the sites of side-chain contacts—for each protein VIII with other proteins [(*22*); proposed details on interactions in table S3B]. For example, every copy of protein VIII interacts with four hexons, two on either side of its body, one to the side of its neck, and one to the side of its head (Fig. 2A, center). The large body domain includes three antiparallel β strands that interact with protein IIIa (Fig. 2A, top right inset). In addition, each of the β strands in the head and body domains joins the β sheets of the VC region of two hexons via β-strand augmentation (Fig. 2A, top insets).

Protein IX. The protein IX network is best viewed from the outside (multicolored in Fig. 3A, center). Each monomer (Fig. 3B) has an N-terminal domain (~50 Å long), a rope domain (~70 Å), and a helix-bundle domain with a long 12-turn helix (~65 Å), all joined by loops. We could visualize the densities of side chains of ~85% of the amino acids in the N-terminal domain and ~70% in the helix-bundle domain (fig. S5, A and B). As above, we use bulky amino acids (table S2) as landmarks to obtain accurate registration of amino acids in our atomic model for these two domains. In addition, we describe protein IX's interactions with other proteins by identifying either visible densities at the sites of side-chain contacts (for the N-terminal and helix-bundle domains) or by close proximity (for the rope domains) [(*22*); proposed details of six sites of interactions in table S3C].

At the N termini of three protein IX monomers, the N-joint regions (Fig. 3B, blue) form a trimeric joint (Fig. 3A, top left inset; fig. S5C; and movie S8). The three contributing monomers radiate from this joint, shown as either three yellow monomers or a red, a green, and a blue (Fig. 3A, center). Four of these N-joints are located in each facet, one at the threefold axis (yellow in Fig. 3A) and three at local threefold axes (each with red, green, and blue monomers in Fig. 3A). The N-joint is tied by a hydrophobic core that includes three tyrosines and three leucines (Fig. 3A, top insets).

At the C terminus of protein IX, four helix-bundle domains coil together to form a ~65 Å long four-helix bundle (Fig. 3A, right insets; fig. S5D; and movie S9). These four-helix bundles, three in each facet, are centered on three local two-fold positions inside the three edges of a facet. The amino acid sequence in the helix-bundle domain of protein IX shows a heptad-repeat motif with the hydrophobic Leu in the *d* position (leucine zipper: L100, L107, L114, and L121), typical of a helix bundle. Indeed, there are additional hydrophobic leucines and valines in the helix-bundle domain, specifically L103, L110, V117, L124, V128, and L131 (table S4).

Three of the helices (blue, yellow, and green) of a four-helix bundle come from the same facet of the capsid and traverse the same distance, two hexagon edges (each ~60 Å), before joining at the base of the bundle (center of Fig. 3A; see also the section "Interaction networks" below). These would run in parallel with each other. However, the fourth helix (red) comes from a neighboring facet, reaches the tip of the helix bundle after traversing the standard two hexagon edges, joins the bundle there, and continues to the base of the helix bundle (black arrows in fig. S5, E and F). Inspired by figure 4 in (*15*), this arrangement, with the red helix running antiparallel to the other three, was already demonstrated by use of peptide-tagged recombinant protein IX (*27*).

Identification of amino acid side chains among the four helices (fig. S5D, table S2) and visualization of the densities of the rope domains of the four proteins IX in an asymmetric unit (movie S10) confirm this unusual arrangement, with three

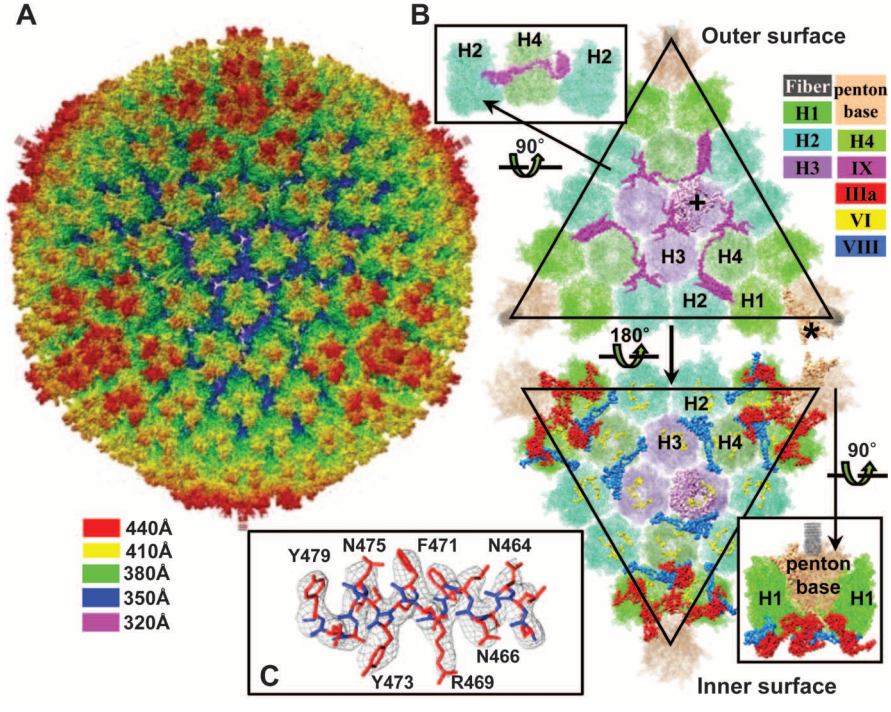

Fig. 1. Overall structure of the Ad5 capsid. (**A**) Radially colored surface of a reconstruction of the capsid, centered on a threefold axis. (**B**) Views of the outer surface (top) showing minor protein IX—and, following rotation—the inner surface (bottom) of a facet showing minor proteins IIIa, VI, and VIII. All hexons, penton bases, and penton fibers are shown semitransparently except for one hexon monomer (+) and one penton-base monomer (*). (Top left inset) Side view of protein IX among hexons. (Bottom right inset) Side view of proteins IIIa and VIII centered on a penton base. (**C**) Atomic model (sticks) of an α helix from a hexon monomer superimposed on its density map (mesh) with some side chains labeled.

Downloaded from www.sciencemag.org on August 27, 2010

parallel helices and one antiparallel helix. Indeed, the hydrophobic leucines and valines listed above create a ladder of hydrophobic interactions between these parallel and antiparallel helix-bundle domains (table S4) to create a hydrophobic core (Fig. 3A, right insets). This arrangement would tack down both ends of the helix bundle and hold the bundle rigidly in place, which may explain why the helix bundle is well resolved in structural studies.

Although filtering to low resolution reveals all of the parts of all four copies of protein IX (fig. S5, E and F, and movie S10), our high-resolution structure shows clearly the entirety of just the blue copy (fig. S5, A and B). Therefore, we use flexible fitting of the blue rope domain to model the green, yellow, and red rope domains in the center of Fig. 3A. Even for the blue copy, amino acid registration for the rope domain is uncertain because of the relatively low density of that domain (fig. S5, A and E). With that caution in mind, we have nonetheless built an atomic model of all three domains of the blue copy of protein IX. For the red, green, and yellow copies, we have built atomic models of only their N-terminal and helix-bundle domains.

Major capsid proteins and conformational adaptability. Derived from the cryo-EM density map of the whole virion, our atomic models of the penton-base and hexon proteins (Fig. 4, A and B, red ribbons) are in excellent agreement with those from x-ray crystallography (*9*–*11*). However, our models reveal features not seen in the crystal structures, as well as many in situ interactions absent from crystal structures of isolated proteins. For example, at the N terminus of each penton-base monomer, we see amino acids 37 to 51 (blue "N-arm" in Fig. 4A). This string of amino acids interacts with two adjacent IIIa proteins (Fig. 2A, bottom right inset; model and densities in fig. S6; and table S3A) and then turns inward to connect with the genome core, all of which anchors the penton base.

We also see an N-terminal extension (amino acids 2 to 7) and a C-terminal extension (amino acids 944 to 950) of the hexon. With four types of hexon (H1 to H4) in an asymmetric unit, there are 12 hexon monomers (fig. S7A), but depending on the location of the subunit and adapting to its interaction with neighboring proteins (see legend of Fig. 4C), the N-terminal extension (Fig. 4C) shows just five different conformations for its short stretch of amino acids. Some of these conformations interact with minor proteins IIIa and VIII on the inner surface (tables S3, A and B), others with neither. Likewise, the C-terminal extension (amino acids 944 to 950 in Fig. 4D and fig. S8A) shows different conformations, six in this case. The first three, like the C-terminal extension type *a* (fig. S8B), interact with protein VIII; the last three do not.

In addition, at the top of the hexon in our cryo-EM model, we see four loops (amino acids 251 to 256, 271 to 278, 431 to 436, 443 to 444) (Fig. 4B, blue ribbons and labels). The first three are within the hypervariable regions HVR4, HVR5, and HVR7 that are important for type-specific immunogenicity (*10*). The one loop (amino acids 251 to 256) in the H4 hexon monomer (fig. S5E) interacts with the tip of the four-helix bundle of protein IX and anchors the latter in the valley between two hexons.

Finally, our 3.6 Å resolution structure shows the amino acids involved in hexon-hexon and hexon-penton base interactions by revealing amino acid residues that are within 7 Å distance (fig. S7 and proposed details of interactions in table S5). Because of the scarcity of visible side-chain contact densities, we suggest that these interactions are generally weaker (like the one shown in fig. S7B) than those between the major and minor proteins. Although these interactions cannot be seen in the crystal structures of the individual proteins, they are largely in agreement with predictions based on fitting the crystal structures to these proteins in their native packing, as revealed in 10 Å cryo-EM maps of the whole virion [table 1 in (*14*)].

Interactions with the genome core. Our map also revealed interactions of two kinds between capsid shell proteins and the genome core, indicating a role for capsid proteins in genome packaging. The first kind is the N-arm of the penton base, extending to the genome core (fig. S9, A to C), consistent with the report that the penton base can bind core protein V (*27*). The second kind is a density underneath and near protein IIIa (fig. S9D), which looks like a rod at low resolution and has the characteristic features of a helix at high resolution. According to its site and copy number, 60 per virion, this rod density is likely to be part of

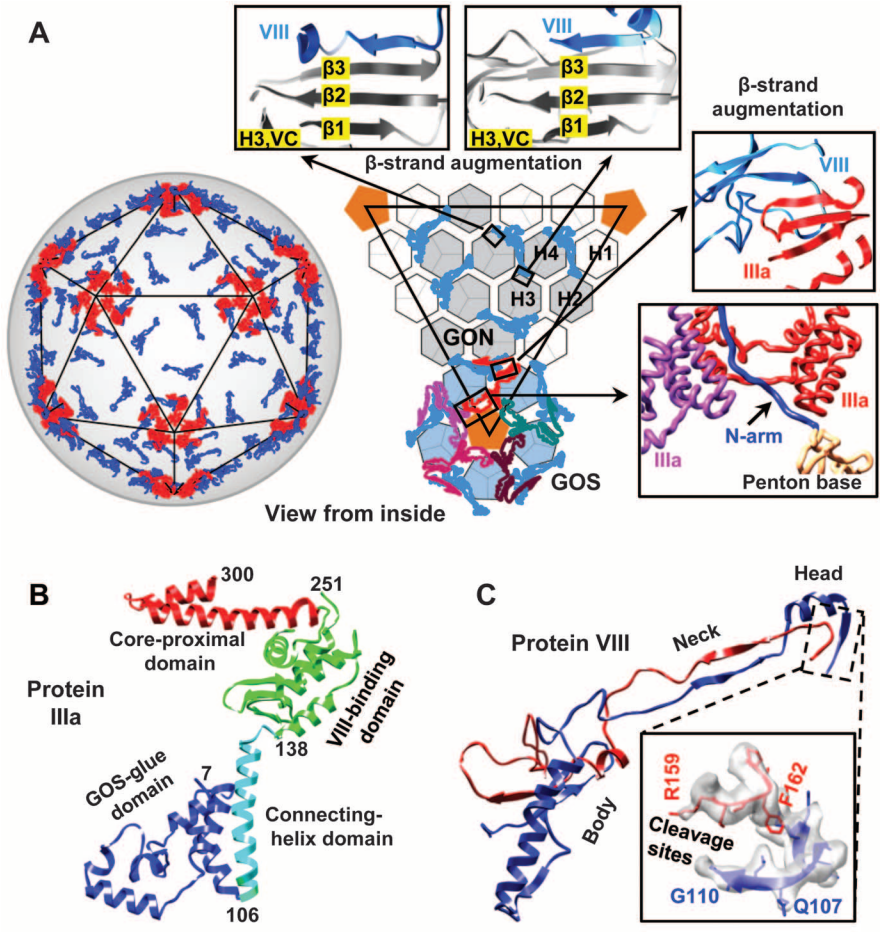

Fig. 2. Interactions among minor and major proteins on the inner surface. (**A**) (Left) Global view of the arrangement of protein IIIa (red) and protein VIII (blue). (Middle) Organization of hexon trimers into a GON (gray shade), peripentonal hexon trimers (light blue shade), and a penton-base pentamer (orange shade) into a GOS. (Top insets) β augmentation at the VC regions of the H3 hexon trimer by the body (left) and the head (right) domains of protein VIII. (Right insets) The top inset shows β augmentation at the VIII-binding domain of protein IIIa by the body domain of protein VIII; the bottom inset shows interactions among the N-arm of a penton base and two adjacent proteins IIIa. (**B**) Ribbon model of protein IIIa (amino acids 7 to 300) with four domains. (**C**) Ribbon model of protein VIII with three domains. (Bottom inset) Head domain density (semitransparent gray) and its atomic model (ribbon), showing cleavage sites G110 and R159 between the N-terminal portion (blue) and the C-terminal portion (red).

Downloaded from www.sciencemag.org on August 27, 2010

the C terminus of protein IIIa, consistent with the ability of protein IIIa also to bind core protein V (*17*, *29*).

Prior reports show that protein VI binds hexons (*30*) and core protein V (*31*) and that its C terminus activates the virion protease that cleaves multiple precursor proteins, required for virion maturation and infectivity (*32*). We find protein VI in the cavity on the underside of the hexon, consistent with these observations.

Interaction networks among minor and major proteins. Using detergent, Smith *et al*. (*18*) obtained dissociation fragments that became known as GONs—groups of nine (*20*) hexons—one in each of the 20 facets (*6*). Following that example, we call the one penton base pentamer and its five peripentonal hexons a GOS—a group of six capsomers—each centered on a vertex (Fig. 5A schematic).

As shown in the sphere in Fig. 2A and in the Fig. 5A schematic, five copies of protein IIIa monomer (red) on the inner surface of the capsid form a network centered on a penton base. This network appears to hold together the penton base and peripentonal hexons to form a GOS, with many contacts between penton base and peripentonal hexons and between peripentonal-hexon neighbors (fig. S10A and table S3A).

From the network point of view, the protein VIII molecule (blue) on the inner surface of the capsid has three kinds of interactions (Fig. 5A schematic, fig. S10A, and table S3B). First, its head and neck domains bind neighboring hexons within each GON. Second, its body domain binds neighboring GONs to each other at a local twofold position (i.e., the SS interface between H3 and H2 hexons in fig. S7A). Third, its body domain joins GON hexons and GOS hexons at another local twofold position (i.e., the SS interface between H4 and H1 hexons in fig. S7A). Indeed, the last type of interaction appears to be the main interaction between GON and GOS tiles.

Protein IX on the outer surface of the capsid forms a network that lines the boundaries between hexons, bonds extensively with them, lashes them together into GONs, and binds GONs to GONs (Fig. 5B). Coextensive with GONs, protein IX essentially avoids GOS tiles, with only one monomer—the red one—having just one interaction site with H1 hexon protein (no. 5 in table S3C). Detergent treatment dissociates adenovirus into GONs and GOS capsomers (*18*). We suppose that this dissociation is the result of disruption of the hydrophobic cores within the three four-helix bundles situated at local twofold positions (TT interfaces between H2 and H4 hexons in fig. S7A) at the edges of each GON (Fig. 5B and table S5). Moreover, dissociation of a protein IX–deletion mutant virus produces isolated hexon and penton-base capsomers but no GONs (*32*).

The schematic (Fig. 5B) also illustrates the argument that the yellow, blue, and green protein IX monomers traverse two hexagon edges before reaching the base of the four-helix bundle, whereas the red monomer traverses two hexagon edges before reaching the tip of the four-helix bundle. The blue protein IX monomer extends along the sides of just one hexon (H4), whereas the others must be more flexible in crossing the valley between two different hexons, which may explain why the density of the blue one is best resolved. Indeed, the four monomers take different combinations of turns at the beginning and at the end of their rope domain; specifically, the parallel blue turns left and left, the parallel yellow turns right and left, the parallel green turns left and right in Fig. 5B, consistent with the diagram in figure 4D of (*15*), and the antiparallel red from the neighboring GON turns left and left. In addition, the green helix domain crosses over the other three and interacts with a hexon (H4) (Fig. 5B and table S3C).

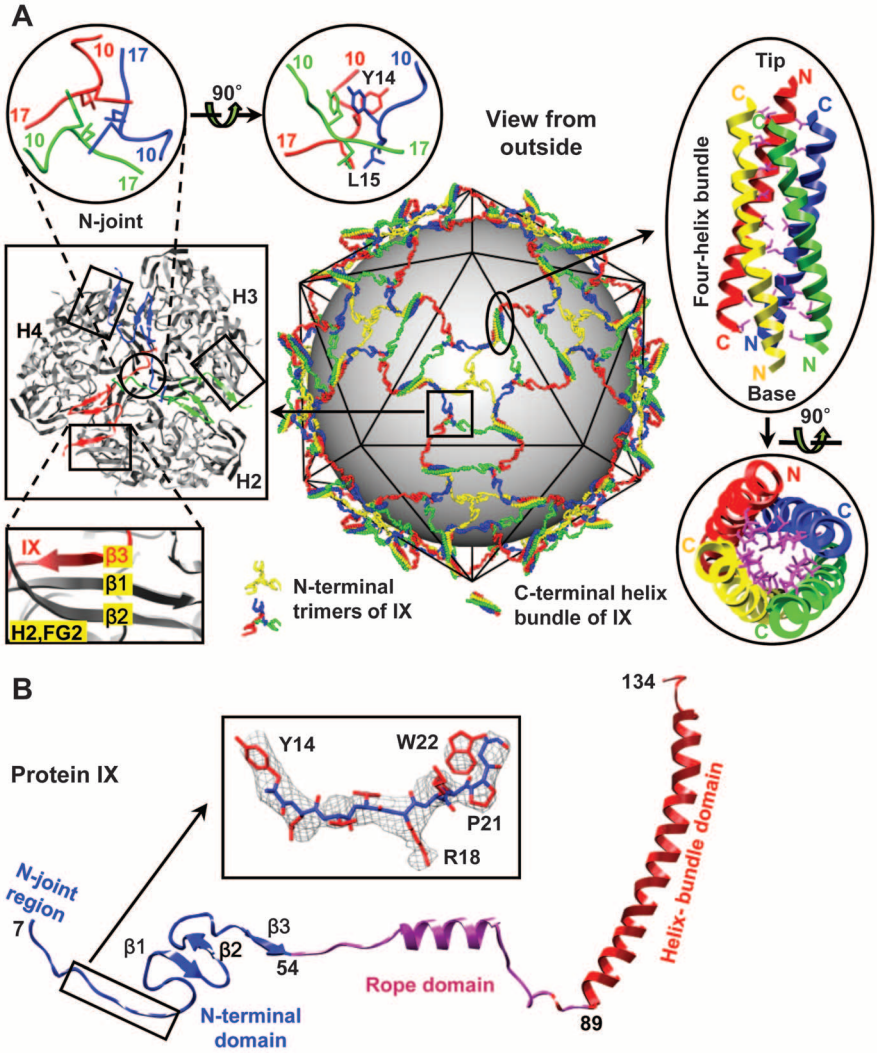

Fig. 3. Interactions among minor and major proteins on the outer surface. (**A**) The physical network of protein IX on the outer surface lashes hexons together into GON tiles but avoids GOS tiles that are each centered on a vertex. Insets: (Center left) Ribbon models of the N-terminal domains of three protein IX monomers (blue, green, and red), overlying the models of three adjacent hexon (H2, H3, and H4) monomers (gray) at a local threefold axis. (Top left insets) N-joint of three protein IX monomers and its side view, showing a hydrophobic core containing a triplet of tyrosines (Y14) and a triplet of leucines (L15). (Bottom left inset) β augmentation at the FG2 region of a hexon H2 by the N termimus of protein IX. (Top right) Four-helix bundle with three parallel and one antiparallel α helices linked by a ladder of hydrophobic residues (leucines and valines, magenta). (Bottom right) Head-on view of the helix bundle and the hydrophobic core. (**B**) Ribbon model of protein IX with three domains and the N-joint region. (See also fig. S5.) (Inset) Density map (mesh) and atomic model (sticks) of a representative loop from the N-terminal domain.

Discussion. Many dsDNA viruses, including some bacteriophages and herpesviruses, assemble a protein capsid first, followed by motor-driven insertion of genomic DNA through a portal complex at one of the 12 vertices into the preformed capsid (*34*, *35*). Indeed, a recent study suggests the presence in adenovirus of a homolog of the bacteriophage portal protein (*36*). Moreover, empty

Downloaded from www.sciencemag.org on August 27, 2010

capsid particles and normal-size particles with a fraction of the normal DNA have been detected (*37*). Therefore, the size of the virion is likely to be determined by its capsid components, probably the assembly of GON and GOS tiles, which depend primarily on interactions between major and minor proteins (Fig. 5). For example, in the absence of protein IX—which may act like the "tape-measure" protein P30 in bacteriophage PRD1 (*38*, *39*)—the adenovirus virion can accommodate a slightly larger than normal genome (*40*). If the protein IX network, with several domains that are tied at both ends—the N-joint at one and the four-helix bundle at the other—is under tension, its elastic cables working in opposition to the outward force from the core stuffed with enough DNA (*41*) may be essential to the stability of the virus. Indeed, adenovirus without protein IX has poor thermostability (*33*).

Our atomic structures have enabled us to identify the amino acids responsible for interactions among the minor and major proteins in the virion (tables S3 to S5). By genetic engineering, these amino acids could be systematically manipulated to generate more stable, less stable, or temperature-sensitive particles, and conceivably, larger capsids. Such larger capsids might permit an increase in the payload of genes carried by an engineered adenovirus for cancer and gene therapy. In addition, our atomic model of the whole virion has revealed which amino acids of protein IX, the hexon, and the penton-base are exposed on the outer surface. These amino acids could serve as targets for genetic engineering to modulate tissue targeting (*41*). Finally, insofar as adenovirus causes illness, especially among young children and immunocompromised adults, it should be possible to rationally design drugs to target those binding sites.

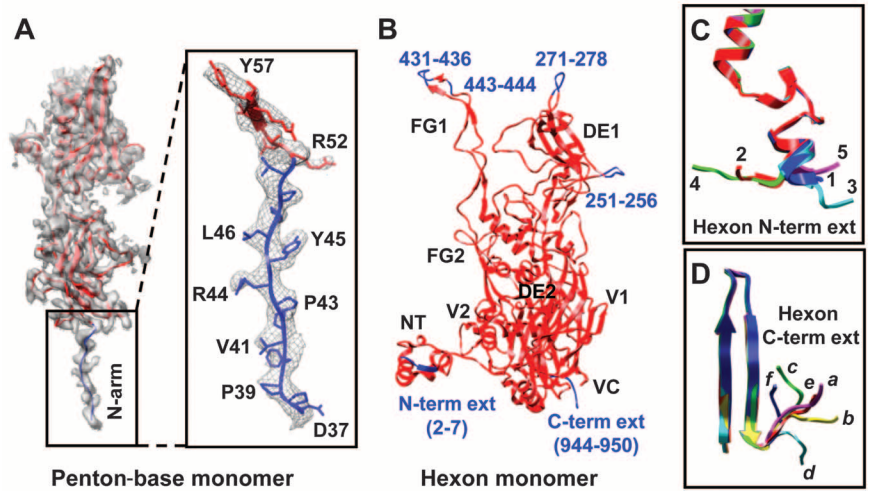

Fig. 4. Newly resolved regions in penton-base and hexon proteins. (**A**) Cryo-EM model (ribbons) of the penton-base protein superimposed on its density map (semitransparent gray). Outside the box, the cryo-EM atomic model (red ribbons) is identical to the x-ray model (*11*). Inside the box is our newly resolved N-arm (blue ribbon, amino acids 37 to 51). (Inset) Enlargement of the boxed region, showing side-chain densities (mesh) and its atomic model (ribbon). (**B**) Cryo-EM model of the hexon protein. Red ribbons show agreement with the x-ray model (*10*). Blue ribbons show our newly resolved pieces, including the N-terminal and C-terminal extensions. Region names in the hexon monomer (e.g., VC and FG) follow (*10*). (**C** to **D**) Conformational adaptation. (C) Twelve hexon monomers exhibit five types of N-terminal extension in an asymmetric unit: four of type 1, two each of types 2 and 3, one of type 4, and three of type 5. (D) Twelve hexon monomers exhibit six types of C-terminal extension: two each of types *a*, *b*, *c* and *d*, three of type *e*, and one of type *f*. Ribbon models superimposed on density (mesh) of these six types are shown in fig. S8A.

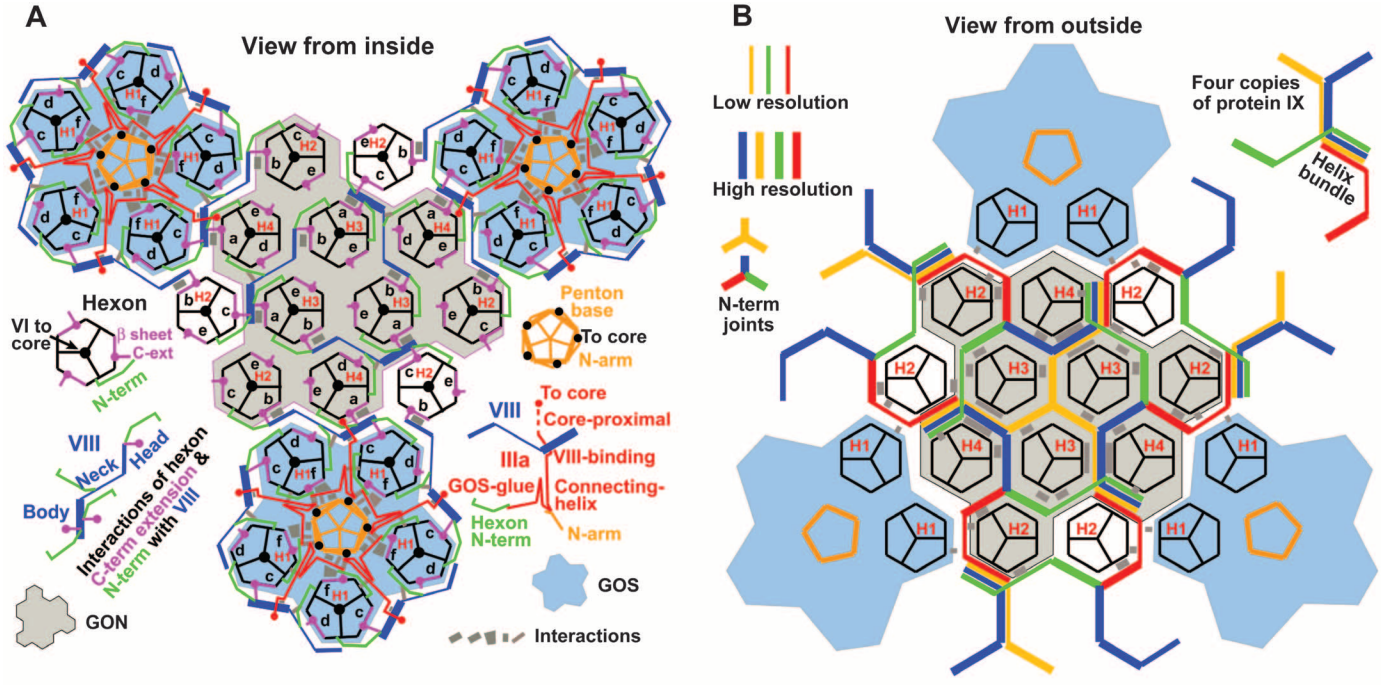

Fig. 5. Schematic illustrations of interactions among minor and major proteins. Interactions are marked here, numbered in fig. S10, and listed in table S3. (**A**) Contacts on the inner surface of the capsid. Letters a to f denote the positions of six types of hexon C-extensions. At each vertex, five copies of protein IIIa link five peripentonal hexon trimers and a penton-base pentamer to make a GOS tile (light blue shading). Protein VIII mediates binding among hexons, links GON tiles (gray shading) to GON tiles, and links GON tiles to GOS tiles. (**B**) Contacts on the outer surface among the four types of hexon trimer (H1, H2, H3, and H4) and the four types of protein IX monomer (red, green, yellow, and blue) that are inlaid into the canyons at the borders between hexons. Protein IX lashes hexons together to form GON tiles and also links GON tiles.

Downloaded from www.sciencemag.org on August 27, 2010

References and Notes

1. D. M. Roberts *et al.*, *Nature* **441**, 239 (2006).
2. M. Everts, D. T. Curiel, *Curr. Gene Ther.* **4**, 337 (2004).
3. N. Tatsis, H. C. J. Ertl, *Mol. Ther.* **10**, 616 (2004).
4. S. N. Waddington *et al.*, *Cell* **132**, 397 (2008).
5. A. J. Berk, in *Fields Virology*, vol. 2, D. M. Knipe *et al.*, Eds. (Lippincott Williams & Wilkins, Philadelphia, 2007), pp. 2356–2395.
6. R. M. Burnett, *J. Mol. Biol.* **185**, 125 (1985).
7. P. L. Stewart, S. D. Fuller, R. M. Burnett, *EMBO J.* **12**, 2589 (1993).
8. W. C. Russell, *J. Gen. Virol.* **90**, 1 (2009).
9. M. M. Roberts, J. L. White, M. G. Grütter, R. M. Burnett, *Science* **232**, 1148 (1986).
10. J. J. Rux, P. R. Kuser, R. M. Burnett, *J. Virol.* **77**, 9553 (2003).
11. C. Zubieta, G. Schoehn, J. Chroboczek, S. Cusack, *Mol. Cell* **17**, 121 (2005).
12. M. J. van Raaij, A. Mitraki, G. Lavigne, S. Cusack, *Nature* **401**, 935 (1999).
13. P. L. Stewart, R. M. Burnett, M. Cyrklaff, S. D. Fuller, *Cell* **67**, 145 (1991).
14. C. M. Fabry *et al.*, *EMBO J.* **24**, 1645 (2005).
15. S. D. Saban, M. Silvestry, G. R. Nemerow, P. L. Stewart, *J. Virol.* **80**, 12049 (2006).
16. M. P. Marsh *et al.*, *J. Virol.* **80**, 11881 (2006).
17. M. Silvestry *et al.*, *J. Virol.* **83**, 7375 (2009).
18. K. O. Smith, W. D. Gehle, M. D. Trousdale, *J. Bacteriol.* **90**, 254 (1965).
19. R. A. Crowther, R. M. Franklin, *J. Mol. Biol.* **68**, 181 (1972).
20. W. G. Laver, H. G. Pereira, W. C. Russell, R. C. Valentine, *J. Mol. Biol.* **37**, 379 (1968).
21. Y. Liang, E. Y. Ke, Z. H. Zhou, *J. Struct. Biol.* **137**, 292 (2002).
22. Materials and methods are available as supporting material on *Science* Online.
23. P. B. Rosenthal, R. Henderson, *J. Mol. Biol.* **333**, 721 (2003).
24. A. J. Pérez-Berná *et al.*, *J. Mol. Biol.* **392**, 547 (2009).
25. Single-letter abbreviations for the amino acids are as follows: A, Ala; C, Cys; D, Asp; E, Glu; F, Phe; G, Gly; H, His; I, Ile; K, Lys; L, Leu; M, Met; N, Asn; P, Pro; Q, Gln; R, Arg; S, Ser; T, Thr; V, Val; W, Trp; and Y, Tyr.
26. E. Lehmberg *et al.*, *J. Chromatogr. B Anal. Technol. Biomed. Life Sci.* **732**, 411 (1999).
27. C. M. S. Fabry *et al.*, *J. Virol.* **83**, 1135 (2009).
28. E. Everitt, L. Lutter, L. Philipson, *Virology* **67**, 197 (1975).
29. M. L. Boudin, J. C. D'Halluin, C. Cousin, P. Boulanger, *Virology* **101**, 144 (1980).
30. C. M. Wiethoff, H. Wodrich, L. Gerace, G. R. Nemerow, *J. Virol.* **79**, 1992 (2005).
31. D. A. Matthews, W. C. Russell, *J. Gen. Virol.* **79**, 1671 (1998).
32. W. J. McGrath, J. Ding, A. Didwania, R. M. Sweet, W. F. Mangel, *Biochim. Biophys. Acta* **1648**, 1 (2003).
33. W. W. Colby, T. Shenk, *J. Virol.* **39**, 977 (1981).
34. W. Jiang *et al.*, *Nature* **439**, 612 (2006).
35. B. Deng, C. M. O'Connor, D. H. Kedes, Z. H. Zhou, *J. Virol.* **81**, 3640 (2007).
36. P. Ostapchuk, P. Hearing, *J. Cell. Biochem.* **96**, 25 (2005).
37. L. Prage, S. Höglund, L. Philipson, *Virology* **49**, 745 (1972).
38. J. J. B. Cockburn *et al.*, *Nature* **432**, 122 (2004).
39. N. G. A. Abrescia *et al.*, *Nature* **432**, 68 (2004).
40. K. L. Sargent, P. Ng, C. Evelegh, F. L. Graham, R. J. Parks, *Gene Ther.* **11**, 504 (2004).
41. A. C. Smith, K. L. Poulin, R. J. Parks, *J. Virol.* **83**, 2025 (2009).
42. M. Yan *et al.*, *Nat. Nanotechnol.* **5**, 48 (2010).

43. We thank A. Berk for advice; W. H. Hui for imaging, C.-O. Yun and O.-J. Kwon for providing the Ad-ΔE1B19/55 virus sample, and X. Zhang and P. Ge for discussion. This project is supported in part by grants from the National Institutes of Health (GM071940 and AI069015 to Z.H.Z.) and (CA101904 to L.W.). We acknowledge use of facilities at the Electron Imaging Center for NanoMachines supported in part by NIH (1S10RR23057). H.L. thanks the National Natural Scientific Foundation of China for support (10874144). S.B.K. was supported by Congressionally Directed Medical Research Programs W81XWH-06-1-055 predoctoral training program. Our structure and atomic model have been deposited in the EM Data Bank and the Protein Data Bank with accession numbers EMD-5172 and 3IYN, respectively.

Supporting Online Material

www.sciencemag.org/cgi/content/full/329/5995/1038/DC1
Materials and Methods
SOM Text
Figs. S1 to S10
Tables S1 to S5
References
Movies S1 to S10

25 January 2010; accepted 18 June 2010
10.1126/science.1187433

Downloaded from www.sciencemag.org on August 27, 2010

Strange Metal Transport Realized by Gauge/Gravity Duality

Thomas Faulkner,[1] Nabil Iqbal,[2] Hong Liu,[2]* John McGreevy,[2] David Vegh[3]

Fermi liquid theory explains the thermodynamic and transport properties of most metals. The so-called non-Fermi liquids deviate from these expectations and include exotic systems such as the strange metal phase of cuprate superconductors and heavy fermion materials near a quantum phase transition. We used the anti–de-Sitter/conformal field theory correspondence to identify a class of non-Fermi liquids; their low-energy behavior is found to be governed by a nontrivial infrared fixed point, which exhibits nonanalytic scaling behavior only in the time direction. For some representatives of this class, the resistivity has a linear temperature dependence, as is the case for strange metals.

During the past decade, developments in string theory have revealed surprising and profound connections between gravity and many-body systems, resulting in the emergence of a new description for strongly coupled many-body systems. The anti–de-Sitter/conformal field theory (AdS/CFT) correspondence (*1*–*3*) relates a gravity theory in a weakly curved $(d+1)$-dimensional anti–de Sitter (AdS_{d+1}) spacetime to a strongly coupled d-dimensional quantum field theory defined on its boundary. This correspondence maps questions about complicated many-body phenomena at strong coupling to solvable single- or few-body classical problems in a curved geometry. Black holes in this geometry play a surprising and universal role in characterizing the dynamics of the boundary theory at finite temperature and density, a development anticipated by the discovery of Hawking and Bekenstein in the 1970s (*4*, *5*) that black holes are intrinsically thermodynamic objects. Important dynamical insight into the thermodynamics (*6*) and transport behavior (*7*) of strongly correlated systems has been obtained from simple geometric aspects of black hole spacetimes.

Very recently, this apparatus has been brought to bear on the problem of fermions near quantum criticality (*8*–*11*). The basic strategy is to perform angle-resolved photoemission (ARPES) thought experiments on a charged black hole, which describes the ground state of a class of strongly coupled many-body systems. The fermionic response, which is proportional to the ARPES intensity, may be computed by studying the scattering of Dirac particles off this black hole. By exploring different regions in parameter space, both Fermi liquid–like (*10*) and non–Fermi-liquid behavior (*9*, *11*) were discovered, establishing the black hole as a new tool for addressing outstanding questions related to interacting fermions at finite density.

A prime example of a theoretical challenge to which such a tool may be applied is the strange metal phase of the cuprate high-temperature superconductors. The metallic state above the superconducting transition temperature T_c near optimal doping has unusual transport properties different from those of a normal metal, and was thus dubbed a strange metal; understanding this phase is believed to be essential for deciphering the mechanism for high-T_c superconductivity. The anomalous behavior of the strange metal (perhaps most prominently the simple and robust linear temperature dependence of the resistivity) implies that the low-

[1]Kavli Institute for Theoretical Physics, University of California, Santa Barbara, CA 93106, USA. [2]Center for Theoretical Physics, Massachusetts Institute of Technology, Cambridge, MA 02139, USA. [3]Simons Center for Geometry and Physics, Stony Brook University, Stony Brook, NY 11794–3636, USA.

*To whom correspondence should be addressed. E-mail: hong_liu@mit.edu

energy excitations near the Fermi surface are not Fermi-liquid–like quasiparticles (*12*, *13*) and suggests that the system may be governed by a quantum critical point at low energies (*14*–*18*). Similar anomalous behavior has also been observed in heavy fermion systems near a quantum phase transition (*19*), where quantum criticality is more firmly established. The anomalous behavior of a strange metal can be characterized by a phenomenological model called the marginal Fermi liquid (MFL) (*12*), which assumes that the spin and charge excitation spectra of the system are only weakly momentum-dependent and have a specific scale-invariant form (*20*).

We report here on a class of non-Fermi liquids discovered using the AdS/CFT correspondence. With a view toward the cuprates, we focus on a (2 + 1)-dimensional boundary theory. For simplicity, we take the field theory to be one with a conformally invariant vacuum, which amounts to working with gravity in an asymptotically AdS_4 spacetime. This conformal symmetry will not affect our results because it will be broken by finite charge density, which we introduce below.

To set up the gravity description of a system with a finite density of fermions, we consider a boundary theory with a $U(1)$ global symmetry and set a finite chemical potential μ for the $U(1)$ charge. This can be described in the bulk by a charged black hole whose horizon is a two plane in AdS_4 spacetime (*21*). The conserved current J_μ of the boundary global $U(1)$ is mapped to a bulk $U(1)$ gauge field A_M, under which the black hole is charged. Many examples exist of boundary gauge theories with such a gravity description. An important fact is that the bulk gravitational Newton's constant G_N is inversely related to the rank N of the boundary gauge group (e.g., $G_N \sim 1/N^2$), meaning that the bulk theory is classical in the large-N limit of the boundary theory.

Now consider a bulk fermionic field ψ, which is dual to some fermionic composite operator O in the boundary system. The charge q of ψ under the $U(1)$ gauge field can be identified with the global $U(1)$ charge q of O, and the conformal dimension Δ of O is related to the mass m of ψ by $\Delta = {}^3/_2 + mR$, where R is the AdS curvature radius. When q is large compared to mR, quanta for ψ can be pair-produced near the horizon. For definiteness, let us take the black hole to be positively charged. Then the negatively charged particle in a pair will fall into the black hole, while the positively charged one moves toward the boundary of the spacetime. However, it cannot escape, because the curvature of AdS pulls all matter toward its center, and thus the particle will eventually fall back toward the black hole. It then has some probability of falling into the black hole or being scattered back toward the boundary. This process will eventually reach an equilibrium, with a positively charged gas of ψ quanta hovering outside the horizon (Fig. 1). In this way, we set up a finite density of fermions in the bulk: This is dual to a finite density of excitations of the fermionic operator O in the boundary theory.

The charge density carried by the black hole is determined by the classical geometry and background fields, giving rise to a boundary theory density on the order of $\rho_0 \sim O(G_N^{-1}) \sim O(N^2)$. In contrast, the density for ψ quanta is produced from quantum pair production, giving rise to a much smaller density of fermions on the order of $\rho_F \sim O(1) \sim O(N^0)$. Thus, in the large N limit, we are studying a small part of a large system, with the background $O(N^2)$ charge density essentially providing a bath for the much smaller $O(1)$ fermionic system we are interested in.

Before describing the results for the spectral function and conductivities, we discuss a feature of the black hole geometry that reveals a crucial dynamical aspect of the boundary system. The coordinate of the extra dimension in the bulk (radial direction r in Fig. 1) can be associated with the energy scale in the boundary field theory. This connection provides an organizing principle that associates geometric aspects of the gravity side to the quantum dynamics of the field theory. The evolution of the geometry from the boundary (at $r = \infty$) toward the interior can be interpreted as the renormalization group flow of the boundary theory from high energies [ultraviolet (UV)] to low energies [infrared (IR)], respectively. As $r \to \infty$, the black hole metric approaches that of AdS_4, which has (2 + 1)-dimensional conformal symmetries. This reflects the fact that at large frequencies $\omega >> \mu$, the effects of the finite density become negligible, and one recovers the conformal invariance of the vacuum. The presence of the black hole breaks various symmetries of AdS_4, a reflection of the fact that in the boundary theory at scales $\omega \sim \mu$, the scaling and Lorentz symmetries are broken by finite density. Close to the horizon, the geometry is $AdS_2 \times R^2$ (Fig. 1). The AdS_2 factor, which involves the time and radial direction of the black hole, has an $SL(2,R)$ isometry, that is, the symmetry group of conformal quantum mechanics, where the scaling symmetry acts in the time direction.

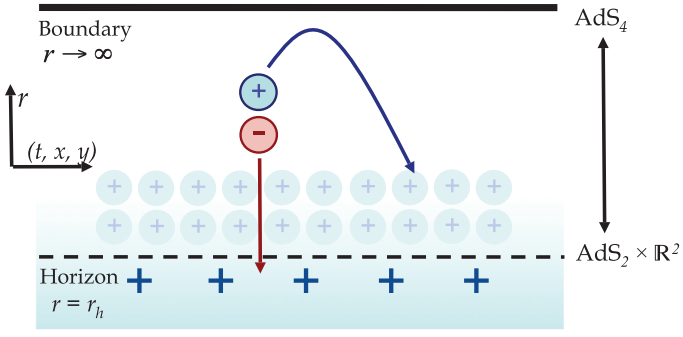

Fig. 1. The geometry of an extremal AdS_4 charged black hole and the Fermi gas hovering outside it. The vertical axis is the radial direction r of the black hole geometry, which is the direction external to the boundary spacetime. The horizontal line at $r = \infty$ denotes the boundary spacetime, which has $d = 2 + 1$ dimensions. The horizon is a plane, R^2. The coordinate r can be interpreted as the energy scale of the boundary theory. The black hole spacetime asymptotes to AdS_4 near the boundary and factorizes into $AdS_2 \times R^2$ near the horizon, with AdS_2 including the r,t directions, and R^2 comprising the spatial x,y directions.

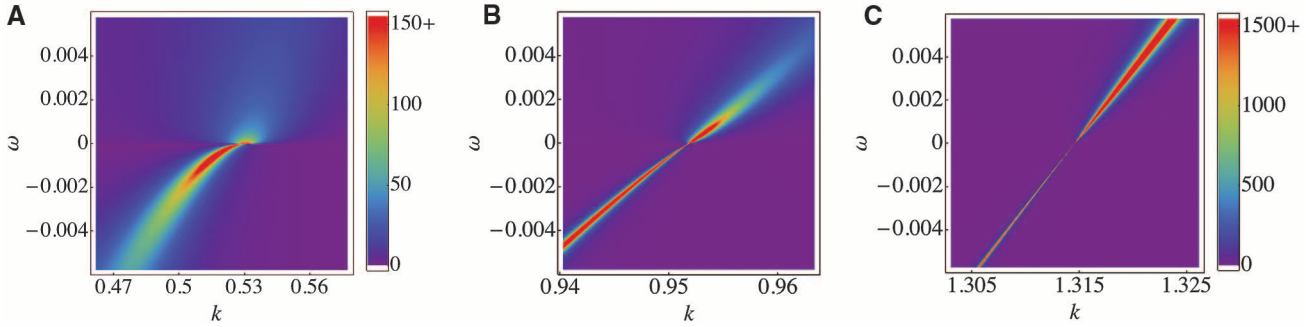

Fig. 2. Density plot of the spectral function $A(\omega,k)$ as a function of ω and k, in units where $\mu = 1$. $m = 0$ in all plots. (**A**) $q = 1$, $k_F = 0.53$, and $v_{k_F} = 0.24 < {}^1/_2$. There is no sharp quasiparticle at the Fermi surface, and the peak dispersion is nonlinear. (**B**) $q = 1.56$, $k_F = 0.952$, and $v_{k_F} = 0.500$, which corresponds to a marginal Fermi liquid. (**C**) $q = 2$, $k_F = 1.315$, and $v_{k_F} = 0.73 > {}^1/_2$. There are stable quasiparticles at the Fermi surface.

Downloaded from www.sciencemag.org on August 27, 2010

The presence of the near-horizon AdS_2 region and associated symmetries indicates that at low frequencies ($\omega \ll \mu$), the boundary system develops an enhanced symmetry group including scale invariance, and in particular is controlled by a conformal theory, which we will denote the IR CFT of the boundary theory. The conformal symmetry of this IR CFT, which only involves the time direction, is emergent, because the microscopic conformal symmetry is broken by the finite density. It is currently not known how to describe this IR CFT using the conventional knowledge of a Lagrangian. However, its properties can be computed from the gravity description: e.g., the fermion operator with momentum $\vec{k}$, $O_{\vec{k}}$ matches onto an IR CFT operator O_k^{IR}, which has a scaling dimension δ_k given by

$$\begin{aligned} \delta_k &= \frac{1}{2} + \nu_k, \\ \nu_k &= \frac{1}{\sqrt{6}}\sqrt{m^2R^2 + \frac{3k^2}{\mu^2} - \frac{q^2}{2}}, \\ k &= |\vec{k}| \end{aligned} \tag{1}$$

and a two-point correlation function $\mathcal{G}_k(\omega)$ given by

$$\mathcal{G}_k(\omega) = c(k)\omega^{2\nu_k} \tag{2}$$

where the prefactor $c(k)$ is complex and analytic in momentum k.

The retarded function $G_R(\omega,\vec{k})$ for O in the full theory is found by solving the bulk Dirac equation in the full black hole geometry. Because of rotational symmetry, G_R only depends on $k = |\vec{k}|$ up to a change of basis. We first describe its properties at zero temperature. Because of the IR CFT described above, in the low-frequency limit $G_R(\omega, k)$ contains nonanalytic behavior as a function of frequency that can be expressed in terms of the IR correlation function $\mathcal{G}_k(\omega)$. For example, at a generic value of k, we find a low-frequency expansion $G_R(\omega, k) = F_0(k) + F_1(k)\omega + F_2(k)\mathcal{G}_k(\omega) + \ldots$ Here the coefficients $F_{0,1,2}(k)$ are related to the UV geometry and are real analytic functions of k. The dissipative part of the correlator and thus the spectral function are controlled by the IR CFT correlation function (Eq. 2).

For $m^2R^2 < \frac{q^2}{3}$, the Dirac equation can have a static normalizable solution at some discrete shell in momentum space, which we call $|\vec{k}| = k_F$. Near such a special value of k, which can be determined numerically, G_R takes a very different form and its small-frequency expansion can be written as (*22*)

$$\begin{aligned} G_R(k,\omega) &= \frac{h_1}{k - k_F - \frac{1}{v_F}\omega - \Sigma(\omega,k)}, \\ \Sigma(\omega,k) &= h\mathcal{G}_{k_F}(\omega) \\ &= hc(k_F)\omega^{2\nu_{k_F}} \end{aligned} \tag{3}$$

The quantities v_F, h_1, and h in Eq. 3 are positive constants that are known numerically. The spectral function $A(\omega,k) = \frac{1}{\pi}\mathrm{Im}G_R(\omega,k)$ is given by

$$\begin{aligned} A(\omega,k) &= \frac{1}{\pi}\frac{h_1\Sigma_2}{(k - k_F - \frac{1}{v_F}\omega - \Sigma_1)^2 + \Sigma_2^2}, \\ \Sigma(\omega,k) &\equiv \Sigma_1(\omega,k) + i\Sigma_2(\omega,k). \end{aligned} \tag{4}$$

The nonanalytic frequency dependence of the spectral density $A(\omega,k)$ is again controlled by the IR CFT correlation function.

Equation 3 has a pole in the lower complex frequency half-plane which approaches $\omega = 0$ as $k \to k_F$. As a result, the associated spectral function has a quasiparticle-like peak at a frequency that approaches $\omega = 0$ for $k \to k_F$. The height and width of the peak approach infinity and zero, respectively. We take this as evidence that the system has a Fermi surface at $k = k_F$. The quantity $\Sigma(k,\omega)$, which only depends on ω (up to analytic corrections in $k - k_F$), can be interpreted as the self-energy for excitations near the Fermi surface, and its imaginary part Σ_2 can be interpreted as the single-particle scattering rate near the Fermi surface (Fig. 2).

The two frequency-dependent terms in the denominator of Eq. 3 have distinct physical origins. The term linear in ω comes from an analytic expansion of UV quantities and is real, whereas the self-energy $\Sigma(\omega)$ comes from the near-horizon AdS_2 region and is complex, scaling with frequency like $\omega^{2\nu_{k_F}}$. The properties of the quasiparticle-like peak depend on the competition between these two terms. For $\nu_{k_F} > \frac{1}{2}$, although the linear analytic term dominates, the self-energy term still makes the leading contribution to the imaginary part. In this case, the system has well-defined quasiparticles with a linear dispersion relation as in a Fermi liquid, even though the scattering rate, which is proportional to $|\omega|^{2\nu_{k_F}} \ll |\omega|$, generically scales differently from that of a Fermi liquid. When $\nu_{k_F} < \frac{1}{2}$, the self-energy dominates over the linear analytic term. As a result: (i) the quasiparticle-like peak has a nonlinear dispersion relation; (ii) the width of the quasiparticle-like peak is always comparable to its real part; and (iii) the residue of the quasiparticle-like pole, which would give the quasiparticle weight, vanishes at the Fermi surface. This is an example of a Fermi surface without quasiparticles. Also note that for $\nu_{k_F} < \frac{1}{2}$, Eq. 3 has a scaling form consistent with the scaling hypothesis for a critical Fermi surface discussed recently in (*23*).

When $\nu_{k_F} = \frac{1}{2}$, the two frequency-dependent terms in Eq. 3 become degenerate in the small frequency limit. As is often the case for such a degenerate situation, a logarithmic term is generated, and the self-energy is given by

$$\begin{aligned} \Sigma(\omega) &\approx \tilde{c}_1\omega\log\omega + id_1\omega, \\ \frac{d_1}{\tilde{c}_1} &= -\frac{\pi}{1 + e^{-\frac{2\pi q}{\sqrt{12}}}} \end{aligned} \tag{5}$$

where $\tilde{c} < 0$ and d_1 are real constants. Thus, in this case the single-particle scattering rate is linear in ω, and the system does not have well-defined quasiparticles. Remarkably, Eq. 5 is of the form (*24*) postulated in (*12*) for the MFL, which fits well with results from ARPES experiments on cuprates in the strange metal region (*25*).

At a nonzero temperature $T \ll \mu$, one finds that the self-energy $\Sigma(\omega)$ in Eq. 3 is replaced by $\Sigma(\omega, T) = h\mathcal{G}_{k_F}(\omega, T)$ where $\mathcal{G}_{k_F}(\omega,T) = (2\pi T)^{2\nu_{k_F}} g_1(\omega/T, k_F/\mu)$ is the finite-temperature IR CFT Green's function and g_1 is a universal scaling function (*26*), which approaches a constant for small ω/T. Thus the scattering rate is now well approximated by $\max(|\omega|^{2\nu_{k_F}}, T^{2\nu_{k_F}})$. At a finite temperature, the pole of Eq. 3 always has a negative nonzero imaginary part, which reflects the familiar fact that the Fermi surface gets smeared at finite temperature.

The contribution of the Fermi surface to the conductivity can be extracted from a one-loop diagram (Fig. 3A), whose evaluation proceeds similarly to that of a Fermi liquid, except for the extra bulk dimension and complications from curved spacetime geometry. We are evaluating the diagram in a spacetime with an event horizon; the fermion running in the loop can go into the horizon. In fact, precisely such processes give the leading contribution to the dissipative part of the current-current correlator and thus the optical and DC conductivities.

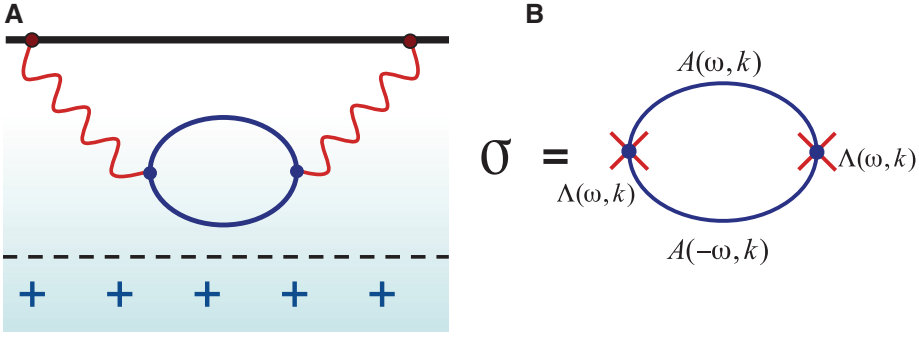

Fig. 3. (**A**) The current-current correlator is computed by evaluating a bulk one-loop diagram, similar to that of a Fermi liquid except for the extra radial dimension. (**B**) Equation 6 can be interpreted in terms of a Fermi liquid picture, with the exact propagator for a fermion running in the loop and an effective vertex Λ.

Downloaded from www.sciencemag.org on August 27, 2010

The system contains a charged background $O(N^2)$ fluid; therefore, the DC conductivity at zero temperature is not well-defined because there is no mechanism to dissipate current. The signature of this in the optical conductivity is a delta function at zero frequency with a coefficient of $O(N^2)$ (*27*). We will instead be interested in the leading low-temperature contribution from the Fermi surface to the conductivity. A well-defined answer for DC conductivity can be extracted, because at any nonzero temperature of $O(N^0)$, the system contains, along with the charged background fluid, a neutral component with density of $O(N^2)$, which can dissipate the $O(N^0)$ momenta of the fermionic quanta (*28*).

The conductivity can be written in terms of boundary theory quantities as

$$\sigma(\omega) = \frac{C}{i\omega}\int d\vec{k}\int \frac{d\omega_1}{2\pi}\frac{d\omega_2}{2\pi} \times \frac{f(\omega_1) - f(\omega_2)}{\omega_1 - \omega - \omega_2 - i\varepsilon} A(\omega_1, \vec{k})\Lambda(\omega_1, \omega_2, \omega, \vec{k}) \times \Lambda(\omega_2, \omega_1, \omega, \vec{k})A(\omega_2, \vec{k}) \quad (6)$$

where $f(\omega) = \frac{1}{\exp(\frac{\omega}{T}) + 1}$ is the Fermi distribution, $A(\omega,\vec{k})$ is the single-particle spectral function Eq. 4, and C is a temperature-independent overall constant. Equation 6 can be interpreted in the boundary theory (Fig. 3B) in terms of standard Fermi liquid theory, with Λ playing the role of an effective vertex. In our construction, Λ can be computed explicitly (*29*); it is in general a complicated function of $\omega, \vec{k}$, and T, but in the low-temperature limit and near the Fermi surface, it becomes a smooth, real function of $|\vec{k}|$, independent of ω and T. In this limit, the conductivity is controlled by the single-particle spectral function near the Fermi surface.

The DC conductivity, given by the $\omega \to 0$ limit of Eq. 6, can be written as

$$\sigma_{DC} = \alpha(q,m)\ T^{-2\nu_{k_F}} \quad (7)$$

with $\alpha(q,m)$ a numerical constant. In particular, for $\nu_{k_F} = 1/2$, which corresponds to the MFL case, we find that the contribution to the resistivity from the Fermi surface is linear in T, as observed for cuprates in the strange metal phase and many other non-Fermi liquid materials (*30*).

The optical conductivity has the advantage that it can diagnose the existence of stable quasiparticles, whose lifetime manifests itself as a transport peak at $\omega = 0$. For $\nu_{k_F} < 1/2$, where there are no stable quasiparticles, we find $\sigma(\omega) = T^{-2\nu_{k_F}} F_1(\omega/T)$ with $F_1(x)$ a universal scaling function approaching a constant as $x \to 0$. For large x, it leads to a conductivity of the form

$$\sigma(\omega) \propto (i\omega)^{-2\nu_{k_F}}, \quad T \ll \omega \ll \mu \quad (8)$$

The phase factor above is fixed by time-reversal symmetry, which requires $\sigma^*(\omega) = \sigma(-\omega)$. The falloff in Eq. 8 has the same exponent seen in single-particle self-energy and is much slower than the Lorentzian form familiar from Drude theory. For $\nu_{k_F} > 1/2$, where the spectral density exhibits a long-lived quasiparticle with a lifetime proportional to $T^{2\nu_{k_F}}$ at small frequencies, there are two low-temperature regimes. At frequencies comparable to $T^{2\nu_{k_F}}$, $\sigma(\omega)$ can be approximated by the Drude form, with the transport scattering time determined by the single-particle lifetime. However, for $\mu >> \omega >> T$, we find scaling behavior

$$\sigma(\omega) = \frac{ia}{\omega} + b(i\omega)^{2\nu_{k_F}-2} \quad (9)$$

where the coefficient a is given by the low-frequency Drude weight and b is a constant. In the MFL liquid case $\nu_{k_F} = 1/2$, we find $\sigma(\omega) = T^{-1} F_2[\omega/T, \log(T/\mu)]$, where F_2 is a universal scaling function that approaches a T-independent constant at small ω. For $\omega < T$, $\sigma(\omega)$ can be approximated by a Drude form with a transport lifetime proportional to T^{-1}. For $\omega >> T$, one finds logarithmic corrections to $1/\omega$

$$\sigma(\omega) \sim \frac{ic}{\omega} \times \left(\frac{1}{log\omega} + \frac{1}{(log\omega)^2}\frac{1 + i\pi}{2}\right) + \cdots \quad (10)$$

with c being a negative constant. This is consistent with the form recently obtained for marginal Fermi liquids from summation of the particle-hole ladder in (*31*).

Our gravity analysis of both single-particle spectral functions and conductivities involves only minimal couplings of ψ to gravity and the $U(1)$ gauge field, which are governed solely by general covariance and gauge symmetry. Thus, our discussion applies to a large class of field theories with an AdS gravity dual with a $U(1)$ global symmetry; the results will depend only on (q,m) and not on the the specific nature of the operator nor the details of the theory. In our discussion, we have treated q, m, and ν_{k_F} as input parameters, even though in any given theory, they are not continuously tunable and only specific values will arise. By varying them we are essentially scanning over a family of possible theories with a gravity dual.

Non-Fermi liquids can also arise from coupling a Fermi liquid to a gapless propagating bosonic mode, such as a transverse magnetic excitation of a gauge field (*32*). The forms of the fermion Green's functions thus obtained fit into the set of functions we have found in Eq. 3. An important difference, however, is that for a gapless boson, small momentum scatterings are strongly preferred because of its linear dispersion relation. As a result, the corresponding resistivity grows with temperature as a higher power than the single-particle scattering rate (*33*). Here quantum-critical fluctuations described by degrees of freedom in the IR CFT are represented in the gravity side by the near-horizon AdS_2 region. These fluctuations are critical for any momentum, similar to that postulated in the MFL description of the cuprates. As a result, the scaling exponent in Eq. 7 is the same as that for Σ in Eqs. 3 and 4.

Our calculations are performed in the large-N limit, in which limit the system under study has a "residual" zero-temperature entropy. A natural question is whether qualitative features of our results extend to small N. Recently it has been argued (*34*, *35*) that back-reaction from the finite density of fermions in the bulk could generate a new energy scale, which goes as $e^{-O(N^2)}$ at large N, below which the entropy vanishes and the Fermi surface behavior is modified. Above this new energy scale, the back-reaction leads to perturbative $1/N$ logarithmic violations of scale invariance in the fermion spectral function (*36*). Although these corrections are small at large N, it is conceivable that at small N, they may become significant.

In a full gravity theory where the extremal black hole arises, there could also be light charged scalar fields. A mechanism similar to the one leading to the bulk Fermi gas in Fig. 1 leads to condensation of those scalar fields and a superconducting state in the boundary theory (*37*). Thus, the Fermi surface state and the IR CFT we are describing could be hidden behind a superconducting state, and our discussion should thus be interpreted as describing a higher-temperature normal state, above the temperature where a superconducting instability would occur. In fact, there are indications that the existence of such light charged scalars may be generic in string theory compactifications (*38*). This is not dissimilar to many known condensed-matter systems, where quantum-critical points tend to be hidden under some superconducting dome. This resemblance may not be an accident, and the "residual" zero-temperature entropy of our system may give a hint about the nature of quantum-critical points observed in realistic condensed-matter systems (*39*). For a reasonable bulk coupling between the superconducting condensate and spinor, it was found in (*40*) that a well-defined gapped quasiparticle appears in the superconducting state.

Finally, it has been an open problem how to construct a framework for non-Fermi liquids. The gauge/gravity framework we are using provides a well-defined way to address physical questions in such a system. Although the underlying UV theories in which our models are embedded most likely have no relation with the UV description of the electronic system underlying the strange metal behavior of cuprates or a heavy fermion system, they do share striking similarities in terms of IR phenomena associated with a Fermi surface without quasiparticles. In particular, the emergence of an IR fixed point and the associated scaling phenomena, which dictate the electron scattering rates and transport, could provide a theoretical

Downloaded from www.sciencemag.org on August 27, 2010

framework to explain the phenomenological success of the MFL description.

References and Notes

1. J. M. Maldacena, *Adv. Theor. Math. Phys.* **2**, 231 (1998).
2. S. S. Gubser, I. R. Klebanov, A. M. Polyakov, *Phys. Lett. B* **428**, 105 (1998).
3. E. Witten, *Adv. Theor. Math. Phys.* **2**, 505 (1998).
4. S. W. Hawking, *Commun. Math. Phys.* **43**, 199 (1975); erratum, **46**, 206 (1976).
5. J. D. Bekenstein, *Phys. Rev. D* **7**, 2333 (1973).
6. S. S. Gubser, I. R. Klebanov, A. W. Peet, *Phys. Rev. D* **54**, 3915 (1996).
7. P. K. Kovtun, D. T. Son, A. O. Starinets, *Phys. Rev. Lett.* **94**, 111601 (2005).
8. S. S. Lee, *Phys. Rev. D* **79**, 086006 (2009).
9. H. Liu, J. McGreevy, D. Vegh, http://arXiv.org/abs/0903.2477.
10. M. Cubrovic, J. Zaanen, K. Schalm, *Science* **325**, 439 (2009).
11. T. Faulkner, H. Liu, J. McGreevy, D. Vegh, http://arXiv.org/abs/0907.2694.
12. C. M. Varma, P. B. Littlewood, S. Schmitt-Rink, E. Abrahams, A. E. Ruckenstein, *Phys. Rev. Lett.* **63**, 1996 (1989).
13. P. W. Anderson, *Phys. Rev. Lett.* **64**, 1839 (1990).
14. G. Aeppli, T. E. Mason, S. M. Hayden, H. A. Mook, J. Kulda, *Science* **278**, 1432 (1997).
15. T. Valla *et al*., *Science* **285**, 2110 (1999).
16. J. L. Tallon *et al*., *Phys. Status Solidi* **215**, 531 (1999).
17. D. van der Marel *et al*., *Nature* **425**, 271 (2003).
18. C. Varma, *Phys. Rev. B* **55**, 14554 (1997).
19. P. Gegenwart, Q. Si, F. Steglich, *Nat. Phys.* **4**, 186 (2008).
20. A microscopic model that produces this critical fluctuation spectrum has been proposed recently in (*41, 42*).
21. A. Chamblin, R. Emparan, C. V. Johnson, R. C. Myers, *Phys. Rev. D* **60**, 064018 (1999).
22. Because we are working with a theory that is scale-invariant in the vacuum, all dimensional quantities can be expressed in units of the chemical potential μ. Throughout the paper, in order not to clutter equations, we often do not write factors of μ explicitly, which can be reinstated on dimensional ground.
23. T. Senthil, *Phys. Rev. B* **78**, 035103 (2008).
24. For marginal Fermi liquids proposed in (*12*), $d_1/\tilde{c}_1$ is equal to $-\pi/2$, for which case there is a particle-hole symmetry; that is, $\Sigma_2(-\omega) = \Sigma_2(\omega)$. In Eq. 5, this happens only for $q = 0$. The particle-hole asymmetry in our case for generic q can be attributed to the fact that quantum-critical fluctuations are charged. In our case, Eq. 5 receives analytic corrections in k in both exponent and prefactors.
25. E. Abrahams, C. M. Varma, *Proc. Natl. Acad. Sci. U.S.A.* **97**, 5714 (2000).
26. For the explicit form of g_1, see eq. S.10 in the supporting online material (SOM). For the $\nu_{k_F} = 1/2$ case there are additional logarithms; see eq. S.18.
27. S. A. Hartnoll, P. K. Kovtun, M. Muller, S. Sachdev, *Phys. Rev. B* **76**, 144502 (2007).
28. The optical conductivity should also contain a piece proportional to $\delta(\omega)$ at the $O(N^0)$ level, which can be interpreted as a correction to the corresponding $O(N^2)$ piece. The contribution from the Fermi surface does not give rise to a delta function at any nonzero temperature.
29. For its explicit form, see the discussion around eq. S.22 in the SOM.
30. G. R. Stewart, *Rev. Mod. Phys.* **73**, 797 (2001).
31. A. Shekhter, C. M. Varma, *Phys. Rev. B* **79**, 045117 (2009).
32. For a recent discussion and references, see (*43*).
33. P. A. Lee, N. Nagaosa, *Phys. Rev. B* **46**, 5621 (1992).
34. S. A. Hartnoll, J. Polchinski, E. Silverstein, D. Tong, *J. High Energy Phys.* **2010**, 120 (2010).
35. There is, however, a range of bulk parameters m,q where this back-reaction effect near the horizon appears not to arise (*34*).
36. T. Faulkner, J. Polchinski, http://arXiv.org/abs/1001.5049.
37. For a review and refences, see (*44*).
38. F. Denef, S. A. Hartnoll, http://arXiv.org/abs/0901.1160.
39. J. Zaanen, *Nature* **462**, 15 (2009).
40. T. Faulkner, G. T. Horowitz, J. McGreevy, M. M. Roberts, D. Vegh, *J. High Energy Phys.* **2010**, 121 (2010).
41. V. Aji, C. M. Varma, *Phys. Rev. Lett.* **99**, 067003 (2007).
42. V. Aji, C. M. Varma, *Phys. Rev. B* **79**, 184501 (2009).
43. S. S. Lee, *Phys. Rev. B* **80**, 165102 (2009).
44. G. T. Horowitz, http://arXiv.org/abs/1002.1722.

44. We thank E. Abrahams, P. Coleman, S. Hartnoll, G. Horowitz, S. Kachru, P. Lee, S.-S. Lee, J. Maldacena, J. Polchinski, K. Rajagopal, S. Sachdev, K. Schalm, E. Silverstein, S. Trivedi, C. M. Varma, J. Zaanen, and in particular T. Senthil for discussions and encouragement. This work was supported in part by funds provided by the U.S. Department of Energy (DOE) under cooperative research agreement DE-FG0205ER41360 and the Outstanding Junior Investigator program, and in part by an Alfred P. Sloan fellowship. Also supported in part by by NSF under grant no. NSF PHY05-51164 and the University of California, Santa Barbara Department of Physics.

Supporting Online Material

www.sciencemag.org/cgi/content/full/science.1189134/DC1
SOM Text
Figs. S1 to S4
References

4 March 2010; accepted 21 July 2010
Published online 5 August 2010;
10.1126/science.1189134
Include this information when citing this paper.

Dynamical Instability Produces Transform Faults at Mid-Ocean Ridges

Taras Gerya

Transform faults at mid-ocean ridges—one of the most striking, yet enigmatic features of terrestrial plate tectonics—are considered to be the inherited product of preexisting fault structures. Ridge offsets along these faults therefore should remain constant with time. Here, numerical models suggest that transform faults are actively developing and result from dynamical instability of constructive plate boundaries, irrespective of previous structure. Boundary instability from asymmetric plate growth can spontaneously start in alternate directions along successive ridge sections; the resultant curved ridges become transform faults within a few million years. Fracture-related rheological weakening stabilizes ridge-parallel detachment faults. Offsets along the transform faults change continuously with time by asymmetric plate growth and discontinuously by ridge jumps.

Mid-ocean ridges sectioned by transform faults are prominent surface expressions of terrestrial plate tectonics and contribute to the overall structure of constructive plate boundaries where new oceanic crust forms [e.g., (*1*–*8*)]. Ridge transform fault patterns and their stability depend on a wide range of physical parameters [e.g., divergence rate (*1*, *7*, *8*), thermal and extensional stresses (*2*, *3*), and pre-existing structures (*9*)], but the physical mechanisms controlling spontaneous nucleation and growth (*1*, *4*) of transform faults remain ambiguous. The geometric correspondence between passive margins and mid-ocean ridges suggests that transform fault patterns result from preexisting structures. It is, therefore, commonly viewed that transform faults develop in regions adjacent to offset ridge segments and that these offsets remain constant through time [e.g., (*1*–*3*)]. However, four lines of evidence from both analog models and nature contradict this common view (*4*, *10*), namely: (i) single straight ridges can develop into an orthogonal pattern (*1*, *11*–*13*), (ii) zero offset fracture zones exist (*5*, *14*), (iii) there is a relation between ridge segment length and spreading rate (*15*), and (iv) transform faults are not inherited from transverse rift structures and nucleate while or after spreading starts (*10*).

Numerical models of transform faults are relatively rare (*2*, *3*, *16*–*18*) because of the intrinsic three-dimensionality of the problem, which only recently became treatable with large-scale computing power. In contrast to freezing wax experiments in which pronounced orthogonal ridge transform fault patterns formed during large plate divergence and growth (*1*, *19*–*21*), previous numerical models focused on short-term processes such as stress and displacement distributions (*16*–*18*) and fault patterns that arise from various thermomechanical loads on plates with predefined ridge offsets (*2*, *3*). These numerical experiments are consistent with analog modeling in that transform faults should be rheologically very weak (*17*); they also delineated conditions under which various fault patterns can nucleate from initially existing plate structure perturbations (*2*, *3*). However, strain reached in these experiments was too small to test the long-term stability of transform faults and investigate their spontaneous nucleation and growth at unsegmented, straight ridges in a self-consistent manner.

This work documents results from high-resolution three-dimensional (3D) thermomechanical numerical models of the long-term plate spreading to investigate the physical conditions for the emergence of orthogonal ridge transform fault patterns (fig. S1). In contrast to previous numerical studies, our Eulerian-Lagrangian model (*22*) can model large strains, which is essential to

Swiss Federal Institute of Technology Zurich, Department of Geosciences, Zurich, Switzerland. E-mail: taras.gerya@erdw.ethz.ch

Downloaded from www.sciencemag.org on August 27, 2010

understand natural processes at divergent, constructive plate boundaries. The modeled spreading rates range from 1.9 to 7.6 cm/year (0.95 to 3.8 cm/year half rates) which simulates (ultra)slow to intermediate spreading ridges (*7*, *23*). Ridge geometries obtained in numerical experiments depend on model parameters (table S2, Figs. 1 to 4, and figs. S2 to S6) and combine several tectonic elements such as straight and curved ridges with hooked ridge tips, normal and detachment faults, ridge-orthogonal and oblique transform faults, intratransform spreading centers, and rotating blocks (microplates). The development of ridge-orthogonal transform faults from a single straight ridge was persistently replicated in numerical experiments.

At the initial stages of plate boundary evolution, the straight boundary is composed of two symmetrical conjugate normal faults along which deformation spontaneously localizes. After 1 million years, the plate boundary becomes gently curved in response to asymmetric plate growth that develops in alternate directions along successive ridge sections (Fig. 1A). Displacement along the dominant conjugate fault locally controls the asymmetric accretion of new lithosphere to the plates. The corresponding fault section gradually turns into a typical, upward convex detachment fault plane (Fig. 1B). Such ridge-parallel detachment faults and asymmetric plate growth exist in relatively slow spreading ridges (*6*, *24*–*26*). Fracture-related weakening, implemented as a brittle/plastic strain weakening in the models, breaks the symmetry by partitioning extensional displacements between the two conjugate faults, as shown in previous 2D numerical experiments on lithospheric extension (*27*) and shortening (*28*). The ridge curvature enhances with time in a self-accelerating manner (Figs. 1 and 2), leading to the emergence of transform faults along rotated ridge segments that became subparallel to the extension direction (Fig. 1, B and C). Transform faults are thus akin to rotated and stretched sections of the mid-ocean ridge. In this process, the proto-transform faults are the former detachment surfaces that gradually changed from normal to strike-slip faults (Fig. 1, B and C). The establishment of their vertical orientation occurs during the offset growth.

The dynamical instability from which transform faults originate has a rheological origin and can develop in the case of no gravity (Fig. 3A). The instability is comparable to extensional necking of a rigid layer in a soft surrounding [i.e., boudinage (*29*, *30*)] with the important difference that new material continuously adds to the stretched and rheologically strong lithospheric layer. The characteristic wavelength of the instability is related to the plate viscosity: 30 to 50 km in models with plate viscosity of 10^{22} Pa s (Figs. 1 and 3) and 10 to 20 km in models with lower plate viscosity of 10^{21} Pa s. Plate/asthenosphere viscosity contrast controls the attitude of transform faults: Larger viscosity contrast ($\geq 10^4$) favors vertical ridge-orthogonal faults, whereas smaller viscosity contrast ($\leq 10^3$) allows faults oblique to the ridge and dipping at shallower angles (table S1 and fig. S2, C and H). The brittle/plastic rheology of the growing plate is another important rheological control of the transform fault orientation: Vertical ridge-orthogonal faults develop faster and more frequently in experiments where wet tensile fracture condition (*22*) is applied. Both spreading rate and thermal conductivity of rocks notably affect the thermal structure of the plates and hence the transform fault nucleation processes (table S1). An increase in the spreading rate has the same effect as a decrease in the thermal conductivity: It causes thinning of the plate boundary, facilitates symmetric plate growth, and weakens the dynamical ridge instability (fig. S2A).

Nucleation of transform faults strongly depends on the ridge orientation relative to the plate motion: A deviation of this orientation by 11 to 27° from perpendicular to spreading direction enhances the development of transform faults (figs.

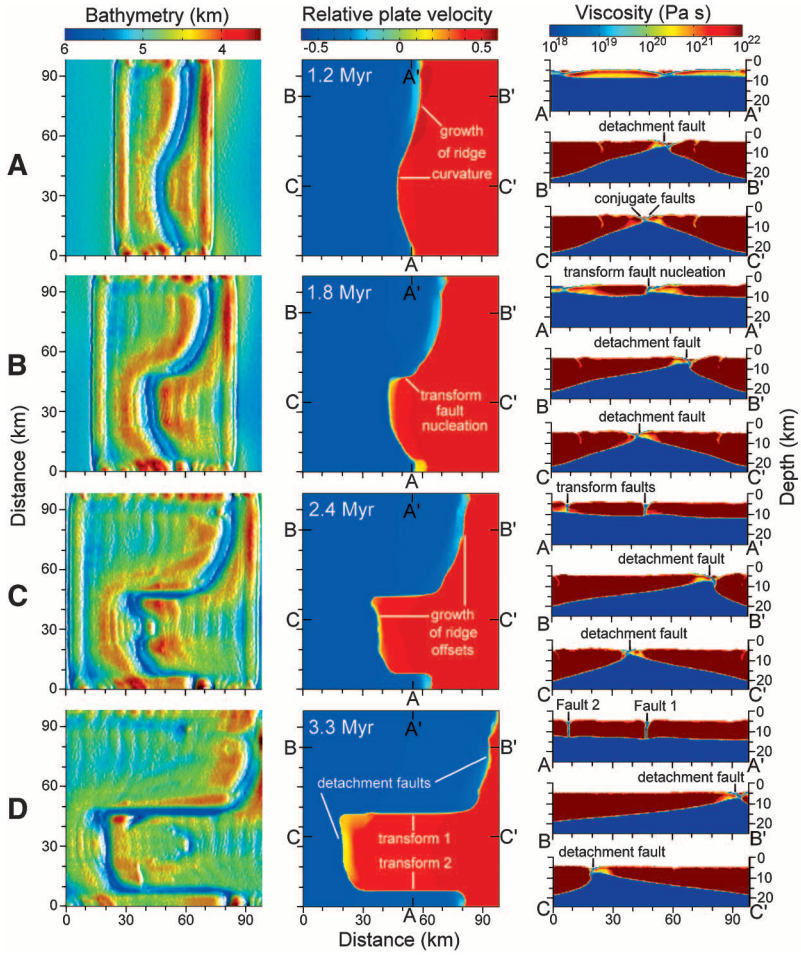

Fig. 1. Typical evolution of a constructive plate boundary with the emergence of transform faults (stages **A** to **D**). Numerical model parameters (*22*): spreading rate 3.8 cm/year, asthenospheric viscosity 10^{18} Pa s, plate viscosity 10^{22} Pa s, initial plate strength 30 MPa, final plate strength 3 MPa, strain weakening interval 0.2 to 1.2 (model named "dahzu" in table S1). Sea level for bathymetry maps (left column) corresponds to the top of the model. Horizontal velocity in the middle column is normalized to the spreading rate.

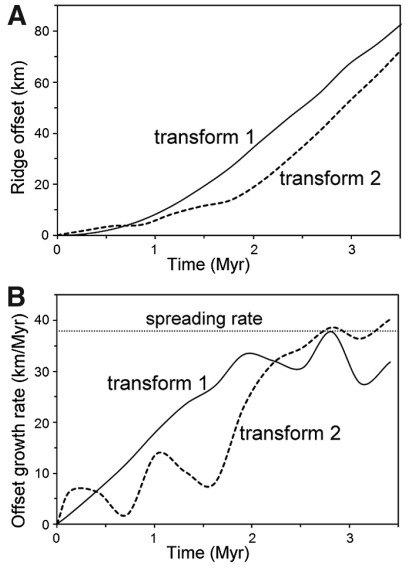

Fig. 2. Dependence of ridge offsets (**A**) and offset growth rates (**B**) versus time for two transform faults shown in Fig. 1.

Downloaded from www.sciencemag.org on August 27, 2010

S4 and S5). This suggests that after the transition from continental breakup to spreading (*10*), transform faults will grow faster from inclined ridge sections. The ensuing pattern will thus reflect to some degree an original large-scale curvature of the rifted margin. This might explain the geometric correspondence between passive margins and mid-ocean ridges. It also explains why transform faults develop rapidly at single straight ridges after a change in the spreading direction (*11*, *12*). Moreover, a similar instability may operate when changes in spreading direction generate extension across a pre-existing transform fault (*31*). In this case, the transform may behave as a ridge and rapidly breaks (*31*) into a series of shorter faults and intratransform spreading centers (*31*) (figs. S5B and S6C).

The growth of oceanic lithosphere by magmatic processes affects the geometry and the topography of mid-ocean ridges (*7*, *8*, *23*, *32*). Dynamic influences of this process were tested (table S1 and fig. S6) with a simple model that incorporates instantaneous melt extraction and deposition (*22*). Although crustal growth notably enhances ridge topography and results in a less-pronounced axial valley (*8*, *23*), the nucleation and development of transform faults is similar to models without magmatism (figs. S5 and S6). Continuous addition of nonfractured magmatic rocks to the surface of the plates dampens the asymmetry of plate accretion and delays growth of transform faults at the beginning of the experiments (figs. S5 and S6). At a later stage, a transition to more symmetric plate accretion and stabilization of transform fault offsets occurs (fig. S6, C and D).

Asymmetric plate growth does not change the relative plate rates across the transform faults (Figs. 1 and 3) because the rates of growth of two plates (A and B) separated by a ridge are partly independent of displacement rates of these plates with relations

$$v_{\mathrm{growth(A)}} + v_{\mathrm{growth(B)}} = v_{\mathrm{displacement(A)}} + v_{\mathrm{displacement(B)}} = v_{\mathrm{spreading}}$$

and

$$v_{\mathrm{ridge}} = [v_{\mathrm{displacement(A)}} - v_{\mathrm{growth(A)}}] = -[v_{\mathrm{displacement(B)}} - v_{\mathrm{growth(B)}}]$$

where $v_{\mathrm{growth(A)}}$ and $v_{\mathrm{growth(B)}}$ are growth rates of plates A and B, respectively, $v_{\mathrm{displacement(A)}}$ and $v_{\mathrm{displacement(B)}}$ are displacement rates of the same plates, $v_{\mathrm{spreading}}$ is the spreading rate, and v_{ridge} is the rate of ridge displacement [$v_{\mathrm{ridge}} = 0$ in the case of symmetric plate growth when $v_{\mathrm{displacement(A)}} = v_{\mathrm{growth(A)}}$ and thus $v_{\mathrm{displacement(B)}} = v_{\mathrm{growth(B)}}$].

The boundary instability is most efficient for the tested spreading rate of 3.8 to 5.7 cm/year (table S1). An 11 to 27° deviation of the initial ridge orientation from perpendicular to the spreading direction produces transform faults at 1.9 cm/year as well (table S1). Faster spreading rates of 7.6 cm/year cause thinning of the plate contact and preclude the development of stable detachment faults, with symmetric plate growth as a result (Fig. 3B and fig. S3). For slower extension rates of 1.9 cm/year, several parallel detachment faults develop simultaneously and preclude focusing deformation within a single boundary. In that case, transform faults are ill-defined and deformation is dominated by growth and rotation of multiple blocks (microplates) and ridge-parallel rolls (fig. S2B). This is consistent with the lack of transform faults in ultraslow spreading ridges (*7*). Numerical experiments thus suggest that transform faults may preferably grow within a certain range of slow to intermediate spreading rates and mark an intermediate stage of plate separation between initial slow rifting and later steady spreading. This was prominent in one numerical experiment where the initial spreading rate of 3.8 cm/year doubled after the appearance of transform faults (Fig. 3B). If

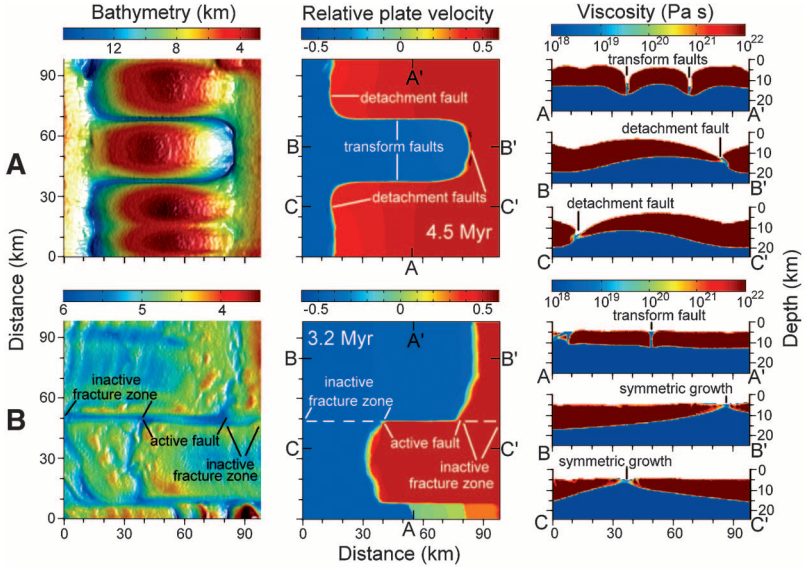

Fig. 3. Variations in model development for different parameters. Model parameters: (**A**) same as in Fig. 1 but without gravity results in larger model topographies, but does not preclude the formation of transform and detachment faults (model named "dahzi" in table S1); (**B**) same as in Fig. 1 but with a gradually increasing spreading rate from 3.8 to 7.6 cm/year within 2 to 2.5 million years after the beginning of the extension. Inactive fracture zones develop as a result of symmetric plate growth (model named "dahzg" in table S1).

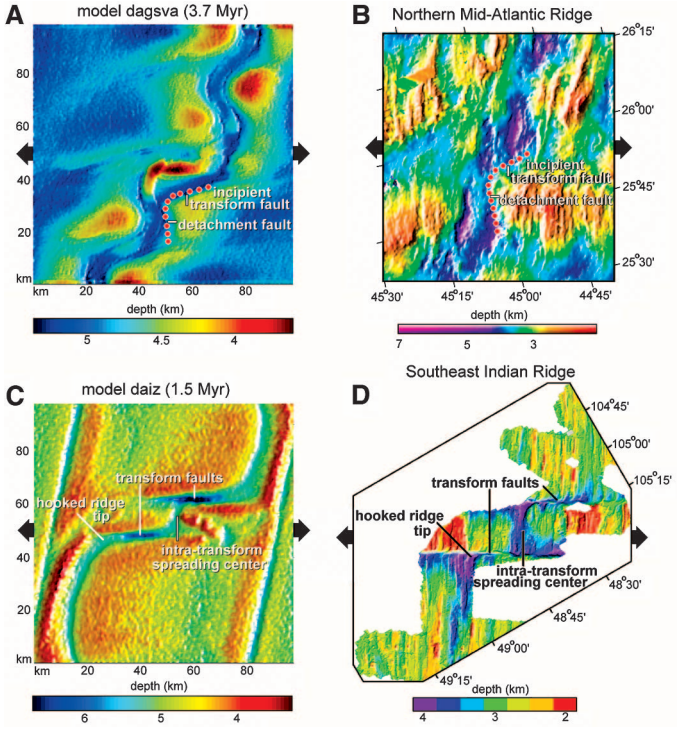

Fig. 4. Comparison of topography patterns developed in amagmatic (**A**) and magmatic (**C**) numerical models with bathymetry data for slow spreading Northern Mid-Atlantic Ridge (*11*) (**B**) and intermediate spreading Southeast Indian Ridge (*34*) (**D**). Model parameters for (A) and (C) are given in table S1.

Downloaded from www.sciencemag.org on August 27, 2010

the final spreading rate is high, symmetric growth will dominate, and offsets of ridge segments may stabilize (Fig. 3B). Stabilization of transform fault offsets with time may also be caused by magmatic processes (fig. S6) that are more intense at faster spreading rates (*7*, *8*, *23*, *32*). The range of spreading rates that favors nucleation and growth of transform faults by the dynamical instability depends on several model parameters, such as initial ridge orientation, thermal conductivity of rocks, plate viscosity, and intensity of magmatic processes. Tuning these parameters within the range of uncertainties for natural systems can provide better fit between nature and models. Also, transient asymmetric magmatic accretion processes indicated by magnetic data (*5*, *25*) may presumably cause transform faults nucleation and growth in magmatically dominated fast spreading ridges.

Spontaneous changes in the growth direction or symmetry of separated ridge segments produced inactive fracture zones in our experiments (Fig. 3B and fig. S3). The periodicity of such changes depends on the degree of strain weakening and is shorter for cases with the least weakening. Another mechanism changing ridge offsets is the formation of new detachment faults away from the ridge crest [i.e., ridge jumps (*6*)]. This process typically reduces the offsets (fig. S3) and may be a mechanical response to increasing stresses in the plate contact along transform faults.

Transform faults obtained in numerical experiments share similarities with natural observations. They are characterized by up to several km deep and wide topographic lows (*33*, *34*) (Figs. 1D, 3B, and 4). Ridge offsets along the faults vary from tens to 100 km (*15*, *34*) (Figs. 1, 3, and 4, and fig. S2). Development of the faults occurs on the time scale of plate separation and thus should react nearly instantaneously to changes in spreading direction (*11*, *12*) (figs. S4 to S6). Curved ridges generated in numerical experiments are similar to some of the natural ridge structures (Fig. 4). They have a pronounced, often asymmetric axial valley characteristic of slow to intermediate spreading ridges [spreading rates below 8 cm/year (*7*, *8*, *23*, *34*)]. Intratransform spreading centers and hooked ridge tips (Fig. 4, C and D, and figs. S5 and S6) are common in nature (*34*). Nucleation and growth of transform faults in numerical models are associated with detachment faults and asymmetric accretion (Fig. 1 and Fig. 4, A and B), which are well documented in nature based on seismic and bathymetric data (*6*, *24*, *26*). Asymmetric patterns of plate age distribution (figs. S4 to S6) and changes of ridge offsets with time (Figs. 1 and 2 and figs. S5 and S6) are indicated by magnetic data (*5*, *25*).

References and Notes

1. D. W. Oldenburg, J. N. Brune, *Science* **178**, 301 (1972).
2. C. F. Hieronymus, *Earth Planet. Sci. Lett.* **222**, 177 (2004).
3. E. Choi, L. Lavier, M. Gurnis, *Phys. Earth Planet. Inter.* **171**, 374 (2008).
4. D. Sandwell, *J. Geophys. Res.* **91** (B6), 6405 (1986).
5. P. R. Stoddard, S. Stein, *Mar. Geophys. Res.* **10**, 181 (1988).
6. K. M. Marks, J. M. Stock, *Mar. Geophys. Res.* **17**, 361 (1995).
7. H. J. B. Dick, J. Lin, H. Schouten, *Nature* **426**, 405 (2003).
8. C. Small, in *Faulting and Magmatism at Mid-Ocean Ridges*, W. R. Buck, P. T. Delaney, J. A. Karson, Y. Lagabrielle, Eds. (American Geophysical Union, Washington, DC, 1998), pp. 1–26.
9. T. Tentler, V. Acocella, *J. Geophys. Res.* **115** (B1), B01401 (2010).
10. B. Taylor, A. Goodliffe, F. Martinez, *C. R. Geosci.* **341**, 428 (2009).
11. H. W. Menard, T. Atwater, *Nature* **219**, 463 (1968).
12. S. A. Merkur'ev, C. DeMets, N. I. Gurevich, *Geotectonics* **43**, 194 (2009).
13. E. L. Winterer, in *The Geophysics of the Pacific Ocean Basin and Its Margin*, G. H. Sutton, M. H. Manghnani, R. Moberly, Eds. (American Geophysical Union, Washington, DC, 1976), pp. 269–280.
14. H. Schouten, R. S. White, *Geology* **8**, 175 (1980).
15. P. J. Fox, D. G. Gallo, *Tectonophys.* **104**, 205 (1984).
16. A. Gudmundsson, *Earth Planet. Sci. Lett.* **136**, 603 (1995).
17. M. D. Behn, J. Lin, M. T. Zuber, *Geophys. Res. Lett.* **29**, 2207 (2002).
18. A. Hashima, Y. Takada, Y. Fukahata, M. Matsuura, *Geophys. J. Int.* **175**, 992 (2008).
19. D. Oldenburg, J. Brune, *J. Geophys. Res.* **80**, 2575 (1975).
20. R. Ragnarsson, J. L. Ford, C. D. Santangelo, E. Bodenschatz, *Phys. Rev. Lett.* **76**, 3456 (1996).
21. R. F. Katz, R. Ragnarsson, E. Bodenschatz, *N. J. Phys.* **7**, 37 (2005).
22. Methods are available as supporting material on *Science* Online.
23. K. A. Kriner, R. A. Pockalny, R. L. Larson, *Earth Planet. Sci. Lett.* **242**, 98 (2006).
24. J. S. Collier, J. J. Danobeitia, CD82 Scientific Party, *Geology* **25**, 1075 (1997).
25. S. Allerton, J. Escartín, R. C. Searle, *Geology* **28**, 179 (2000).
26. J. Escartín *et al.*, *Nature* **455**, 790 (2008).
27. R. S. Huismans, C. Beaumont, *Geology* **30**, 211 (2002).
28. S. M. Schmalholz, B. J. P. Kaus, J.-P. Burg, *Geology* **37**, 775 (2009).
29. R. B. Smith, *Geol. Soc. Am. Bull.* **88**, 312 (1977).
30. W. R. Buck, L. L. Lavier, A. N. B. Poliakov, *Philos. Trans. R. Soc. London Ser. A* **357**, 671 (1999).
31. R. A. Pockalny, P. J. Fox, D. J. Fornari, K. C. Macdonald, M. R. Perfit, *J. Geophys. Res.* **102** (B2), 3167 (1997).
32. W. R. Buck, L. L. Lavier, A. N. B. Poliakov, *Nature* **434**, 719 (2005).
33. P. M. Gregg, J. Lin, M. D. Behn, L. G. J. Montési, *Nature* **448**, 183 (2007).
34. C. DeMets, R. G. Gordon, D. F. Argus, *Geophys. J. Int.* **181**, 1 (2010).

35. I thank Y. Podladchikov, J.-P. Burg, B. Kaus, P. Tackley, and three anonymous reviewers for suggestions and discussions. This work was supported by the TopoEurope and 4D-Adamello projects of Swiss National Science Foundation.

Supporting Online Material

www.sciencemag.org/cgi/content/full/329/5995/1047/DC1
Methods
Figs. S1 to S6
Table S1
References

23 April 2010; accepted 23 July 2010
10.1126/science.1191349

The Chlorine Isotope Composition of the Moon and Implications for an Anhydrous Mantle

Z. D. Sharp,[1]* C. K. Shearer,[1,2] K. D. McKeegan,[3] J. D. Barnes,[4] Y. Q. Wang[5]

Arguably, the most striking geochemical distinction between Earth and the Moon has been the virtual lack of water (hydrogen) in the latter. This conclusion was recently challenged on the basis of geochemical data from lunar materials that suggest that the Moon's water content might be far higher than previously believed. We measured the chlorine isotope composition of Apollo basalts and glasses and found that the range of isotopic values [from −1 to +24 per mil (‰) versus standard mean ocean chloride] is 25 times the range for Earth. The huge isotopic spread is explained by volatilization of metal halides during basalt eruption—a process that could only occur if the Moon had hydrogen concentrations lower than those of Earth by a factor of ~10^4 to 10^5, implying that the lunar interior is essentially anhydrous.

The origin of the Moon is constrained by geophysical models of angular momentum, density and mass, and geochemical arguments based on chemical and isotopic similarities and differences between Earth and the Moon. It is now generally accepted that the Moon was formed from the impact of a Mars-sized body sometime after formation of Earth's core (*1*, *2*), although a number of observations have not been adequately explained. Geodynamic models indicate that the impactor came from a different region of our solar system and that the bulk of the Moon originated from the impactor rather than Earth (*3*). This result is at odds with geochemical data, such as the fact that Earth and the Moon have identical oxygen and chromium isotope ratios (*4*, *5*). If the two bodies came from different regions of our solar system, it is expected that they would have different isotope ratios (*6*). Turbulent mixing between the molten Earth and the Moon immediately after impact has been proposed as a

[1]Department of Earth and Planetary Sciences, University of New Mexico, Albuquerque, NM 87122, USA. [2]Institute of Meteoritics, University of New Mexico, Albuquerque, NM 87122, USA. [3]Department of Earth and Space Sciences, University of California, Los Angeles, CA 90095, USA. [4]Department of Geological Sciences, University of Texas, Austin, TX 78712, USA. [5]Materials Science and Technology Division, Los Alamos National Laboratory, Los Alamos, NM 87545, USA.

*To whom correspondence should be addressed. E-mail: zsharp@unm.edu

Downloaded from www.sciencemag.org on August 27, 2010

means of homogenization (*6*), but such intense mixing would also tend to homogenize volatiles between the two bodies. The recognition that the Moon is strongly depleted in volatile elements and is effectively anhydrous was established soon after the return of Apollo samples (*7*, *8*). Several explanations for the absence of hydrogen in the Moon have been suggested: an anhydrous impactor (*9*), exclusion of water in the Moon because of low water solubility in molten silicate at high temperature and low pressure (*10*), or Earth and the Moon both having been anhydrous during formation, with volatiles delivered to Earth at a later date (*11*).

Recently, it was proposed that the water content of the Moon may be far higher than previously recognized. Saal *et al*. (*12*) measured water contents of lunar glass beads and concluded that the water content of the Moon may be equivalent to that of typical terrestrial mid-ocean ridge basalts (MORBs). Similar high water contents of lunar basalts have been estimated from H contents of apatite grains (*13*–*15*). Here, we present Cl isotope data from lunar basalts, volcanic glasses, and apatite grains to assess the water content of the Moon. Chlorine is extremely hydrophilic, tracking closely with water on Earth (*16*). It is also incompatible in nearly all silicates and extremely volatile. If the Moon were anhydrous, the unique degassing and partition behavior of Cl should lead to Cl isotope fractionations that are distinct from those observed on Earth.

We used gas source mass spectrometry to determine Cl isotope ratios and concentrations of water-soluble leachates and silicate residues from lunar basalts and glasses. A wide range of sample types were chosen to allow us to assess the effects of chemical composition/mineralogy and surface processing. Apatite grains were analyzed in situ with the Cameca 1270 ion microprobe at the University of California, Los Angeles (UCLA). To assess the potential effect of solar wind on the Cl isotope ratio of the lunar regolith and soils, we irradiated a thin film of NaCl with a 100-keV proton beam at the Ion Beam Materials Laboratory, Los Alamos National Laboratory, and then analyzed the irradiated sample for its Cl isotope composition (*17*).

The Cl isotope compositions of typical terrestrial materials and meteorites are clustered around 0‰ (*18*) or –1.6‰ (*19*) with a spread of ±0.5‰ (Fig. 1). Large variations in δ^{37}Cl values are seen only in the specific case where HCl gas is evolved from volcanic fumaroles (*16*). The enrichment of ^{37}Cl in the vapor is due to the large isotopic fractionation between the solvated Cl^- ion in an aqueous solution and HCl gas.

In contrast to terrestrial basalts, lunar samples show a range of δ^{37}Cl values from –1 to +24‰ (Fig. 1). The large spread is indicative of conditions that do not exist on Earth. We consider three possible explanations for the large spread: (i) initial heterogeneities retained from the Moon-forming event; (ii) isotopic fractionation associated with solar wind and micrometeorite bombardment; and (iii) devolatilization and isotopic fractionation specific to the anhydrous character of lunar basalts.

The first of these possibilities is unlikely. Volatilization and fractionation could certainly occur during accretion of the Moon with preferential loss of the light isotope during volatile escape to space. However, maintaining such large isotopic variations in a system that was certainly molten and went through a magma ocean stage (*20*) would not be expected and has not been observed for other volatile elements, such as K (*21*).

The second scenario is similarly unlikely. Because micrometeorite bombardment and solar wind sputtering can preferentially remove the light isotopes of volatile elements, we chose samples that have experienced both minimum and maximum degrees of surface processing (Table 1) to test for a correlation between the extent of surface exposure (soil maturity) and δ^{37}Cl values. Lunar soil sample 64501,232, with a high maturity index and the highest δ^{34}S value (+11.7‰) of any of our samples, has an intermediate δ^{37}Cl value, similar to that of immature soil sample 61220,39 (*22*), arguing against preferential ^{35}Cl loss due to formation and removal of light HCl (HCl gas) to space. In addition, the δ^{37}Cl value of the surface volatile chlorides are always lower than the rock-bound Cl in the same sample, in some cases as much as 10‰. If the surface chlorides interacted with solar wind, they should be enriched in ^{37}Cl, not depleted. Apatite grains in KREEP (potassium–rare earth element–phosphorus) basalt sample 72275,491 were almost certainly shielded from solar wind, and yet this sample has the highest δ^{37}Cl value of all measured samples. As a final test, a thin film of NaCl was found to be isotopically unfractionated after bombarded by a 5×10^{17} ions/cm^2 proton source (Table 1). Preferential formation of H^{35}Cl during proton bombardment should raise the δ^{37}Cl values of the residual salt, a trend that is not seen here.

The third possibility, that devolatilization of anhydrous lunar basalts caused the range of δ^{37}Cl values is supported by several trends. First, the lowest measured δ^{37}Cl values of all samples overlap the range for both terrestrial and meteorite samples. This is consistent with the idea of a well-mixed Cl isotope ratio for the inner solar system. All higher δ^{37}Cl values, as discussed below, are explained by fractionation during degassing. Second, the δ^{37}Cl values of the leached material, representing vapor deposition of the volatile chloride species, are always lower than the coexisting silicate. These data strongly support the idea that the light isotope of Cl is lost during devolatilization.

In terrestrial magmas and lavas, there is always an excess of H relative to Cl, and the dominant volatile chloride species is HCl gas. The fractionation between HCl gas and a basalt melt must be close to 0‰, because the δ^{37}Cl values of terrestrial basalts have very little variation, despite varying Cl contents. Two factors control Cl isotope fractionation during volatilization on Earth: (i) the preferential loss of ^{35}Cl to the vapor phase (due to its higher translational velocities and vapor pressure relative to ^{37}Cl), and (ii) the preferential incorporation of ^{37}Cl into HCl gas (due to the covalent character of the bond) (*16*, *23*). The two factors tend to cancel one another, resulting in near-zero fractionation between melt

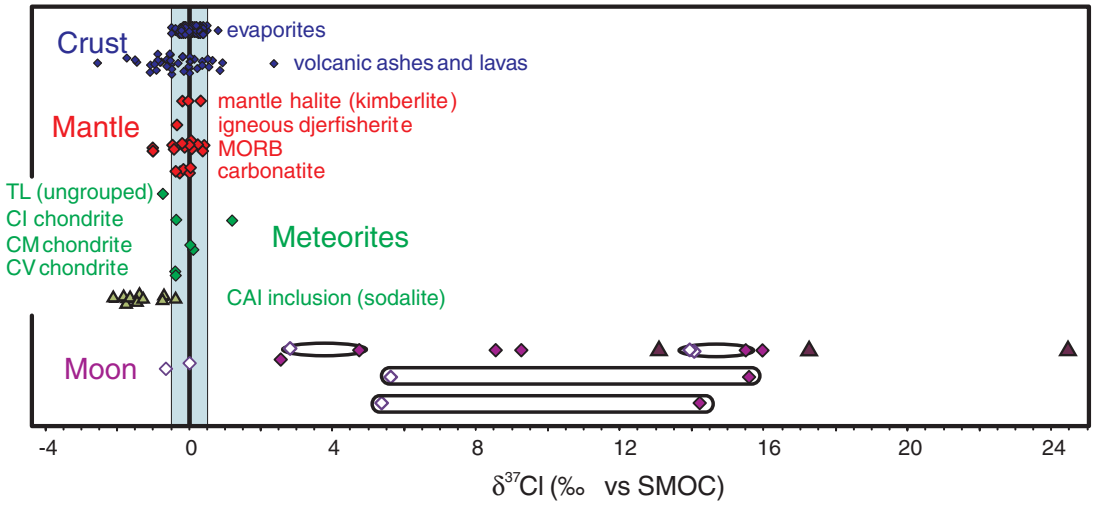

Fig. 1. Chlorine isotope composition of selected terrestrial materials and lunar samples (triangles, ion microprobe; diamonds, gas source mass spectrometry). Silicate and leachate samples are shown as solid and open symbols, respectively. Matched leachate-silicate pairs are circled. Terrestrial and meteorite data are from (*18*, *32*, *33*), and references therein. Error bars are smaller than the size of symbols. See (*18*) for meteorite abbreviations.

Downloaded from www.sciencemag.org on August 27, 2010

Table 1. Cl contents and δ^{37}Cl values for lunar samples and irradiated salt experiment. Initial Cl contents were calculated assuming Rayleigh distillation, an α value of 0.99, and an initial δ^{37}Cl value of 0‰. SMOC, standard mean ocean chloride. All apatite grains were analyzed by secondary ion mass spectrometry.

Sample	Notes	Surface exposure	Cl concentration (ppm)	δ^{37}Cl (‰ vs. SMOC)	Calculated initial Cl content (ppm)
74220,862	Pyroclastic, glass	Yes	50*	8.6,* 9.3*	
10017,34	Vesicular basalt; ilmenite (high K) basalt	No	24.7,† 12.3	4.7,† 2.7*	40
12040,214	Mare basalt		11*	0.0*	
64501,232	Mature soil	Yes	8,† 19*	15.7,† 5.6*	38
61220,39	Immature trench soil	Yes	10,† 16*	14.3,† 6.1*	42
66095	"Rusty rock" with $FeCl_2$, fumarole?, regolith breccia	Yes	117*	15.6,† 14.0,* 14.1*	
12034,116	Regolith, breccia	Yes		16.0†	
12052	Pigeonite basalt	No	5	2.5†	6
74002,36	Hand-picked glass beads	Yes	80	–0.7*	
15555,207	Apatite; olivine normative MARE basalt	No	0.56‡	13.1	
12040,46	Apatite; olivine basalt	No	0.83‡	17.2	
72275,491	Apatite; KREEP basalt clast in fragmental breccia	Minor	1.22‡	24.5	
Non-irradiated salt				+0.1	
Irradiated salt				–0.1	

*Leachate. †Nonleachable. ‡Weight percent in apatite.

and vapor. In a water-free melt, the volatile chloride species are metal chlorides (*24*, *25*). Under such conditions, the bonding of Cl in the vapor and melt phase is similar, so that the preferential kinetic loss of the light isotope is not cancelled out by a different bonding energies of the melt and vapor phase. Vapor loss should increase the δ^{37}Cl value of the residual magma, which explains the extraordinary isotopic range of lunar samples. NaCl, $ZnCl_2$, $FeCl_2$, and other metal chlorides have been observed as surface coatings on lunar volcanic materials (*26*, *27*), consistent with deposition of metal chloride vapor phases. Thermodynamic calculations also support metal halide vapor as the dominant Cl species when the Cl/H ratio is substantially greater than 1 (*8*).

The change in the δ^{37}Cl value of the melt during vapor loss of a metal chloride can be modeled assuming Rayleigh distillation, where $\delta_{final} = \delta_{initial} + [(1000 + \delta_{initial})(F^{(\alpha-1)} - 1)]$, F is the fraction of Cl remaining in the silicate melt, and α is the fractionation between vapor and melt given by $\alpha = [(1000 + \delta_{vapor})/(1000 + \delta_{silicate\ melt})]$. For volatilization of a liquid into a vacuum, $\alpha = \sqrt{m_1/m_2}$, where m_1 and m_2 are the masses of the light and heavy isotopolog of the vaporizing species (*28*). For the common chloride species NaCl, $FeCl_2$, and $ZnCl_2$, α is 0.983, 0.992, and 0.993, respectively. These fractionations are similar to the measured Δ^{37}Cl (silicate−vapor) value from samples 64501,232 ($\alpha = 0.990$) and 61220,39 ($\alpha = 0.992$). Actual fractionations less than those computed from relative mass differences have been observed experimentally (*29*) and are expected when diffusion rates are insufficient to maintain isotopic homogeneity in the melt. Nonetheless, the lighter isotope diffuses faster through the melt, so that fractionation during volatilization will still occur. Volatilization can only increase the δ^{37}Cl value of the residual Cl in the melt. The lowest value of all samples is –0.7‰, measured on leachates of a fire-fountain glass (sample 74002,36). This value is similar to bulk Earth and meteorite samples (*18*) and may be slightly lighter than bulk Moon because it is a vapor condensate sample and is likely the product of some fractionation. This sample is also anomalously volatile rich and is the only sample that has indigenous hydrogen (*12*). As a result, the volatile Cl species could have been HCl, and little fractionation during degassing would be expected. Mare basalt sample 12040,214 has both δ^{37}Cl and δ^{34}S values of 0‰, suggesting minor fractionation during degassing. We conclude that the undifferentiated Moon appears to have a δ^{37}Cl value close to 0‰, similar to Earth.

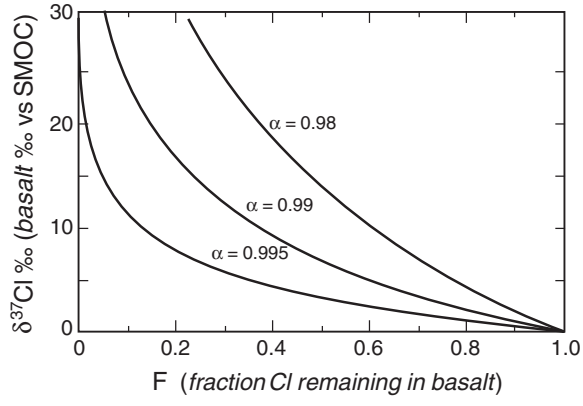

Fig. 2. Calculated trajectories of δ^{37}Cl values of basalt during loss of metal chloride volatiles. A δ^{37}Cl value of 20‰ is obtained at >70% (NaCl) to >90% ($FeCl_2$ or $ZnCl_2$) volatilization ($F < 0.3$) assuming an initial δ^{37}Cl value of 0‰. The α values of 0.983 and 0.992 are obtained from the relationship $\alpha = \sqrt{m_1/m_2}$ for NaCl and $FeCl_2$ or $ZnCl_2$, respectively.

Initial Cl contents were calculated assuming Rayleigh distillation and an initial δ^{37}Cl value of 0‰ (*17*). The amount of Cl vapor loss necessary to reach a ^{37}Cl enrichment equivalent to a δ^{37}Cl value of +20‰ ranges from 63 to 98% for a value of α between 0.983 and 0.992, respectively (Fig. 2). These are minimum degrees of degassing because diffusion-limited exchange will cause a reduction in the fractionation between melt and vapor. The calculated Cl contents of the undegassed basalts (and apatite grains for the ion microprobe analyses) have a positive correlation with the δ^{37}Cl values (Table 1). It is reasonable that samples with high initial Cl contents would lose proportionally more Cl than Cl-poor ones, and therefore evolve to higher δ^{37}Cl values.

The H contents of lunar magmas must have been substantially lower than their Cl contents, or else HCl gas rather than metal chlorides would have been the volatilizing species, and no isotopic fractionation would have occurred. Excepting one pigeonite basalt sample, the calculated initial Cl concentrations of three undifferentiated lunar basalts are all close to 40 parts per million (ppm) (Table 1). Cl volatilization is expected to have occurred only after 90 to 95% crystallization has taken place (*14*), concentrating Cl in the remaining liquid. Primitive melts therefore had Cl concentrations that were lower by at least a factor of 10, or ~4 ppm. Finally, primitive melts generated in the mantle should be concentrated in incompatible elements relative to bulk lunar man-

Downloaded from www.sciencemag.org on August 27, 2010

tle by a factor of ~10 (*30*), so that the lunar mantle should have a Cl concentration of ~400 parts per billion (ppb), with H contents around 10 ppb (given that the Cl/H atomic mass unit ratio is 35.45/1.01), versus the bulk Earth value of ~260 ppm (*17*, *31*).

Isotopic anomalies in lunar samples have been seen in other elemental systems, but never with the extreme variations observed for the Cl isotopes. What makes Cl unique is its hydrophilic affinity and high volatility relative to all other isotopic systems studied in lunar samples. It is therefore an extremely sensitive indicator of H contents. If lunar basalts had initial H contents anywhere close to terrestrial magmas (e.g., MORB), then the extreme fractionations observed in the lunar materials would not have occurred. We suggest that the Moon was anhydrous as initially proposed (*7*) and that the high H contents calculated for some lunar samples are atypical. High H contents are found only in anomalous samples with extreme volatile contents and are likely the product of igneous processes that resulted in extreme volatile enrichment. In contrast to other samples, they have δ^{37}Cl values close to 0‰ and are inconsistent with the high and variable δ^{37}Cl values reported for the majority of lunar samples.

References and Notes

1. A. G. W. Cameron, *Icarus* **126**, 126 (1997).
2. W. K. Hartmann, D. R. Davis, *Icarus* **24**, 504 (1975).
3. R. M. Canup, E. Asphaug, *Nature* **412**, 708 (2001).
4. R. W. Carlson, G. W. Lugmair, in *Origin of the Earth and Moon*, R. M. Canup, K. Righter, Eds. (Univ. of Arizona Press, Tucson, AZ, 2000), pp. 25–44.
5. U. Wiechert *et al.*, *Science* **294**, 345 (2001).
6. K. Pahlevan, D. J. Stevenson, *Earth Planet. Sci. Lett.* **262**, 438 (2007).
7. A. E. Ringwood, *Origin of the Earth and Moon* (Springer-Verlag, New York, 1979).
8. B. J. Fegley, T. D. Swindle, in *Resource of Near-Earth Space*, M. S. M. Lewis, M. L. Guerrieri, Eds. (Univ. of Arizona Press, Tucson, AZ, 1993), pp. 367–426.
9. S. N. Raymond, T. Quinn, J. I. Lunine, *Icarus* **168**, 1 (2004).
10. Y. Abe, E. Ohtani, T. Okuchi, K. Righter, M. Drake, in *Origin of the Earth and Moon*, R. M. Canup, K. Righter, Eds. (Univ. of Arizona Press, Tucson, AZ, 2000), pp. 413–433.
11. F. Albarède, *Nature* **461**, 1227 (2009).
12. A. E. Saal *et al.*, *Nature* **454**, 192 (2008).
13. J. P. Greenwood *et al.*, *Lunar Planet. Sci. Conf.* **41**, 2439.pdf (2010).
14. Y. Liu *et al.*, *Lunar Planet. Sci. Conf.* **41**, 2647.pdf (2010).
15. F. M. McCubbin *et al.*, *Proc. Natl. Acad. Sci. U.S.A.* **107**, 11223 (2010).
16. Z. D. Sharp, J. D. Barnes, T. P. Fischer, M. Halick, *Geochim. Cosmochim. Acta* **74**, 264 (2010).
17. See supporting material on *Science* Online.
18. Z. D. Sharp *et al.*, *Nature* **446**, 1062 (2007).
19. M. Bonifacie *et al.*, *Science* **319**, 1518 (2008).
20. C. K. Shearer *et al.*, in *New Views of the Moon*, B. L. Jolliff, M. A. Wieczorek, C. K. Shearer, C. R. Neal, Eds. (Mineralogical Society of America, Chantilly, VA, 2006), vol. 60, pp. 365–518.
21. M. Humayun, R. N. Clayton, *Geochim. Cosmochim. Acta* **59**, 2131 (1995).
22. R. V. Morris, *Proc. Lunar Planet. Sci.* **9**, 2287 (1978).
23. E. A. Schauble, G. R. Rossman, H. P. Taylor, *Geochim. Cosmochim. Acta* **67**, 3267 (2003).
24. B. J. Fegley Jr., *Geophys. Res. Lett.* **18**, 2073 (1991).
25. R. O. Colson, *Proc. Lunar Planet. Sci.* **22**, 427 (1992).
26. C.-L. Chou, W. V. Boynton, L. L. Sundberg, J. T. Wasson, *Proc. Lunar Planet. Sci. Conf.* **2**, 1701 (1975).
27. D. S. McKay, S. J. Wentworth, *Lunar Planet. Sci. Conf.* **24**, 961 (1993).
28. T. M. Esat, *Geochim. Cosmochim. Acta* **52**, 1409 (1988).
29. F. M. Richter, P. E. Janney, R. A. Mendybaev, A. M. Davis, M. Wadhwa, *Geochim. Cosmochim. Acta* **71**, 5544 (2007).
30. C. K. Shearer, J. J. Papike, *Am. Mineral.* **84**, 1469 (1999).
31. W. F. McDonough, in *The Mantle and Core: Treatise on Geochemistry*, vol. 2, R. W. Carlson, Ed. (Elsevier, Amsterdam, 2003), pp. 547–568.
32. J. D. Barnes, Z. D. Sharp, T. P. Fischer, D. R. Hilton, M. J. Carr, *Geochem. Geophys. Geosyst.* **10**, Q11S17 (2009).
33. J. D. Barnes, Z. D. Sharp, T. P. Fischer, *Geology* **36**, 883 (2008).

34. Supported by NASA Origins grant 07-SSO07-0077 (Z.D.S.), NASA LASER grant NNX08AY786 (C.K.S.), and a NASA Cosmochemistry grant (K.D.M.). The UCLA ion microprobe facility is partially supported by a grant from the NSF Instrumentation and Facilities Program. We thank lunar curator G. Lofgren and staff of the Johnson Space Center, Houston. P. Burger provided imaging and quantitative elemental analyses of apatite. The Ion Beam Materials Laboratory at Los Alamos is partially supported by DOE Office of Basic Energy Sciences programs.

Supporting Online Material

www.sciencemag.org/cgi/content/full/science.1192606/DC1
Materials and Methods
Table S1
References

20 May 2010; accepted 26 July 2010
Published online 5 August 2010;
10.1126/science.1192606
Include this information when citing this paper.

An Adaptable Peptide-Based Porous Material

J. Rabone, Y.-F. Yue, S. Y. Chong, K. C. Stylianou, J. Bacsa, D. Bradshaw, G. R. Darling, N. G. Berry, Y. Z. Khimyak, A. Y. Ganin, P. Wiper, J. B. Claridge, M. J. Rosseinsky

Porous materials find widespread application in storage, separation, and catalytic technologies. We report a crystalline porous solid with adaptable porosity, in which a simple dipeptide linker is arranged in a regular array by coordination to metal centers. Experiments reinforced by molecular dynamics simulations showed that low-energy torsions and displacements of the peptides enabled the available pore volume to evolve smoothly from zero as the guest loading increased. The observed cooperative feedback in sorption isotherms resembled the response of proteins undergoing conformational selection, suggesting an energy landscape similar to that required for protein folding. The flexible peptide linker was shown to play the pivotal role in changing the pore conformation.

The sorption of a guest molecule by a rigid porous material such as a zeolite (*1*) or active carbon (*2*) is controlled by the fixed size and shape of the pores, whereas in some metal-organic framework [MOF (*3*)] materials the geometry of the porosity can change in response to guest species (*4*, *5*), producing complex behaviors that challenge classical sorption models (*5*, *6*). The adaptability of MOF porosity is limited by both the metal coordination geometry and the degrees of freedom available to the linkers. When the geometry of the metal coordination is fixed (as is usual), MOFs built from rigid linkers are limited to configurations that can be accessed by uniaxial rotations (*7*) and displacement of the linkers. In contrast, proteins are characterized by an adaptable response to their environment, produced by conformational selection of an appropriate functional structure (e.g., for enzyme catalysis) from a large ensemble of energetically low-lying and kinetically accessible states (*8*). This is enabled by the manifold torsions available to polypeptide chains, which allow folding into the required structures. In this work, we used a dipeptide (glycylalanine, Gly-Ala) linker to assemble a crystalline porous framework through metal binding. The resulting material combines preformed pores with the degrees of freedom from a peptide linker required for conformational selection, displaying adaptable porosity that evolves continuously from an open to a partially disordered closed structure in response to the level of guest loading.

There is a spectrum of porous materials that can sorb guest species, from amorphous swelling polymers (*9*) through crystalline molecular assemblies (*10*–*12*) and flexible MOFs (*5*) to entirely rigid systems such as the zeolites (*1*) and other classical sorbents (*2*). While several peptide-based open frameworks are known (*13*–*23*), sorption data (*13*, *14*, *20*) and reports on their guest-loss behavior are rare (*17*, *18*), although sorption mechanisms in metal-peptide frameworks (*17*, *18*, *21*–*23*) could provide insights into protein behavior otherwise obscured by atomic disorder. We have used Gly-Ala as a dipeptide linker possessing the conformational degrees of freedom involved in protein folding with the Zn^{2+} cation characterized by its ability to adopt a range of coordination environments. This combination of preformed pores with a conformationally flexible linker opens the possibility of materials that lie on the boundary between ordered MOFs and amorphous systems.

Crystals of the metal-dipeptide framework $[Zn(Gly\text{-}Ala)_2]\cdot(solvent)$, **1**, were obtained by reacting zinc nitrate with Gly-Ala in 90% methanol/

Department of Chemistry, University of Liverpool, Liverpool, L69 7ZD, UK.

*To whom correspondence should be addressed. E-mail: m.j.rosseinsky@liverpool.ac.uk

Downloaded from www.sciencemag.org on August 27, 2010

10% aqueous NaOH [supporting online material (SOM) section S1 describes synthesis, handling, and compositional and chiral purity analysis]. In **1** (SOM section S2 describes crystallographic characterization) (Fig. 1), the zinc ions are tetrahedrally coordinated (fig. S6A and table S4) to four dipeptide ligands; two dipeptide ligands are coordinated by the C-terminal Ala carboxylate groups and two by N-terminal Gly amine groups. Each ligand is coordinated to two zinc ions, forming layers with a gridlike structure (Fig. 1A). The layers are aligned in an AA fashion in the third dimension by hydrogen bonds between all of the amide groups in adjacent layers to form one-dimensional, square-shaped pores running parallel to the crystallographic *c* axis (Fig. 1B). The amide groups line the walls of the pore and are linked by hydrogen bonds (Fig. 1C) with an alignment similar to that in β-sheet structures of polypeptides, controlled by the torsional conformation of the dipeptide, which is defined by four torsion angles ψ, ϕ, ψ_T, ϕ_T (Fig. 1D, fig. S4, and table S4). The zinc ions impose a porous structure [solvent-accessible volume 532.7 Å^3 per unit cell at 100 K (28%)] distinct from the β sheet because they are tetrahedral rather than linear connectors of the dipeptide units. The resulting porosity has a complex topography that is defined by the positions of the methyl side chains of the L-alanine component of the dipeptide within the channels. Two methyl groups from opposite sides of the grid project into the channels, producing constrictions in the porosity and conferring a bilobal "hourglass" shape on the void space (Fig. 1, B and E, and fig. S7). The polar methanol guests occupying this porosity in as-made **1** are located within two regions by hydrogen bonding interactions with the pore wall to carboxylate and amide groups (figs. S9 and S10). The ^{13}C cross-polarization/magic angle spinning nuclear magnetic resonance (CP/MAS NMR) spectrum of **1** displays the five expected resonances from the single crystallographically distinct peptide itself, slightly shifted from the positions in the isolated ligand (Fig. 2A and SOM section S7), together with a sixth resonance at 49.5 parts per million (ppm) from the CH_3OH solvent guest species. The observed methyl shift of 20.7 ppm is entirely consistent with the 19- to 24-ppm range expected for the β-sheet–like peptide conformation seen in the structure of **1** (*24*).

The solvent in **1** can be removed reversibly to give a desolvated material **1′** stable to 250°C (fig. S1). The powder x-ray diffraction pattern of **1′** indicates a strong structural response to guest loss, with a pronounced shift (1.115 Å to smaller d-spacing) of the most intense reflection (110 in **1**) and a marked decrease in crystallinity. The diffraction pattern of **1′** can be indexed with a triclinic cell related to a 2 × 1 × 4 supercell of **1** as shown by Le Bail fitting (figs. S12 and S13) but cannot be solved, consistent with the reduction in crystalline order manifested in the ^{13}C CP/MAS NMR resonances broadening and splitting into multiple peaks in **1′** (Fig. 2A and SOM section S7). The main changes in the spectra are observed for the Ala residue—the carboxyl C1 shows at least three nonequivalent sites and the tertiary C2 site shows at least five resonances. The most pronounced changes are seen in the C5 resonance from the Ala methyl, which is a powerful probe of the conformational state of the residue and is particularly affected by the ϕ torsion, and the packing of methyl groups in solid materials (SOM section S9) (*25*). In **1′**, at least seven Ala methyl resonances with chemical shifts in the range 15.7 to 23 ppm are observed (Fig. 2A, inset, and table S10). This is consistent with the development of considerable heterogeneity in the Ala conformation in desolvated **1′**, including conformations not present in the solvated material, as indicated by the distinct shift at 15.7 ppm. The disorder on guest loss can be related to trapping of local differences in torsional states found in some protein tertiary structures on water removal (*26*) when hydrogen bond exchange becomes more difficult.

The structural changes associated with the NMR and x-ray scattering observations were identified from molecular dynamics (MD) simulations (SOM section S3-5). Simulations were performed using a 8 × 8 × 12 supercell of the as-grown structure **1**, and using the same supercell with the solvent removed to access the structure of desolvated **1′**. In these simulations, the cell shrinks within a few tens of picoseconds to form an ordered structure with greatly reduced porosity (fig. S15A), which then gradually becomes partially disordered over a period of 100 ps (fig. S15B). The pore closing is attributable to van der Waals interactions between the methyl groups within the collapsed **1′** structure, as confirmed using van der Waals–corrected density functional theory (DFT) calculations (SOM section S6). Consistent with the NMR observations, there is a pronounced increase in the number of distinct Ala methyl environments in the final MD structure of desolvated **1′**, with cluster analysis giving at least four methyl environments compared to the single environment observed in **1** (SOM section S8). The methyl position is controlled by the torsional conformation of the Gly-

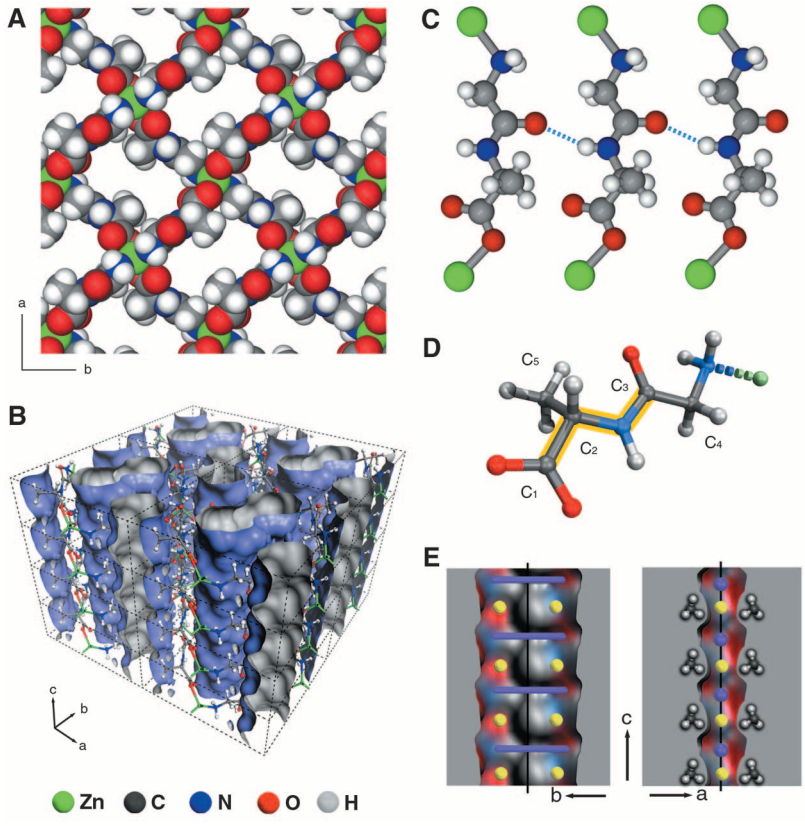

Fig. 1. Structure of **1** [298 K, orthorhombic $P2_12_12$; a =14.109(16) Å, b = 14.455(17) Å, c = 4.799(6) Å] (**A**) Space-filling representation showing the one-dimensional hourglass-shaped cavities projected along the *c* axis of **1**. (**B**) Perspective view of channels in **1**. (**C**) Stacking of the layers by alignment of hydrogen bonds (shown as dashed lines) and the walls of the channels –Zn···Zn = 4.816(7) Å, N_1-O_3 (at x, y, $1 + z$) = 3.06 (1) Å. (**D**) The Gly-Ala dipeptide ligand with carbon atom labels and the ϕ torsion highlighted in yellow (the other torsions are shown in fig. S4). (**E**) Cross sections of a pore Connolly surface with the larger volumes within the pores highlighted in purple and constrictions highlighted in yellow. The constrictions are formed by the methyl groups that project into the pore; the position of the methyl groups is shown in the right panel. The maximum-solvent accessible pore area was 29.2 Å^2 (maximum and minimum dimensions of 6.2 and 3.7 Å) and the minimum was 15.6 Å^2 (maximimum and minimum dimensions of 5.2 and 2.0 Å) as calculated with HOLE (*34*).

Downloaded from www.sciencemag.org on August 27, 2010

Ala dipeptide linker (Fig. 1D and fig. S4), which affords a convenient measure of the local structural disorder. A 6° ± 1° change in the peptide torsion angles allows the methyl side chains to fill and thus close the porosity. Comparison of the torsion angle distributions obtained for **1′** and **1** shows that in **1′**, in addition to the ligands covering a greater conformational range (fig. S18), the ligands can be resolved into different clusters by the time averages of their torsion angles (figs. S17 and S19). The match between the calculated (not fitted) total x-ray scattering function of the MD-simulated structures of **1′** and experiment improves as the structure disorders, capturing the positional shift of the most intense observed reflection noted above (fig. S16).

The simulations suggest that changes in the peptide torsional state in desolvated **1′** produce the multiple methyl environments seen in NMR spectra, and predict that these changes act to close the porosity of **1**. This is confirmed by gas sorption experiments: **1′** does not sorb N_2 at 77 or 195 K, nor H_2 at 77 K (fig. S21 E to G). MD simulations of desorption (*27*) that allow the structure to relax in response to the extent of guest loading (SOM section S11) show that both H_2 and N_2 sorption by **1′** are thermodynamically unfavorable.

The sorption response of **1′** to CO_2, MeOH, and water, however, is quite different. **1′** is nonporous to these guests at low pressure, but sorption occurs above a temperature-dependent gate pressure (*28*) (Fig. 2B and fig. S21). Such sigmoidal dependencies have previously been observed as a result of lattice expansion and polymorph switching in soft porous materials (*11*, *12*), and guest rearrangements in rigid hosts (*29*) (SOM text S12), and also in the cooperative binding of substrates to proteins, e.g., oxygen in hemoglobin [with hysteresis found in the case of sickle cell hemoglobin (*30*)]. Indeed, the Hill model (*31*), which relates the cooperative feedback of guest sorption to a power of the guest concentration (or pressure), provides a good description of the desorption isotherms (Fig. 2C), and thus the functional form of the isotherm is consistent with cooperative sorption of guests by **1′** just above the gate pressure (fig. S35). MD simulations show that the uptake of these guests is thermodynamically favorable. The simulations reveal that the porosity adapts to variations in loading of these guests by small, coupled torsional, orientational, and displacive changes of the peptide. These changes reduce the pore volume smoothly from that of **1** by continuous methyl-group repositioning as the guest loading decreases. The ϕ torsion, which defines the relative positions of the methyl groups of the Ala residue, must change for the porosity to close upon guest removal (Fig. 3 and animations). If the ϕ torsion angle were fixed, steric interactions between methyl groups on opposite sides of the pores would prevent the pore from closing. Rotation of two opposing Ala residues in the same sense about the ϕ torsions moves the methyl groups in opposite directions (Fig. 3, A and B), allowing them to slide past each other and thus enable displacement of the dipeptide molecules (Fig. 3C) to close the pore. The conformational changes at the Ala residue are matched by a conformational change in Gly, which is required to retain the tetrahedral coordination around the zinc ions, because the carboxylate groups necessarily move with the methyl groups.

The coupled torsional degrees of freedom allow the pores to close cooperatively in response to reduced guest loading without large energy changes (figs. S29 to S32). This allows sorption equilibrium in **1′** to be established between many thermally accessible sorption states separated by low energy barriers rather than between the gas phase and a single sorbed phase. This ability of the structure to respond locally to guest molecules provides an explanation for the observed gating. Once sorption commences in **1′** and the pores start to open, the barriers to sorption are reduced, allowing greater uptake. The observed gate pressure is then a consequence of the dependence of the sorption rate on the amount of guest already sorbed, with the adaptation of the host structure to guest loading allowing different sorption and desorption paths consistent with the observed hysteresis (SOM section S12). The MD enthalpies predict separation into low-loading and high-loading phases at partial MeOH or CO_2 loadings, confirmed by powder x-ray diffraction and NMR measurements (SOM section S10).

To understand the interplay of forces that allow certain molecules to sorb into **1′** by triggering the opening of the initially closed pores, we performed MD simulations of CO_2 diffusion (*32*) in partially closed pores (loading = 2.3% by mass) (SOM section S13). At 195 and 273 K, the diffusion of CO_2 along the pores was too slow to be observed on normal simulation time scales, but at 400 K the rate was fast enough for several diffusion events to occur within a typical 40 ps simulation (fig. S37 and animations). Analysis of the diffusion events reveals that for most of the time, CO_2 molecules occupy the larger volumes within the pores (Fig. 1 E, purple spheres) but they occasionally make rapid hops between them when aligned along the *c*-axis channel direction, passing through the constrictions (Fig. 1 E, yellow spheres). The larger volumes lie between

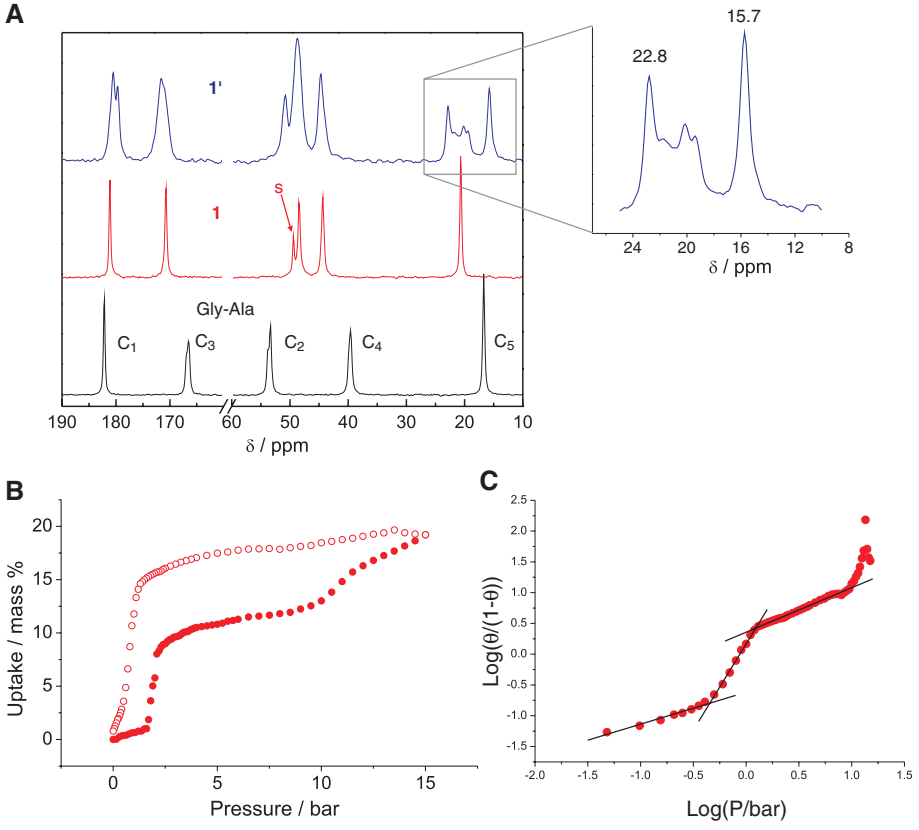

Fig. 2. (**A**) Solid-state ^{13}C CP/MAS NMR (100.56 MHz) of peptide ligand Gly-Ala (bottom, black), as-made **1** (middle, red), and desolvated **1′** (top, blue) measured at room temperature. The resonances of the Ala methyl carbon for the desolvated and as-made samples are enlarged for clarity. Atom labels are given in Fig. 1D; for **1**, the peak labeled "s" shows the resonance from the guest methanol. (**B**) Experimental CO_2 isotherms of **1′** at 273 K (closed and open symbols show adsorption and desorption, respectively) exhibiting gating above a pressure of 2 bar on the sorption branch. (**C**) Hill plot of the experimental desorption branch of the isotherm in (B), where θ is the fractional loading. The fitted solid lines show three sorption regimes with the high-gradient region corresponding to strongly cooperative sorption and Hill coefficient of 2.8 (SOM section S12).

Downloaded from www.sciencemag.org on August 27, 2010

pairs of methyl groups that project into the pore, whereas the constrictions are formed by the pairs of methyl groups themselves. The steric repulsion acting between the methyl groups and the CO_2 molecules when they pass a constriction is partially alleviated by polar interactions with the amide bonds, which coincide with the constriction. Figure 4, A and B, and animations (SOM section S14) show the detailed trajectory of a single CO_2 molecule diffusing along a channel during the 40-ps simulation. This requires coupled torsion and displacement of a ligand to remove the methyl side chain from its initial position obstructing the pore. The extensive conformational space that the peptide ligands can adopt with minimal energy penalties facilitates these motions (Fig. 4C). A notable feature of the diffusion through the constriction is the cooperative manner in which the CO_2 molecules interact with the ligands. Favorable interactions between the polar groups on one side of the pore (amide, carboxylate, and amine) and the CO_2 molecule (at the point where the CO_2 molecule is colored yellow in Fig. 4) are strong enough to force the Gly-Ala ligand on the opposite side (ligand labeled b in Fig. 4) into the pore wall, particularly as the CO_2 molecule is aligned with the carbonyl moiety of the amide along the *c* axis so as to maximize polar interactions—this is a specific chemical trigger of the diffusion event.

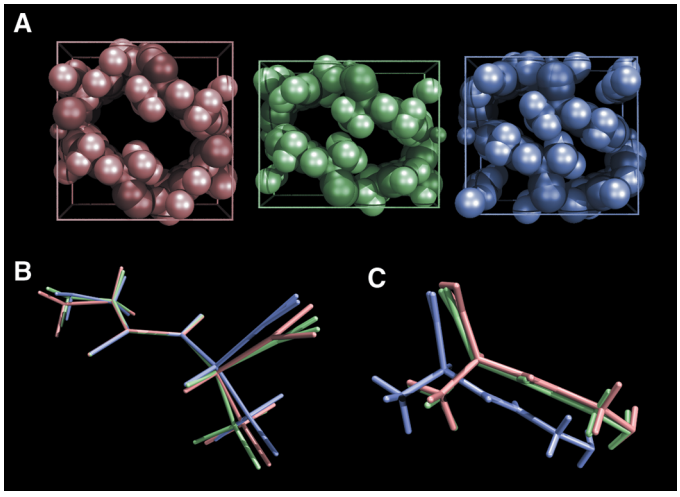

Fig. 3. A single pore at three CO_2 loadings. The intermediate loading demarcates the transition from the first to the second stage of closure, and both stages show that gradual changes in the torsion angles of the ligand occur (see fig. S30 for more details and SOM section S14 for animations). The color represents CO_2 loading with pink = 9.00 (fully loaded), green = 5.25 (after the initial stage of collapse), and blue = 0.75 molecules per unit cell. (**A**) Space-filling representations of the pore as it closes. (**B**) Overlaid images of the peptide ligand during pore closing, aligned on the amide group to show the changes in the ϕ torsion of the alanine residue and the ψ torsion of the glycine residue (fig. S4). (**C**) Overlaid images of the peptide ligand during pore closing, showing their relative positions in the unit cell.

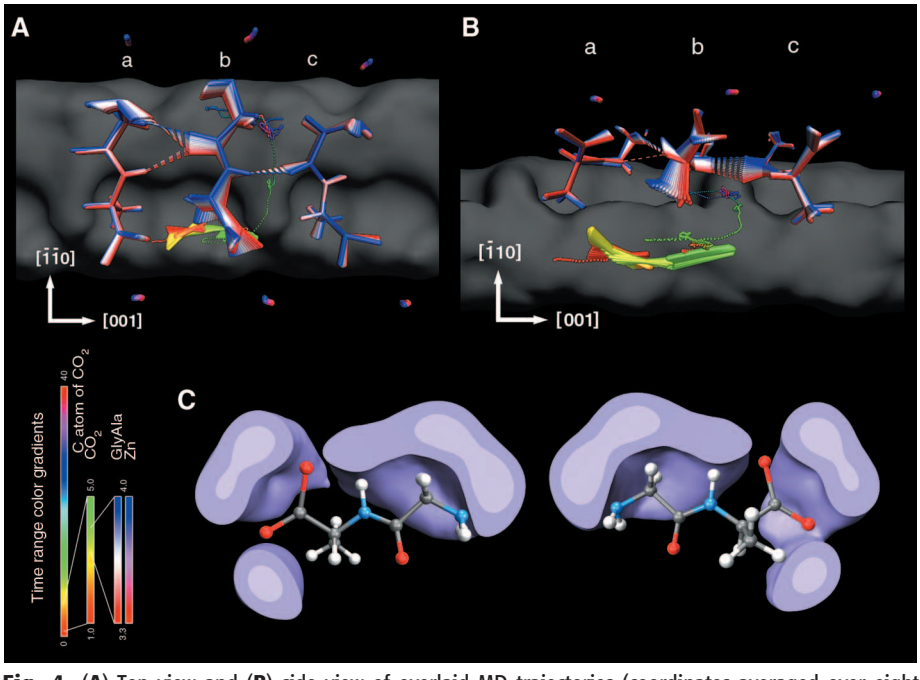

Fig. 4. (**A**) Top view and (**B**) side view of overlaid MD trajectories (coordinates averaged over eight consecutive snapshots 0.05 ps apart to reduce thermal noise) showing a CO_2 molecule diffusing in partly loaded **1′** (see SOM sections S13 for details and S14 for animations). Different color gradients are used to represent different time ranges for various components of the structure (see scale), and the gray isosurface represents the Connolly surface of the pore wall. Hydrogen bonds between the peptide ligands are shown as dashed cylinders. (**C**) Thermally accessible conformations for the Gly-Ala ligand at 273 K displayed as an isosurface (SOM section S13). The purple isosurface encloses the regions where zinc ions can bind to the carboxylate or amine groups as the four peptide torsions cover the thermally accessible range of angles. The isosurface is cut by a plane to show the ligand in the conformation it adopts in **1** with the lighter shade depicting a volume of higher binding probability. The range of the isosurface is much greater than, for example, in terephthalate (fig. S38).

The experimental isotherms and desorption simulations of the peptide-linked framework **1′** show that the pores block when no guests are present, gradually and cooperatively opening when triggered by small molecules possessing polar bonds. This adaptable porosity is a direct consequence of the peptide linkers. The four synergistic torsional degrees of freedom of the dipeptide (Fig. 4C) allow the methyl group to control the accessible void volume, the resulting conformations being identified by MASNMR. The low-energy states accessed during this deformation of the host are defined by the cooperative torsions thermally available in the arrangement of the dipeptides in **1′** by the coordinate (from the metal center) and hydrogen bonding (from the rigidly planar amide unit) interactions. This allows the framework to be maintained during the adaptation despite the large change in guest-available space. The complex sorption behavior of **1′** is attributable to the accessibility of the resulting many sorption states with low energy barriers between them, in contrast to the binary switching effect observed in rigid-linker MOF materials (*33*), in which a single kinetic barrier controls the transition between open- and closed-pore forms. This suggests a cooperative sorption mechanism analogous to conformational selection in proteins, due to an energy landscape defined by low-energy torsional motions of the peptide unit that control both responses. The energy landscape may allow selective sorption capable of addressing complex separation, sorting, and reaction problems reminiscent of those addressed by biological systems. (*34*)

References and Notes

1. M. E. Davis, *Ind. Eng. Chem. Res.* **30**, 1675 (1991).
2. K. S. W. Sing, in *Porosity in Carbons*, J. W. Patrick, Ed. (Arnold, London, 1995), pp. 49–66.
3. D. J. Tranchemontagne, J. L. Mendoza-Cortés, M. O'Keeffe, O. M. Yaghi, *Chem. Soc. Rev.* **38**, 1257 (2009).
4. C. Serre *et al.*, *Science* **315**, 1828 (2007).
5. S. Horike, S. Shimomura, S. Kitagawa, *Nat. Chem.* **1**, 695 (2009).
6. H. J. Choi, M. Dincă, J. R. Long, *J. Am. Chem. Soc.* **130**, 7848 (2008).
7. E. B. Winston *et al.*, *Phys. Chem. Chem. Phys.* **10**, 5188 (2008).
8. D. D. Boehr, R. Nussinov, P. E. Wright, *Nat. Chem. Biol.* **5**, 789 (2009).

Downloaded from www.sciencemag.org on August 27, 2010

9. O. Okay, *Prog. Polym. Sci.* **25**, 711 (2000).
10. J. L. Atwood, L. J. Barbour, A. Jerga, *Science* **296**, 2367 (2002).
11. S. A. Allison, R. M. Barrer, *J. Chem. Soc. A* **11**, 1717 (1969).
12. D. V. Soldatov, *J. Chem. Crystallogr.* **36**, 747 (2006).
13. R. Anedda, D. V. Soldatov, I. L. Moudrakovski, M. Casu, J. A. Ripmeester, *Chem. Mater.* **20**, 2908 (2008).
14. A. Comotti, S. Bracco, G. Distefano, P. Sozzani, *Chem. Commun. (Camb.)* **3**, 284 (2009).
15. C. H. Görbitz, *Chemistry* **13**, 1022 (2007).
16. C. H. Görbitz, F. Rise, *J. Pept. Sci.* **14**, 210 (2008).
17. H. Y. Lee, J. W. Kampf, K. S. Park, E. N. G. Marsh, *Cryst. Growth Des.* **8**, 296 (2008).
18. A. Mantion *et al.*, *J. Am. Chem. Soc.* **130**, 2517 (2008).
19. M. Peterca *et al.*, *J. Am. Chem. Soc.* **128**, 6713 (2006).
20. D. V. Soldatov, I. L. Moudrakovski, J. A. Ripmeester, *Angew. Chem. Int. Ed.* **43**, 6308 (2004).
21. T. Takayama *et al.*, *Soc. Jpn.* **69**, 1579 (1996).
22. M. Tiliakos *et al.*, *Inorg. Chem. Commun.* **8**, 1085 (2005).
23. E. Ueda *et al.*, *Soc. Jpn.* **77**, 981 (2004).
24. T. Asakura, Y. Nakazawa, E. Ohnishi, F. Moro, *Protein Sci.* **14**, 2654 (2005).
25. K. Ohgo, T. Kawase, J. Ashida, T. Asakura, *Biomacromolecules* **7**, 1210 (2006).
26. J. A. Bell, *Protein Sci.* **8**, 2033 (1999).
27. T. Düren, Y. S. Bae, R. Q. Snurr, *Chem. Soc. Rev.* **38**, 1237 (2009).
28. R. Kitaura, K. Seki, G. Akiyama, S. Kitagawa, *Angew. Chem. Int. Ed.* **42**, 428 (2003).
29. D. H. Olson, G. T. Kokotailo, S. L. Lawton, W. M. Meier, *J. Phys. Chem.* **85**, 2238 (1981).
30. H. Mizukami, A. G. Beaudoin, D. E. Bartnicki, B. Adams, *Proc. Soc. Exp. Biol. Med.* **154**, 304 (1977).
31. A. V. Hill, *Proc. Phys. Soc.* **40**, 4 (1910).
32. D. Dubbeldam, R. Q. Snurr, *Mol. Simul.* **33**, 305 (2007).
33. F. Salles *et al.*, *Angew. Chem. Int. Ed.* **47**, 8487 (2008).
34. O. S. Smart, J. M. Goodfellow, B. A. Wallace, *Biophys. J.* **65**, 2455 (1993).

35. We thank the UK Engineering and Physical Sciences Research Council for funding under grant EP/F027443.

Supporting Online Material

www.sciencemag.org/cgi/content/full/329/5995/1053/DC1
Materials and Methods
Figs. S1 to S38
Tables S1 to S18
References
Movies S1 to S6

8 April 2010; accepted 7 July 2010
10.1126/science.1190672

Trapping a Diradical Transition State by Mechanochemical Polymer Extension

Jeremy M. Lenhardt,[1] Mitchell T. Ong,[2] Robert Choe,[1] Christian R. Evenhuis,[2] Todd J. Martinez,[2]* Stephen L. Craig[1]*

Transition state structures are central to the rates and outcomes of chemical reactions, but their fleeting existence often leaves their properties to be inferred rather than observed. By treating polybutadiene with a difluorocarbene source, we embedded *gem*-difluorocyclopropanes (*g*DFCs) along the polymer backbone. We report that mechanochemical activation of the polymer under tension opens the *g*DFCs and traps a 1,3-diradical that is formally a transition state in their stress-free electrocyclic isomerization. The trapped diradical lives long enough that we can observe its noncanonical participation in bimolecular addition reactions. Furthermore, the application of a transient tensile force induces a net isomerization of the *trans-g*DFC into its less-stable cis isomer, leading to the counterintuitive result that the *g*DFC contracts in response to a transient force of extension.

The rates and outcomes of chemical reactions are typically interpreted via the concept of transition states: the highest energy conformations through which molecules must pass during the course of a reaction. Transition states are central to our understanding of chemical reactivity, but their ephemeral existence (a single bond vibration, ~10^{-13} s) prohibits their capture and presents a formidable challenge to their direct characterization. Ultrafast (*1*, *2*) and photoelectron (*3*) spectroscopy experiments have been used to capture structural and dynamic details of these fleeting structures, shedding light on transition states and their properties. In this realm, recent studies have shown that strong and directional coupling of a reactive molecule to an external force can lead to unanticipated reactivity and provide opportunities for mechanistic insight (*4*–*10*). We describe how this idea can be extended to literally force *gem*-difluorocyclopropanes (*g*DFCs) into tension-locked conformations at or near that of a transition state.

The *g*DFCs exhibit good long-term stability under ambient conditions, but the C-C bond opposite the difluoromethylene is substantially weaker than a typical C-C single bond because of a combination of ring strain and stereoelectronic effects (*11*, *12*). When the *g*DFCs are generated by the addition of difluorocarbene to alkenes along the backbone of 1,4-polybutadiene (PB), the weak bond is formed in the main chain of the polymer, and the tensile stresses associated with polymer extension are naturally coupled to its activation (*4*, *13*, *14*). The addition of difluorocarbene to PB is stereospecific, and so a mixture of cis and trans alkenes in the PB leads to a similar mixture of cis and trans stereoisomers in the *g*DFC-functionalized polymer (*15*). The as-synthesized polymer features a cis:trans *g*DFC ratio of 1:1.2. This ratio is kinetically rather than thermodynamically determined during the synthesis; the trans isomer is ~1.0 kcal mole^{-1} more stable than the cis (*16*), and thermal isomerization of the polymer at 200°C overnight in a microwave reactor leads to the expected equilibrium product ratio (cis:trans = 1:2.6), confirming the greater stability of the *trans-g*DFC (Fig. 1).

Vastly different results are observed when the isomerization is induced mechanically, rather than thermally, by coupling the *g*DFC to large elongational shear fields generated by ultrasonication. Embedding the *g*DFCs within the 209-kD PB backbone provides a scaffold that is sufficiently large to experience a substantial elongational force gradient, leading to extension of the polymer chain and an externally generated tension within the constituent C-C bonds (*4*, *14*, *17*, *18*). Whereas thermal isomerization takes hours, shear-induced isomerization is observed in minutes at ~6° to 9°C. More compelling than the rate of isomerization, however, is that its direction is reversed; there is a steady and unexpected conversion of the more-stable *trans-g*DFC into its less-stable cis isomer, resulting in a cis:trans ratio of 3.5:1 after 60 min (Fig. 1). The mechanical nature of polymer sonochemistry is well established (*4*, *14*, *17*, *18*), as supported here by a series of observations and control experiments. First, the fact that the conversion occurs from more- to less-stable isomer rules out thermal activation. Second, the kinetics of *g*DFC reactivity have a characteristic polymer molecular weight (MW) dependence that is very similar to those of chain scission and the electrocyclic rearrangement of *gem*-dichlorocyclopropanes to 2,3-dichloroalkenes (fig. S26 and S32), processes whose mechanical origins have been previously demonstrated (*17*, *18*). Third, an 8.2-kD *g*DFC-functionalized polymer is below the critical MW necessary to experience significant elongational shear forces necessary for mechanical activation, and identical sonication conditions produce no evidence of isomerization.

The direction of the isomerization rules out simple mechanical acceleration of the cis-trans equilibration (*19*), which will always lead to an excess of the more-stable trans isomer. Rather, the applied tension must effectively create a distinct, transient equilibrium by populating one or more new intermediates that are more stable than the closed cyclopropanes. These intermediates must subsequently convert preferentially to the cis isomer once the tension is removed. The basis for such a process is found in the mechanism of the thermal, stress-free *g*DFC ring-opening reaction, which occurs through a concerted, disrotatory motion (*16*): Coupled rotation in the *cis-g*DFC ring opening proceeds through an s-trans/s-trans diradical, whereas the *trans-g*DFC preferentially opens through an s-trans/s-cis diradical. Because the same orbital symmetry rules apply to the ring closing, the majority of ring-opening and -closing

[1]Department of Chemistry, Duke University, Durham, NC 27708, USA. [2]Department of Chemistry, Stanford University, Stanford, CA 94305, USA.

*To whom correspondence should be addressed. E-mail: todd.martinez@stanford.edu (T.J.M.); stephen.craig@duke.edu (S.L.C.)

Downloaded from www.sciencemag.org on August 27, 2010

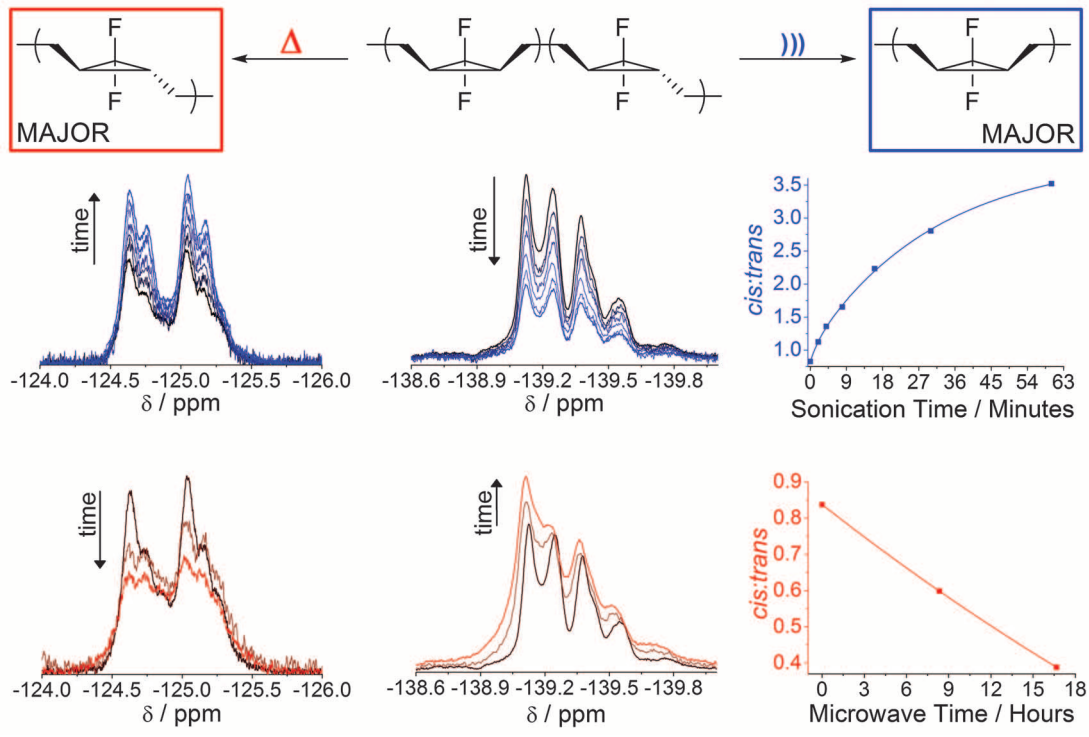

Fig. 1. Sonication (11.9 W cm^{-2}, 6 to 9°C) of a mixture of *cis*- and *trans*-*g*DFC–PB dissolved in tetrahydrofuran (THF) under N_2 leads to formation of the less-stable cis isomer [chemical shift (δ) = –125 parts per million (ppm) in the ^{19}F–nuclear magnetic resonance (NMR) spectrum], whereas microwave thermolysis of the polymer in *o*-dichlorobenzene (200°C under N_2) leads to equilibration to the expected cis:trans ratio (with *trans*-*g*DFC resonating at –139.2 ppm). Similar results are observed for reactions in benzene (fig. S31).

reactions do not lead to interconversion of *cis*- and *trans*-*g*DFCs (*16*). Under tension, however, the formation of the cis isomer suggests that mechanical activation of both the *cis*- and *trans*-*g*DFC leads to an s-trans/s-trans diradical whose extended conformation is favored by the coupling to the polymer tension. The s-trans/s-trans diradical is first formed under the transient mechanical stress of the elongational flow and then relaxes through a disrotatory ring closing to the *cis*-*g*DFC once the external tension is released, in effect, acting as a molecular ratchet (*20*, *21*) that is driven by the periodic oscillation between states of high and low tension.

Molecular dynamics simulations support this view. Ab initio steered molecular dynamics (AISMD) (*22*) techniques were used to analyze the mechanical reactivity of *g*DFC. The potential energy surface was determined on the fly by using the complete active space self-consistent field method (CASSCF) (*23*) with second-order perturbative corrections [i.e., CAS(2/2)-PT2] (*24*). In the simulations, an external force was applied to hydrogen atoms of the adjacent methylene groups, which were set either trans or cis relative to each other in order to model trans or cis attachment of the surrounding polymer chain. In both cases, we followed the dynamics for 1 ps under the applied force. Snapshots of representative reactive trajectories are shown in Fig. 2, A and B, for cis and trans attachment, respectively. On application of a 2-nN force to cis attachment points, 6 out of 20 trajectories opened in disrotatory fashion to form the diradical, which is the thermally allowed pathway (Fig. 2C). The other 14 trajectories did not undergo ring opening within 1 ps but would be expected to do so if

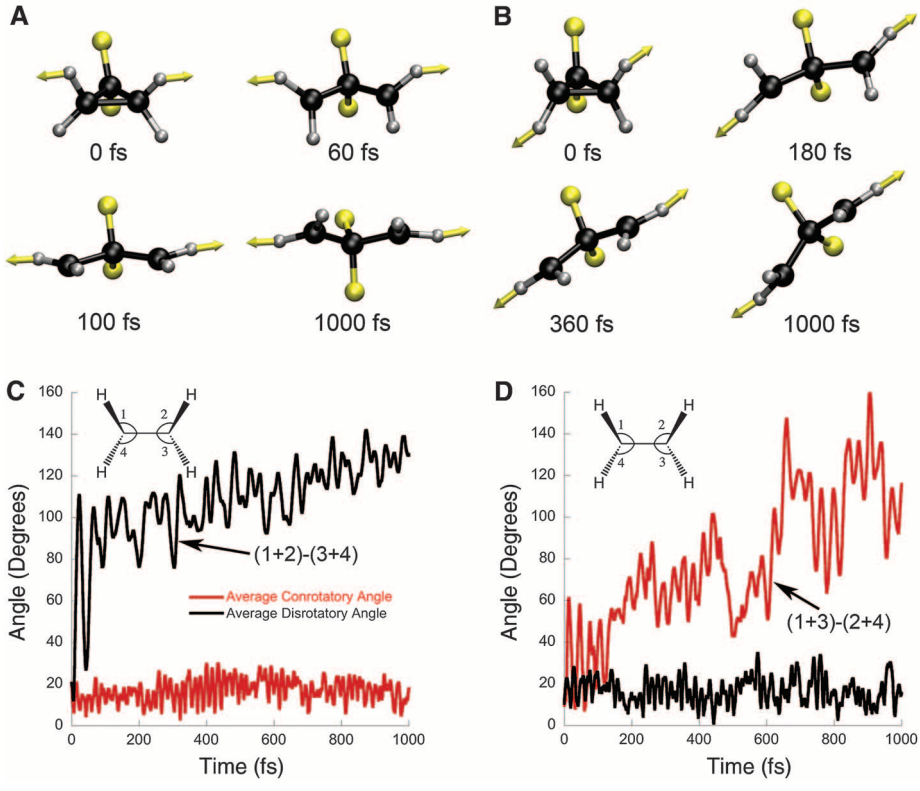

Fig. 2. Mechanical activation of the *gem*-difluorocyclopropane from AISMD simulations. Snapshots of representative trajectories pulling on (**A**) cis attachment points at an applied force of 2 nN and (**B**) trans attachment points at an applied force of 3 nN. Cis and trans pulling result in predominantly disrotatory and conrotatory ring opening, respectively. Yellow arrows designate the pulling direction. The average conrotatory (red) and disrotatory (black) angles are shown as a function of time for (**C**) all six trajectories that opened in disrotatory fashion for cis pulling at 2 nN and (**D**) all four trajectories that opened in conrotatory fashion for trans pulling at 3 nN. The insets define the conrotatory and disrotatory angles.

Downloaded from www.sciencemag.org on August 27, 2010

followed for longer time. A larger 3-nN applied force was required to observe ring opening within the 1-ps simulation window for the trans attachment case, whereupon 1 out of 20 trajectories ring-opened via the thermally forbidden conrotatory pathway (Fig. 2D).

The forces of 2 to 3 nN in the simulations are relevant to the experimental conditions, as evidenced by force-induced polymer chain scission that accompanies isomerization (fig. S23). Although the chain scission events occur in much smaller numbers than the isomerizations, their presence establishes a lower bound for the forces generated along the polymers. The time scale of the bubble collapse, and therefore the duration of the tension, is on the order of microseconds or less (*17*), and polymer MW degradation by bond scission on this time scale requires transient forces of nearly 5 nN (*25*). Longer periods of exposure would require less force (*25*), but even if the polymers were held under constant tension for the relevant experimental time scale of several minutes, forces in excess of 3 nN would be required to account for the observed MW degradation. Thus, our simulations predict that both cis and trans attachment lead to formation of the s-trans/s-trans diradical in the presence of an applied force.

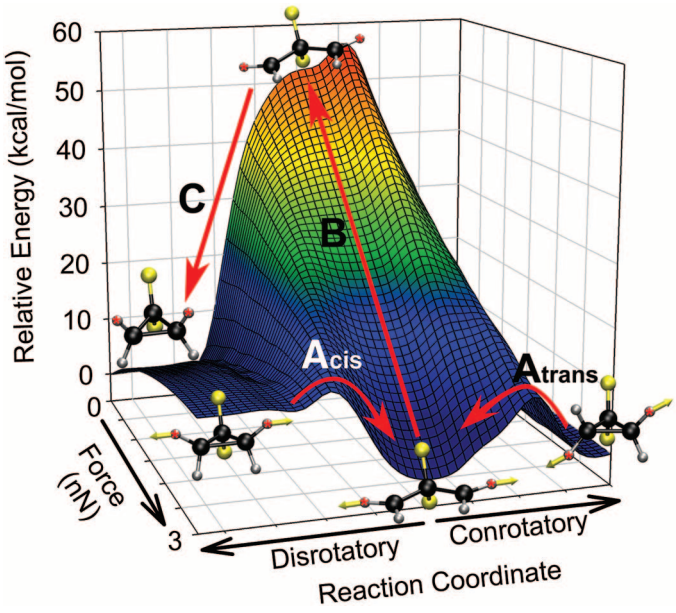

Fig. 3. Force-modified potential energy surface of the conrotatory and disrotatory pathways for *gem*-difluorocyclopropane. Yellow arrows and red asterisks indicate the pulling direction and the attachment points, respectively. (Pathways A_{cis} and A_{trans}) At 3 nN, *cis*- and *trans*-gDFC open to the 1,3-diradical, which is a minimum on the force-modified potential energy surface. (Pathway B) When the force is removed, the 1,3-diradical becomes a transition state along the disrotatory inversion path from *trans*- to *cis*-gDFC. A small energy barrier prevents conrotatory ring closure to *trans*-gDFC and (pathway C) disrotatory ring closure produces *cis*-gDFC. Note that complete relaxation to zero force in step B is not required before ring closure in order to favor the disrotatory pathway.

Once the diradical is formed, we do not observe ring closure within the 1-ps simulation window at the applied force for either the cis or trans attachment, a result consistent with our hypothesis that the stereochemical preference for ring closure to *cis*-gDFC is imposed after the external tension is released. To further test this hypothesis, we carried out AISMD simulations under no force starting with the diradical intermediate (figs. S62 and S63). These simulations were carried out on the singlet state surface, which has been reported previously (*12*), and verified by our calculations here (tables S4 and S5) to be the ground state of the diradical. In all cases, prompt ring closure is observed within 500 fs. Furthermore, this ring closure predominantly (in more than 95% of the samples) occurs in the thermally allowed disrotatory fashion, leading to a cis conformation of the attachment points. Therefore, simulations at experimentally relevant forces predict (i) that the s-trans/s-trans diradical is formed regardless of the cis or trans arrangement of the attachment points; (ii) that, when coupled to the applied force, the ring-opened diradical is lower in energy than the ring-closed cyclopropanes; and (iii) that ring closure occurs almost exclusively to the cis conformation upon removal of the applied force. The selective closure to the cis conformation is confirmed by sonication of the pure *cis*-gDFC–PB copolymer, which shows <2% isomerization under identical experimental conditions (fig. S28). The final 3.5:1 ratio of cis:trans *g*DFC in the sonication of mixed *cis*- and *trans*-gDFC–PB is therefore not strictly determined by the relative probabilities of the two ring-closing pathways but is instead limited by not all *g*DFCs experiencing sufficiently high forces (which are focused in the center of the polymer) for activation (*4*, *17*).

This picture is confirmed by further calculations in which we used the nudged elastic band method (*22*, *26*, *27*) to compute minimum energy pathways for conrotatory and disrotatory ring opening and closure in the presence and absence of applied force (Fig. 3). In the absence of force, the calculations reproduce Borden's earlier observation (*28*) that the 1,3-diradical is a transition state of the thermal ring-opening reactions. At forces exceeding 1 nN, the diradical becomes a local minimum as opposed to a transition state. Furthermore, at forces of 3 nN or greater, the 1,3 diradical

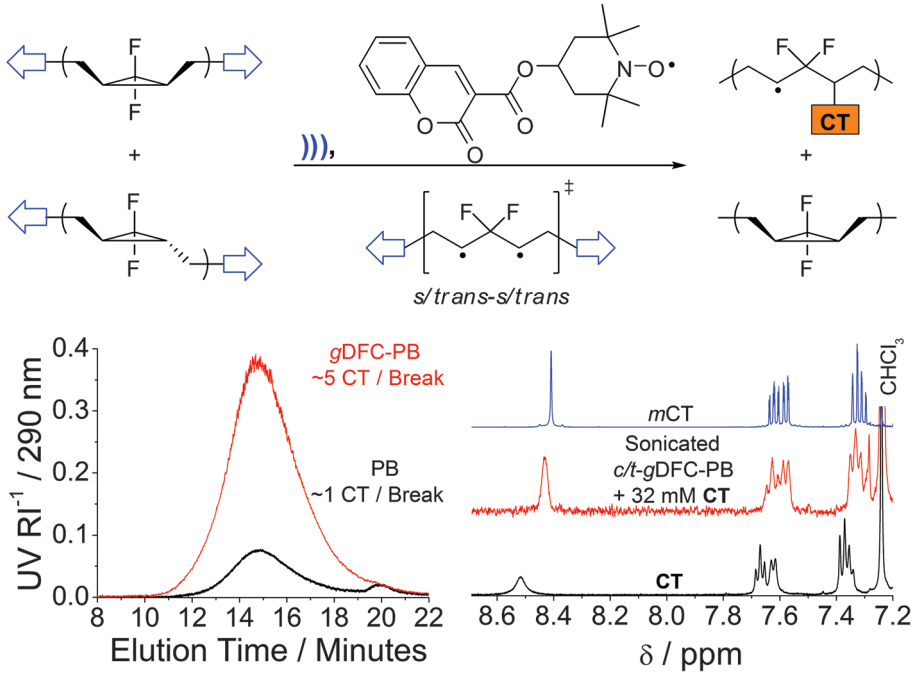

Fig. 4. Tension trapping of the 1,3-diradical by CT during sonication (THF, 11.9 W cm^{-2}, N_2, 6° to 9°C). Normalized absorbance data (bottom left) show CT incorporation along the main chain of the *g*DFC-PB polymer, whereas PB alone incorporates CT only at the chain ends formed as a result of chain scission. The ^{1}H-NMR spectrum of the polymer-CT adduct shows shifts in the CT resonances that are consistent with carbon addition to the oxygen-centered radical (*m*CT is the *O*-methylated CT model compound). Additional details of the spectral characterization are provided in fig. S4. UV, ultraviolet; RI, refractive index.

Downloaded from www.sciencemag.org on August 27, 2010

becomes the global minimum and is therefore expected to be long-lived. These threshold forces are expected to be even lower for the more reactive disubstituted *g*DFC studied here (*12*). Thus, on application of the force, both *cis*- and *trans*-gDFC isomers open to the diradical (pathways A_{cis} and A_{trans} in Fig. 3). Once the force is removed (for example, at the end of a bubble collapse in the sonication experiments), the diradical returns to the force-free potential energy surface (pathway B in Fig. 3), where there is no barrier to disrotatory ring closure to the cis product (there is an additional barrier of about 4 kcal mol^{-1} that must be surmounted in order to close in conrotatory fashion). Thus, the 1,3-diradical (whether generated from the *cis*- or the *trans*-*g*DFC) closes almost exclusively to give the cis conformation (pathway C in Fig. 3), as observed both experimentally and in our dynamics simulations.

Further experimental support that ring closure occurs under reduced tension comes from another counterintuitive result of the mechanical activation: The calculated (*15*) methylene-methylene (C-C) separation in the cis mechanoisomerization product (~3.2 Å) is shorter than that in the trans reactant (~4.0 Å), even though an elongational stress is applied. That is, the C-C distance contracts ~18% in response to being pulled. As shown in Fig. 3, however, the presence of tension during ring closing would bias the pathway, both kinetically and thermodynamically, toward the unobserved conrotatory process, throughout which the attachment points are farther apart than in the observed disrotatory ring closing.

Although the dialkyl-1,3-diradical is typically invoked as a waypoint along the thermal isomerization of *g*DFCs (*12*), Borden has pointed out the primary challenge precluding its more direct characterization (*28*): As a transition state, the 1,3-diradical is expected to persist only for a single bond vibration, ~10^{-13} s, far too short a time, for example, to be caught by a radical trap. Here, however, the tension-induced stabilization of the conformationally extended 1,3-diradical in the polymer affords the opportunity to reactively probe this trapped transition state structure. In this vein, sonication of the *g*DFC-functionalized polymer in the presence of a coumarin–2,2,6,6-tetramethylpiperidine-1-oxyl (CT) adduct (a chromophore known to add to carbon-centered radicals at its persistent nitroxide radical site) (*29*) led to incorporation of multiple chromophores along the polymer backbone (Fig. 4). Similar results were observed for the pure *cis*-*g*DFC–PB (fig. S44), confirming that the *cis*-*g*DFC is activated but closes back to cis rather than isomerizing to trans. The *g*DFC-PB mechanochemistry does not otherwise change in the presence of CT, and control experiments on both PB and a *gem*-dichlorocyclopropanated polybutadiene show only low levels of CT incorporation that are attributed to radical addition at the polymer chain ends derived from polymer scission. Because the rate constants for addition of persistent nitroxides to carbon-centered radicals are typically ~10^8 M^{-1} s^{-1} (*29*), the 1 to 2% efficiency of CT trapping suggests that the lifetime of the diradical exceeds 10^{-9} s (*30*) (table S3).

Our results complement previous work by Hickenboth *et al*. (*4*), who showed that mechanical activation could override Woodward-Hoffman orbital symmetry rules in the activation of benzocyclobutene to an *ortho*-quinodimethane intermediate. For benzocyclobutene, the cis isomer was pulled down the thermally forbidden disrotatory pathway, whereas here it is the *trans*-*g*DFC that is pulled down the thermally forbidden conrotatory pathway. More broadly, the use of a coupled restoring force to extend the lifetime of selected, transient intermediates—including, as shown here, transition states—provides a tool for the study of reactive intermediates that complements, for example, the use of encapsulation complexes (*31*–*33*). Here, the scope of the technique is governed not by an appropriate fit inside a protective capsule but instead by appropriate coupling to a vector of applied force.

References and Notes

1. D. H. Paik, D. S. Yang, I. R. Lee, A. H. Zewail, *Angew. Chem. Int. Ed.* **43**, 2830 (2004).
2. S. T. Roberts *et al*., *Proc. Natl. Acad. Sci. U.S.A.* **106**, 15154 (2009).
3. D. M. Neumark, *J. Chem. Phys.* **125**, 132303 (2006).
4. C. R. Hickenboth *et al*., *Nature* **446**, 423 (2007).
5. S. S. Sheiko *et al*., *Nature* **440**, 191 (2006).
6. F. R. Kersey, W. C. Yount, S. L. Craig, *J. Am. Chem. Soc.* **128**, 3886 (2006).
7. S. R. Koti Ainavarapu, A. P. Wiita, L. Dougan, E. Uggerud, J. M. Fernandez, *J. Am. Chem. Soc.* **130**, 6479 (2008).
8. Q. Yang *et al*., *Nat. Nanotechnol.* **4**, 302 (2009).
9. T. J. Kucharski *et al*., *Angew. Chem. Int. Ed.* **48**, 7040 (2009).
10. M. K. Beyer, H. Clausen-Schaumann, *Chem. Rev.* **105**, 2921 (2005).
11. W. R. Dolbier Jr., M. A. Battiste, *Chem. Rev.* **103**, 1071 (2003).
12. S. J. Getty, D. A. Hrovat, W. T. Borden, *J. Am. Chem. Soc.* **116**, 1521 (1994).
13. D. A. Davis *et al*., *Nature* **459**, 68 (2009).
14. A. Piermattei, S. Karthikeyan, R. P. Sijbesma, *Nat. Chem.* **1**, 133 (2009).
15. Materials and methods are available as supporting material on *Science* Online.
16. F. Tian, S. B. Lewis, M. D. Bartberger, W. R. Dolbier Jr., W. T. Borden, *J. Am. Chem. Soc.* **120**, 6187 (1998).
17. M. W. A. Kuijpers, P. D. Iedema, M. F. Kemmere, J. T. F. Keurentjes, *Polymer (Guildf.)* **45**, 6461 (2004).
18. J. M. Lenhardt, A. L. Black, S. L. Craig, *J. Am. Chem. Soc.* **131**, 10818 (2009).
19. K. M. Wiggins *et al*., *J. Am. Chem. Soc.* **132**, 3256 (2010).
20. S. Matthias, F. Müller, *Nature* **424**, 53 (2003).
21. A. van Oudenaarden, S. G. Boxer, *Science* **285**, 1046 (1999).
22. M. T. Ong, J. Leiding, H. Tao, A. M. Virshup, T. J. Martínez, *J. Am. Chem. Soc.* **131**, 6377 (2009).
23. B. O. Roos, *Adv. Chem. Phys.* **69**, 399 (1987).
24. B. O. Roos, *Acc. Chem. Res.* **32**, 137 (1999).
25. M. K. Beyer, *J. Chem. Phys.* **112**, 7307 (2000).
26. G. Henkelman, B. P. Uberuaga, H. Jonsson, *J. Chem. Phys.* **113**, 9901 (2000).
27. J. Ribas-Arino, M. Shiga, D. Marx, *Angew. Chem. Int. Ed.* **48**, 4190 (2009).
28. W. Adam *et al*., *J. Am. Chem. Soc.* **120**, 593 (1998).
29. J. Sobek, R. Martschke, H. Fischer, *J. Am. Chem. Soc.* **123**, 2849 (2001).
30. We note that nitroxide trapping rates of carbon centered radicals depend on the structure and spin state of the radical, and the bimolecular rate constant of 10^8 M^{-1} s^{-1} used here is likely an upper limit for CT trapping of the 1,3-diradical.
31. T. Iwasawa, R. J. Hooley, J. Rebek Jr., *Science* **317**, 493 (2007).
32. V. M. Dong, D. Fiedler, B. Carl, R. G. Bergman, K. N. Raymond, *J. Am. Chem. Soc.* **128**, 14464 (2006).
33. P. Mal, B. Breiner, K. Rissanen, J. R. Nitschke, *Science* **324**, 1697 (2009).

34. This material is based on work supported by the U.S. Army Research Laboratory and the Army Research Office under grant number W911NF-07-1-0409. J.M.L. is supported by the American Chemical Society Division of Organic Chemistry Schering-Plough Fellowship.

Supporting Online Material

www.sciencemag.org/cgi/content/full/329/5995/1057/DC1
Materials and Methods
SOM Text
Figs. S1 to S64
Tables S1 to S5
References
Movies S1 to S6

8 June 2010; accepted 20 July 2010
10.1126/science.1193412

Induction of Broadly Neutralizing H1N1 Influenza Antibodies by Vaccination

Chih-Jen Wei,[1] Jeffrey C. Boyington,[1] Patrick M. McTamney,[1] Wing-Pui Kong,[1] Melissa B. Pearce,[2] Ling Xu,[1] Hanne Andersen,[3] Srinivas Rao,[1] Terrence M. Tumpey,[2] Zhi-Yong Yang,[1] Gary J. Nabel[1]*

The rapid dissemination of the 2009 pandemic influenza virus underscores the need for universal influenza vaccines that elicit protective immunity to diverse viral strains. Here, we show that vaccination with plasmid DNA encoding H1N1 influenza hemagglutinin (HA) and boosting with seasonal vaccine or replication-defective adenovirus 5 vector encoding HA stimulated the production of broadly neutralizing influenza antibodies. This prime/boost combination increased the neutralization of diverse H1N1 strains dating from 1934 to 2007 as compared to either component alone and conferred protection against divergent H1N1 viruses in mice and ferrets. These antibodies were directed to the conserved stem region of HA and were also elicited in nonhuman primates. Cross-neutralization of H1N1 subtypes elicited by this approach provides a basis for the development of a universal influenza vaccine for humans.

Seasonal influenza outbreaks are driven by the evolution of diverse viral strains that evade human immunity. Immune protection is mediated predominantly by neutralizing antibodies directed to the hemagglutinin (HA) of these viruses, and the coevolution of HA and

Downloaded from www.sciencemag.org on August 27, 2010

neuraminidase (NA) generates variant strains that become resistant to neutralization. Yearly influenza vaccine programs have relied on surveillance of circulating viruses and the identification of strains likely to emerge and cause disease (*1*). An alternative approach to influenza prevention is the generation of universal influenza vaccines. This strategy is based on the premise that invariant regions of the viral proteins can be identified as targets of the immune response. Several broadly neutralizing antibodies directed against the viral HA have been identified (*2*–*6*), and the structural basis of antibody recognition and neutralization has been recently elucidated (*3*, *4*). Although this knowledge has identified at least one functionally conserved and constrained target of neutralizing antibodies, it has not been possible to elicit such broadly neutralizing antibodies by vaccination. Gene-based vaccination offers the potential to improve the priming of immune responses that can subsequently enhance immunity induced by the appropriate heterologous boost (*7*). In this study, we examined whether gene-based priming could potentiate the neutralizing antibody response elicited by the seasonal influenza vaccine or by replication-defective adenovirus 5 (rAd5) encoding HA by evaluating the potency, breadth, and efficacy of cross-protection in relevant animal models.

To elicit neutralizing antibody responses with greater breadth and potency, plasmid expression vectors encoding H1N1 or H3N2 HAs were prepared based on the 2006–2007 vaccine strains A/New Caledonia/20/99 (NC) (1999 NC) and A/Wisconsin/67/05 (2005 WI) (*8*), respectively. Mice were immunized with an empty plasmid (control) or a HA-encoding plasmid, followed by a boost with a trivalent 2006–2007 seasonal vaccine that expressed matching H1 or H3 HA. Gene-based vaccination with 1999 NC HA followed by 2006–2007 seasonal vaccine boosting stimulated a greater than 50-fold increase in neutralizing antibody titer than that produced by one dose of seasonal vaccine alone or DNA alone (Fig. 1A). To evaluate the breadth of neutralization, antisera were analyzed for their ability to neutralize heterologous H1N1 strains. Remarkably, the DNA/seasonal vaccine antiserum neutralized previous H1N1 strains dating back to 1934 (Fig. 1B). This antiserum also inhibited the activity of A/Brisbane/59/2007 (Fig. 1B). Priming with HA from a different subtype, H3N2 (2005 WI), failed to stimulate an increase in neutralization titer to 1999 NC after a 2006–2007 seasonal vaccine boost (Fig. 1C), though it did increase H3N2 neutralization titers against both autologous and heterologous H3N2 viruses (fig. S1). DNA priming with matched H1N1 HA was therefore required to boost the seasonal vaccine neutralizing antibody response to homologous and heterologous H1N1 strains. Because it stimulates strong boosting capacity for antibodies and also allows for evaluation of a single matched HA strain boost, we also evaluated the ability of a rAd5 HA vector to stimulate this response. Immune sera from mice immunized with H1 HA DNA/vaccine or DNA/rAd5 HA also neutralized other group 1 influenza strains such as H2N2 and H5N1 viruses (fig. S2), indicating that this prime/boost immunization

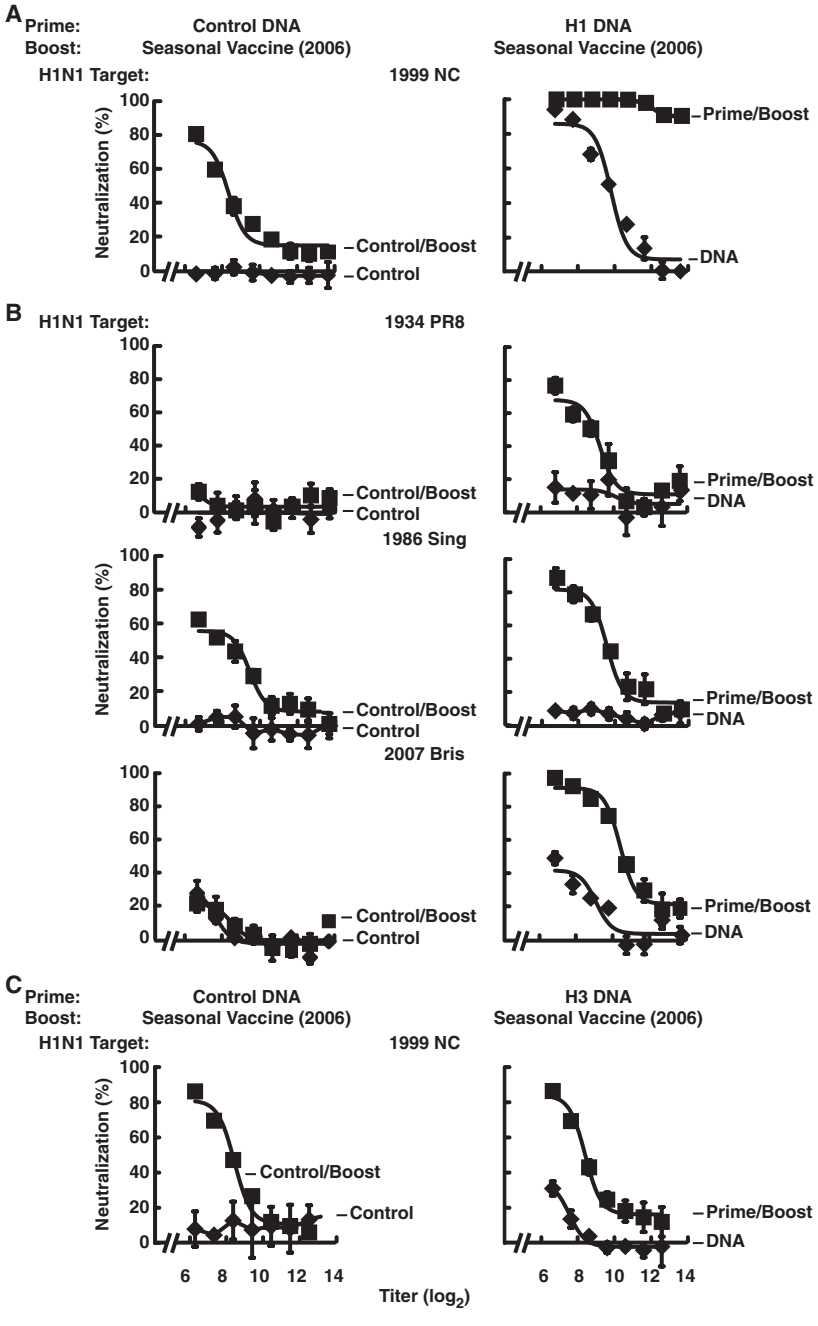

Fig. 1. Increased titer and breadth of neutralizing antibodies to H1N1 strains elicited by DNA/seasonal flu vaccine immunization. (**A**) Pseuotyped neutralization assay to measure the neutralizing antibody response in mice immunized with homologous H1N1 1999 NC HA DNA vaccine, seasonal flu vaccine, or a DNA prime and seasonal flu vaccine boost regimen. (**B**) The neutralizing antibody response in mice against 1934 PR8, A/Singapore/6/1986 (1986 Sing), and 2007 Bris HA-pseudotyped lentivirus reporters after a DNA prime/vaccine boost regimen. (**C**) The neutralizing antibody response against a 1999 NC HA pseudotyped lentivirus reporter in response to an H3N2 HA DNA (A/Wisconsin/67/2005) prime/seasonal vaccine boost.

[1]Vaccine Research Center, National Institute of Allergy and Infectious Diseases (NIAID), National Institutes of Health (NIH), Bethesda, MD 20892–3005, USA. [2]Influenza Division, National Center for Immunization and Respiratory Diseases, Centers for Disease Control and Prevention, Atlanta, GA 30333, USA. [3]BIOQUAL, Rockville, MD 20850, USA.

*To whom correspondence should be addressed. E-mail: gnabel@nih.gov

Downloaded from www.sciencemag.org on August 27, 2010

strategy broadens neutralization beyond the H1N1 subtype.

We next evaluated whether these antibodies would confer protection against lethal challenge in mice. Protective immunity was tested using the most distant H1N1 strain, derived from the 1934 virus (1934 PR8). Animals were immunized with DNA alone, seasonal vaccine alone, or the prime/boost combination. A 1934 PR8 DNA prime followed by boost with rAd5 encoding 1934 PR8 HA served as a positive control. Animals immunized with the 1999 NC DNA/seasonal vaccine showed significantly increased survival rates (Fig. 2A, left; $P < 0.0001$) and less body weight loss (Fig. 2A, right) as compared to DNA alone–, seasonal vaccine alone–, or sham-immunized controls. Although the survival rates for the matched DNA/rAd5 1934 PR8 trended higher than the 1999 NC DNA/seasonal vaccine group, the difference was not statistically significant (Fig. 2A, $P = 0.3714$). For the prime/boost vaccine, survival did not correlate with the hemagglutination inhibition (HAI) or microneutralization titer to 1934 PR8 or 1999 NC viruses. Rather, the increase in neutralization of the 1934 PR8 strain by DNA/seasonal vaccine sera was detected with a pseudotyped lentiviral reporter assay (Fig. 2A), which provides a more sensitive measure of HA-specific viral neutralization (*9*–*11*).

Infectious challenge in ferrets is widely considered a better model to predict vaccine efficacy in humans (*12*). To evaluate immune protection in ferrets, animals were first immunized with the prime/boost combination that conferred cross-neutralization in mice. Under this vaccine regimen and as seen in mice, we also observed cross-reactive neutralizing antibodies to H1N1 viruses (Table 1, A and B). These animals were next tested by challenge with a seasonal 2007 virus, the Brisbane (Bris) strain. The DNA prime/vaccine boost immunization conferred protection against the 2007 virus, as indicated by the significantly reduced viral titers in the nasopharynx (Fig. 2B). We also evaluated the ability of DNA prime/rAd5 HA immunization to elicit broadly neutralizing antibodies and protection. Ferrets immunized with this gene-based combination generated higher titers of cross-neutralizing antibodies (Table 1B)

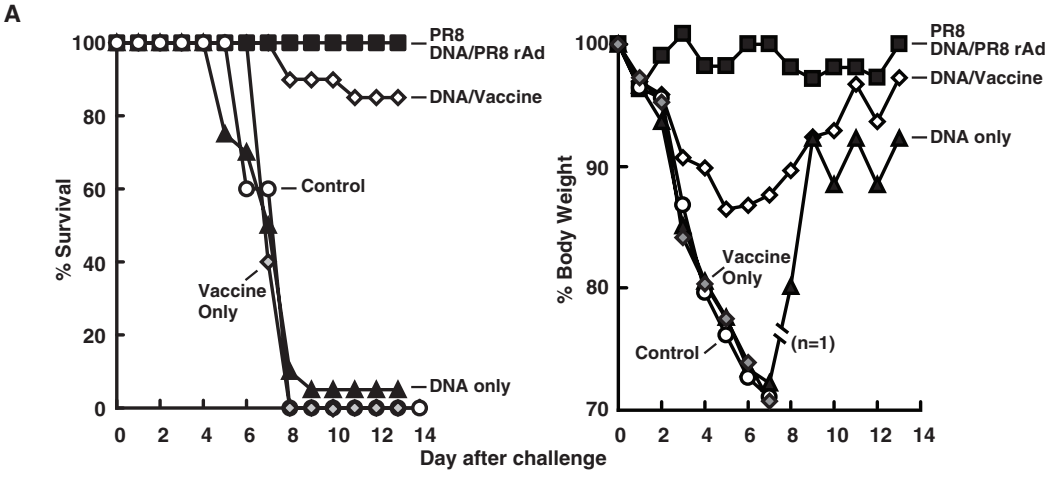

HAI Titer

Group \ Virus	1934 PR8	1999 NC
Control	<20	20
PR8 DNA/rAd	2,560	20
DNA	<20	160
Vaccine	<20	40
DNA/Vaccine	<20	2,560

Microneutralization Titer

Group \ Virus	1934 PR8	1999 NC
Control	<20	<20
PR8 DNA/rAd	>2,560	20
DNA	<20	640
Vaccine	<20	320
DNA/Vaccine	<20	>2,560

Pseudotype Titer

Group \ Virus	1934 PR8	1999 NC
Control	0	0
PR8 DNA/rAd	>12,800	787
DNA	0	879
Vaccine	0	330
DNA/Vaccine	574	>12,800

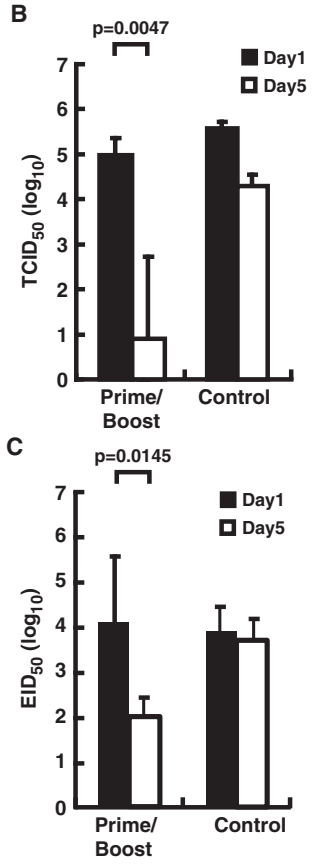

Fig. 2. Immune protection conferred against lethal challenge by 1934 PR8 influenza virus in mice and against infection by 1934 PR8 or 2007 Bris in ferrets. (**A**) Protection of prime/boost immune mice after heterologous virus challenge (upper panel). Mice were immunized with control vector ($n = 5$ mice), PR8 HA DNA/PR8 rAd5 ($n = 5$), H1 HA DNA ($n = 20$), seasonal vaccine ($n = 5$), or H1 HA DNA/seasonal vaccine ($n = 20$). Three weeks after the final immunization, the animals were challenged with 50 median lethal doses of 1934 PR8 virus, and survival (left) and weight loss (right) were recorded and evaluated. $P = 0.3713$ between the PR8 DNA/PR8 rAd and DNA/vaccine groups; $P < 0.0001$ for DNA/vaccine as compared to DNA-only or vaccine-only groups by Kaplan-Meyer analysis. (Lower panel) The antibody responses to homologous (1999 NC) or heterologous (1934 PR8) HAs elicited by HA DNA alone, seasonal vaccine alone, or HA DNA prime/seasonal vaccine boost immunization were measured by HAI (left), microneutralization (middle), and pseudotyping (right) assays. Median inhibitory concentration (IC_{50}) titers for the pseudotyped lentiviral vector reporter assay are shown. Titers of 100 to 1000 are shown in yellow and of ≥2560 in red. (**B**) Protection of ferrets from 2007 Bris viral challenge. $TCID_{50}$, median tissue culture infective dose. Two groups of four ferrets were immunized with 1999 NC HA DNA/seasonal flu vaccine or control vector and challenged with heterologous 2007 Bris virus [$10^{6.5}$ egg infective dosage (EID_{50})]. Virus titers in the nasal swabs from day 1 and day 5 after challenge were determined by means of end-point titration in Madin-Darby canine kidney cells. $P = 0.0104$ between day 5 control and day 5 prime/boost. (**C**) Protection of ferrets from 1934 PR8 viral challenge. Two groups of six ferrets were immunized with 1999 NC HA DNA/rAd5 vaccine or control vector and challenged with heterologous 1934 PR8 virus ($10^{6.5}$ EID_{50}). Virus titers in the nasal swabs from day 1 and day 5 after challenge were determined in eggs from an initial dilution of 1:10 in phosphate-buffered saline and expressed as EID_{50}/ml. The limit of virus detection was $10^{1.5}$ EID_{50}/ml. $P = 0.0004$ between day 5 control and day 5 prime/boost.

Downloaded from www.sciencemag.org on August 27, 2010

and were protected against challenge with a more divergent strain, 1934 PR8, showing a >2 log reduction in nasopharyngeal viral loads (Fig. 2C).

We analyzed the target of neutralization breadth further by testing DNA, vaccine (one or two doses as currently recommended for human vaccines), or DNA prime/seasonal vaccine boost sera against a variety of strains. In mice, the highest neutralization titers were generated against the homologous 1999 NC strain or an earlier strain, A/Beijing/262/1995 (1995 Bei), by all vaccine regimens; however, minimal cross-neutralization of other strains was observed with DNA or seasonal vaccine immune sera as compared to DNA/seasonal vaccine (Table 1A). Two doses of seasonal vaccine increased the neutralization titer against the homologous 1999 NC HA but had a minimal effect on heterologous neutralization. In nonhuman primates, a similar increase in titer and breadth of neutralizing antibodies to H1N1 viruses was elicited by this prime/boost immunization (Table 1C).

To document that neutralizing antibodies were directed to the highly conserved HA stem, we included wild-type 1999 NC HA trimer (WT) or a matched stem mutant protein (ΔStem) as competitors in the neutralization assay. The stem mutant trimer showed minimal reactivity with the previously defined C179 monoclonal antibody (mAb) directed to this region, in contrast to WT 1999 NC HA trimer (Fig. 3A). The specificity of this stem mutant was also confirmed by size-exclusion column chromatography, showing that it forms a trimer of the appropriate size (fig. S3A) recognized by a mAb to the 1999 NC HA head, and yet it fails to react with three mAbs specific for the conserved region of the HA stem (*2*–*4*): C179, CR6261, and F10 (fig. S3B). When included as competitors in the neutralization assay, WT 1999 NC HA trimer, but not the stem mutant, blocked neutralization against 1934 PR8 virus by the stem-directed C179 mAb (Fig. 3A), further documenting the specificity of this stem mutation. When mouse sera from DNA/vaccine- or DNA/rAd5 HA–immunized animals were analyzed in this way, both WT and stem mutant HAs inhibited neutralization against homologous 1999 NC virus, but the stem mutant failed to block neutralization against heterologous 1934 PR8 virus (Fig. 3B). In ferrets, which showed protection against the 1934 PR8 and 2007 Bris virus, as expected, both WT and stem mutant HA trimers blocked neutralization against homologous 1999 NC virus; however, only the WT protein inhibited the neutralization against heterologous 2007 Bris virus or 1934 PR8 virus (Fig. 3C). Additional competition assays were performed with the stem-directed CR6261 mAb to further document the specificity of these antisera. Antisera from DNA/rAd5 HA–immunized ferrets were preabsorbed with cells expressing the stem mutant of the 1999 NC HA to remove non–stem-directed HA antibodies. By enzyme-linked immunosorbent assay (ELISA), we examined the ability of the CR6261 antibody to block the binding of ferret sera to homologous or heterologous H1N1 HAs as compared to a control immunoglobulin G (IgG). CR6261, in contrast to control antibody, inhibited the binding of ferret sera to these HA trimers, further confirming the presence of stem-specific antibodies in the ferret sera (Fig. 3D). We also demonstrated the presence of antistem antibodies in monkeys immunized with a DNA/seasonal vaccine prime/boost combination. Monkey sera were absorbed with cells (*10*) expressing WT or stem mutant 1999 NC HA. Absorption with the WT HA removed reactivity to homologous and heterologous HAs (Fig. 3E). In contrast, antisera absorbed with cells expressing the stem mutant retained reactivity with heterologous HA trimers while retaining a lower level of homologous binding as expected (Fig. 3E). Together these results demonstrate the specificity of the antistem antibodies elicited by the prime/boost immunization in mice, ferrets, and nonhuman primates.

Protection by antibodies directed to the conserved stem of the HA in ferrets is probably relevant to influenza immunity in humans. The presence of these antibodies was highly correlated with efficacy and suggested that neutralization function contributes to protection. The generation of these antibodies was dependent on gene-based priming, which can increase the number and diversity of CD4 clones (*7*) that stimulate B cells to secrete antibodies of greater magnitude and diversity. In fact, we observed that the DNA prime/vaccine boost elicited higher HA-specific T cell responses as compared to vaccine alone (fig. S4). Multiple doses of vaccine with inclusion of a B cell adjuvant, or other immunization approaches, could possibly help achieve this effect. Recent publications have shown that priming with vaccine elicits cross-reactive $CD4^+$ T cells (*13*), and the MF59 adjuvant expands the antibody repertoires against H5N1 influenza virus (*14*).

Vaccine-elicited antisera almost exclusively target the variable head region of HA rather than the conserved stem. Although broadly neutralizing antibodies to HA have been derived from mice (*2*), humans (*5*, *6*), or recombinant antibody libraries (*3*, *4*), it has not been possible to specifically elicit them through vaccination, a difficulty shared by other viruses, such as HIV-1 [reviewed in (*15*)]. In addition to H1N1, this prime/boost combination also elicited an increase in the titer and breadth of antibodies to H3N2 HAs (fig. S1), and it could potentially be applied to influenza B. Stem-focused HA immunogens could also be developed using rational structure-based protein design to increase breadth still more (*16*). We have

Table 1. Neutralization activity of mouse, ferret, and monkey antisera against H1N1 pseudotyped viruses. (**A**) Neutralization activity of murine antisera from DNA-, seasonal vaccine– (one or two doses), or DNA/seasonal vaccine–immunized mice against H1N1 pseudotyped viruses (1986 Sing; A/Beijing/262/1995, 1995 Bei; 1999 NC; A/Solomon Islands/3/2006, 2006 SI; 2007 Bris). (**B**) Neutralization activity of antisera from DNA/seasonal vaccine– or DNA/rAd5–immunized ferrets against the indicated H1N1 pseudotyped viruses. (**C**) Neutralization activity of antisera from DNA-, seasonal vaccine–, or DNA/seasonal vaccine–immunized monkeys against the indicated H1N1 pseudotyped viruses. IC_{50} titers are shown for all panels. Titers of <100 (low) are shown in green, of 100 to 1000 (medium) in yellow, and >1000 (high) in red.

A Mouse

Immunization \ Virus	1934 PR8	1986 Sing	1995 Bei	1999 NC	2006 SI	2007 Bris
DNA	0	0	631	879	<100	<100
Vaccine	0	693	677	330	574	0
Vaccine/Vaccine	<100	366	625	2778	851	728
DNA/Vaccine	574	735	3083	>12800	1808	1251

B Ferret

Immunization \ Virus	1934 PR8	1986 Sing	1995 Bei	1999 NC	2007 Bris
DNA/Vaccine	<100	576	2683	1287	105
DNA/rAd	246	552	16497	48951	1584

C Monkey

Immunization \ Virus	1986 Sing	1995 Bei	1999 NC	2007 Bris
DNA	<50	223	100	<50
Vaccine	<50	<50	<50	<50
DNA/Vaccine	485	4182	1176	334

Downloaded from www.sciencemag.org on August 27, 2010

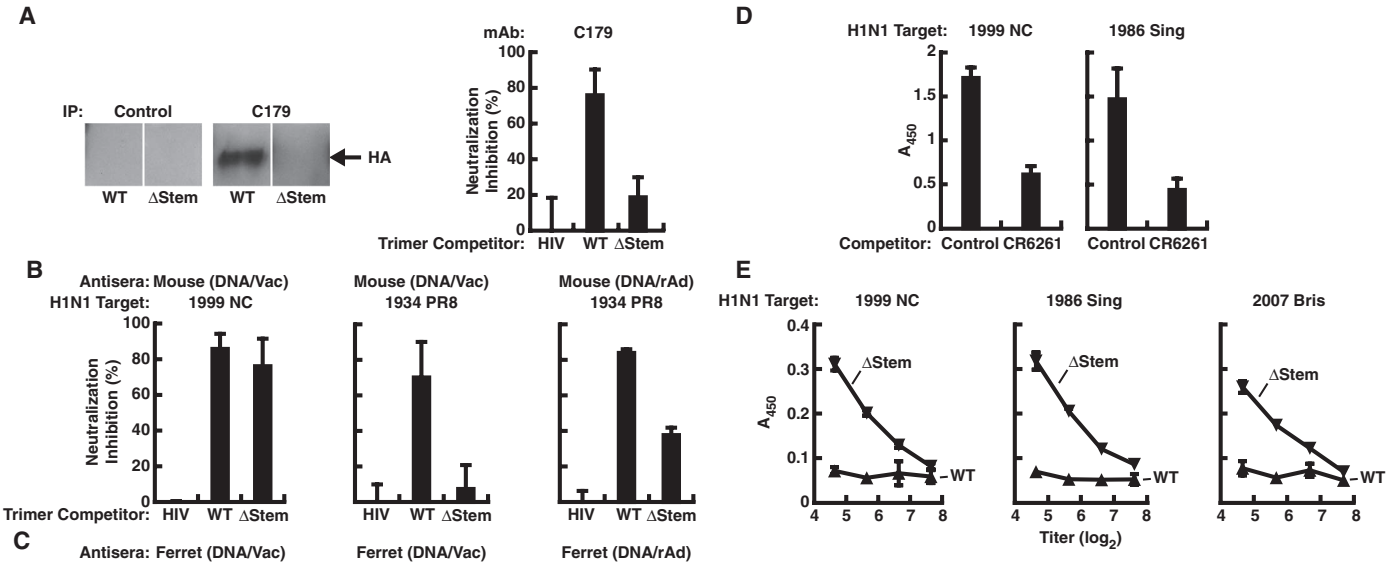

Fig. 3. Stem-directed antisera elicited by HA DNA/seasonal flu vaccine immunization. (**A**) WT or ΔStem HA protein was immunoprecipitated with C179 mAb or a nonreactive isotype control (IgG2a) and was detected with an antibody to a histidine tag (left panel). mAb C179 was preabsorbed with HIV Env (HIV), WT 1999 NC trimer (WT), or stem mutant 1999 NC trimer (ΔStem), and the neutralization activities of the preabsorbed antibody were measured with 1934 PR8 HA-pseudotyped lentiviral vectors (right panel). The percent reduction in neutralization was determined at 5 μg of C179 per milliliter. (**B**) Immune sera from mice immunized with H1 HA DNA/seasonal flu vaccine or H1 HA DNA/rAd5 were preabsorbed as described in (A), and the neutralization activities of the preabsorbed antisera were measured with 1999 NC or 1934 PR8 HA-pseudotyped lentiviral vectors (at a 1:200 serum dilution). (**C**) Immune sera from ferrets immunized with H1 HA DNA/seasonal flu vaccine or H1 HA DNA/rAd5 were preabsorbed as above, and the neutralization activities of the preabsorbed antibody or antisera were measured with 1999 NC, 2007 Bris, or 1934 PR8 HA-pseudotyped lentiviral vectors (at a 1:200 serum dilution). (**D**) Antisera from DNA/rAd5 HA immunized ferrets were preabsorbed with cells expressing the stem mutant of the 1999 NC HA to remove non–stem-directed HA antibodies. ELISA plates coated with 1999 NC or 1986 Sing HA trimers were preincubated with a control IgG or CR6261 before the addition of the preabsorbed sera. Detection of the presence of ferret antibodies was performed with an anti-ferret secondary antibody. (**E**) Antisera from monkeys immunized with H1 HA DNA/seasonal vaccine were preabsorbed with 293F cells expressing either WT or ΔStem of 1999 NC HA, and the binding of preabsorbed sera to 1999 NC, 1986 Sing, or 2007 Bris HA trimers was examined by ELISA.

recently assessed the efficacy of a DNA/rAd5 prime/boost immunization for enhancing antibody responses in humans with HIV-1 Env immunogens (*17*). As observed in other nonhuman primate and rodent studies (*18*, *19*), this vaccine platform elicited an enhancement of antibody responses in humans similar to those to the DNA/rAd HA vaccine described here. Together, these data support the applicability of this vaccine strategy to humans. In such studies, it will be important to define immune correlates of protection, which will probably differ from those for seasonal vaccines. Pre-existing influenza immunity in humans could possibly affect vaccine efficacy. In this case, the vaccine could still be deployed in influenza-naïve children or infants. Evaluation of this first-generation universal H1N1 vaccine candidate in clinical studies will determine its ability to protect against natural infection and improve the public health benefit of influenza vaccination.

References and Notes

1. World Health Organization, "About WHO Global Influenza Programme," http://www.who.int/csr/disease/influenza/mission/en/ (2010).
2. Y. Okuno, Y. Isegawa, F. Sasao, S. Ueda, *J. Virol.* **67**, 2552 (1993).
3. D. C. Ekiert *et al.*, *Science* **324**, 246 (2009).
4. J. Sui *et al.*, *Nat. Struct. Mol. Biol.* **16**, 265 (2009).
5. A. K. Kashyap *et al.*, *Proc. Natl. Acad. Sci. U.S.A.* **105**, 5986 (2008).
6. D. Corti *et al.*, *J. Clin. Invest.* **120**, 1663 (2010).
7. L. Wu, W.-P. Kong, G. J. Nabel, *J. Virol.* **79**, 8024 (2005).
8. Materials and methods are available as supporting material on *Science* Online.
9. W.-P. Kong *et al.*, *Proc. Natl. Acad. Sci. U.S.A.* **103**, 15987 (2006).
10. C. J. Wei *et al.*, *Sci. Transl. Med* **2**, 24ra21 (2010).
11. Z.-Y. Yang *et al.*, *Science* **317**, 825 (2007).
12. J. W. van der Laan *et al.*, *Expert Rev. Vaccines* **7**, 783 (2008).
13. G. Del Giudice *et al.*, *Sci. Transl. Med* **1**, 12re1 (2009).
14. S. Khurana *et al.*, *Sci. Transl. Med* **2**, 15ra5 (2010).
15. P. D. Kwong, I. A. Wilson, *Nat. Immunol.* **10**, 573 (2009).
16. D. C. Douek, P. D. Kwong, G. J. Nabel, *Cell* **124**, 677 (2006).
17. R. A. Koup *et al.*, VRC 009 Study Team; VRC 010 Study Team, *PLoS ONE* **5**, e9015 (2010).
18. J. R. Mascola *et al.*, *J. Virol.* **79**, 771 (2005).
19. Z.-Y. Yang *et al.*, *J. Virol.* **78**, 4029 (2004).

20. We thank A. Ault, J.-P. Todd, A. Zajac, and C. Chiedi for help with the animal studies; K. Dai, W. Shi, and S. Y. Ko for technical support; M. Lewis (BIOQUAL), B. Sanders (BIOQUAL), and members of the Nabel lab for helpful discussions; A. Tislerics and B. Hartman for manuscript preparation; and Y. Okuno for providing the C179 mAb. NIH has filed a patent application (U.S. patent E-341-2008l; international patent WO 2010/036958 A2) on this work (authors: C-J.W., Z-y.Y, and G.J.N.), related to gene- and protein-based approaches to influenza vaccination. This research was supported by the Intramural Research Program of the Vaccine Research Center, NIAID, NIH. The findings and conclusions in this report are those of the authors and do not necessarily reflect the views of the funding agency.

Supporting Online Material

www.sciencemag.org/cgi/content/full/science.1192517/DC1
Materials and Methods
Figs. S1 to S4
References

19 May 2010; accepted 1 July 2010
Published online 15 July 2010;
10.1126/science.1192517
Include this information when citing this paper.

Downloaded from www.sciencemag.org on August 27, 2010

Secreted Peptide Signals Required for Maintenance of Root Stem Cell Niche in *Arabidopsis*

Yo Matsuzaki, Mari Ogawa-Ohnishi, Ayaka Mori, Yoshikatsu Matsubayashi*

Stem cells are maintained in the niche by intercellular interactions and signaling networks. In this work, we study extracellular signals required for maintenance of the root stem cell niche in higher plants. We identify a family of functionally redundant homologous peptides that are secreted, tyrosine-sulfated, and expressed mainly in the stem cell area and the innermost layer of central columella cells. We name these peptides root meristem growth factors (RGFs). RGFs are required for maintenance of the root stem cell niche and transit amplifying cell proliferation in *Arabidopsis*. RGF1 defines expression levels and patterns of the stem cell transcription factor PLETHORA, mainly at the posttranscriptional level. The RGFs function independently of the auxin pathway. These peptide signals play a crucial role in postembryonic root development.

Secreted peptides are now recognized as important members of intercellular signals that coordinate and specify cellular functions in plants. Some of the secreted peptide hormones undergo complex posttranslational modifications that are mediated by specific enzymes that recognize particular sequences of multiple target peptides. Because such modifications are generally critical for the functions of individual peptide hormones, the presence of previously unidentified peptide hormones should be revealed through phenotypic analysis of the mutants of posttranslational modification enzymes.

Tyrosine sulfation is a posttranslational modification that has been found in several peptide hormones in both animals and plants (*1*). This modification is mediated by tyrosylprotein sulfotransferase (TPST), which catalyzes the transfer of sulfate to the phenolic group of tyrosine. *Arabidopsis* TPST (AtTPST) is a type I transmembrane protein localized in cis-Golgi (*2*). Because *AtTPST* is a single-copy gene, phenotypes of its loss-of-function mutant should reflect the deficiency in the biosynthesis of all the functional tyrosine-sulfated peptides found in *Arabidopsis*.

Of the pleiotropic phenotypes of the *tpst-1* mutant, we focused on the severe short-root phenotype characterized by reduction in root meristem size and loss of coordination between cell elongation and expansion in the elongation-differentiation zone (Fig. 1, A to C) (*3*). Impaired expression of a cell-cycle marker *CYCB1;1:GUS* (*4*) indicates that root meristematic activity of *tpst-1* is considerably decreased compared with that of the wild type (Fig. 1, D and E, and fig. S1A). We occasionally observed extra quiescent center (QC) cells in *tpst-1*, as indicated by the expression of *WOX5*, a QC-specific gene (Fig. 1, F and G, and fig. S1, B to D) (*5*). In addition, starch granules accumulate in all columella layers including cells at the position of the columella stem cells, indicating that *tpst-1* fails to maintain root stem cells (Fig. 1, H and I, and table S1). In contrast, the auxin maximum in *tpst-1* visualized by *DR5:GUS* marker (*6*) was comparable to that of the wild type (Fig. 1, J and K), suggesting that this short-root phenotype is not directly associated with auxin distribution. Embryogenesis is normal in *tpst-1*, suggesting that only postembryonic root development is affected by this mutation (fig. S1, E to H).

To further understand the defects in *tpst-1* plants, we added peptide hormones phytosulfokine (PSK) (*7*) and PSY1 (*8*), both of which are tyrosine sulfated and also expressed in roots. These peptides restored cell-elongation activity in the elongation-differentiation zone (figs. S2 and S3, A to D) but did not promote meristematic activity in *tpst-1*, as evidenced by meristem size (fig. S3, A to E), root length (fig. S3F), and *CYCB1;1:GUS* expression (fig. S3, G to I). Extra QC cells were still observed in *tpst-1* in the presence of PSK and PSY1 (fig. S3, J to L). In addition, starch-granule staining showed no rescue of columella stem cells, indicating that *tpst-1* fails to maintain root stem cells, even in the presence of PSK and PSY1 (fig. S3M and table S1).

On the basis of these observations, we speculated that an as-yet undiscovered tyrosine-sulfated peptide(s) regulates root meristematic activity and maintenance of the stem cell niche in *Arabidopsis*. To identify this peptide signal, we searched the *Arabidopsis* genome for genes likely to encode the sulfated peptide(s). Hormones PSK and PSY1 are encoded by multiple paralogous genes whose primary translated polypeptides are ~70 to 110 amino acids in length, are relatively poor in cysteine residues (Cys < 6), contain a secretion signal, and contain Asp-Tyr sequences that function as tyrosine-sulfation motifs (*8*, *9*). On the basis of these criteria, we found a candidate polypeptide family with a C-terminal con-

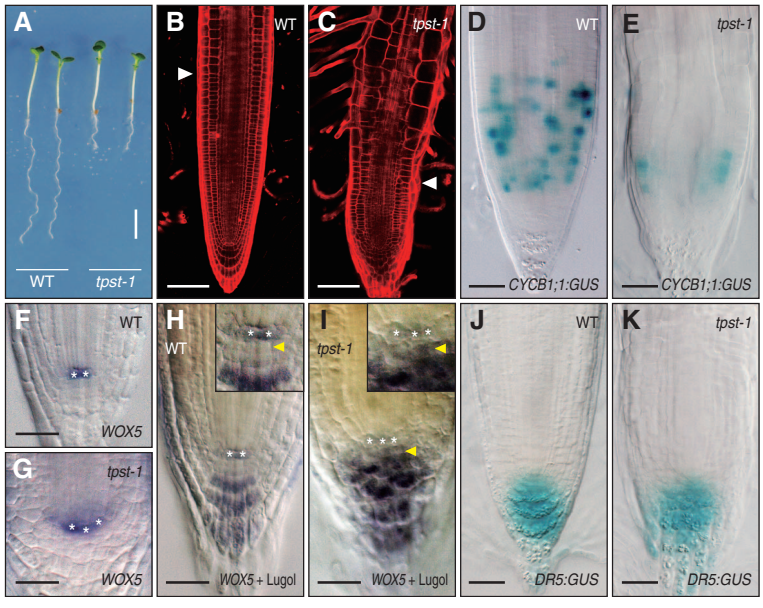

Fig. 1. Root meristem phenotype of *tpst-1*. (**A**) WT and *tpst-1* seedlings at 7 days after germination (DAG). (**B** and **C**) Confocal images of root meristem of WT and *tpst-1* seedlings at 5 DAG. White arrowheads indicate the root meristem boundary. (**D** and **E**) *CYCB1;1:GUS* expression at 5 DAG. (**F** and **G**) Whole-mount in situ hybridization of *WOX5* mRNA. Asterisks denote *WOX5*-expressing cells at the QC position. (**H** and **I**) Starch granules stained by Lugol. Asterisks indicate the QC position counterstained by in situ hybridization with *WOX5*. Yellow arrowheads indicate the position of columella stem cells. Insets show close-up views. (**J** and **K**) *DR5:GUS* expression. Scale bars, (A) 5 mm; (B and C) 100 μm; (D to K) 50 μm.

Graduate School of Bio-Agricultural Sciences, Nagoya University, Chikusa, Nagoya 464-8601, Japan.

*To whom correspondence should be addressed. E-mail: matsu@agr.nagoya-u.ac.jp

Downloaded from www.sciencemag.org on August 27, 2010

served domain containing Asp-Tyr sequences (fig. S4, A and B). We overexpressed one of these peptides, At5g60810, in *Arabidopsis* and used nano–liquid chromatography–tandem mass spectrometry to analyze the apoplastic peptides derived from the transgenic plants to determine the peptide's mature structure (fig. S5A). We determined that mature peptide derived from At5g60810 is 13 amino acids long, carries a tyrosine sulfation, and derives from the C-terminal conserved domain of the encoded protein through proteolytic processing (Fig. 2, A and B, and figs. S4A and S5B).

To test whether the At5g60810 peptide is responsible for the *tpst-1* root phenotype, we cultured *tpst-1* seedlings in liquid medium containing the chemically synthesized sulfated form of At5g60810 peptide. At5g60810 peptide suppressed formation of extra QC cells (Fig. 2, C and D) and restored columella stem cells to a level comparable to the wild type (Fig. 2E and table S1), which indicates that At5g60810 peptide is sufficient for maintenance of root stem cell niche. At5g60810 peptide also restored meristematic activity of *tpst-1* to ~70% of the wild-type (WT) level, as indicated by root meristem size (Fig. 2, F and G) and *CYCB1;1:GUS* expression (Fig. 2, H and I). We named this peptide root meristem growth factor 1 (RGF1). RGF1 further increased meristematic activity of *tpst-1* to a level comparable to that of the wild type in the presence of PSK and PSY1, suggesting that PSK and PSY1 are required for full activity of RGF1 (fig. S6, A to D). RGF1 fully restored root growth of *tpst-1* in the presence of PSK and PSY1 (fig. S6, E to H and table S1).

RGF1 is active at concentrations above 0.1 nM in a dose-dependent manner (fig. S7, A to F and H). Tyrosine sulfation is critical for the function of this peptide (fig. S7, G and H). The earliest detectable increase in meristem size occurred 6 to 12 hours after RGF1 treatment (fig. S8, A to E). Root meristem activity of *tpst-1* was also recovered, albeit to varying degrees, by the application of the synthetic sulfated peptides corresponding to the 13–amino acid conserved domain of the other members of this RGF peptide family; the only exception was RGF8, which shows no activity (Fig. 2B and fig. S9, A to M).

In situ hybridization revealed that the expression of *RGF1* is limited to the QC and columella stem cells (Fig. 2J and fig. S10J). In addition, two of the homolog peptides that showed strong activity (RGF2 and RGF3) mainly expressed in the innermost layer of central columella cells (fig. S10, B and C). Whole-mount immunostaining with the use of an antibody that specifically recognizes RGF1 and several of its homologs revealed that RGF1 and cross-reactive homologs diffuse into the meristematic region (Fig. 2K and fig. S11, A and B).

To analyze the functions of *RGFs*, we compared the root phenotype of transgenic seedlings overexpressing *RGF1* and WT seedlings treated with RGF1 peptide. Both types of seedlings

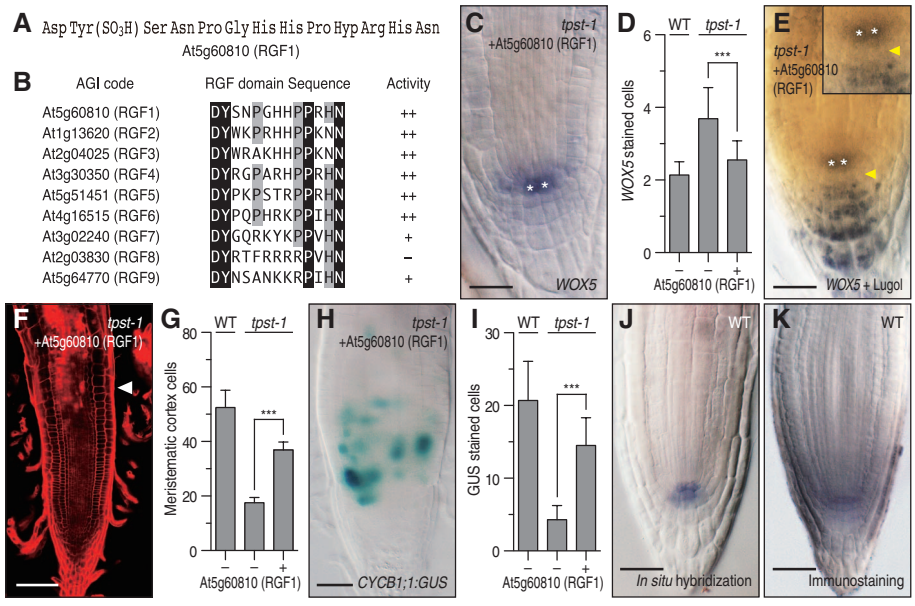

Fig. 2. A tyrosine-sulfated peptide family that maintains root stem cell niche and regulates meristematic activity. (**A**) Sequence of the mature At5g60810 (RGF1) peptide. (**B**) Multiple sequence alignments of the conserved 13–amino acid domain of the At5g60810 (RGF1) peptide family. ++, strong acitivity; +, weak activity; –, no activity (see also fig. S9). (**C**) Whole-mount in situ hybridization of *WOX5* mRNA in *tpst-1* root meristem at 5 DAG cultured in the presence of At5g60810 (RGF1) peptide. (**D**) Changes in number of *WOX5*-expressing cells at the QC position. Data represent mean values ± SD (error bars) (n = 9, ***P < 0.001; paired t test). (**E**) Starch granules stained by Lugol. The yellow arrowhead indicates the position of columella stem cells. Inset shows a close-up view. (**F**) Confocal image of root meristem of *tpst-1* seedling grown in the presence of At5g60810 (RGF1) peptide. (**G**) Quantitative analysis of the number of meristematic cortex cells (n = 10). (**H**) *CYCB1;1:GUS* expression in *tpst-1* root meristem cultured in the presence of At5g60810 (RGF1) peptide. (**I**) Quantification of *CYCB1;1:GUS* spots (n = 10). (**J**) Whole-mount in situ hybridization of *RGF1* mRNA. (**K**) Whole-mount immunostaining with antibodies against RGF1. Scale bars, (C, E, H, J, and K) 50 μm; (F) 100 μm.

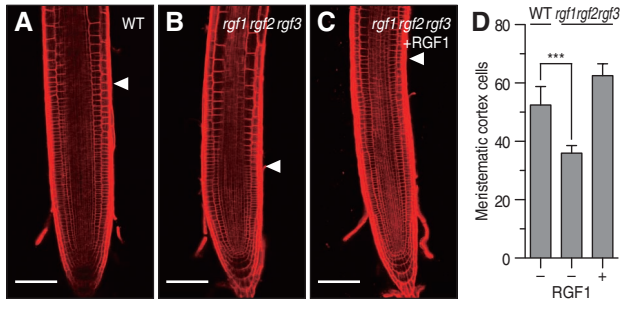

Fig. 3. Phenotype of *rgf1 rgf2 rgf3* triple mutant. (**A** to **C**) Confocal images of the root meristem of WT (A), *rgf1 rgf2 rgf3* triple mutant (B), and *rgf1 rgf2 rgf3* triple mutant treated with RGF1 (C) at 5 DAG. (**D**) Quantitative analysis of the number of meristematic cortex cells (n = 10). Scale bars in (A) to (C), 100 μm.

showed enlarged meristems, indicating that RGF1 peptide treatment phenocopies *RGF1* overexpression (fig. S12, A to D). We confirmed that the *pskr1-2 pskr2-1 pskrl1-1* triple mutant (*8*), which lacks PSK receptors and the putative PSY1 receptor, also showed enlarged meristems in the presence of RGF1 (fig. S12, E to G). Plants carrying transferred DNA insertion mutations in the promoter region of *RGF1* (*rgf1-1*) and in the introns of *RGF2* (*rgf2-1*) and *RGF3* (*rgf3-1*) (fig. S12H) showed no *RGF1*, *RGF2*, and *RGF3* transcripts [quantitative reverse transcription polymerase chain reaction (RT-PCR); fig. S12, I to K]. Immunostaining confirmed the decrease in RGF peptides in the root meristem of the *rgf1 rgf2 rgf3* triple mutant (fig. S12L). Although single mutants did not exhibit any obvious phenotypes in roots, the *rgf1 rgf2 rgf3* triple mutant showed a short-root phenotype characterized by the decrease in meristematic cell number (Fig. 3, A, B, and D, and fig. S12M). Externally applied RGF1 restored meristem activity in the *rgf1 rgf2 rgf3* triple mutant (Fig. 3, B to D). Thus, we concluded that RGFs redundantly regulate root meristem activity.

To dissect the molecular mechanisms by which RGFs maintain the stem cell niche and

Downloaded from www.sciencemag.org on August 27, 2010

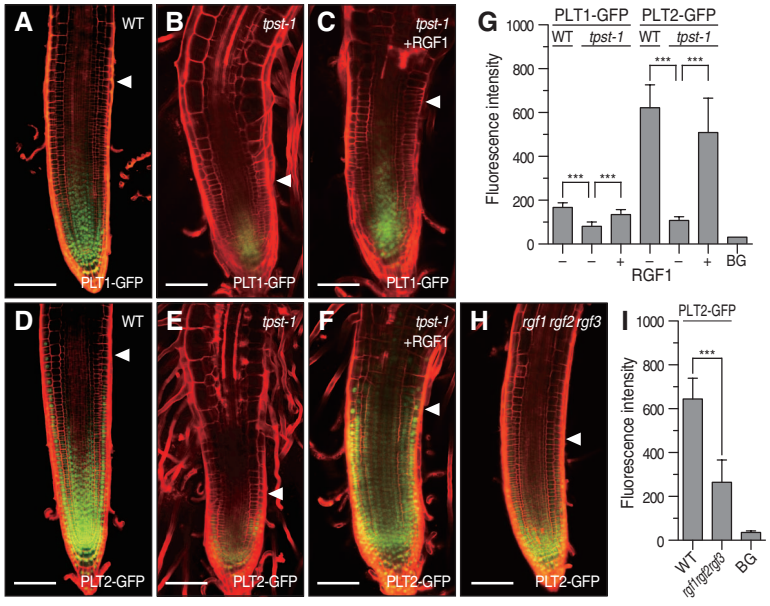

Fig. 4. RGF1 defines expression levels of PLETHORA transcription factors. (**A** and **B**) Confocal image of root meristem of WT and *tpst-1* seedlings expressing *PLT1-GFP* at 5 DAG. (**C**) Root meristem of *tpst-1* seedling expressing *PLT1-GFP* treated with RGF1 for 24 hours. (**D** and **E**) Confocal image of root meristem of WT and *tpst-1* seedlings expressing *PLT2-GFP*. (**F**) Root meristem of *tpst-1* seedling expressing *PLT2-GFP* treated with RGF1 for 24 hours. (**G**) Quantitative analysis of PLT-GFP signals. BG, background fluorescence ($n = 7$). (**H**) Confocal image of root meristem of *rgf1 rgf2 rgf3* triple-mutant seedling expressing *PLT2-GFP* at 5 DAG. (**I**) Quantitative comparison of PLT2-GFP signal between WT and *rgf1 rgf2 rgf3* triple mutant ($n = 6$). Scale bars in (A) to (F) and (H), 100 μm.

regulate meristem activity, we analyzed the response of several root-specific transcription factor mutants to RGF1 by exogenous application of RGF1 peptide. We found that a loss-of-function mutant of *PLETHORA* (*PLT*) transcription factors (*plt1-4 plt2-2* double mutant) shows little or no response to RGF1 (fig. S13, A to E). *PLT* genes, specifically expressed in root meristem, encode AP2-domain transcription factors that mediate patterning of the root stem cell niche (*10*). PLT proteins display gradient distributions with maxima in the stem cell area, and these gradients are essential for maintenance of the root stem cell niche and transit-amplifying cell proliferation (*11*).

To determine whether the amount of RGF regulates PLT expression, we observed expression of *PLT1pro:PLT1-GFP* and *PLT2pro:PLT2-GFP* in WT and *tpst-1* backgrounds. In WT seedlings, PLT1–green fluorescent protein (GFP) and PLT2-GFP fusions in WT seedlings show gradients that extend into the region of transit-amplifying cells and, for the PLT2 fusion, as far as the elongation zone (*11*) (Fig. 4, A and D). In *tpst-1* seedlings, both PLT1-GFP and PLT2-GFP signals were reduced, with weak expression in the meristematic zone (Fig. 4, B, E, and G). We confirmed that expression of PLT1-GFP and PLT2-GFP in *tpst-1* was recovered when treated with RGF1 for 24 hours, irrespective of the absence or presence of PSK (Fig. 4, C, F, and G, and fig. S13, F to J). PLT2-GFP signal was also reduced in the *rgf1 rgf2 rgf3* triple mutant (Fig. 4, H and I). These results indicate that RGFs positively regulate PLT expression levels.

Quantitative RT-PCR analysis revealed that the *PLT1* level in *tpst-1* is comparable to that of the wild type (fig. S14A). *PLT2* transcripts were decreased but not absent in *tpst-1* (fig. S14G), suggesting that PLT expression is regulated at both transcriptional and posttranscriptional levels. Consistent with this, in situ hybridization confirmed that most *PLT1* and *PLT2* transcripts are detected in *tpst-1* root meristem, with the highest amounts found in the stem cell region (fig. S14, B to E and H to K). We next treated WT seedlings expressing PLT2-GFP with RGF1 for 24 hours and observed that the PLT2-GFP–expression domain expanded into the basal zone (fig. S13K). Accumulation of *PLT2* transcripts, however, is restricted to the stem cell region (fig. S14L), suggesting that expanded expression of PLT2 protein may be due to posttranscriptional regulation, possibly through stabilization of PLT2 protein by RGF1 signaling. Similarly, localization of *PLT1* transcripts was also not altered by RGF1 treatment (fig. S14F). When RGF1-treated seedlings expressing PLT2-GFP were further incubated in the absence of RGF1 for 24 hours, gradient expression of PLT2-GFP was restored in the meristematic region (fig. S13L). Thus, RGF acts posttranscriptionally to define PLT expression levels and patterns.

We predict that modulation of local concentration of RGF would alter PLT expression patterns. To confirm this, we placed dextran microbeads containing RGF1 directly on the surface of the meristematic region of WT roots expressing PLT2-GFP (fig. S15A). In the absence of RGF1 beads, PLT2-GFP displayed vertically symmetric distributions, as indicated by pseudocolor intensity images (fig. S15B). In contrast, when RGF1 beads were placed on the meristematic region for 6 hours, PLT2-GFP expression was up-regulated, specifically at the side in contact with the beads, resulting in asymmetric distributions of PLT2-GFP protein (fig. S15, C to E). These results suggest that RGF acts directly on individual cells to define PLT expression levels. *RGF* expression is not affected by auxin levels (fig. S16).

Thus, RGFs, a redundant family of sulfated peptides, maintain the postembryonic root stem cell niche by defining expression levels and patterns of PLT transcription factors independently of the auxin pathway. The physiological and molecular characteristics of RGFs are such that they might act as morphogens (*12*). It will be very interesting to unravel how individual cells perceive and integrate the concentration-dependent information provided by RGFs and auxin to generate precise root meristem patterning during root development.

References and Notes

1. K. L. Moore, *J. Biol. Chem.* **278**, 24243 (2003).
2. R. Komori, Y. Amano, M. Ogawa-Ohnishi, Y. Matsubayashi, *Proc. Natl. Acad. Sci. U.S.A.* **106**, 15067 (2009).
3. Materials and methods are available as supporting material on *Science* Online.
4. A. Colón-Carmona, R. You, T. Haimovitch-Gal, P. Doerner, *Plant J.* **20**, 503 (1999).
5. A. K. Sarkar *et al.*, *Nature* **446**, 811 (2007).
6. T. Ulmasov, J. Murfett, G. Hagen, T. J. Guilfoyle, *Plant Cell* **9**, 1963 (1997).
7. Y. Matsubayashi, Y. Sakagami, *Proc. Natl. Acad. Sci. U.S.A.* **93**, 7623 (1996).
8. Y. Amano, H. Tsubouchi, H. Shinohara, M. Ogawa, Y. Matsubayashi, *Proc. Natl. Acad. Sci. U.S.A.* **104**, 18333 (2007).
9. Y. Matsubayashi, M. Ogawa, H. Kihara, M. Niwa, Y. Sakagami, *Plant Physiol.* **142**, 45 (2006).
10. M. Aida *et al.*, *Cell* **119**, 109 (2004).
11. C. Galinha *et al.*, *Nature* **449**, 1053 (2007).
12. H. L. Ashe, J. Briscoe, *Development* **133**, 385 (2006).
13. We thank P. Doerner for providing the *CYCB1;1:GUS* seeds, T. Guilfoyle for the *DR5:GUS* seeds, and B. Scheres for the *plt1-4 plt2-2* seeds. This research was supported by a Grant-in-Aid for Scientific Research for Priority Areas from the Ministry of Education, Culture, Sports, Science, and Technology (no. 19060010) and a Grant-in-Aid for Creative Scientific Research from the Japan Society for the Promotion of Science (no. 19GS0315).

Supporting Online Material

www.sciencemag.org/cgi/content/full/329/5995/1065/DC1
Materials and Methods
Figs. S1 to S16
Table S1
References

19 April 2010; accepted 15 July 2010
10.1126/science.1191132

Downloaded from www.sciencemag.org on August 27, 2010

Genomic Comparison of the Ants *Camponotus floridanus* and *Harpegnathos saltator*

Roberto Bonasio,[1]* Guojie Zhang,[2,3]* Chaoyang Ye,[4]* Navdeep S. Mutti,[5]* Xiaodong Fang,[3]* Nan Qin,[3]* Greg Donahue,[4] Pengcheng Yang,[3] Qiye Li,[3] Cai Li,[3] Pei Zhang,[3] Zhiyong Huang,[3] Shelley L. Berger,[4]† Danny Reinberg,[1,6]† Jun Wang,[3,7]† Jürgen Liebig[5]†

The organized societies of ants include short-lived worker castes displaying specialized behavior and morphology and long-lived queens dedicated to reproduction. We sequenced and compared the genomes of two socially divergent ant species: *Camponotus floridanus* and *Harpegnathos saltator*. Both genomes contained high amounts of CpG, despite the presence of DNA methylation, which in non-Hymenoptera correlates with CpG depletion. Comparison of gene expression in different castes identified up-regulation of telomerase and sirtuin deacetylases in longer-lived *H. saltator* reproductives, caste-specific expression of microRNAs and SMYD histone methyltransferases, and differential regulation of genes implicated in neuronal function and chemical communication. Our findings provide clues on the molecular differences between castes in these two ants and establish a new experimental model to study epigenetics in aging and behavior.

As eusocial insects, ants live in populous colonies in which up to millions of individuals delegate the reproductive role to one or few queens, while nonreproductive workers carry out all tasks required for colony maintenance (*1*). These mutually exclusive morphologies and behaviors arise from a single genome and are typically dictated not by genetic differences, but by environmental factors (*2*). The first fertilized (diploid) eggs laid by a founder queen develop into workers, but as the colony enlarges, some diploid embryos take a different developmental path to become virgin queens, which leave the nest, mate, and establish new colonies. As colonies mature, queens transition from a broad behavioral repertoire that allows them to forage, excavate nests, and rear offspring, to one restricted to egg-laying and total dependence on workers. Queens also live up to 10 times longer than workers and 500 times longer than males (*3*).

We compared the genomes of the ants *Camponotus floridanus* and *Harpegnathos saltator*, because of contrasts in their behavioral flexibility, caste specialization, and social organization. *C. floridanus* lives in large organized colonies, in which only the queen lays fertilized eggs; when the queen dies, so does the colony (*1*). Nonreproductive individuals belong to two separate castes, major and minor workers, which exhibit differences in morphology and behavior established during development purely on environmental grounds. In contrast, the *H. saltator* social system and division of labor are more basal: dimorphism between queens and workers is limited, and when the queen dies she is replaced by workers that become functional queens, called gamergates (*4*).

These two ant species differ in other respects as well. *C. floridanus* are scavengers, forage diurnally and nocturnally, and lay pheromone trails that mark paths to food sources. *H. saltator* workers prey on small arthropods in a solitary and diurnal fashion. *C. floridanus* exhibits high territoriality, strong nestmate recognition, and elaborate task specialization. In contrast, *H. saltator* displays low territoriality, loses nestmate recognition in the laboratory, and has only basic task specialization.

The Illumina Genome Analyzer platform was used to sequence genomic libraries for *C. floridanus* and *H. saltator*, obtaining more than 100-fold coverage. Draft genomic assemblies reached scaffold N50 size of ~600 kb (table S1), although for *C. floridanus* most genome-wide analyses reported here were conducted on an earlier version (v3), with scaffold N50 size of 444 kb (table S1). Assembly resulted in only small gaps and large N50 size, which assured us that most genomic features, particularly gene models, were predicted with reasonable accuracy. We verified the assemblies by sequencing 9 (*C. floridanus*) and 10 (*H. saltator*) randomly selected fosmid inserts (average size, 37 kb) (table S2). Additionally, we sequenced ~5000 expressed sequence tags from each ant and mapped them to the assembled scaffolds; more than 95% matched the assemblies (table S3).

The *C. floridanus* and *H. saltator* assemblies cover more than 90% of the genomes, which we estimate at 240 and 330 Mb in size, respectively (fig. S1 and table S4). The *H. saltator* assembly contains 45% G+C, similar to *Drosophila melanogaster* (42%), and *Nasonia vitripennis* (42%), whereas the *C. floridanus* genome is A+T rich, with a G+C frequency of 34%, similar to *Apis mellifera* (33%) (*5*) (table S4). Organisms that use DNA methylation for gene regulation typically display a depletion of CpG dinucleotides in their genome (table S5); however, CpG dinucleotides are overrepresented in both ant genomes

[1]Department of Biochemistry, New York University School of Medicine, 522 First Avenue, New York, NY 10016, USA. [2]Chinese Academy of Sciences–Max Planck Junior Research Group, State Key Laboratory of Genetic Resources and Evolution, Kunming Institute of Zoology, Chinese Academy of Sciences, Kunming, Yunnan 650223, China. [3]Beijing Genomics Institute–Shenzhen, Shenzhen 518083, China. [4]Department of Cell and Developmental Biology, University of Pennsylvania School of Medicine, Philadelphia, PA 19104, USA. [5]School of Life Sciences, Arizona State University, Tempe, AZ 85287, USA. [6]Howard Hughes Medical Institute, New York University Medical School, New York, NY 10016, USA. [7]Department of Biology, University of Copenhagen, Copenhagen DK-2200, Denmark.

*These authors contributed equally to this work.
†To whom correspondence should be addressed. E-mail: bergers@mail.med.upenn.edu (S.L.B.); danny.reinberg@nyumc.org (D.R.); wangj@genomics.cn (J.W.); juergen.liebig@asu.edu (J.L.)

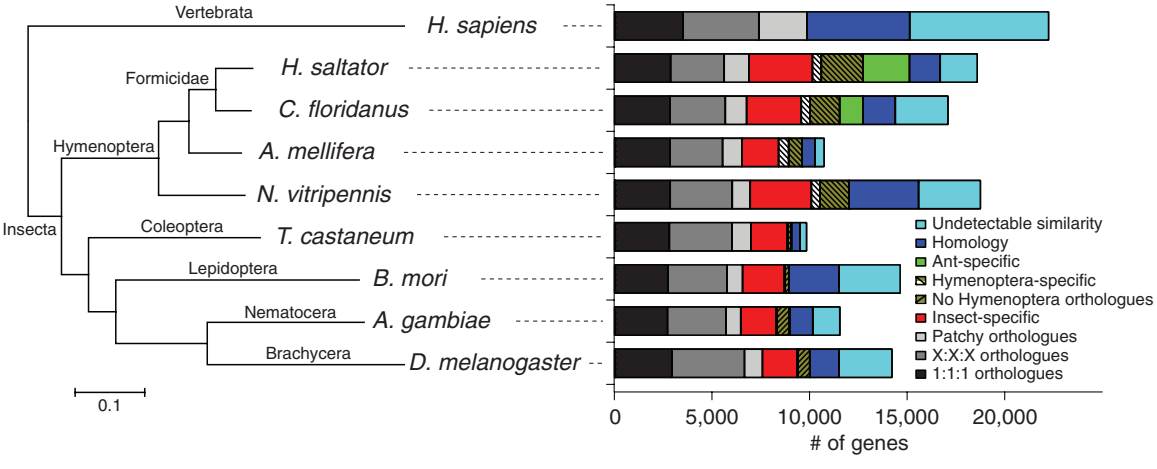

Fig. 1. Ant proteome. Phylogenetic tree based on maximum likelihood analyses of a concatenated alignment of single-copy proteins (**left**), and orthology relationships in multiple insects (**right**), using *Homo sapiens* as outgroup. The scale bar indicates 0.1 substitution per site. *T. castaneum*, *Tribolium castaneum*; *B. mori*, *Bombyx mori*; *A. gambiae*, *Anopheles gambiae*.

Downloaded from www.sciencemag.org on August 27, 2010

(table S4 and fig. S2), despite the presence of cytosine methylation. CpG dinucleotides are also overrepresented in *A. mellifera* (*5*) and in *N. vitripennis*; thus, this genomic feature may be specific to the Hymenoptera.

Repetitive elements constitute 15% of the assemblies in *C. floridanus* and 27% in *H. saltator* (table S4 and fig. S3), which is probably an underestimate, because genome regions that cannot be assembled are enriched in repeats. Both genomes contain copies of the *piggyBac* transposon [234 in total and 6 with intact open reading frames (ORFs) in *C. floridanus*, 976 in total and 23 with intact ORFs in *H. saltator*], which has been used for insect transgenesis (*6*, *7*) and may also prove useful in ants.

Segmental duplications (SDs) account for 9.6% and 14.8% of the *C. floridanus* and *H. saltator* genomes, respectively (table S6). The 1810 (*C. floridanus*) and 2858 (*H. saltator*) gene models found in SDs are enriched in Gene Ontology (GO) terms associated with chemodetection, olfactory function, and protease/peptidase activity (table S7). *C. floridanus* SDs are also enriched for genes belonging to the cytochrome P450 family—perhaps as a result of detoxifying needs related to their generalist feeder life-style.

The predicted proteomes of *C. floridanus* and *H. saltator* share most protein families with *A. mellifera* and *N. vitripennis*, but also contain a large number of ant-specific (690) and species-specific families (3230 in *C. floridanus* and 2617 in *H. saltator*) without homologs in the other two Hymenoptera (fig. S4). When more insect genomes are included in the comparison, one-third of the ant protein-coding genes are conserved with vertebrates and two-thirds are conserved with insects, leaving 506 ant-specific protein families and 2000 to 3000 species-specific families (Fig. 1). Ant-specific genes were enriched not only in GO terms "olfactory receptor activity," "sensory perception of smell," "G protein–coupled receptor activity," and "odorant binding," but also in terms related to detoxification, including "monooxygenase activity" and "heme binding" (table S8).

We annotated 96 microRNA (miRNA) genes in *C. floridanus* and 159 in *H. saltator*. These accounted for most of the small RNA reads in adult specimens, with the exception of *H. saltator* gamergates, which showed a larger proportion of small RNAs mapping to unannotated regions of the genome (Fig. 2A and table S9). Gamergates also expressed the most diverse miRNA repertoire (table S10). The two *C. floridanus* worker castes displayed differential expression of miRNAs, with cflo-mir-64 up-regulated in minor workers (Fig. 2B) and cflo-mir-7 in major workers (fig. S5). This suggests that, in addition to being developmentally regulated (Fig. 2, C and D), some miRNAs might contribute to the differences among ant castes.

We examined the ant genomes and transcriptomes for signatures related to aging. Telomere shortening is a hallmark of cellular senescence in multicellular eukaryotes, and the enzyme telomerase (TERT), which counteracts telomere shortening, prolongs life span upon overexpression (*8*). *TERT* RNA levels were highest in eggs and lower in adults in both *C. floridanus* and *H. saltator*, but they were up-regulated in *H. saltator* gamergates (Fig. 3A). This may be explained by the gamergates acquiring many physiological characteristics of queens, including longer life span (*9*). Aging has also been linked to the sirtuin lysine deacetylases enzymes SIRT1 and SIRT6, homologous to the *Saccharomyces cerevisiae* Sir2p implicated in replicative senescence (*10*). In *H. saltator* gamergates, both of these genes are expressed at higher levels compared to workers (Fig. 3B). These results suggest that the regulation of life span in gamergates may share common mechanisms with other organisms.

The caste system in ant societies in general, and the social flexibility of *H. saltator* in particular, allow us to study the role of epigenetics in behavior, aging, and development. Here, we use the term "epigenetics" as the ensemble of molecular pathways that select genomic regions (chromatin domains) for activation or repression, transmit these states through cell division, and stabilize them in differentiated cell types. These mechanisms include DNA methylation, histone posttranslational modifications, and trans-acting mechanisms involving noncoding RNAs (*11*).

Unlike in *Drosophila*, DNA methylation pathways in *A. mellifera* and *N. vitripennis* are similar to those of mammalian systems (*5*, *12*). In the two ant species, we found single copies of cytosine methyltransferases *DNMT1* and *DNMT3B* genes and the noncatalytic *DNMT3L*, as well as four genes containing methyl-CpG binding domains (table S11). Consistent with these and previous observations (*13*), we detected the presence of 5-methylcytosine in the ants genomic DNA. *H. saltator*, which shows more ancestral characteristics, had less DNA methylation than its more derived relative, *C. floridanus* (Fig. 4A).

Histone acetyltransferases (HATs) and deacetylases (HDACs) add and remove acetyl groups on histone tails, regulate genes through chromatin structure (*14*), and are linked to the aging process (*10*). We identified 26 putative HATs in *C. floridanus* and 27 in *H. saltator*, with an expansion of GCNL2 homologs (table S12). Humans have four classes of HDACs, comprising HDAC1–11 and the NAD^+-dependent sirtuin family proteins (SIRT1–7). In contrast, only four HDACs and six sirtuins are found in *A. mellifera* (*5*). We identified five HDACs in *C. floridanus* and four in *H. saltator*, as well as six sirtuins in both ant species (table S11). Compared with mammals, these two ants and the honeybee lack SIRT3 (*10*).

Histone methylation is suspected to participate in epigenetic processes (*11*). We identified 27 proteins containing the conserved SET histone methyltransferase domain in *C. floridanus* and 22 in *H. saltator* (table S13). All major SET families are conserved in ants, including Polycomb/trithorax group, NSDs, SMYDs, and SETDs, and the arginine methyltransferase family. The SMYD family appears to have undergone multiple duplication events during the evolution of insects (fig. S6). We found five homologs in *C.*

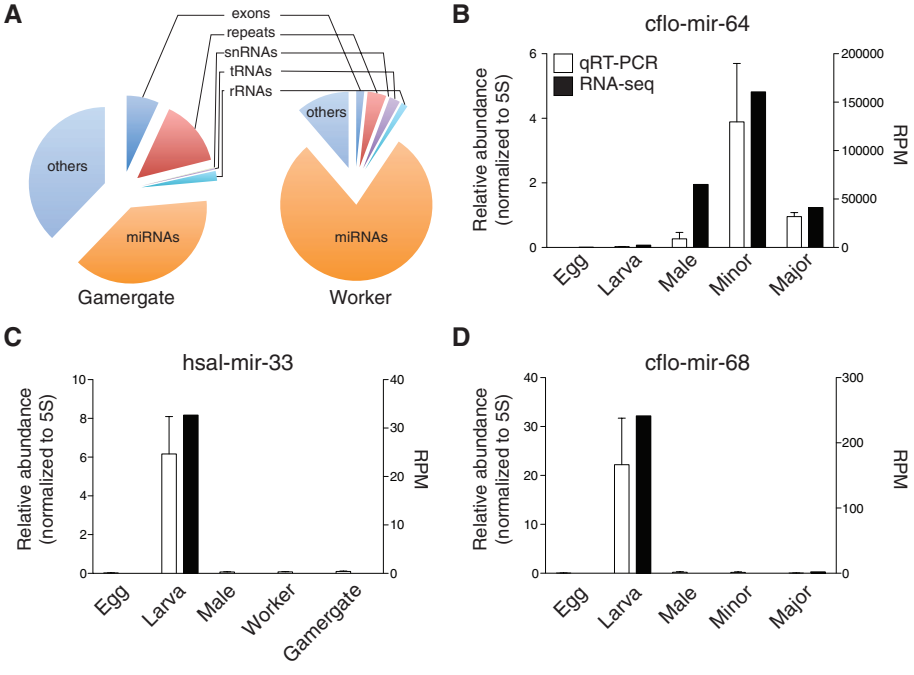

Fig. 2. Small RNA–seq and miRNA. (**A**) Classification of small RNA-seq reads from *H. saltator* gamergates (left) or workers (right). snRNAs, small nuclear RNAs; rRNAs, ribosomal RNAs. (**B** to **D**) Caste- and stage-specific expression of miRNAs in *C. floridanus* [(B) and (D)] and *H. saltator* (C). White bars represent quantitative reverse transcription–polymerase chain reaction (qRT-PCR) and indicate the mean ± SEM, $n = 7$ biological replicates. Black bars are scaled on the right y axis and indicate reads per million (RPM).

Downloaded from www.sciencemag.org on August 27, 2010

floridanus and six in *H. saltator* of *SMYD4*, which is involved in muscle development and breast cancer (*15*, *16*). SMYD family members are differentially regulated among different ant castes and developmental stages (fig. S7); among them, a *SMYD3* homolog (Hsal_14941) is up-regulated in gamergates (Fig. 4B), whereas a *SMYD4* homolog (Hsal_08142) is up-regulated in nonreproductive workers (Fig. 4C).

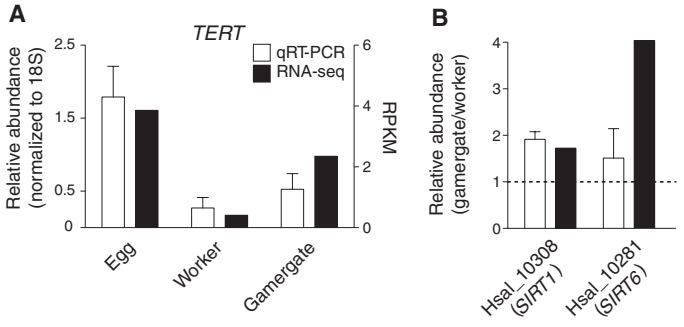

Fig. 3. Aging pathways in *H. saltator*. (**A**) *TERT* transcript levels in egg, workers, and gamergates. RPKM, read per kb per million reads. (**B**) Transcript levels in gamergates versus workers for *SIRT1* and *SIRT6* homologs. White bars, qRT-PCR mean ± SEM, $n = 7$. Black bars, RNA-seq. The dashed horizontal lines indicate a ratio of 1 (no difference).

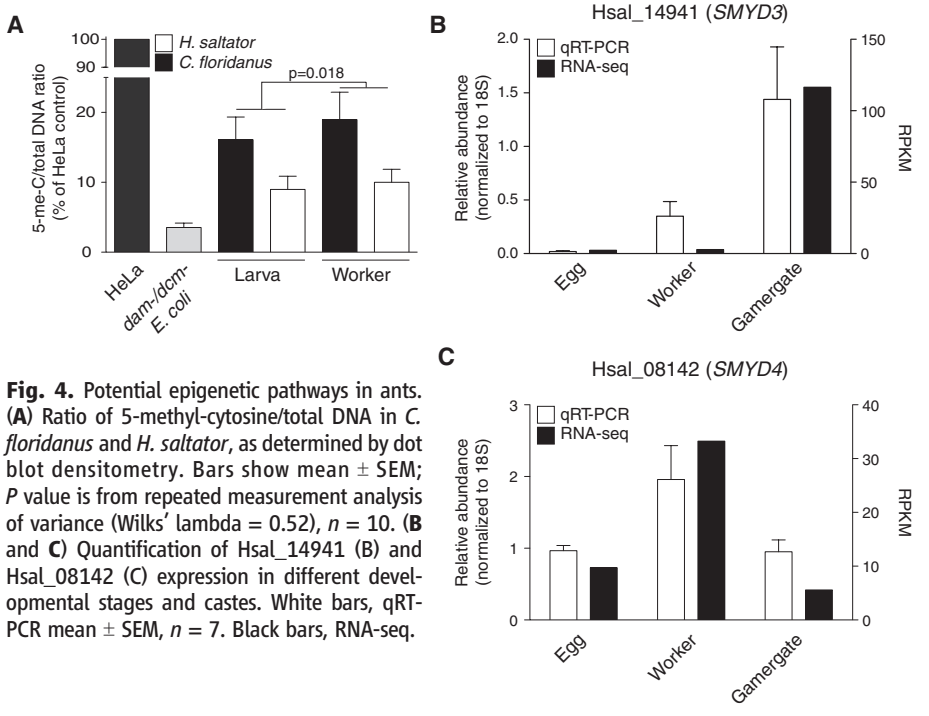

Fig. 4. Potential epigenetic pathways in ants. (**A**) Ratio of 5-methyl-cytosine/total DNA in *C. floridanus* and *H. saltator*, as determined by dot blot densitometry. Bars show mean ± SEM; *P* value is from repeated measurement analysis of variance (Wilks' lambda = 0.52), $n = 10$. (**B** and **C**) Quantification of Hsal_14941 (B) and Hsal_08142 (C) expression in different developmental stages and castes. White bars, qRT-PCR mean ± SEM, $n = 7$. Black bars, RNA-seq.

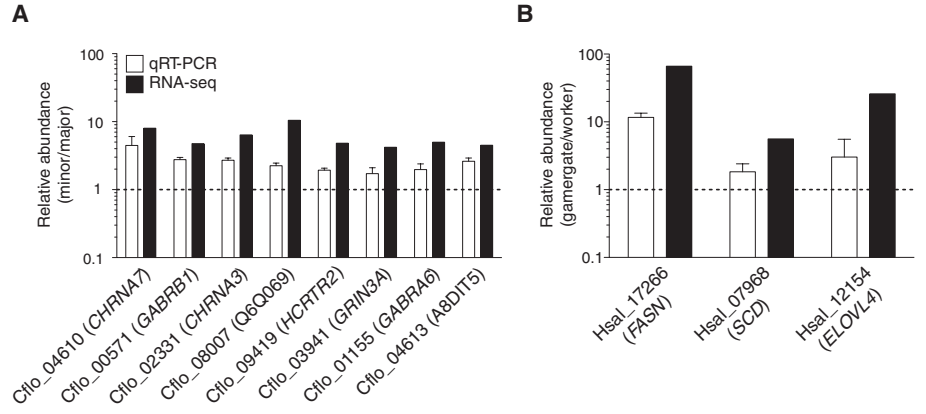

Fig. 5. Neurobiology and communication. (**A**) Quantification of 8 "GO:neurotransmitter binding" genes in head and thorax from major and minor workers in *C. floridanus*. White bars, qRT-PCR mean ± SEM, $n = 9$. Black bars, RNA-seq. (**B**) Quantification of fatty acid biosynthesis genes in *H. saltator* gamergates compared to nonreproductive workers. White bars, qRT-PCR mean ± SEM, $n = 7$. Black bars, RNA-seq.

The elaborate social organization in ant colonies is attributed to a sophisticated communication system, made up of chemical signals that elicit behavioral responses via the nervous system (*1*). Many enriched GO terms associated with differentially expressed genes in *C. floridanus* (table S14) and *H. saltator* (table S15) castes are related to neuronal function and chemical communication. In *C. floridanus* major and minor workers, we detected differences in the expression levels of genes associated with GO terms including "postsynaptic membrane," "ligand-gated channel activity," "sensory perception of smell" (table S14), and "neurotransmitter binding" (Fig. 5A). This suggests that the different behaviors exhibited by distinct workers castes may in part be encoded in the brain at the transcriptional level.

Olfactory receptors (ORs) are G protein–coupled receptors (GPCRs) that function in behavioral responses and chemical communication in animals (*17*). We found 139 genes containing the *Drosophila* olfactory receptor domain (IPR004117) in *C. floridanus* and 105 in *H. saltator* (tables S16 and 17). Similar to the *A. mellifera* genome, the ant genomes contain fewer gustatory receptors and odorant binding proteins than *Drosophila* (tables S16 and 17). The number of identified ORs is much smaller than the number of glomeruli observed in the antennal lobe for both ant species (*18*, *19*), apparently contradicting findings in other insects, which showed that most ORs are individually represented in the brain by a dedicated glomerulus (*20*). However, our homology-based approach might be insufficient to detect all ant-specific ORs.

In ants, cuticular hydrocarbons play a key role in nestmate recognition and regulation of reproduction (*21*). GO terms associated with the metabolism of hydrocarbons were enriched in ant-specific protein families (table S8) and in protein families expanded in ants (table S18 and fig. S8). *C. floridanus* and *H. saltator* have 19 and 14 genes, respectively, containing a beta-ketoacyl synthase domain (IPR014030), whereas *A. mellifera* has 3 and *D. melanogaster* has 4. Genes with putative roles in hydrocarbon metabolism show altered expression levels across castes and developmental stages (fig. S9). Compared to nonreproductive workers, *H. saltator* gamergates up-regulated several hydrocarbon metabolism genes, including homologs of a fatty acid synthase (*FASN*), an acetyl–coenzyme A desaturase (*SCD*), and an elongase of very long fatty acid (*ELOVL4*) (Fig. 5B). *H. saltator* gamergates advertise their reproductive status to nestmates via long cuticular hydrocarbons (*22*), and we found that expression of most genes with homology to human *ELOV* genes was up-regulated in gamergates (fig. S10). Because of the complexity of the metabolic pathways involved, we cannot conclude that transcriptional regulation of these genes is directly linked to communication; however, these observations suggest a molecular basis for

Downloaded from www.sciencemag.org on August 27, 2010

the interplay between pheromone production, olfaction, and behavior in ants.

Our initial analysis of the genomes of two socially divergent ant species has captured major molecular features that make ants an attractive model for genomic and epigenetic studies. Ant species vary widely in the extent to which eusociality is implemented, ranging from small and less organized colonies to massive and complex societies (*1*). The diversity and flexibility of ants may provide experimental avenues to address long-standing hypotheses on the relationships among epigenetics, neurobiology, and behavior (*23*), as well as life-span regulation.

References and Notes

1. B. Hölldobler, E. O. Wilson, *The Ants* (Harvard Univ. Press, Cambridge, MA, 1990).
2. D. E. Wheeler, *Am. Nat.* **128**, 13 (1986).
3. S. Jemielity, M. Chapuisat, J. Parker, L. Keller, *Age (Omaha)* **27**, 241 (2005).
4. C. Peeters, J. Liebig, B. Hölldobler, *Insectes Soc.* **47**, 325 (2000).
5. Honeybee Genome Sequencing Consortium, *Nature* **443**, 931 (2006).
6. M. D. Lorenzen *et al.*, *Insect Mol. Biol.* **16**, 265 (2007).
7. M. Sumitani, D. S. Yamamoto, K. Oishi, J. M. Lee, M. Hatakeyama, *Insect Biochem. Mol. Biol.* **33**, 449 (2003).
8. E. Sahin, R. A. Depinho, *Nature* **464**, 520 (2010).
9. A. Hartmann, J. Heinze, *Evolution* **57**, 2424 (2003).
10. A. Vaquero, D. Reinberg, *Genes Dev.* **23**, 1849 (2009).
11. C. D. Allis, T. Jenuwein, D. Reinberg, *Epigenetics*, M. Caparros, Ed. (Cold Spring Harbor Laboratory, Cold Spring Harbor, NY, ed. 1, 2007).
12. J. H. Werren *et al.*, Nasonia Genome Working Group, *Science* **327**, 343 (2010).
13. M. R. Kronforst, D. C. Gilley, J. E. Strassmann, D. C. Queller, *Curr. Biol.* **18**, R287 (2008).
14. Z. Wang *et al.*, *Cell* **138**, 1019 (2009).
15. E. C. Thompson, A. A. Travers, L. Randau, *PLoS ONE* **3**, e3008 (2008).
16. L. Hu, Y. T. Zhu, C. Qi, Y. J. Zhu, *Cancer Res.* **69**, 4067 (2009).
17. J. G. Hildebrand, G. M. Shepherd, *Annu. Rev. Neurosci.* **20**, 595 (1997).
18. C. Zube, C. J. Kleineidam, S. Kirschner, J. Neef, W. Rössler, *J. Comp. Neurol.* **506**, 425 (2008).
19. S. C. Hoyer, J. Liebig, W. Rössler, *Arthropod Struct. Dev.* **34**, 429 (2005).
20. E. Fishilevich, L. B. Vosshall, *Curr. Biol.* **15**, 1548 (2005).
21. G. J. Blomquist, A. G. Bagnères, *Insect Hydrocarbons: Biology, Biochemistry, and Chemical Ecology* (Cambridge Univ. Press, Cambridge, 2010).
22. J. Liebig, C. Peeters, N. J. Oldham, C. Markstädter, B. Hölldobler, *Proc. Natl. Acad. Sci. U.S.A.* **97**, 4124 (2000).
23. C. Dulac, *Nature* **465**, 728 (2010).

24. We thank T. Bloss for ant colony maintenance, B. Kopenhaver for technical help, A. Alekseyenko and J. Wang for bioinformatic support, W. Wang for advice on evolutionary analysis, and P. Voigt and D. Simola for careful reading of the manuscript. R.B. is a fellow of the Helen Hay Whitney Foundation. This work was funded by Howard Hughes Medical Institute Collaborative Innovation Award #2009005 to S.L.B., D.R., and J.L. Raw sequencing data have been deposited in the National Center for Biotechnology Information as SRA020747 (*C. floridanus* genome), SRA020748 (*H. saltator* genome), and GSE22680 (RNA-seq). Assemblies and annotations have been deposited at DNA Data Bank of Japan–European Molecular Biology Laboratory–GenBank under the accession AEAB00000000 and AEAC00000000. The versions described in this paper are the first deposited versions: AEAB01000000 and AEAC01000000.

Supporting Online Material

www.sciencemag.org/cgi/content/full/329/5995/1068/DC1
Materials and Methods
SOM Text
Figs. S1 to S24
Tables S1 to S40
References

18 May 2010; accepted 20 July 2010
10.1126/science.1192428

Crystal Structure of Human Adenovirus at 3.5 Å Resolution

Vijay S. Reddy,[1]* S. Kundhavai Natchiar,[1] Phoebe L. Stewart,[2] Glen R. Nemerow[1]*

Rational development of adenovirus vectors for therapeutic gene transfer is hampered by the lack of accurate structural information. Here, we report the x-ray structure at 3.5 angstrom resolution of the 150-megadalton adenovirus capsid containing nearly 1 million amino acids. We describe interactions between the major capsid protein (hexon) and several accessory molecules that stabilize the capsid. The virus structure also reveals an altered association between the penton base and the trimeric fiber protein, perhaps reflecting an early event in cell entry. The high-resolution structure provides a substantial advance toward understanding the assembly and cell entry mechanisms of a large double-stranded DNA virus and provides new opportunities for improving adenovirus-mediated gene transfer.

Human adenoviruses (HAdV) are nonenveloped double-stranded DNA (dsDNA) viruses that are associated with acute infections (*1*–*3*). Although these infections are generally self-limiting, the reemergence of certain HAdV types has also been linked to potentially fatal respiratory infections in both civilian and military populations (*4*). Severe disseminated diseases also occur in patients receiving bone marrow–derived stem cells (*5*, *6*). In addition to their disease associations, replication-defective or conditionally replicating HAdVs continue to be evaluated in ~25% of approved phase I to III clinical trials for vaccine and therapeutic gene transfer (*7*, *8*). However, the lack of accurate details of the virus structure limits the reengineering of HAdV vectors and prevents a better understanding of the virus life cycle. High-resolution HAdV structure determination presents a challenge because of the large size (910 Å average diameter, 150 megadalton) and complexity (pseudo-$T = 25$) of the virus. The crystal structures of the major HAdV capsid proteins, the fiber (*9*), penton base (PB) (*10*), and hexon (*11*), have been solved. The hexon and penton base crystal structures were subsequently used to derive pseudo-atomic models of the HAdV capsid at moderately high resolution (7 to 10 Å) (*12*–*14*) by cryoelectron microscopy (cryoEM). CryoEM structural analyses provided considerable insight into HAdV organization; however, they did not furnish detailed information on the interactions between the major and accessory (cement) proteins (IIIa,VI,VIII, and IX).

We report here the crystal structure of a recombinant HAdV-5 vector, designated Ad35F, that is equipped with a short and flexible fiber protein derived from HAdV-35 (*15*). Details of the crystallization (*16*), diffraction data statistics (table S1), and structure determination of Ad35F at near-atomic resolution (3.5 Å) are described in (*17*).

The architecture of the HAdV capsid is shown in Fig. 1, A and B. The hexon is the most abundant protein in the capsid, with 720 subunits arranged as 240 trimers on a pseudo-$T = 25$ icosahedral lattice. Five PB monomer subunits occupy each of the icosahedral vertices and are associated with the trimeric fiber protein. Each of the 20 facets of the capsid contains 12 hexon trimers and a penton at each vertex. The icosahedral asymmetric unit consists of four hexon trimers and one PB monomer. As previously described, each hexon monomer contains two eight-stranded jelly-roll domains, V1 and V2 (*11*), whereas the PB subunit contains a single jelly-roll domain (*10*). Three sets of V1 and V2 domains give the hexon trimer a pseudo-hexagonal shape at the base, which in turn gives rise to a pseudo-$T = 25$ architecture for the HAdV capsid. Large insertions between the strands of the hexon jelly-roll domains form triangular towers on top of the hexagonal base. Representative electron density for a hexon subunit [amino acids (aa) 579 to 582] is shown in fig. S1. Some of the hypervariable region loops (aa 186 to 193 and 250 to 258) that were disordered in the isolated hexon structure are visible in the HAdV capsid crystal structure (fig. S1) because they are involved in multiple, symmetry-related interhexon contacts (figs. S2 and S3). The tertiary structures of the 12 structurally independent hexon subunits are nearly identical, having a root mean square deviation of ~1 Å upon superposition with a few differences found mainly at the amino and carboxy termini.

[1]The Scripps Research Institute, 10550 North Torrey Pines Road, La Jolla, CA 92037, USA. [2]Vanderbilt University Medical Center, 2215 Garland Avenue, 710 Light Hall, Nashville, TN 37232, USA.

*To whom correspondence should be addressed. E-mail: gnemerow@scripps.edu (G.R.N.); reddyv@scripps.edu (V.S.R.)

Downloaded from www.sciencemag.org on August 27, 2010

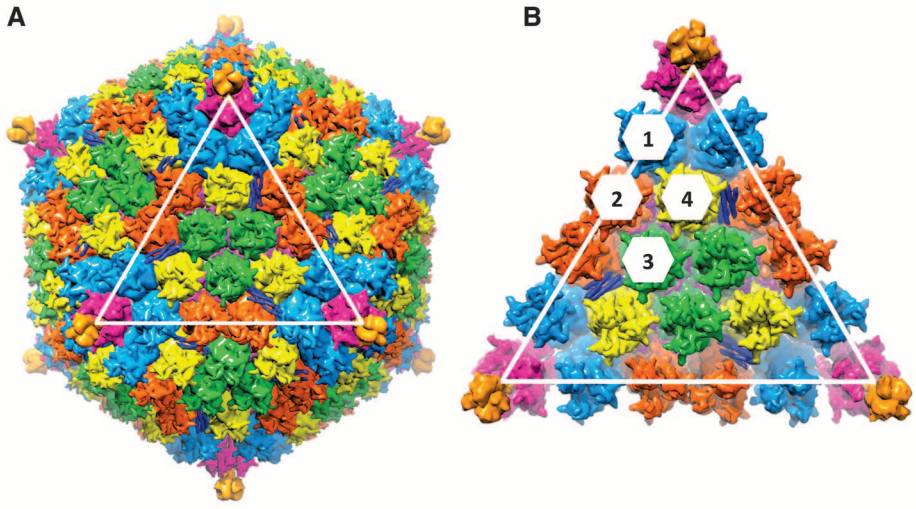

Fig. 1. Surface rendering and subunit associations of Ad35F. The icosahedral asymmetric unit is composed of one of the PB (pink) subunits and four hexon trimers [cyan (1), orange-red (2), green (3), and yellow (4)]. Cement proteins on the outside of the capsid are shown in blue (four-helix bundle) and magenta (IX triskelion). Twelve hexon trimers occupy one facet of the Ad35F capsid; however, a total of 18 hexons are shown for clarity. A model of the trimeric fiber docked into each penton base is shown in orange. (**A**) Outer capsid viewed down the particle threefold axis with a facet circumscribed by the white triangle. (**B**) A zoom-in view of the single facet.

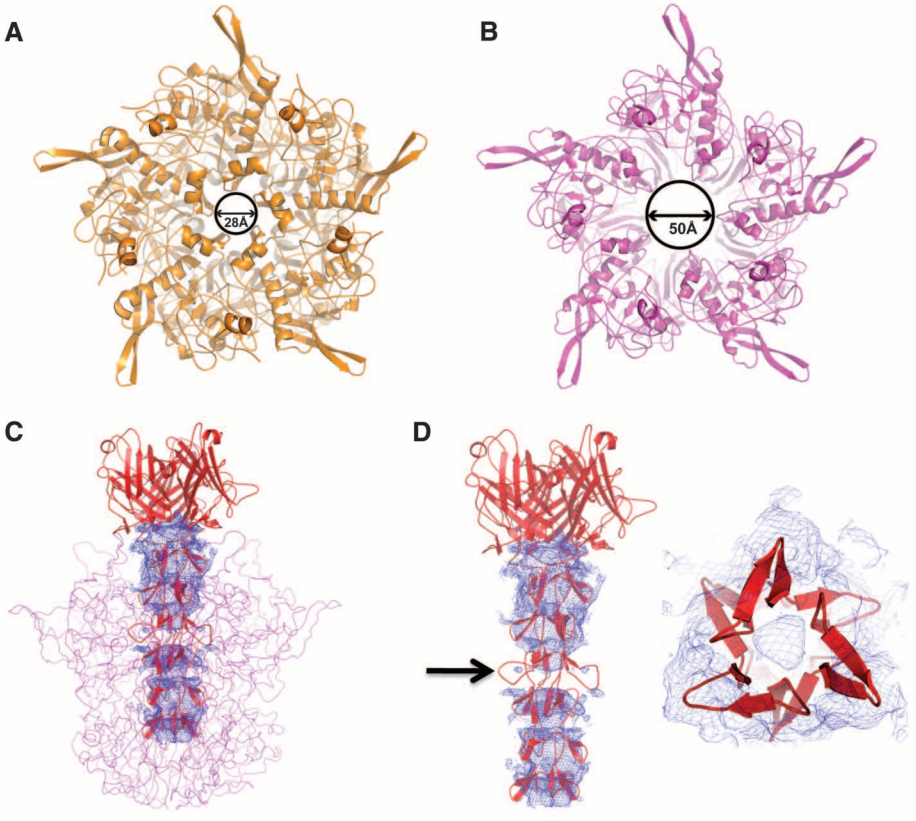

Fig. 2. Structure of the penton complex. (**A**) The structure of the isolated PB shown in gold (*10*) with a maximum pore diameter of 28 Å. (**B**) The structure of the PB in the Ad35F particle shown in magenta with a maximum pore dimension of 50 Å. (**C**) The threefold averaged difference ($F_o - F_c$) electron density (in blue, contoured at 2.5σ) corresponding to the fiber molecule along the fivefold axis of the PB, shown as magenta trace. Structure of the HAdV-35 fiber molecule based on the partial HAdV-2 fiber structure (*9*), represented as ribbon diagram (red) and fitted into the difference density. (**D**) A vertical view of the fit of the fiber shaft to the difference density (left). The flexible third repeat of the shaft is indicated by an arrow. A view down the fiber axis showing the fit of one of the shaft repeats (right).

An unusual molecular interaction in the HAdV particle occurs between the fivefold symmetric PB and the threefold symmetric fiber protein. The "symmetry mismatch" that occurs between the PB and fiber is of particular interest because of its potential impact on cell receptor interactions as well as subsequent disassembly processes. Previous cryoEM structural analyses of HAdV at moderate resolution and a cocrystal structure of PB with an N-terminal fiber peptide suggested that the fiber protein interacts on the outer surface of the PB (*18*, *19*). Consistent with this model, the crystal structure of recombinant PB alone (Fig. 2) indicated that the central pore of the PB pentamer is too narrow to allow fiber insertion (*10*). However, in the Ad35F particle the central pore of the PB has a diameter nearly twice that of the isolated (fiberless) PB (*10*) (Fig. 2B). Hence, the dimensions for the PB pore in the Ad35F structure but not in the isolated PB would allow insertion of the fiber shaft domain into the central cavity of the PB. Consistent with this, Fig. 2, C and D, shows strong $F_o - F_c$ electron density along the icosahedral fivefold symmetry axes, generated by using local threefold symmetry, originating from deep inside the PB pore and extending to its outer surface. We assign this to the shaft region of the fiber protein. This fiber shaft corresponds to a length of 90 Å and accommodates five to six β-spiral repeats that are each about 13 to 15 Å along the fiber axis (Fig. 2, C and D) in agreement with the 5.5 repeats predicted for the HAdV-35 fiber shaft (*20*). The density corresponding to the fiber knob was not visible. The ability of the penton base to adapt to large changes is striking. Conformational changes observed in the crystal structure may reflect early events in cell entry.

The C termini of hexon subunits are involved in two different types of interactions. First, the C termini stabilize the threefold junctions inside the capsid within each group of nine hexons (GONs) in a facet. The C-terminal tail (green) (residue 944 to the last ordered residue—946, 949, or 951 in different subunits) forms an extra strand that interacts with a β sheet in the V2 domain of the adjacent (clockwise; threefold related) hexon subunits in neighboring trimers (Fig. 3, A and B).

The second type of interaction occurs between two C-terminal tails of hexon subunits, with the two tails coming from adjacent GONs or with one of the tails coming from a peripentonal hexon. The two tails stack on top of each other. Although there are no direct interactions between the C-terminal tails themselves, each interacts with residues in apposing hexon subunits primarily via hydrogen bonds. A highly ordered helix from protein VIII (residues 40 to 60) lies beneath and coplanar with these stacked C termini, further supporting the interface between hexon subunits at the capsid interior (Fig. 3, A and C). In contrast to the C termini, none of the N termini of the hexons are involved in "direct" interhexon interactions. They are, however, involved in critical interactions with the cement proteins, thus indirectly stabilizing the interhexon associations (detailed below).

Downloaded from www.sciencemag.org on August 27, 2010

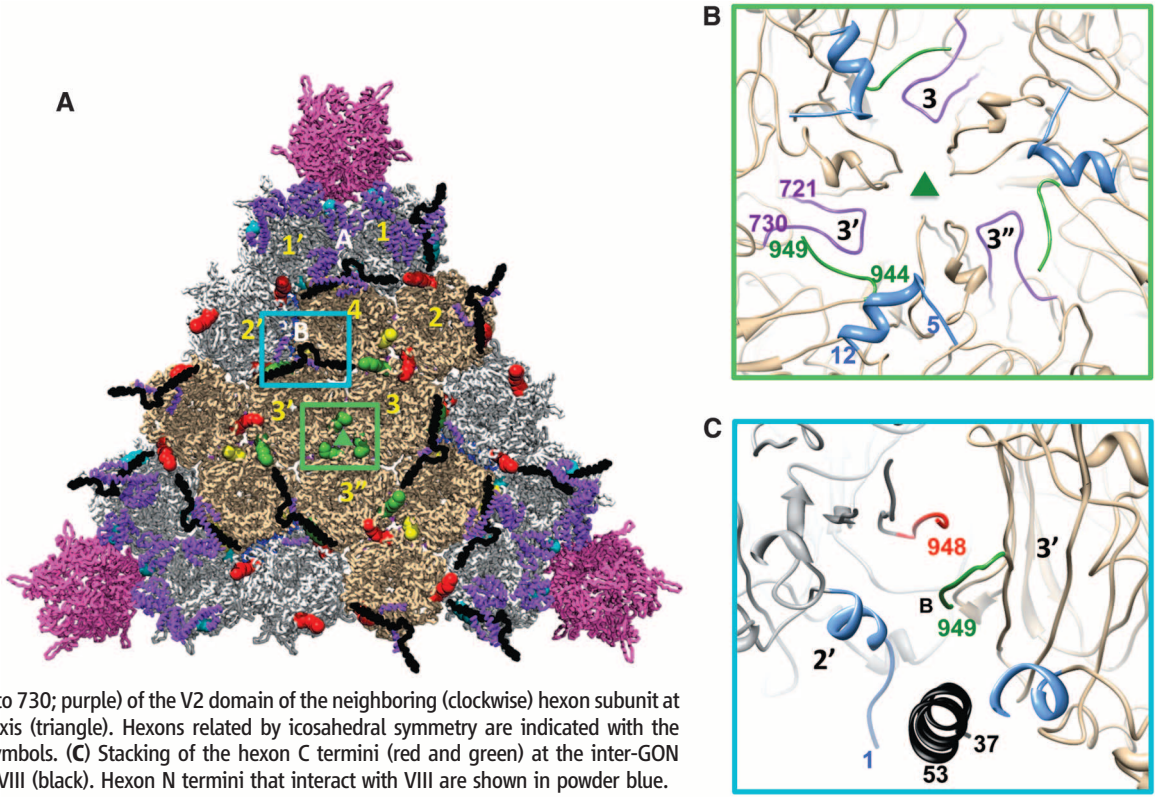

Fig. 3. Hexon associations at the inner capsid surface. (**A**) Inner surface of a facet showing the locations of hexon C termini, shown as spheres according to the hexon color coding used in Fig. 1A. GON hexons in the facet are shown in tan, and the rest of the hexons are shown in gray for clarity. VIII molecules are shown in black. PB subunits are shown in pink and additional cement proteins in purple. Structurally distinct locations (A and B) of VIII molecules as well as the four hexon trimers (1, 2, 3, and 4) of the icosahedral asymmetric unit are indicated. (**B**) Formation of extended β sheets by the hexon C termini (green) with the EF strands (aa 721 to 730; purple) of the V2 domain of the neighboring (clockwise) hexon subunit at the icosahedral threefold axis (triangle). Hexons related by icosahedral symmetry are indicated with the prime and double prime symbols. (**C**) Stacking of the hexon C termini (red and green) at the inter-GON interface with a helix from VIII (black). Hexon N termini that interact with VIII are shown in powder blue.

The contiguous shell of the Ad35F capsid contains four cement proteins, IIIa, VI, VIII, and IX, that play important roles in stabilizing the virion. Their locations have been tentatively assigned to the outer and inner surface of the capsid on the basis of their copy number, cryoEM, and biochemical analysis (*12*, *14*, *21*). We did not observe significant side-chain densities needed to definitively assign their sequence with the exception of VIII (see below). The triskelion-like structures, formed by N-terminal regions of three protein IX subunits (*12*, *13*), are located at four different positions per facet (Fig. 1) and stabilize the threefold GON junctions on the capsid exterior. The Ad35F crystal structure revealed a very-well-ordered four-helix bundle, 80 Å in length, that is located on the capsid exterior between hexon-4 of one GON and hexon-2 of the neighboring GON (molecule in blue; Fig. 1, A and B). Early cryoEM analyses (*12*, *22*) tentatively assigned density at this location to IIIa, which is the largest cement protein (63 kD) in the HAdV capsid shell. However, a recent 6 Å resolution cryoEM analysis revealed the coiled coil shape of this density and led to the alternate hypothesis that this region might correspond to the C termini of four IX molecules (*14*). This assignment to protein IX was also suggested by cryoEM analysis of Ad vectors with peptide-tagged IX (*23*). Interestingly, the x-ray structure revealed that two of the helices in this four-helix bundle appear to be connected at one end (fig. S4a inset). This finding, as well as the different distances observed from the visible ends of the (trimeric) triskelions of protein IX to the nearest helix of the (tetrameric) four-helix bundle, raises the question as to whether the helical bundle is formed by four C-terminal helices of IX. Another possibility is that this helical bundle represents a domain of IIIa as originally proposed. A higher-resolution density map will be required to definitively assign an amino acid sequence to this region.

The Ad35F structure also revealed multiple helices, organized primarily as two domains (fig. S4b), on the inside of the virus capsid at the vertex region. The connectivity between these helices is not clear. Although this region has been tentatively assigned as IIIa on the basis of a cryoEM analysis (*14*), it is possible that at least some of these helices could correspond to the membrane lytic VI molecule (*24*) that participates in endosomalysis and whose N-terminal 80 residues have a high degree of α-helical content. The helical domain, closest to the vertex, "cements" the contacts between two peripentonal hexons, whereas the second domain appears to interact with the base of one peripentonal hexon. There is also a helix layered on top of one of the molecules of VIII (A) (fig. S4b). This helix, along with two other short helices, could belong to yet another cement protein. Interestingly, difference maps also showed that all of the hexon cavities are filled with electron density (fig. S5), suggesting that at least part of the putative protein VI molecules could be sequestered inside the hexon trimers, as previously suggested (*25*). These densities could account for over 200 VI molecules present in the HAdV capsid.

The HAdV particle contains 120 copies of protein VIII, a key cement protein that has been tentatively assigned to the interior of the capsid on the basis of its copy number and predicted α-helical content (*12*, *14*). Our x-ray structure confirmed the location of VIII and provided more detailed information on its interactions with nearby hexon proteins (Fig. 4). We fit the VIII sequence into the electron density on the basis of multiple criteria, including the presence of a single predicted α helix, the location of key proline residues associated with a prominent U-shaped bend in the central portion of the VIII segment, and the direction of the densities for the residues with long side chains (facing toward the N terminus of the helix) in the sharpened maps. The ordered part of VIII molecule has an extended fold with an end-to-end span of 83 Å, starting with a helix of ~20 residues, followed by a distinct inverted U-shaped structure, and succeeded by an extended polypeptide chain (Fig. 4A). Furthermore, a large portion of the aligned sequence (residues 37 to 90) exhibited favorable side chain interactions with the residues from the nearby hexon subunits (Fig. 4, C and D). Fifty-four residues of the mature form of VIII, resulting from cleavage by the virus cysteine protease, are visible at two independent locations in the electron density maps. The two structurally distinct VIII molecules (A and B) closely trace the base of individual hexons (inside) along the outer edge of the GON hexons and mediate the interactions between GONs as well as between peripentonal hexons (Fig. 4B). Each VIII molecule in the Ad35F particle interacts with the N termini of three subunits of hexon trimers related by local threefold symmetry. One of the protein VIII molecules, designated A, is located close to vertex region and

Downloaded from www.sciencemag.org on August 27, 2010

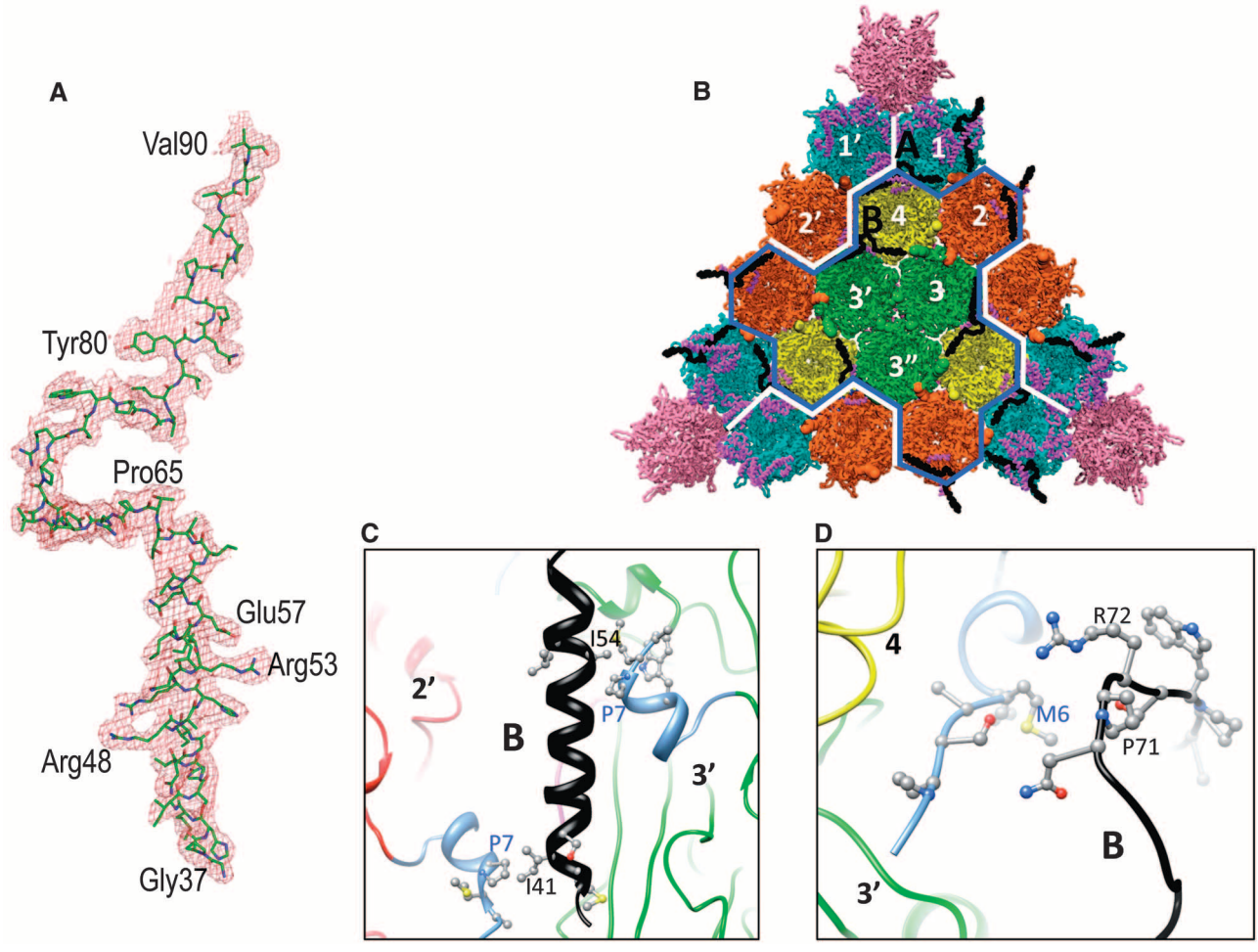

Fig. 4. Structure and interactions of pVIII with the hexons. (**A**) Display of $2F_o - F_c$ electron density (contoured at 1.0σ) of the ordered part of an VIII molecule. (**B**) An interior view of the facet showing the locations of proteins VIII (black) and additional cement proteins (purple). An outline of the GONs is shown by a thick blue line. A line trace (in white) corresponding to the location of three P30 molecules from PRD1 (*9*) is shown in comparison with protein VIII and in the context of the Ad35F structure. Hexons are color coded and numbered according to the scheme described in Fig. 1A and (A), respectively. (**C**) Nonpolar interactions between an VIII helix (black) with the N termini (powder blue) of two neighboring hexons viewed from the inside of the virus. I indicates Ile; P, Pro; R, Arg; and M, Met. (**D**) Close approach of the inverted U-shaped bend in VIII (black) to the N terminus of a hexon subunit. However, the interactions of the U-shaped structure are not as close and specific as those mediated by the helix in (C).

interacts with two peripentonal hexons, whereas the second one, designated B, closely interacts with hexon-4 and hexon-3′ (Figs. 3A and 4B). The ordered parts of each of these molecules closely associate with three hexon trimers.

Specifically, residues Ile^{41} and Ile^{54} in the N-terminal leg of the VIII molecule (A) mediate nonpolar interactions with Pro^{7} and flanking residues at the N terminus of a peripentonal hexon (hexon-1′) (Fig. 4B) and hexon-4 in the reference icosahedral asymmetric unit, respectively (Fig. 4, B and C). The inverted U-shaped kink comprising VIII residues 63 to 77 interacts with N-terminal residues 1 to 7 of one of the subunits of another peripentonal hexon (hexon-1) (Fig. 4D). Thus, VIII molecule-A staples two peripentonal hexons with hexon-4. Likewise, the second VIII molecule-B mediates associations between three hexons, hexon-2′ of a neighboring GON with hexon-3′ and hexon-4 from the reference GON, by using the quasi-equivalent interactions as described for VIII molecule-A (Fig. 4, B to D).

The Ad35F structure provides insights into the virus-host interactions. Although interhexon contacts are extensive and are augmented by the cement proteins, the interactions between the penton base and peripentonal hexons are rather tenuous (fig. S6). This would favor efficient capsid disassembly and release of the penton complex during cell entry. The crystal structure of the entire HAdV particle also provides an initial assessment of the folds and interactions of cement proteins with the hexon subunits. Improved knowledge of HAdV assembly from its individual capsid proteins could lead to the development of novel antiviral strategies to block infection at multiple cell entry steps and facilitate the development of HAdV vectors with improved tissue targeting.

References and Notes

1. A. L. Butt, J. Chodosh, *Cornea* **25**, 199 (2006).
2. Y. J. Gordon, T. P. Araullo-Cruz, Y. F. Johnson, E. G. Romanowski, P. R. Kinchington, *Invest. Ophthalmol. Vis. Sci.* **37**, 2774 (1996).
3. M. R. Hilleman, J. H. Werner, *Proc. Soc. Exp. Biol. Med.* **85**, 183 (1954).
4. D. Metzgar *et al.*, *J. Infect. Dis.* **196**, 1465 (2007).
5. J. A. Hoffman, *Pediatr. Transplant.* **10**, 17 (2006).
6. L. Lenaerts, E. De Clercq, L. Naesens, *Rev. Med. Virol.* **18**, 357 (2008).
7. M. L. Edelstein, M. R. Abedi, J. Wixon, R. M. Edelstein, *J. Gene Med.* **6**, 597 (2004).
8. T. D. Henry *et al.*, *J. Am. Coll. Cardiol.* **50**, 1038 (2007).
9. M. J. van Raaij, A. Mitraki, G. Lavigne, S. Cusack, *Nature* **401**, 935 (1999).
10. C. Zubieta, G. Schoehn, J. Chroboczek, S. Cusack, *Mol. Cell* **17**, 121 (2005).
11. J. J. Rux, R. M. Burnett, *Mol. Ther.* **1**, 18 (2000).
12. C. M. Fabry *et al.*, *EMBO J.* **24**, 1645 (2005).
13. S. D. Saban, R. R. Nepomuceno, L. D. Gritton, G. R. Nemerow, P. L. Stewart, *J. Mol. Biol.* **349**, 526 (2005).
14. S. D. Saban, M. Silvestry, G. R. Nemerow, P. L. Stewart, *J. Virol.* **80**, 12049 (2006).
15. T. A. Smith *et al.*, *Hum. Gene Ther.* **14**, 777 (2003).
16. V. S. Reddy *et al.*, *Virology* **402**, 209 (2010).
17. Materials and methods are available as supporting material on *Science* Online.
18. P. Fuschiotti *et al.*, *J. Mol. Biol.* **356**, 510 (2006).
19. D. J. Von Seggern, C. Y. Chiu, S. K. Fleck, P. L. Stewart, G. R. Nemerow, *J. Virol.* **73**, 1601 (1999).
20. D. M. Shayakhmetov, A. Lieber, *J. Virol.* **74**, 10274 (2000).

Downloaded from www.sciencemag.org on August 27, 2010

21. J. van Oostrum, R. M. Burnett, *J. Virol.* **56**, 439 (1985).
22. P. L. Stewart, S. D. Fuller, R. M. Burnett, *EMBO J.* **12**, 2589 (1993).
23. S. K. Campos, M. A. Barry, *Curr. Gene Ther.* **7**, 189 (2007).
24. C. M. Wiethoff, H. Wodrich, L. Gerace, G. R. Nemerow, *J. Virol.* **79**, 1992 (2005).
25. M. Silvestry *et al.*, *J. Virol.* **83**, 7375 (2009).
26. The authors express their deep gratitude to J. E. Johnson for advice and guidance during all phases of the structure determination and for reading the manuscript; T.-M. Mullen and L. Gritton for the outstanding technical support for vector production; S. Venkataraman for help with the early crystallization setups of HAdV; I. Mathews of the Stanford Synchrotron Radiation Lightsource for initial help with the data collection; W. Minor and I. Minor for generously providing the larger version of the SCALEPACK program; E. Ollmann-Saphire and J. G. Smith for comments on the manuscript; T. McCarthy for preparation of this paper; and R. Fischetti, N. Sanishvili, and other members at General Medicine and Cancer Institutes Collaborative Access Team (GM/CA CAT) for discussions and technical support. GM/CA CAT has been funded in whole or in part with federal funds from the National Cancer Institute (Y1-CO-1020) and the National Institute of General Medical Science (Y1-GM-1104). The use of the Advance Photon Source was supported by the U.S. Department of Energy, Basic Energy Sciences, Office of Science (contract no. DE-AC02-06CH11357). The coordinates of Ad35F crystal structure have been deposited in the Protein Data Bank (PDB) with the identification code 1VSZ. This work was supported by NIH grants R01 AI070771 to V.S.R., HL054352 and EY011431 to G.R.N., and AI042929 to P.L.S. This is manuscript no. 20538 from the Scripps Research Institute. G.R.N. holds a patent titled "Adenovirus vectors, packaging cell lines, compositions, and methods for preparation and use" (patent no. 7,232,899).

Supporting Online Material
www.sciencemag.org/cgi/content/full/329/5995/1071/DC1
Materials and Methods
Figs. S1 to S6
Table S1
References

20 January 2010; accepted 21 June 2010
10.1126/science.1187292

Insects Betray Themselves in Nature to Predators by Rapid Isomerization of Green Leaf Volatiles

Silke Allmann[1,2] and Ian T. Baldwin[1]*

Plants emit green leaf volatiles (GLVs) in response to herbivore damage, thereby attracting predators of the herbivores as part of an indirect defense. The GLV component of this indirect defense was thought to be a general wound signal lacking herbivore-specific information. We found that *Manduca sexta*–infested *Nicotiana attenuata* attract the generalist hemipteran predator *Geocoris* spp. as the result of an herbivore-induced decrease in the (*Z*)/(*E*) ratio of released GLVs, and that these changes in the volatile bouquet triple the foraging efficiency of predators in nature. These (*E*)-isomers are produced from plant-derived (*Z*)-isomers but are converted by a heat-labile constituent of herbivore oral secretions. Hence, attacking herbivores initiate the release of an indirect defense a full day before the attacked plants manufacture their own defensive compounds.

Plants defend themselves against herbivore attack by producing chemical and physical defenses that decrease herbivore performance, but they also release distinct volatile bouquets when attacked. These herbivore-induced plant volatiles (HIPVs) can function as indirect defenses by attracting carnivores. Although the attraction of natural enemies to HIPVs has frequently been observed in laboratory studies (*1*), few studies have demonstrated that HIPVs attract carnivores in nature (*1*–*3*).

Elicitors in herbivore oral secretions introduced into plant wounds during feeding (*4*–*6*), as well as the rhythm of caterpillar feeding (*7*), provide the plant with the information required to activate herbivore-specific defenses, including the release of specific volatiles. The composition of the HIPV blend can differ among plant and herbivore species, abiotic conditions, and over time (*2*, *8*–*10*). HIPVs have several different metabolic origins, of which the isoprene-derived terpenoids and fatty acid–derived green leaf volatiles (GLVs) are the best-studied classes. Terpenoids are released with a delay from the whole plant, not just attacked leaves, after a few hours or with the plant's next photosynthetic phase (i.e., often a day after the start of herbivore attack) (*11*–*13*). Because of their delayed, systemic release, the terpenoids likely function in the long-distance attraction of carnivores. GLVs—which consist of six-carbon aldehydes, alcohols, and their esters—are, unlike terpenoids, immediately and likely passively released from wounded leaves (*11*, *14*). Consequently, GLVs likely provide rapid, but nonspecific information about the exact location of a feeding herbivore. GLVs were shown to play a role in host-location of predators and parasitic wasps (*15*–*17*). Although changes in constitutive GLV ratios can alter the ability of herbivores to locate their host (*18*), the degree to which natural enemies use induced GLVs to find plants with prey remains unclear (*19*, *20*).

The GLV blend of mechanically wounded *Nicotiana attenuata* plants contains large amounts of (*Z*)-GLVs and proportionally smaller amounts of (*E*)-GLVs (Fig. 1). These different isomers result from rearrangements of the double bonds. However, plants that had been attacked for 24 hours by 1, 5, or 10 *Manduca sexta* neonates, a specialist herbivore of this native tobacco, released (*Z*)- and (*E*)-isomers in nearly equal amounts (Fig. 1A) (*21*). We compared changes in the (*Z*)/(*E*) ratio of GLVs released from mechanically wounded leaves of which the wounds were treated with water (w + w) or *M. sexta* oral secretions (OS) (w + OS; fig. S1) (*22*). We found that w + w–treated plants emitted high levels of (*Z*)-GLVs and low levels of (*E*)-GLVs, whereas treating wounds with *M. sexta* OS decreased emissions of (*Z*)-GLVs and increased those of (*E*)-GLVs, resulting in a distinct change in the (*Z*)/(*E*) ratio (Fig. 1, B and C, and table S1). To determine whether the OS-elicited (*Z*)/(*E*) shift is a transient response, we monitored the GLV bouquet for several hours after a single elicitation. Although the GLV burst occurred immediately after a single wounding and vanished after a few hours (fig. S2A), the OS-elicited changes in the (*Z*)/(*E*) ratio persisted for the duration of the GLV burst (fig. S2B).

Saliva or OS from herbivores can elicit specific responses in a plant, and two main classes of endogenously produced elicitors have been characterized in lepidopteran larvae: fatty acid–amino acid conjugates (FACs) and enzymes such as β-glucosidase and glucose oxidase (*6*). In addition, OS contains elicitors of plant origin, such as inceptins, which are processed in the oral cavity and reintroduced into the plant during feeding (*6*). FACs are central elicitors in *M. sexta*'s OS. In *N. attenuata* they amplify the wound-induced bursts of the phytohormones, jasmonic acid (JA), and ethylene, as well as the release of the sesquiterpene (*E*)-α-bergamotene (*5*, *6*). We trapped volatiles from plants that had been wounded and treated with the two most abundant FACs in *M. sexta*'s OS: *N*-linolenoyl-glutamate (18:3-Glu) or *N*-linolenoyl-glutamine (18:3-Gln) (*5*). Neither of the two elicited the OS-induced change in the (*Z*)/(*E*) ratio (fig. S3D). Because the alkaline pH of *M. sexta* OS (pH = 9) elicits the release of methanol during herbivory by activating pectin methyl esterases in leaves (*23*), we tested the influence of pH on the GLV emissions. In theory, alkaline conditions could convert the relatively unstable (*Z*)-hex-3-enal into its more stable (*E*)-isomer, (*E*)-hex-2-enal. However, an alkaline buffer (0.1 M Tris, pH 9, in 0.02% Tween-20) equal to the pH of *M. sexta* OS sufficient to elicit the methanol release did not change the (*Z*)/(*E*) ratio relative to w + w–treated plants when

[1]Department of Molecular Ecology, Max Planck Institute for Chemical Ecology, Hans-Knöll-Str. 8, DE-07745 Jena, Germany. [2]Department of Plant Physiology, Swammerdam Institute for Life Sciences, Science Park 904, 1098 XH Amsterdam, Netherlands.

*To whom correspondence should be addressed. E-mail: baldwin@ice.mpg.de

Downloaded from www.sciencemag.org on August 27, 2010

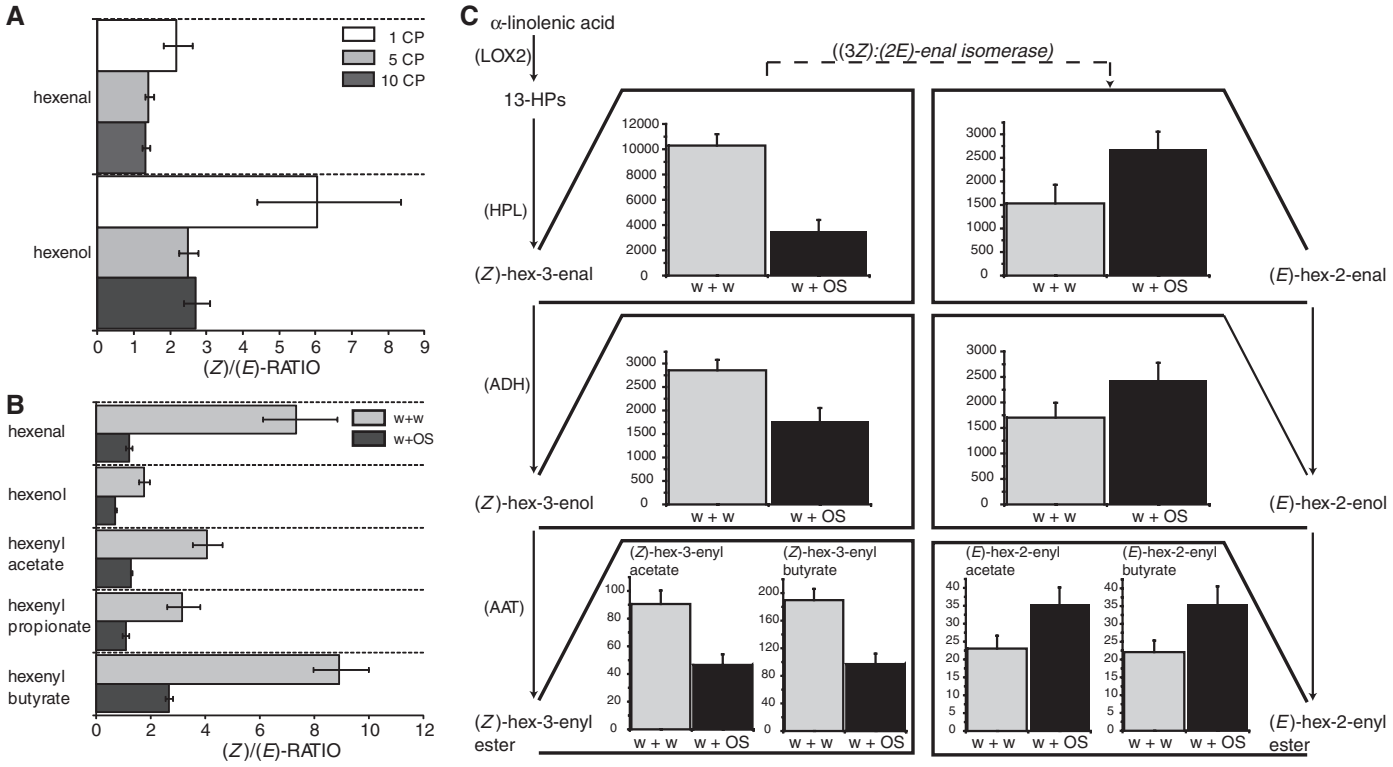

Fig. 1. Herbivory and the application of *Manduca sexta*'s oral secretions to the wounds of wild-type *Nicotiana attenuata* plants lead to a marked change in GLV emissions. (**A**) Mean (*Z*)/(*E*) ratios, with 95% confidence limits, of *N. attenuata* plants attacked by 1, 5, or 10 *M. sexta* neonates (*22*); CP, caterpillar. (**B**) Wounded plants release GLVs with a high (*Z*)/(*E*) ratio, whereas OS-elicited plants emit a GLV bouquet with a much lower ratio (*22*). Bars represent the average ratio (n = 5) and their 95% confidence limits. (**C**) Mean (+ SE) release of GLVs in w + w–treated and w + OS–treated plants in the first 20 min after elicitation (n = 5). Values are indicated in nanograms per gram of fresh mass per 20-min period. LOX2, lipoxygenase 2; HPL, hydroperoxide lyase; ADH, alcohol dehydrogenase; AAT, alcohol acetyltransferase; 13-HPs, 13-hydroperoxides.

applied to puncture wounds (fig. S3, A and B). FACs are relatively heat-stable compounds, and heating OS to 90°C for 10 min did not reduce the concentration of FACs in OS (fig. S3, E and F). However, heated OS no longer elicited the shift in the (*Z*)/(*E*) ratio (fig. S3C). Therefore, we conclude that FACs are not involved, but that a heat-labile elicitor of *M. sexta*'s OS directly converts (*Z*)- into (*E*)-GLVs or indirectly activates an isomerase in the plant. Additional tests revealed that the *M. sexta* OS-mediated (*Z*)/(*E*) shift is independent of the plant's JA, salicylic acid, and ethylene-dependent defense signaling pathways (fig. S4 and tables S2 and S3) (*22*).

To determine whether the OS elicitor responsible for the (*Z*)/(*E*) shift functions directly as an isomerase, we added (*Z*)-hex-3-enal to *M. sexta*'s OS in an in vitro system and quantified the conversion to (*E*)-hex-2-enal. More than 50% of the added (*Z*)-hex-3-enal was converted, which did not occur when water or heated OS were used as the converting solution and only slightly with an alkaline buffer (Fig. 2). Additionally, we tested two OS-derived enzymes, glucose oxidase and β-glucosidase, both of which elicit specific responses in plants (*6*). However, these enzymes did not increase the release of (*E*)-hex-2-enal. Bovine serum albumin (BSA) has lipophilic properties and increased the isomerization of cis- to trans-JA when added to plant cell cultures

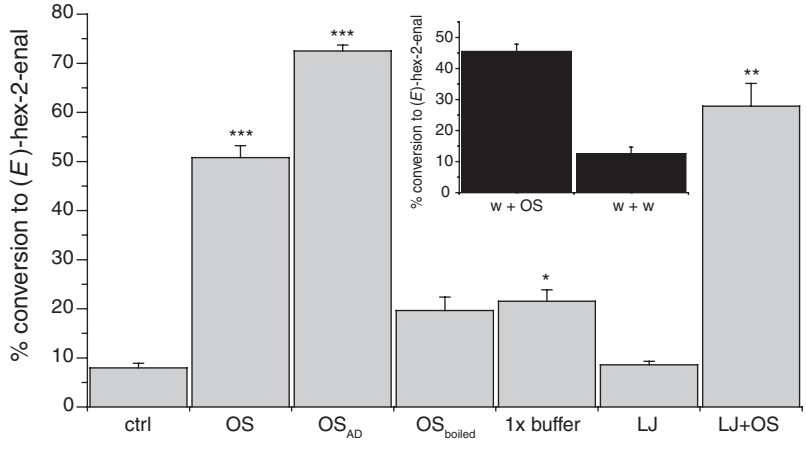

Fig. 2. Percentage conversion to (E)-hex-2-enal in vitro (n = 6; gray bars) and in vivo (n = 6; black bars) (Fig. 1) (*22*). Asterisks indicate significant differences from the control treatment (*$P \leq 0.05$, **$P \leq 0.01$, ***$P \leq 0.001$); univariate analysis of variance, $F_{6,37} = 99.957$, $P \leq 0.001$, followed by a Tamhane post hoc test; oral secretions (OS), $P \leq 0.001$; OS from artificial diet–fed caterpillars (OS_{AD}), $P \leq 0.001$; OS heated to 90°C for 10 min (OS_{boiled}), $P = 0.051$; 1× buffer (pH 9), $P \leq 0.05$; leaf juice (LJ), $P = 1.000$; LJ + OS, $P \leq 0.01$; the control was 0.02% Tween-20 (*22*).

(*24*). However, BSA had no effect on the (*Z*) to (*E*) conversion of leaf aldehydes (fig. S5).

An (3*Z*):(2*E*)-enal isomerase that converts the (*Z*)-aldehyde to its (*E*) isomer has been proposed for several plant species; (3*Z*):(2*E*)-enal isomerase activity has been found in crude extracts of alfalfa and soybean (*25*, *26*). However, we showed that a plant-derived isomerase was not responsible for the (*Z*) to (*E*) conversion of leaf aldehydes, but an unknown OS-derived, heat-unstable compound was necessary and sufficient for the conversion. The addition of crude leaf extract did not increase the conversion rate, and OS from caterpillars never fed on leaf material,

Downloaded from www.sciencemag.org on August 27, 2010

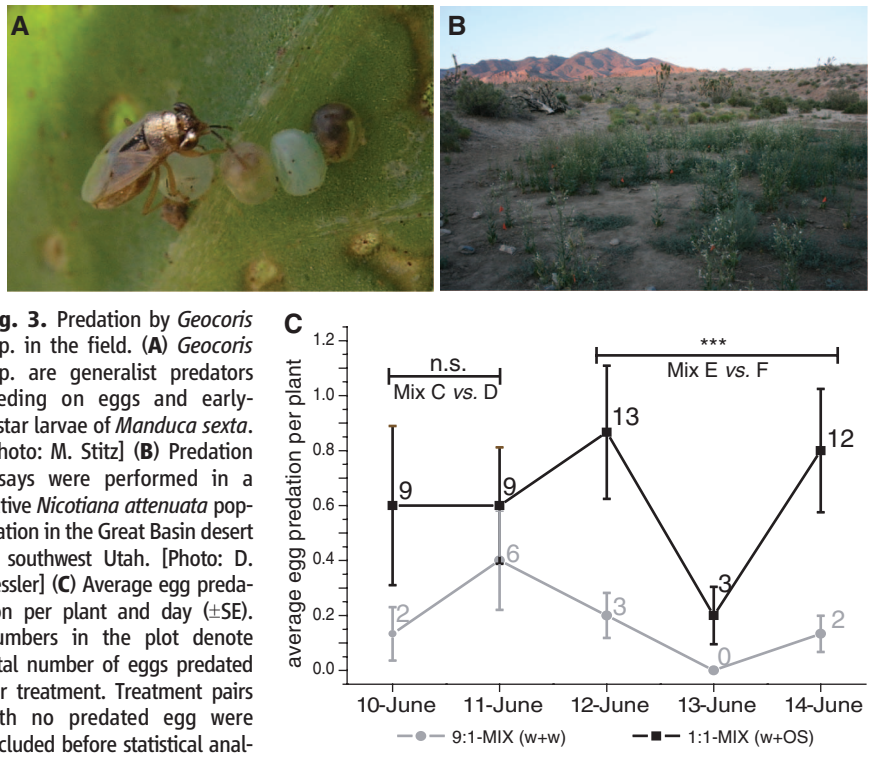

Fig. 3. Predation by *Geocoris* spp. in the field. (**A**) *Geocoris* spp. are generalist predators feeding on eggs and early-instar larvae of *Manduca sexta*. [Photo: M. Stitz] (**B**) Predation assays were performed in a native *Nicotiana attenuata* population in the Great Basin desert of southwest Utah. [Photo: D. Kessler] (**C**) Average egg predation per plant and day (±SE). Numbers in the plot denote total number of eggs predated per treatment. Treatment pairs with no predated egg were excluded before statistical analysis. Asterisks indicate significant differences between treatments (paired-sample *t* test, mix E versus F, t_{17} = 4.600, ***$P \leq 0.001$; mix C versus D, t_{12} = 1.594, P = 0.137). The composition of the different mixes tested (mixes C, D, E, and F) are explained in table S5. n.s., not significant.

but only on an artificial diet (*22*), converted (*Z*)-aldehydes to (*E*)-aldehydes as efficiently as OS from plant-fed caterpillars (Fig. 2). The observed (*Z*) to (*E*) conversion also appears to be species-specific, as the OS from two other generalist lepidopteran species (*Spodoptera exigua* and *S. littoralis*) that can feed on *N. attenuata* were not nearly as active as the OS from *M. sexta* larvae (fig. S6).

Whether this herbivory-specific change is relevant for tritrophic interactions hinges on whether carnivores can use these isomeric changes to augment their prey-hunting abilities. Insects are known to distinguish different isomeric forms of volatiles (*27*, *28*), and two structural isomers elicit responses in distinct antennal olfactory receptor neurons (*29*). *Geocoris* spp. are generalist predators feeding on eggs and early larval instars of *M. sexta*. They use individual HIPVs, including terpenoids and GLVs, to locate their prey on herbivore-attacked plants (*3*, *16*). We tested whether *Geocoris* could distinguish between (*Z*)- and (*E*)-GLVs, and used the changes in the (*Z*)/(*E*) ratio to discriminate between an herbivore-attacked and a mechanically wounded *N. attenuata* plant in nature.

We created two mixtures (A and B) in lanolin containing either (*Z*)- or (*E*)-GLVs (*30*). We also created GLV mixtures to mimic the GLV emissions of w + w–treated or w + OS–treated plants. To do so, we combined both isomeric alcohols and hexenyl esters (table S5, C and D) or all eight GLVs used for mix A and B (table S5, E and F) and added different amounts of each isomer to mimic the 1:1 (*Z*)/(*E*) ratio released by OS-elicited plants or the 9:1 ratio to mimic mechanically wounded plants.

We tested the attractiveness of these mixtures to *Geocoris* spp. in a native *N. attenuata* population in the Great Basin desert of southwest Utah by gluing three *M. sexta* eggs per plant to the underside of a lower stem leaf of 21 pairs of plants, as described (*3*). Plants were of the same size and developmental stage. Developmental stage did not influence the OS-induced (*Z*)/(*E*) shift (fig. S7) (*22*). On each day, two different mixes were tested by dipping a cotton swab into lanolin paste containing different GLV mixes and placing them immediately adjacent to the leaf with the *M. sexta* eggs.

Predated eggs were counted after 12 and 24 hours. We started with mixes that contained either (*Z*)- or (*E*)-GLVs (table S5, mixes A and B), and *Geocoris* spp. showed a clear preference for those scented with the (*E*)-GLVs. Whereas 8% of the (*Z*)-baited eggs were predated, 24% of the (*E*)-baited eggs were predated (fig. S9). These results demonstrated that *Geocoris* may distinguish between (*Z*)- and (*E*)-GLVs. We tested GLV mixes that consisted of both isomers (table S5C versus S5D; table S5E versus S5F) in different ratios to determine whether *Geocoris* detected changes in the (*Z*)/(*E*) ratio similar to those of OS-elicited plants. In both experiments, predation rates were higher on plants scented with equal amounts of (*Z*)- and (*E*)-GLVs [(*Z*)/(*E*) = 1:1] relative to those scented with a 9:1 ratio of (*Z*)/(*E*)-GLVs (Fig. 3) (*22*).

These results show that attack by the specialist herbivore *M. sexta* and the addition of their oral secretions to mechanical wounds elicits a rapid (*Z*)/(*E*) isomeric change in the GLV release of *N. attenuata* plants. This change, which lowers the (*Z*)/(*E*) ratio of the GLV blend, increases the predation rate of the generalist predator *Geocoris* spp., likely by betraying the location of the feeding caterpillar in a rapid, herbivore-specific, and spatially explicit manner. Why *Manduca* larvae would produce such an apparently maladaptive elicitor in their OS remains to be determined, but the larvae may benefit from the enhanced antimicrobial properties of a GLV blend enhanced in (*E*)-hex-2-enal (*31*).

References and Notes

1. J. D. Allison, J. Daniel Hare, *New Phytol.* **184**, 768 (2009).
2. C. M. De Moraes, W. J. Lewis, P. W. Pare, H. T. Alborn, J. H. Tumlinson, *Nature* **393**, 570 (1998).
3. A. Kessler, I. T. Baldwin, *Science* **291**, 2141 (2001).
4. H. T. Alborn *et al.*, *Science* **276**, 945 (1997).
5. R. Halitschke, U. Schittko, G. Pohnert, W. Boland, I. T. Baldwin, *Plant Physiol.* **125**, 711 (2001).
6. J. Q. Wu, I. T. Baldwin, *Plant Cell Environ.* **32**, 1161 (2009).
7. A. Mithöfer, G. Wanner, W. Boland, *Plant Physiol.* **137**, 1160 (2005).
8. J. Takabayashi, M. Dicke, *Trends Plant Sci.* **1**, 109 (1996).
9. C. M. De Moraes, M. C. Mescher, J. H. Tumlinson, *Nature* **410**, 577 (2001).
10. S. P. Gouinguené, T. C. J. Turlings, *Plant Physiol.* **129**, 1296 (2002).
11. T. C. J. Turlings, U. B. Lengwiler, M. L. Bernasconi, D. Wechsler, *Planta* **207**, 146 (1998).
12. M. Dicke, *Plant Cell Environ.* **32**, 654 (2009).
13. M. R. Kant, K. Ament, M. W. Sabelis, M. A. Haring, R. C. Schuurink, *Plant Physiol.* **135**, 483 (2004).
14. J. C. D'Auria, E. Pichersky, A. Schaub, A. Hansel, J. Gershenzon, *Plant J.* **49**, 194 (2007).
15. M. E. Hoballah, T. C. J. Turlings, *J. Chem. Ecol.* **31**, 2003 (2005).
16. R. Halitschke, J. A. Stenberg, D. Kessler, A. Kessler, I. T. Baldwin, *Ecol. Lett.* **11**, 24 (2008).
17. K. Shiojiri *et al.*, *J. Chem. Ecol.* **32**, 969 (2006).
18. T. J. A. Bruce, L. J. Wadhams, C. M. Woodcock, *Trends Plant Sci.* **10**, 269 (2005).
19. M. Rostás, J. Ton, B. Mauch-Mani, T. C. J. Turlings, *J. Chem. Ecol.* **32**, 1897 (2006).
20. K. Shiojiri *et al.*, *Proc. Natl. Acad. Sci. U.S.A.* **103**, 16672 (2006).
21. GLV esters were near or below the detection limit; thus, only the ratios for the aldehyde and the alcohol are shown.
22. See supporting material on *Science* Online.
23. C. C. von Dahl, M. Hävecker, R. Schlögl, I. T. Baldwin, *Plant J.* **46**, 948 (2006).
24. M. J. Mueller, W. Brodschelm, *Anal. Biochem.* **218**, 425 (1994).
25. M. A. Noordermeer, G. A. Veldink, J. F. G. Vliegenthart, *FEBS Lett.* **443**, 201 (1999).
26. H. Takamura, H. W. Gardner, *Biochim. Biophys. Acta Lipids Lipid Metab.* **1303**, 83 (1996).
27. B. S. Hansson, M. C. Larsson, W. S. Leal, *Physiol. Entomol.* **24**, 121 (1999).
28. J. A. Klun *et al.*, *Science* **181**, 661 (1973).
29. M. C. Stensmyr, M. C. Larsson, S. Bice, B. S. Hansson, *J. Comp. Physiol. A* **187**, 509 (2001).
30. We used the four most abundant GLVs of both isomers in *N. attenuata*: mix A, (*Z*)-hex-3-enal, (*Z*)-hex-3-en-1-ol, (*Z*)-hex-3-enyl acetate, and (*Z*)-hex-3-enyl butyrate; mix B, (*E*)-hex-2-enal, (*E*)-hex-2-en-1-ol, (*E*)-hex-2-enyl acetate, and (*E*)-hex-2-enyl butyrate (tables S5 and S6).

Downloaded from www.sciencemag.org on August 27, 2010

31. I. Prost *et al.*, *Plant Physiol.* **139**, 1902 (2005).
32. Supported by the Max Planck Society. We thank M. Kant, R. Schuurink, E. Gaquerel, G. Bonaventure, and three anonymous reviewers for comments on the manuscript; S. Meldau for providing ir-*sipk* × ir-*wipk* seeds; D. Kessler and C. Diezel for help with the field experiments and enzyme assays; M. Kallenbach and A. Weinhold for analytical help; and Brigham Young University for the use of their Lytle Ranch Preserve field station.

Supporting Online Material
www.sciencemag.org/cgi/content/full/329/5995/1075/DC1
Materials and Methods
SOM Text
Figs. S1 to S13
Tables S1 to S6
References

29 April 2010; accepted 13 July 2010
10.1126/science.1191634

Substrate Elasticity Regulates Skeletal Muscle Stem Cell Self-Renewal in Culture

P. M. Gilbert,[1]* K. L. Havenstrite,[1,2]* K. E. G. Magnusson,[1,3] A. Sacco,[1]† N. A. Leonardi,[1,4] P. Kraft,[1] N. K. Nguyen,[1] S. Thrun,[5] M. P. Lutolf,[4] H. M. Blau[1]‡

Stem cells that naturally reside in adult tissues, such as muscle stem cells (MuSCs), exhibit robust regenerative capacity in vivo that is rapidly lost in culture. Using a bioengineered substrate to recapitulate key biophysical and biochemical niche features in conjunction with a highly automated single-cell tracking algorithm, we show that substrate elasticity is a potent regulator of MuSC fate in culture. Unlike MuSCs on rigid plastic dishes (~10^6 kilopascals), MuSCs cultured on soft hydrogel substrates that mimic the elasticity of muscle (12 kilopascals) self-renew in vitro and contribute extensively to muscle regeneration when subsequently transplanted into mice and assayed histologically and quantitatively by noninvasive bioluminescence imaging. Our studies provide novel evidence that by recapitulating physiological tissue rigidity, propagation of adult muscle stem cells is possible, enabling future cell-based therapies for muscle-wasting diseases.

Many adult tissues harbor stem cells with a defined identity and marked regenerative capacity. This property is retained if stem cells are immediately transplanted from one individual to another following isolation, but it is lost as soon as the stem cells are plated in culture in order to increase their numbers for therapeutic applications. The muscle microenvironment (niche) enables freshly isolated muscle stem cells (MuSCs) to contribute extensively to skeletal muscle regeneration when transplanted in mice (*1*–*8*). In contrast, muscle stem cells grown on standard tissue culture plastic lose "stemness," yielding progenitors with greatly diminished regenerative potential (*3*, *7*, *9*) and therapeutic potency (*10*). Indeed, the propagation of functional adult stem cells, including MuSCs, is currently not possible in culture, despite extensive research on biochemical signals. Biophysical properties such as matrix rigidity are known to alter the differentiation of cells in culture (*11*). Here, we test the hypothesis that the elastic modulus plays a crucial role in muscle stem cell self-renewal and function in muscle regeneration. We report that when MuSCs are cultured on a substrate that mimics the rigidity of muscle tissue, they self-renew to generate stem cell progeny that can potently repair damaged muscle, establishing a paradigm for overcoming a major roadblock to adult stem cell therapeutic utility. In contrast to induced pluripotent stem (iPS) or embryonic stem cells whose differentiation must be directed, this strategy capitalizes on the existence of native tissue stem cells with defined identities and functions.

To recapitulate muscle rigidity and uncouple biophysical from biochemical effects, we engineered a tunable polyethylene glycol (PEG) hydrogel platform. By altering the percentage of PEG polymer in the precursor solution we produced hydrogels with a range of rigidities (Fig. 1, A and B, top) including a formulation that mimics the elastic modulus of adult murine skeletal muscle (Fig. 1, A and C) (*12*). Notably, polystyrene plastic traditionally used for cell culture, has an elastic modulus of ~3 GPa, more than five orders of magnitude stiffer than skeletal muscle (*13*). Laminin, a component of the native MuSC niche, was covalently cross-linked to the hydrogel network and used as an adhesion ligand (Fig. 1B, bottom). To ensure that laminin density and surface chemistry remained consistent between hydrogel and plastic culture conditions, we generated gels that do not swell after polymerization (Fig. 1D and fig. S1) and cast a thin layer of PEG hydrogel (≤1 μm) on the plastic surface, allowing MuSCs to sense the stiffness of the plastic beneath [see supporting online material (SOM)] (Fig. 1D) (*12*).

MuSCs were prospectively isolated (*7*) and analyzed at the single-cell level on pliant or stiff culture surfaces patterned with arrays of microwells (Fig. 1E) (*14*), because even when enriched by fluorescence-activated cell sorting, stem cell populations are inherently heterogeneous (*4*, *6*–*8*, *14*, *15*). Time-lapse acquisition of hundreds of single stem cells is possible using microwell technology (*14*); however, analysis of the resulting immense data sets remains a major challenge. To enable rapid analysis, we developed a highly automated algorithm termed the Baxter algorithm (SOM), which, in contrast to most commercially available software, is able to track lineage relationships over multiple cell divisions. This algorithm reduced data analysis time by ~90% with a mere 1% error rate.

The genealogic history of clones derived from a single cell was established by time-lapse acquisition and automated tracking (Fig. 1E and movie S1). MuSC velocity increased on stiff (120 μm/hour) compared with pliant (99 μm/hour) culture substrates (Fig. 1F, $P < 0.0001$), in agreement with previous reports investigating cell lines (*16*). In addition, we observe that cell area increases as cells duplicate their content, returning to initial cell area after mitosis, further validating our segmentation parameters (fig. S2).

MuSCs propagated on pliant hydrogel substrates do not undergo the "crisis," or massive cell death, previously reported in culture (*9*, *17*). After 1 week of culture in soft microwells, twice as many cells give rise to clones as compared with cells cultured in rigid microwells (fig. S3). Using the Baxter algorithm, we characterized this phenomenon at the clonal level. On rigid substrates, the overall cell number does not change over time because division is offset by death; however, on pliant substrates death is reduced and the total number of cells increases over time (Fig. 1G and figs. S4 and S5). In both conditions, death is not sudden; indeed, it is independent of time and cell division number (Fig. 1G and fig. S4). This data demonstrates that culture on soft substrates augments MuSC survival.

Substrate rigidity also impacts gene expression, suggesting that MuSC stemness is retained on soft surfaces. MuSCs cultured for 1 week on soft substrates give rise to one-third as many cells that express myogenin, a myogenic transcription factor expressed by differentiated MuSCs, than MuSCs cultured on rigid substrates (fig. S6). Time-lapse analysis excludes the possibility that gene expression differences are due to differences in cell division, because we observe no statistically significant difference in MuSC time to first

[1]Baxter Laboratory for Stem Cell Biology, Department of Microbiology and Immunology, Institute for Stem Cell Biology and Regenerative Medicine, Stanford University School of Medicine, Stanford, CA 94305, USA. [2]Department of Chemical Engineering, Stanford University, Stanford, CA 94305, USA. [3]School of Electrical Engineering, Signal Processing Lab, Royal Institute of Technology (KTH), SE-100 44 Stockholm, Sweden. [4]Institute of Bioengineering and Laboratory of Stem Cell Bioengineering, Ecole Polytechnique Fédérale de Lausanne (EPFL), CH-1015 Lausanne, Switzerland. [5]Stanford Artificial Intelligence Lab, Department of Computer Science, Stanford, CA 94305, USA.

*These authors contributed equally to this work.
†Present address: Sanford-Burnham Medical Research Institute, La Jolla, CA 92037, USA.
‡To whom correspondence should be addressed. E-mail: hblau@stanford.edu

Downloaded from www.sciencemag.org on August 27, 2010

division (fig. S7) or time between divisions (fig. S8). In addition, division rate is not different on pliant compared with rigid substrates (fig. S9 and SOM). These in vitro studies demonstrate that substrate rigidity has no effect on cell division rate in culture but likely prevents differentiation and leads to increased cell numbers by enhancing viability.

To establish definitively that MuSCs cultured on pliant substrates retain stemness, their function was assessed in vivo. MuSCs were isolated from mice constitutively expressing firefly lucif-

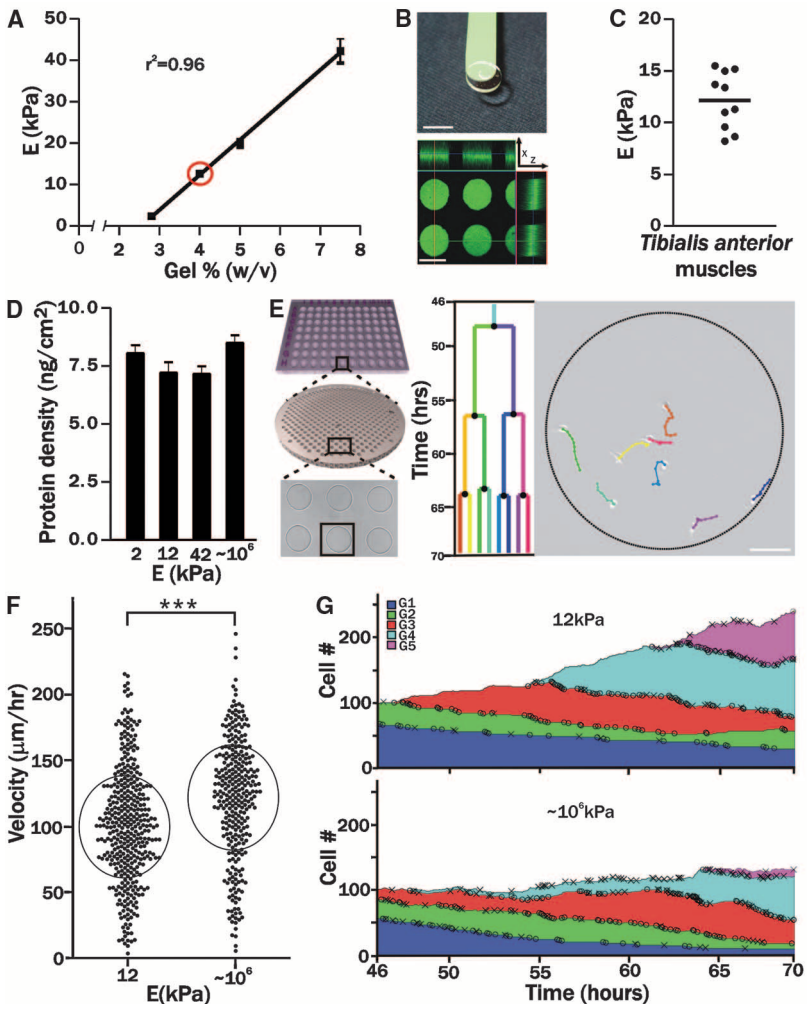

Fig. 1. Pliant hydrogel promotes MuSC survival and prevents differentiation in culture. (**A**) PEG hydrogels with tunable mechanical properties. Young's modulus (E) is linearly correlated with precursor polymer concentration ($n = 4$); red circle indicates muscle elasticity. (**B**) Image of a pliant PEG hydrogel on a green spatula. Scale bar, 7 mm (top). Confocal immunofluorescence image of hydrogel microcontact printed with laminin specifically at the bottom of hydrogel microwells (i.e., from the "tips" of the micropillars). Scale bar, 125 μm (bottom). (**C**) Dissected tibialis anterior muscles ($n = 5$ mice, 10 muscles total) were analyzed by rheometry (horizontal line indicates the mean). (**D**) Gel surface protein density did not differ significantly on PEG hydrogels of different rigidities (E; $P > 0.05$) and was 7.6 ng/cm^2 ± 1.0 ng/cm^2 ($n \geq 4$). (**E**) Scheme of Baxter algorithm analysis of time-lapse videos. Hydrogel arrays with hundreds of microwells containing single MuSCs were followed by time-lapse microscopy for 3 days. Videos were automatically processed and analyzed (SOM). Scale bar, 100 μm. (**F**) Single MuSC (black data points) velocity on pliant or rigid culture substrates. Circles denote mean velocity ± SD ($P < 0.0001$). (**G**) Change in total MuSC number on soft (top plot) or stiff (bottom plot) substrates during time-lapse acquisition. Deaths (X) and divisions (O) are shown, and colors designate five cell generations (G1 to G5). The proportion of cells in each generation at all time points is shown. Cell number is normalized to a starting population of 100 single MuSCs.

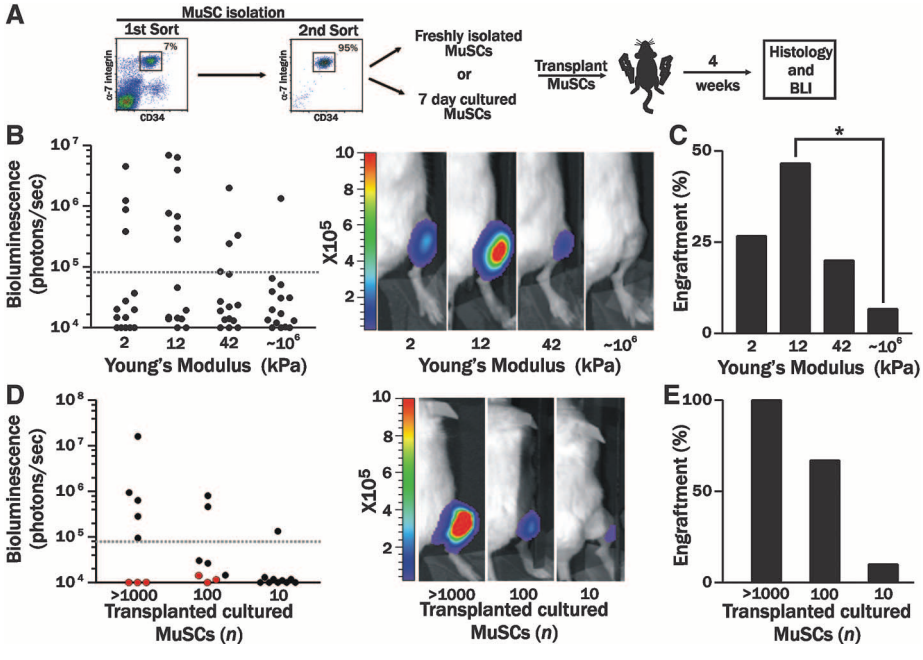

Fig. 2. Cultured MuSC engraftment is modulated by substrate elasticity. (**A**) Scheme of in vivo transplantation experiments. (**B**) Scatter graph of BLI values of recipient mice 1 month after transplantation with 100 GFP/*Fluc* MuSCs after 7-day culture on substrates of varying stiffness (left; $n = 15$). Representative bioluminescence images of mice transplanted with each culture condition are shown (right; photons s^{-1} cm^{-2} sr^{-1}). (**C**) Percentage of mice from each experimental condition that had a BLI value above the engraftment threshold. Fisher's exact test $P < 0.05$. (**D**) Scatter graph of BLI values of recipient mice 1 month after transplantation with different numbers of *Fluc* MuSCs cultured for 7 days on either hydrogel (black) or plastic (red). Representative bioluminescence images of mice transplanted with each culture condition are shown (right; photons s^{-1} cm^{-2} sr^{-1}). (**E**) Percentage of total transplanted mice in each experimental condition exhibiting a BLI value above the engraftment threshold.

Downloaded from www.sciencemag.org on August 27, 2010

erase (Fluc) (*18*) and green fluorescent protein (GFP) and cultured for 7 days. Cells were harvested and counted, and cultured MuSC progeny were transplanted into the tibialis anterior (TA) muscles of immunodeficient mice depleted of endogenous MuSCs by 18 Gy leg-irradiation (*15*, *19*). We assayed donor cell behavior quantitatively over time by noninvasive in vivo bioluminescence imaging (BLI) of luciferase activity, which correlates with cell number (Fig. 2A) (*7*). The engraftment threshold was set as the bioluminescence value corresponding with histological detection of donor-derived myofibers (fig. S10). This in vivo functional assay is critical for validating the stemness of cultured MuSCs.

In vivo functional assays show that MuSCs cultured on substrates matching the physiological modulus of muscle tissue most potently retain stemness. Hydrogel substrates were tuned to mimic the endogenous in vivo mechanical properties of brain, muscle, and cartilage (2, 12, or 42 kPa) compared with polystyrene plastic (~10^6 kPa). In agreement with previous reports (*3*, *7*, *9*), we observe markedly reduced engraftment from MuSCs cultured on plastic (Fig. 2B). Strikingly, the highest bioluminescent signals are obtained from mice transplanted with MuSCs cultured on the most pliant hydrogels, whereas both the extent and rate of engraftment are decreased on the stiffest culture substrates (Fig. 2B). Notably, the culture substrate that recapitulates skeletal muscle elasticity (12 kPa) is the only condition that leads to a statistically significant increase in the percentage of mice with MuSC engraftment compared with tissue culture plastic (Fig. 2C).

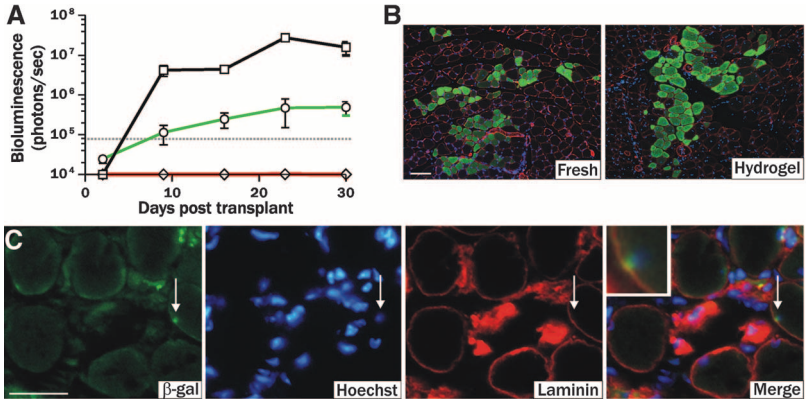

Fig. 3. Culture on pliant hydrogel promotes muscle stem cell engraftment and niche repopulation in vivo. (**A**) Engraftment of freshly isolated (black line, squares; 500 cells) and pliant (green line, circles; 1500 cells) or rigid (red line, diamonds; 1500 cells) substrate-cultured MuSCs monitored by BLI for a period of 30 days after transplantation ($P < 0.05$). (**B**) Immunofluorescence of GFP expression in transverse sections of muscles 1 month after transplantation with freshly isolated (left; 500 transplanted cells) or 1 week pliant hydrogel-cultured MuSCs (right; 2500 transplanted cells). GFP, green; laminin, red; Hoechst, blue. Scale bar, 100 μm. (**C**) Immunohistochemical analysis of transverse muscle tissues 1 month after transplant with pliant substrate-cultured MuSCs. Arrow points to a donor-derived cell in satellite cell position. β-galactosidase, green; laminin, red; Hoechst, blue. Scale bar, 50 μm.

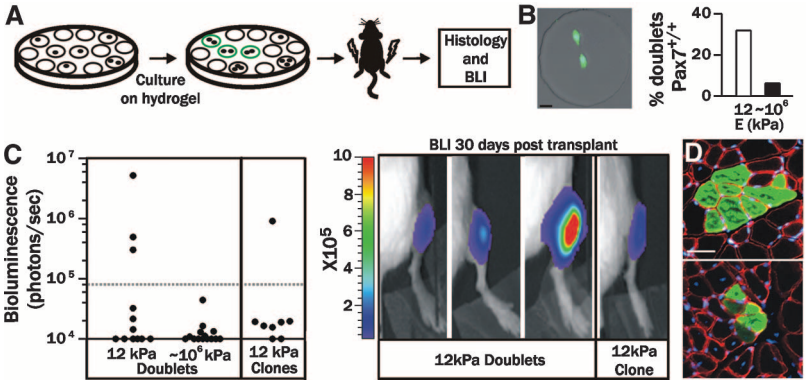

Fig. 4. Culture on pliant hydrogel promotes muscle stem cell self-renewal. (**A**) Scheme of in vivo self-renewal assay. (**B**) Percentage of total doublets exhibiting a Pax7$^{+/+}$ gene signature in pliant ($n = 47$) or stiff ($n = 32$) microwells (right). Representative image of a Pax7$^{+/+}$ doublet (left). Native Pax7-ZsGreen, green; Hoechst, blue. Scale bar, 20 μm. (**C**) Scatter graph (left) of bioluminescent values from mice transplanted with doublets derived from pliant ($n = 12$) or stiff ($n = 14$) microwells or clones collected from pliant microwells ($n = 8$). Images of mice with bioluminescent values above threshold are shown (right; photons s^{-1} cm^{-2} sr^{-1}). (**D**) Immunohistochemistry of GFP expression in transverse sections of muscles 1 month after transplantation with five MuSC doublets (top, GFP$^+$ fibers persist ~13 mm longitudinally) or a single clone (bottom, fibers persist ~7 mm longitudinally) cultured on pliant hydrogel. GFP, green; laminin, red; Hoechst, blue. Scale bar, 100 μm.

To determine the proportion of cultured cells with engraftment potential, we cultured MuSCs for 1 week on either soft or rigid substrates and then performed dilution analysis. None of the mice transplanted with stem cells cultured on a rigid plastic substrate exhibit a BLI signal above the threshold of detection (Fig. 2D, red circles). By contrast, engraftment occurs with 100% frequency when ≥1000 hydrogel-cultured (12 kPa) stem cells are transplanted (Fig. 2D, black circles), similar to freshly isolated cells (*7*). Moreover, 10% of mice transplanted with only 10 hydrogel cultured cells exhibit engraftment (Fig. 2E), on par with transplantations of 10 freshly isolated cells (16%) (*7*).

MuSCs cultured on a substrate that mimics muscle tissue exhibit dynamic proliferative behavior similar to freshly isolated MuSCs when transplanted in vivo. Both cell populations undergo a period of extensive proliferation that ultimately plateaus and stabilizes when homeostasis is achieved (Fig. 3A). Histology identifies GFP$^+$ myofibers resulting from regeneration in mice transplanted with MuSCs that were freshly isolated or cultured on soft substrates (Fig. 3B). Although the engraftment rate of freshly isolated MuSCs (*7*) and those grown on soft substrates is comparable (Fig. 2C), the extent of engraftment from cultured MuSCs is not as robust as that of freshly isolated cells (Fig. 3A), suggesting that exposure to additional biochemical cues in vitro may be required to recapitulate other key niche components necessary for maximal function in vivo.

MuSCs cultured on soft substrates can home to their native satellite cell niche upon transplantation into muscle, a defining characteristic of freshly isolated MuSCs (*3*, *7*). MuSCs isolated from mice expressing *LacZ* under the regulation of the *Myf5* promoter (*20*) were cultured on soft hydrogel and subsequently transplanted into mice. Before harvesting tissues, recipient muscles were damaged with notexin (*21*), which activates MuSCs and up-regulates expression of the myogenic transcription factor Myf5 (*7*, *20*). Histological analysis of β-galactosidase (β-gal) staining reveals that, like freshly isolated cells (*7*), transplanted hydrogel cultured cells expressing Myf5 are found in the satellite cell niche, beneath the basal lamina and atop myofibers (Fig. 3C).

One of the defining characteristics of stem cells is their ability to make more copies of themselves upon division, or self-renew. Several elegant in vitro approaches have provided strong evidence that MuSC asymmetric and symmetric divisions occur in culture, consistent with self-renewal (*4*, *22*–*27*). Our in vitro analysis of MuSC gene expression using MuSCs isolated from a Pax7-ZsGreen transgenic mice (*28*) suggests that a pliant substrate supports self-renewal. We observe that 32% of doublets (two cells that arose from a single cell division) in pliant microwells

Downloaded from www.sciencemag.org on August 27, 2010

are positive for the MuSC marker Pax7 (Fig. 4, A and B, and fig. S11). In contrast, only 6% of doublets in plastic microwells have this gene expression pattern, suggesting that a pliant substrate enables MuSC expansion. Although gene expression data are suggestive, an in vivo functional assay is necessary to conclude definitively that a self-renewal division event occurred in culture.

We show conclusively that stem cell self-renewal occurs using an in vivo functional assay. The transplantation of MuSCs at a population level demonstrates engraftment (Figs. 2 and 3) but does not definitively show that self-renewal divisions occurred in culture, because the population could include nondividing cells that maintained stem cell properties. Accordingly, in this experiment, we plated MuSCs in hydrogel microwell arrays and obtained images immediately after plating and 2 to 3 days after culturing to identify microwells that contained only one doublet. Doublets from 5 microwells were picked and pooled using a micromanipulator, and 10 cells total were transplanted per mouse (Fig. 4A). A detectable BLI signal indicates engraftment resulting from a self-renewal division event that must have occurred in at least one of the five transplanted doublets. Notably, 25% (3 of 12) of mice transplanted with doublets cultured on soft substrates demonstrate detectable engraftment (Fig. 4C) and contribution to regenerating myofibers (Fig. 4D, top), providing in vivo functional evidence that MuSC self-renewal division events occur in culture on pliant substrates. In contrast, doublets grown on rigid plastic microwells never exhibit engraftment after transplantation (0 of 14) (Fig. 4C), indicating that their regenerative potential is rapidly lost.

MuSC self-renewal on pliant hydrogel occurs even after multiple divisions. We transplanted clones that arose from a single cell that underwent 3 to 5 divisions. Remarkably, 12% (1 of 8) of mice transplanted with a single clone show engraftment, demonstrating that MuSC self-renewal capacity is retained on pliant substrates even after multiple divisions (Fig. 4, C and D, bottom).

Here, we provide insight into the potency of tissue rigidity, a biophysical property of the skeletal muscle microenvironment, on stem cell fate regulation. Using a single-cell tracking algorithm to interrogate MuSC behaviors at the single-cell level, we demonstrate that soft substrates enhance MuSC survival, prevent differentiation, and promote stemness. Functional assays in mice demonstrate conclusively that pliant substrates permit MuSC self-renewal in culture. Although the underlying mechanisms remain to be elucidated, we hypothesize that decreased rigidity preserves stemness by altering cell shape, resulting in cytoskeletal rearrangements and altered signaling, as shown for cell lines (*16*). Despite the remarkable retention of stemness in response to a single parameter, rigidity, we anticipate further enhancement of stemness through incorporation of additional biochemical cues into our reductionist platform. Studies employing biomimetic culture platforms, such as described here for MuSCs, will broadly affect stem cell studies by facilitating in vitro propagation while maintaining stemness and the capacity to regenerate tissues, a critical step toward the development of cell-based therapies. As an alternative to embryonic stem cells and iPS cells that must be directed toward a differentiated fate, our approach exploits the existence of native stem cells within tissues that have a well-defined tissue-specific identity.

References and Notes

1. D. D. Cornelison, M. S. Filla, H. M. Stanley, A. C. Rapraeger, B. B. Olwin, *Dev. Biol.* **239**, 79 (2001).
2. S. Fukada *et al.*, *Exp. Cell Res.* **296**, 245 (2004).
3. D. Montarras *et al.*, *Science* **309**, 2064 (2005).
4. S. Kuang, K. Kuroda, F. Le Grand, M. A. Rudnicki, *Cell* **129**, 999 (2007).
5. M. Cerletti *et al.*, *Cell* **134**, 37 (2008).
6. C. A. Collins *et al.*, *Cell* **122**, 289 (2005).
7. A. Sacco, R. Doyonnas, P. Kraft, S. Vitorovic, H. M. Blau, *Nature* **456**, 502 (2008).
8. R. I. Sherwood *et al.*, *Cell* **119**, 543 (2004).
9. Z. Qu-Petersen *et al.*, *J. Cell Biol.* **157**, 851 (2002).
10. E. Gussoni *et al.*, *Nature* **356**, 435 (1992).
11. M. P. Lutolf, P. M. Gilbert, H. M. Blau, *Nature* **462**, 433 (2009).
12. A. J. Engler, S. Sen, H. L. Sweeney, D. E. Discher, *Cell* **126**, 677 (2006).
13. W. D. Callister, *Fundamentals of Materials Science and Engineering: An Interactive E-Text* (Wiley, Somerset, NJ, ed. 5, 2000).
14. M. P. Lutolf, R. Doyonnas, K. L. Havenstrite, K. Koleckar, H. M. Blau, *Integr. Biol.* **1**, 59 (2009).
15. L. Heslop, J. E. Morgan, T. A. Partridge, *J. Cell Sci.* **113**, 2299 (2000).
16. R. J. Pelham Jr., Y. Wang, *Proc. Natl. Acad. Sci. U.S.A.* **94**, 13661 (1997).
17. T. A. Partridge, in *Basic Cell Culture Protocols,* J. W. Pollard, J. M. Walker, Eds. (Humana Press, Totowa, NJ, 1997), vol. 75, pp. 131–144.
18. Y. A. Cao *et al.*, *Proc. Natl. Acad. Sci. U.S.A.* **101**, 221 (2004).
19. S. Wakeford, D. J. Watt, T. A. Partridge, *Muscle Nerve* **14**, 42 (1991).
20. S. Tajbakhsh *et al.*, *Dev. Dyn.* **206**, 291 (1996).
21. J. B. Harris, M. A. Johnson, *Clin. Exp. Pharmacol. Physiol.* **5**, 587 (1978).
22. R. Abou-Khalil *et al.*, *Cell Stem Cell* **5**, 298 (2009).
23. V. Shinin, B. Gayraud-Morel, D. Gomès, S. Tajbakhsh, *Nat. Cell Biol.* **8**, 677 (2006).
24. M. J. Conboy, A. O. Karasov, T. A. Rando, *PLoS Biol.* **5**, e102 (2007).
25. I. M. Conboy, T. A. Rando, *Dev. Cell* **3**, 397 (2002).
26. F. Le Grand, A. E. Jones, V. Seale, A. Scimè, M. A. Rudnicki, *Cell Stem Cell* **4**, 535 (2009).
27. P. S. Zammit *et al.*, *J. Cell Biol.* **166**, 347 (2004).
28. D. Bosnakovski *et al.*, *Stem Cells* **26**, 3194 (2008).

29. We thank K. Koleckar, R. Tran, IBM Almaden, the Stanford Center for Innovation in In-Vivo Imaging, and the Stanford Shared FACS Facility core facilities for technical support; J. Sly, R. D. Miller, S. Kobal, S. Gobaa, R. Doyonnas, and A. Barron for valuable discussions; and F. Rossi and M. Kyba for providing alpha-7 integrin antibody and Pax7-ZsGreen mice, respectively. This work was financially supported by PHS CA09151 and CIRM TG2-01159 (P.M.G.); Leukemia and Lymphoma Society Fellow and European Young Investigator Award (M.P.L.); NSF and NIH Training Grant 2 T32 HD007249 (K.H.); Muscular Dystrophy Association (MDA) grant 4063 (A.S.); EPFL Excellence Scholarship and the Swiss Study Foundation (N.A.L.); John och Karin Engbloms Stipendiefond (K.E.G.M.); Bio X Undergraduate Research Award and Howard Hughes Medical Institute grant 52005886 (N.K.N.); and NIH grants HL096113, AG009521, AG020961, U01 HL100397, JDRF 34-2008-623, MDA grant 4320, LLS grant TR6025-09, CIRM grant RT1-01001, Stanford Bio-X Award IIP3-34, and the Baxter Foundation (H.M.B.).

Supporting Online Material

www.sciencemag.org/cgi/content/full/science.1191035/DC1
Materials and Methods
Figs. S1 to S11
References
Movie S1

16 April 2010; accepted 30 June 2010
Published online 15 July 2010;
10.1126/science.1191035
Include this information when citing this paper.

Optimally Interacting Minds

Bahador Bahrami,[1,2,3]* Karsten Olsen,[3] Peter E. Latham,[4] Andreas Roepstorff,[3] Geraint Rees,[1,2] Chris D. Frith[2,3]

In everyday life, many people believe that two heads are better than one. Our ability to solve problems together appears to be fundamental to the current dominance and future survival of the human species. But are two heads really better than one? We addressed this question in the context of a collective low-level perceptual decision-making task. For two observers of nearly equal visual sensitivity, two heads were definitely better than one, provided they were given the opportunity to communicate freely, even in the absence of any feedback about decision outcomes. But for observers with very different visual sensitivities, two heads were actually worse than the better one. These seemingly discrepant patterns of group behavior can be explained by a model in which two heads are Bayes optimal under the assumption that individuals accurately communicate their level of confidence on every trial.

To come to an optimal joint decision, individuals must share information with each other and, importantly, weigh that information by its reliability (*1*, *2*). It has been well established that isolated individuals can accurately weigh information when combining different sources of sensory information (*3*–*5*). Little is known, however, about how, or even whether, two individuals can accurately combine information that they communicate with each other. To investigate this issue, we examined the behavior of pairs of individuals in a simple perceptual decision task, and we asked how signals from the same sensory modality (vision) in the brains of two different individuals could be combined through social interaction.

Downloaded from www.sciencemag.org on August 27, 2010

Work on perceptual decision-making has shown that when combining information from different senses, individuals have access not just to magnitudes of sensory signals, but also to their probability distributions, or at least to their means and variances (*3*–*8*). However, this may not be true for interpersonal communication. Whereas probability distributions arising from different sensory modalities are available within an individual's brain, it is not clear whether such distributions can be passed directly to another person or what types of information can be communicated. To answer this, we considered four models (*9*), each of which proposes that different types of information could be communicated, and quantitatively compared the predictions of those models to empirical data in a low-level visual decision-making task.

The first model proposes that nothing except the decision about the visual stimulus is communicated, and when there is disagreement, the joint decision is no better than a coin flip (CF model). This strategy is expected from previous work on collective decision-making without feedback (*10*). The second model proposes that nothing except the decision is communicated, but that pairs of individuals learn, from trial-to-trial feedback, which of them is more accurate, so they eventually use that individual's decisions [the behavior and feedback (BF) model]. This model was motivated by previous work showing that collective decisions are dominated by the most competent group member in situations where clear feedback about "the truth" (in our case, the correct answer) is available (*11*, *12*). The third model, put forward here for the first time, proposes that confidence, which we define as an internal estimate of the probability of being correct (*13*), is communicated [the weighted confidence sharing (WCS) model] (*9*). Finally, the fourth model proposes that the mean and standard deviation of the sensory response to the stimulus about which the decision is made are communicated [direct signal sharing (DSS) model]. This model is used to account for multisensory integration within an individual (*3*, *4*) and also for collective decisions in groups (*14*). To anticipate our findings, we determined that the WCS model was quantitatively consistent with our empirical data, whereas the other three models were not.

Our empirical data were obtained from pairs of participants (dyads) who viewed brief visual displays containing a faint target (contrast oddball; Fig. 1A) in either the first or second viewing interval (*9*). We performed a series of four experiments, each of which followed very similar procedures. Initially, each participant chose the interval that they thought contained the target, without consulting the other. Individual decisions were then shared, and if participants disagreed, they discussed the matter until they reached a joint decision. Subsequently, both participants were informed of the correct choice (with the exception of experiment 4 in which no feedback was given). Individual and dyad psychometric functions (Fig. 1B, left and middle panels) were fit with a cumulative Gaussian function, from which we extracted the slope *s*. The slope provided an estimate of sensitivity (the steeper the slope, the higher the sensitivity). More sensitive observers were, by definition, more reliable in their estimates of contrast.

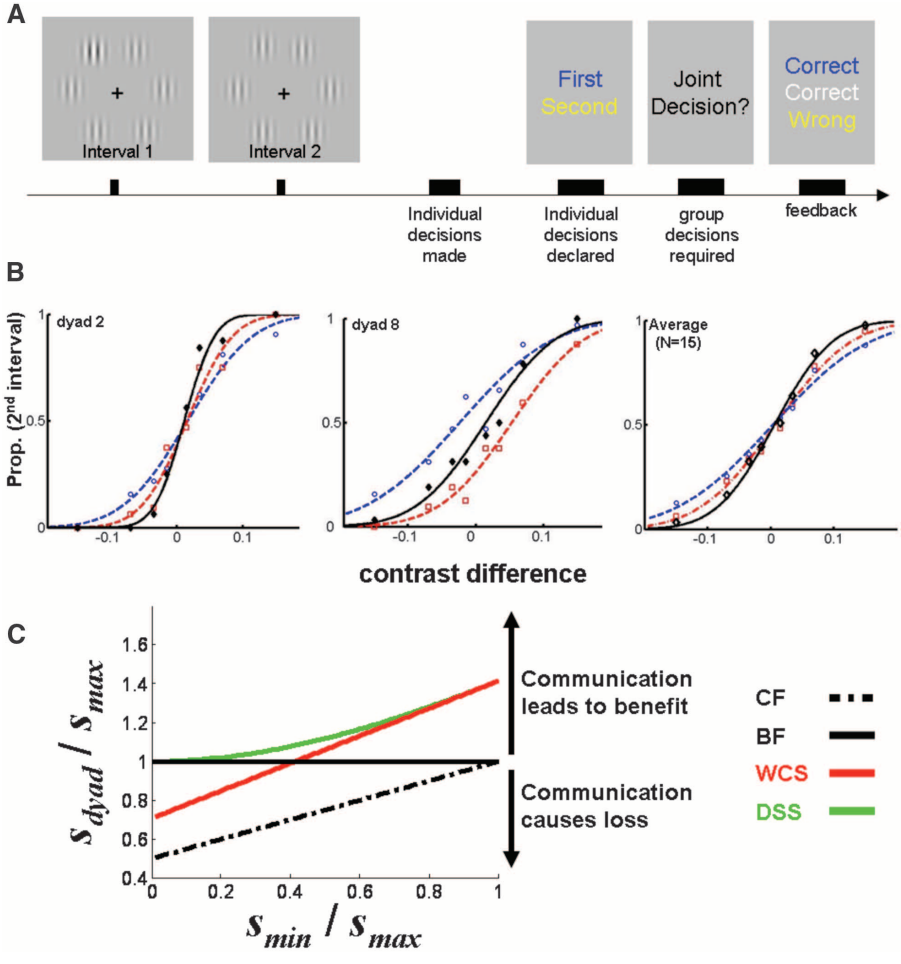

Fig. 1. (**A**) Experimental paradigm. Each trial consisted of two observation intervals. In each interval, six vertically oriented Gabor patches were displayed equidistantly around an imaginary circle (duration: 85 ms). In either the first or second interval, there was one oddball target that had slightly higher contrast than all of the others (in this example, upper-left target in interval 1). (**B**) Two example psychometric functions and the group average in experiment 1. The proportion of trials in which the oddball was reported to be in the second interval is plotted against the contrast difference at the oddball location (i.e., contrast in the second interval minus contrast in the first). A highly sensitive observer would produce a steeply rising psychometric function with a large slope. Blue circles, performance of the less sensitive observer (s_{min}) of the dyad; red squares, performance of the more sensitive observer (s_{max}); and black diamonds, performance of the dyad (s_{dyad}). The blue and red dashed curves are the best fit to a cumulative Gaussian function (*9*); the solid black curve is the prediction of the WCS. $N = 15$ dyads. (**C**) Predictions of the four models (see Eqs. 1 to 4). The *x* axis shows the ratio of individual sensitivities (s_{min}/s_{max}), with values near one corresponding to dyad members with similar sensitivities and values near zero to dyad members with very different sensitivities. The *y* axis shows the ratio of dyad sensitivity to the more sensitive member (s_{dyad}/s_{max}). Values above the horizontal line indicate communication benefit; in this range the dyad is better than the more sensitive observer. The red curve, which corresponds to the WCS model, is above the horizontal line only if s_{min}/s_{max} is larger than ~0.4, reflecting the prediction that communication by WCS is beneficial only if dyad members have approximately the same competence. The green curve, which corresponds to the DSS model, never crosses the black horizontal line, so for this model, communication will invariably be beneficial. The dot-dashed and solid black lines indicate the CF and BF models, respectively.

[1]University College London Institute of Cognitive Neuroscience, University College London, Alexandra House, 17 Queen Square, London WC1N 3AR, UK. [2]Wellcome Trust Centre for Neuroimaging, Institute of Neurology, University College London, 12 Queen Square, London WC1N 3BG, UK. [3]Interacting Minds Project, Institute of Anthropology, Archaeology, Linguistics, Aarhus University, and Centre of Functionally Integrative Neuroscience, Aarhus University Hospital, Norrebrogade 44, Building 10 G, 8000 Aarhus C, Denmark. [4]Gatsby Computational Neuroscience Unit, London WC1N 3AR, UK.

*To whom correspondence should be addressed. E-mail: bbahrami@gmail.com

Downloaded from www.sciencemag.org on August 27, 2010

The four models made different predictions for the relation between the slope of the psychometric function for each individual and the collective dyad; thus, by comparing predicted and observed dyad slopes, we could distinguish the models. For each of the four models (*9*), we computed the predicted dyad slopes, s_{dyad}^{model}, in terms of the individual slopes, s_1 and s_2, of observers 1 and 2. For the CF model, the predicted dyad slope is related to the individual slopes by

$$s_{dyad}^{CF} \approx \frac{s_1 + s_2}{2} \quad (1)$$

for the BF model by

$$s_{dyad}^{BF} = \max(s_1, s_2) \quad (2)$$

for the WCS model by

$$s_{dyad}^{WCS} = \frac{s_1 + s_2}{2^{1/2}} \quad (3)$$

and for the DSS model by

$$s_{dyad}^{DSS} = (s_1^2 + s_2^2)^{1/2} \quad (4)$$

These equations provide upper bounds on performance for each model: For example, Eq. 3 provides the largest possible dyad slope, given that participants share only confidence. If the dyads reach that slope, then they are Bayes optimal, given the model assumptions, where by "Bayes optimal" we mean that participants made decisions that maximized their probability of being correct, given their model assumptions.

Fig. 1C shows the predictions (from Eqs. 1 to 4) for the collective benefit (the ratio s_{dyad}/s_{max}) versus relative sensitivity (s_{min}/s_{max}), where s_{min} and s_{max} are the minimum (less sensitive) and maximum (more sensitive) of the individual slopes, respectively. The models clearly make different predictions, but to distinguish them requires experiments with a broad range of s_{min}/s_{max}; we would need to investigate dyad members with nearly identical performance ($s_{min}/s_{max} \sim 1$), as well as those with very different performance ($s_{min}/s_{max} << 1$). Experiments 1 and 2 were performed to test the model predictions in different ranges of s_{min}/s_{max}.

In experiment 1, participants viewed identical stimuli, and individual sensitivities of the dyad members were similar ($s_{min}/s_{max} > 0.5$) (Fig. 2B). The CF model (Eq. 1 and Fig. 1C, black dot-dashed line) predicted that dyad sensitivity would never be higher than that of the better participant. The BF model (Eq. 2 and Fig. 1C, solid black line) predicted that dyad sensitivity would be as good as that of the better participant. In contrast, the WCS model (Eq. 3 and Fig. 1C, red line) and DSS model (Eq. 4 and Fig. 1C, green curve) both predicted that, within the relative sensitivity range tested here ($s_{min}/s_{max} > 0.5$), dyad sensitivity would be higher than that of the better participant.

We found that the dyad slope was significantly larger than that of the better participant [$t(14) = 5.24$, $p < 10^{-3}$, paired t test]. Thus, these data ruled out both the CF (Fig. 2A; $p < 10^{-5}$) and BF (Fig. 2A; $p < 10^{-3}$) models, for which the dyad slope can be no larger than that of the better participant, and instead favored the sharing models ($p > 0.1$), for which the dyad can outperform the individuals. The sharing models were also able to accurately predict, via Eqs. 3 and 4, the dyad slopes on a case-by-case basis (fig. S1). Thus, communication conferred a significant benefit, and, at least on this task, two heads did perform better than one.

Experiment 1 favored the WCS and DSS models, but was not able to distinguish between them. For the range of relative sensitivities tested in experiment 1, the two models made very similar predictions (Fig. 2B). To distinguish the models, we sought to study dyads with very different individual sensitivities ($s_{min}/s_{max} << 1$) for which the WCS model (Fig. 1C, red line) made a counterintuitive prediction: If one participant's sensitivity was no better than ~40% of the other's (e.g., $s_{min}/s_{max} < 2^{1/2} - 1 \approx 0.4$), then two heads should do worse than the better one ($s_{dyad}/s_{max} < 1$), even when individuals accurately communicated their confidence. In contrast, the DSS model (Fig. 1C, green curve) invariably predicted a benefit for dyads, consistent with the fact that when signals are directly available (as in multisensory integration within a single brain), putting them together is never worse than either one alone (*4*).

We tested these predictions in experiment 2. In randomly chosen trials, we surreptitiously reduced one or the other (or both) participants' sensitivity by adding a substantial amount of noise to their stimuli (*9*) without having told the participants about this manipulation. The four noise regimes were randomized, so on each trial, noise was given to both participants ("equal" condition), to one but not the other (both possibilities combined together as the "unequal" condition), or to neither participant ("none" condition). For each participant and dyad, four psychometric functions (corresponding to the four noise regimes) were constructed, and the slopes were estimated (fig. S2). Figure 3 shows that, in equal and none conditions—in which participants received identical amounts of noise—robust group benefits were obtained [Fig. 3A; for equal condition: $t(10) = 2.50$, $p = 0.03$, paired t test; for none condition: $t(10) = 3.38$, $p = 0.007$, paired t test]. This replicated the results of experiment 1. However, in the unequal condition, dyads did not perform better than the better participant, and reliable group benefit was not observed [Fig. 3A; $t(21) = 0.68$, $p = 0.54$, paired t test].

In all three conditions, the results were consistent with the predictions of the WCS model (Fig. 3B). Importantly, the majority of the data points for which $s_{min}/s_{max} < 0.4$ fell below the black line in Fig. 3D, indicating that, in these instances, two heads did worse than the better one. The DSS model, on the other hand, was rejected in the unequal condition [Fig. 3C; $t(21) = 4.52$, $p < 10^{-3}$, paired t test]. Moreover, randomized addition of noise resulted in a wide range of relative sensitivity, and a highly significant linear correlation was observed between collective benefit and relative sensitivity [Fig. 3D; dotted blue line $R^2 = 0.51$, $F_{42,1} = 43.22$, $p < 10^{-7}$] with a slope (0.6 ± 0.09) and intercept (0.74 ± 0.05) that were very close to the slope ($1/2^{1/2} \approx 0.71$) and intercept ($1/2^{1/2} \approx 0.71$) predicted by the WCS model.

In these experiments, two aspects of social information contributed to collective decision-making: communication and feedback. However, the experiments could not tell us whether either or both types of information were necessary for collective benefit in sensitivity. To address this issue, we conducted two more experiments: Experiment 3 tested whether communication was necessary, whereas experiment 4 tested whether feedback was necessary. We found that communication was necessary, but, surprisingly, feedback was not.

It is conceivable that, even if the participants were not able to communicate their confidence on each trial, they would still be able to estimate each other's average reliability (defined explicitly as the slope of the psychometric curves; see Fig. 1B), not through direct trial-by-trial interaction and confidence sharing, but by accumulating information about one another's accuracy through feed-

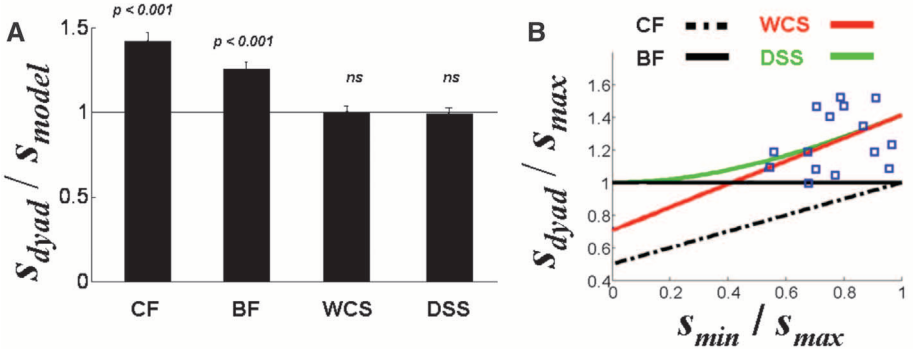

Fig. 2. Results of experiments 1. (**A**) Plot of the ratio of the dyad slope to the slope predicted by each model. The BF model comparison also depicts collective benefit over the more sensitive observer. Error bars indicate SEM ($N = 15$). (**B**) Distribution of data points and model predictions. Collective benefit (s_{dyad}/s_{max}) is plotted against relative sensitivity (s_{min}/s_{max}). Each blue square represents one dyad.

Downloaded from www.sciencemag.org on August 27, 2010

back. Armed with such an estimate, dyads might conceivably be able to match the performance of those that did communicate, and so match the performance of the WCS model. On theoretical grounds, we did not expect this; instead, we expected performance without communication to match the BF model. We hypothesized that trial-by-trial communication was necessary and that feedback alone would not be sufficient for achieving collective benefit.

Experiment 3 tested this prediction using the same paradigm as experiment 1, modified so that participants were now not allowed to communicate anything but their choice. Whenever the participants disagreed in their decision, one of the two (chosen randomly by the computer) made a decision individually by arbitrating between their own choice and that of the other participant. Feedback about the correct choice was then given to both participants (*9*). The results were unequivocal. In contrast to experiment 1, dyad sensitivity did not exceed that of the more sensitive observer [Fig. 4A, red bar; $t(13) = 0.18$, $p = 0.85$, paired t test], as predicted by the BF model. More important, dyad sensitivity was significantly lower than the upper bound predicted by the WCS model [Fig. 4B, red bar; $t(13) = 5.91$, $p < 10^{-4}$, paired t test], demonstrating that knowledge of current choice and previous outcomes was not adequate for the dyads to reach the level of performance observed in experiment 1, expected from the WCS model.

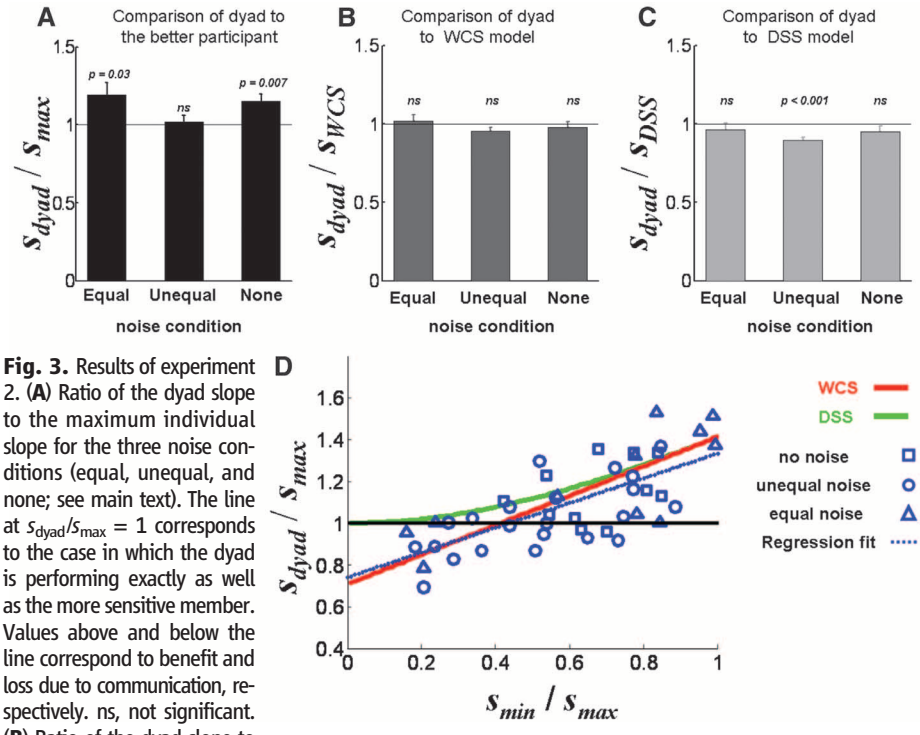

Fig. 3. Results of experiment 2. (**A**) Ratio of the dyad slope to the maximum individual slope for the three noise conditions (equal, unequal, and none; see main text). The line at $s_{dyad}/s_{max} = 1$ corresponds to the case in which the dyad is performing exactly as well as the more sensitive member. Values above and below the line correspond to benefit and loss due to communication, respectively. ns, not significant. (**B**) Ratio of the dyad slope to the slope predicted by the WCS model, the latter denoted s_{WCS}. This ratio was not significantly different from zero for any of the noise conditions. (**C**) Ratio of the dyad slope to the slope of the DSS model. For the unequal noise condition, this ratio was significantly smaller than 1 ($p < 10^{-4}$). (**D**) Distribution of data points and model predictions (the latter taken from Fig. 1C). Collective benefit (s_{dyad}/s_{max}) is plotted against relative sensitivity (s_{min}/s_{max}). Each dyad contributed four sets of data points (one triangle for equal, one square for none, and two circles for unequal conditions). The solid black line indicates the boundary of collective benefit (see Fig. 1C). In (A) to (C), error bars denote SEM ($N = 11$ data points for equal and none conditions; $N = 22$ for unequal condition).

Experiment 3 showed that communication was necessary and that feedback alone was not sufficient for dyads to achieve a collaboration benefit. However, the results do not address the question of whether communication alone, without feedback, is sufficient for achieving collaboration benefit. Could dyads achieve any group benefit at all without ever receiving any objective feedback about the accuracy of their decisions? This is an important question, because feedback is not formally incorporated in the confidence-sharing model (*9*). Taking this model seriously at face value, one may make the extremely counter-intuitive assumption that, as long as accurate communication of confidence is ensured, dyad benefit can still be achieved without any feedback (that is, without any definitive knowledge of decision outcomes).

In experiment 4, we removed the feedback stage of the task to test this prediction (*9*): After the joint decision was made (either automatically in the agreement trials or after interaction in the disagreement trials), the participants were not told the correct answer. All other aspects of the experiment were identical to experiment 1. Consistent with our prediction, even without feedback, the dyads nevertheless achieved a significant collaboration benefit [Fig. 4A, blue bar; $t(10) = 2.68$, $p = 0.022$, paired t test], and dyad sensitivity was statistically indistinguishable from the prediction of the confidence sharing model [Fig. 4B, blue bar; $t(10) = 1.16$, $p = 0.27$, paired t test]. These findings indicate that objective feedback was not necessary, and communication alone was sufficient for achieving collective benefit.

Our results show that interactive decision-making between two individuals can significantly improve perceptual sensitivity, but, importantly, only for similarly sensitive observers. Moreover, such joint behavior is Bayes optimal under the assumption that participants accurately communicate their internal estimate that they are correct. Our findings show that human-to-human interpersonal communication is adequately rich to permit sharing of subjective estimates of confidence, and humans are adequately perceptive to make optimal use of this information. Moreover, communication of trial-by-trial confidence is necessary for collective benefit, but, somewhat surprisingly, feedback about decision outcomes is not.

Quantitatively, we tested four models, and only one—the WCS model, in which participants communicated only an internal estimate of their reliability on each trial—was consistent with the data. Of the three models that were not consistent with the data, one, the DSS model, posited that participants communicated both the perceived contrast and their estimate of its reliability on

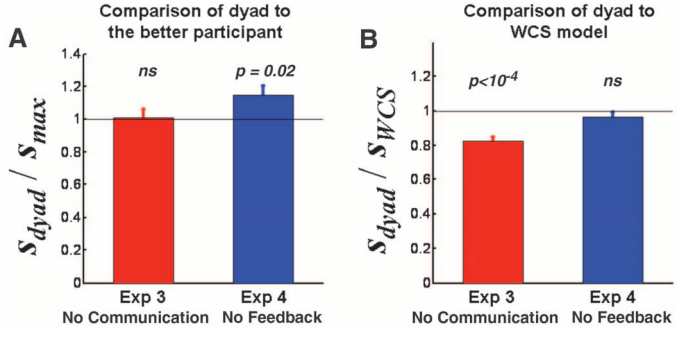

Fig. 4. Results of experiments 3 and 4. *y*-axis conventions are the same as in Fig. 3, A and B. (**A**) Collective benefit (s_{dyad}/s_{max}) is plotted for experiment 3 (red, without communication) and for experiment 4 (blue, without feedback). (**B**) Ratio of the dyad slope to the slope predicted by the WCS model for experiment 3 (red, without communication), and experiment 4 (blue; without feedback). In all panels, error bars denote SEM ($N = 14$ for experiment 3; $N = 11$ for experiment 4).

Downloaded from www.sciencemag.org on August 27, 2010

each trial. That model was rejected because it outperformed the dyads in experiment 2. This leaves open the possibility that the participants did communicate contrast and reliability, but used that information suboptimally, which seems unlikely, as we never observed any dyads explicitly communicating contrast and reliability separately. However, our data cannot definitively rule out this idea, and further research is needed to distinguish between optimal use of WCS versus suboptimal DSS.

The general consensus from extensive earlier work on collective decision-making is that groups rarely outperform their best members (*11*, *15*). Even in one of the rare cases in which consistent collaborative benefit was established, group performance failed to reach the bound predicted by the proposed ideal combination of individual decisions (*14*). That study employed the DSS model (see Eq. 4) to estimate the ideal, expected group sensitivity. As shown in experiments 1 and 2, however, the predictions of that model deviate significantly from empirical data if individuals' sensitivities differ markedly. In particular, experiment 2 demonstrated the detrimental side effect of collective decision-making based on Bayesian combination of confidence: Individuals with very different sensitivities are best advised to avoid collaboration and instead should rely entirely on the more sensitive individual. In fact, the WCS model and the results of experiment 2 (Fig. 3D) set a quantitative limit on the usefulness of cooperation that, to our knowledge, is not predicted by current economic and social theories of collective decision-making (*15*). An important next step for future research is to test the generality of this limit in other types of dyadic interactions.

Our findings have direct bearing on studies in social psychology that have discovered numerous situations in which groups fail to do better than their individuals. Many explanations for such "process loss" have been proposed, such as reduced effort in the presence of others [e.g., "social loafing" (*16*)], interpersonal competition (*11*), and groupthink (*17*). Our results raise the rather different possibility that, when the communicated evidence (perceived contrast) cannot be separated from its reliability (slope), such failures of collective decision-making may be the natural consequence of a perfectly reasonable strategy (for instance, WCS). Indeed, we know all too well about the catastrophic consequences of consulting "evidence" of unknown reliability on problems as diverse as the existence of weapons of mass destruction and the possibility of risk-free investments.

References and Notes

1. L. Bovens, S. Hartmann, *Bayesian Epistemology* (Oxford Univ. Press, Oxford, 2003).
2. S. Nitzan, J. Paroush, *Collective Decision Making: An Economic Outlook* (Cambridge Univ. Press, Cambridge, 1985).
3. D. Alais, D. Burr, *Curr. Biol.* **14**, 257 (2004).
4. M. O. Ernst, M. S. Banks, *Nature* **415**, 429 (2002).
5. K. P. Körding, D. M. Wolpert, *Nature* **427**, 244 (2004).
6. S. Deneve, P. E. Latham, A. Pouget, *Nat. Neurosci.* **4**, 826 (2001).
7. D. M. Green, J. A. Swets, *Signal Detection Theory and Psychophysics* (Wiley, New York, 1966).
8. W. J. Ma, J. M. Beck, P. E. Latham, A. Pouget, *Nat. Neurosci.* **9**, 1432 (2006).
9. For details of methods, models, and additional results, see the supporting material on *Science* Online.
10. G. W. Hill, *Psychol. Bull.* **91**, 517 (1982).
11. R. Hastie, T. Kameda, *Psychol. Rev.* **112**, 494 (2005).
12. P. R. Laughlin, A. L. Ellis, *J. Exp. Soc. Psychol.* **22**, 177 (1986).
13. In our model, this internal estimate of the probability of being correct is a function of the ratio of stimulus contrast in a given trial to its standard deviation. The standard deviation is found by fitting a cumulative Gaussian to the participant's psychometric function.
14. R. D. Sorkin, C. J. Hays, R. West, *Psychol. Rev.* **108**, 183 (2001).
15. N. L. Kerr, R. S. Tindale, *Annu. Rev. Psychol.* **55**, 623 (2004).
16. B. Latané, K. Williams, S. Harkins, *J. Pers. Soc. Psychol.* **37**, 822 (1979).
17. M. E. Turner, A. R. Pratkanis, *Organ. Behav. Hum. Decis. Process.* **73**, 105 (1998).

18. We thank D. Bang for generous help with data collection in experiments 2 and 4 and F. Scharnowski for his insightful comments in the early stages of the project. This work was supported by the European Union MindBridge project (B.B.), the Danish National Research Foundation and the Danish Research Council for Culture and Communication (A.R. and C.D.F.), the Gatsby Charitable Foundation (P.E.L.), and the Wellcome Trust (G.R.). Support from the MIND Lab UNIK initiative at Aarhus University was funded by the Danish Ministry of Science, Technology and Innovation.

Supporting Online Material

www.sciencemag.org/cgi/content/full/329/5995/1081/DC1
Materials and Methods
Figs. S1 and S2
References

8 December 2009; accepted 28 June 2010
10.1126/science.1185718

Downloaded from www.sciencemag.org on August 27, 2010

Phosphatidic Acid Is a pH Biosensor That Links Membrane Biogenesis to Metabolism

Barry P. Young,[1]* John J. H. Shin,[1]* Rick Orij,[2] Jesse T. Chao,[1] Shu Chen Li,[1] Xue Li Guan,[3,4] Anthony Khong,[5] Eric Jan,[5] Markus R. Wenk,[4,6,7] William A. Prinz,[8] Gertien J. Smits,[2] Christopher J. R. Loewen[1,9]†

Recognition of lipids by proteins is important for their targeting and activation in many signaling pathways, but the mechanisms that regulate such interactions are largely unknown. Here, we found that binding of proteins to the ubiquitous signaling lipid phosphatidic acid (PA) depended on intracellular pH and the protonation state of its phosphate headgroup. In yeast, a rapid decrease in intracellular pH in response to glucose starvation regulated binding of PA to a transcription factor, Opi1, that coordinately repressed phospholipid metabolic genes. This enabled coupling of membrane biogenesis to nutrient availability.

The hydrophobic portions of lipids can be sensed by hydrophobic protein domains that are often membrane inserted. Soluble protein domains recognize lipids by interacting predominately with their hydrophilic headgroups. Recruitment of proteins to membranes is dependent on the concentration of their target lipid in the bilayer. Membrane-associated transcription factors sense changes in the levels of key signaling lipids, enabling direct feedback regulation of lipid metabolism (*1*–*3*). In yeast, phospholipid metabolism is regulated by the transcriptional repressor Opi1, part of a lipid-sensor complex in the endoplasmic reticulum (ER) (fig. S1) (*3*). Opi1 is sequestered on the ER by binding both PA and the tail-anchored ER protein Scs2. Addition of inositol results in the rapid depletion of PA, release of Opi1 from the ER, and translocation of Opi1 to the nucleus (*3*). Nuclear Opi1 represses the Ino2/4 transcriptional activator complex, which binds a cis regulatory element, UAS_{INO}, found in many phospholipid metabolic genes (*4*).

Of the genes regulated by inositol and Opi1, *INO1* is the most highly regulated (*4*). *INO1* encodes the rate-limiting enzyme in inositol biosynthesis; thus, inositol auxotrophy is a sensitive measure of expression of the *INO1* gene and the status of the ER lipid sensor. We screened the

[1]Department of Cellular and Physiological Sciences, University of British Columbia, Vancouver, British Columbia, V6T 1Z3, Canada. [2]Department of Molecular Biology and Microbial Food Safety, University of Amsterdam, Amsterdam, 1018 WV, Netherlands. [3]Department of Biochemistry, Yong Loo Lin School of Medicine, National University of Singapore, Singapore 119077. [4]Department of Biochemistry, University of Geneva, Sciences II, 30 Quai Ernest Ansermet, CH-1211 Geneva, Switzerland. [5]Department of Biochemistry and Molecular Biology, University of British Columbia, Vancouver, British Columbia, V6T 1Z3, Canada. [6]Department of Biological Sciences National University of Singapore, Singapore 119077. [7]Swiss Tropical and Public Health Institute, University of Basel, Socinstrasse 57, P.O. Box 4002, Basel, Switzerland. [8]Laboratory of Cell Biochemistry and Biology, National Institute of Diabetes and Digestive and Kidney Diseases, National Institutes of Health, Bethesda, MD 20892, USA. [9]The Brain Research Centre, University of British Columbia, Vancouver, British Columbia, V6T 1Z3, Canada.

*These authors contributed equally to this work.
†To whom correspondence should be addressed. E-mail: christopher.loewen@ubc.ca

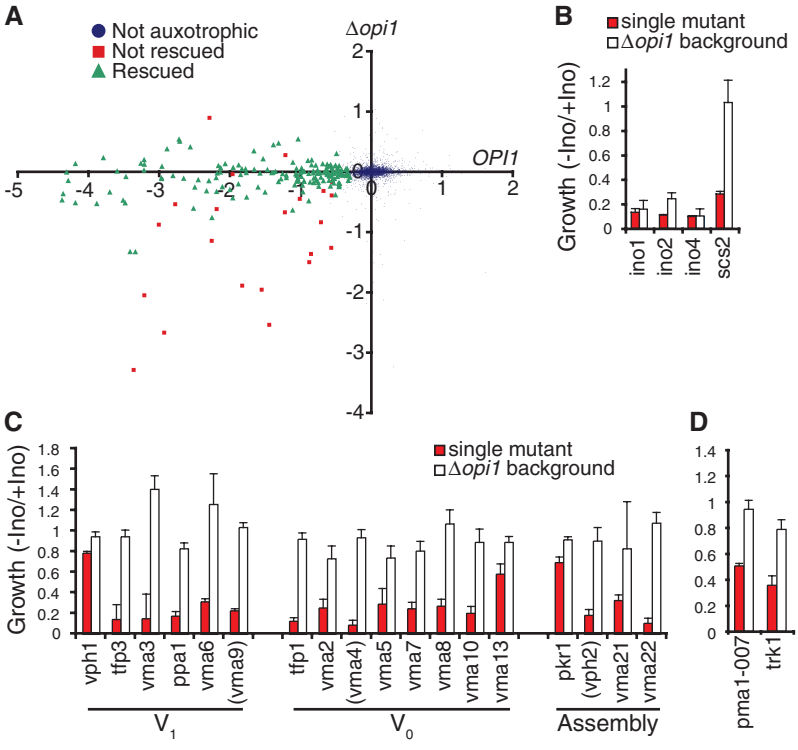

Fig. 1. Genome-wide screen for regulators of phospholipid metabolism. (**A**) Inositol auxotrophy of ~4800 deletion mutants and effect of deletion of *OPI1*. Plotted are $\log_2$ values of ratios of colony sizes for growth of mutants in the absence or presence of inositol (*5*). Single mutants are plotted on the *x* axis and double mutants with *Δopi1* on the *y* axis. (**B**) Inositol auxotrophy of known regulators of phospholipid metabolism and rescue by *Δopi1*. Plotted are ratios of colony sizes for growth of mutants in the absence (–Ino) or presence (+Ino) of inositol. (**C**) Inositol auxotrophy of V-ATPase deletion mutants. Mutants are grouped by V-ATPase domain (V_1, peripherally associated subunits; V_0, membrane-associated subunits) or factors required for V-ATPase assembly. Genes in parentheses indicate deletion of an overlapping dubious open reading frame and may not be true nulls. (**D**) Inositol auxotrophy of *pma1-007* and *Δtrk1* mutants. Error bars indicate SD.

haploid yeast deletion collection for sensitivity to growth in the absence of inositol (*5*). We identified 231 mutants with notable growth defects (fig. S2 and table S1). Most of these were rescued by deletion of Opi1 (Fig. 1A and table S2). The *Δino1*, *Δino2*, and *Δino4* mutants, which act downstream of the ER lipid-sensor, were not rescued (Fig. 1B). The *Δscs2* mutant was rescued as expected. Genes that govern intracellular pH (pH_i) were enriched in our data set (fig. S2 and table S3), including all 14 subunits of the vacuolar adenosine triphosphatase (V-ATPase) complex and the four factors in the ER responsible for its assembly (*6*) (Fig. 1C). The V-ATPase governs pH_i in part through regulation of Pma1 (*7*), a P-type H^+ ATPase of the plasma membrane (PM) that is the master regulator of pH_i (*8*). A hypomorphic allele of *PMA1* (*pma1-007*) that results in a 50% reduction in expression and activity of the Pma1 protein (*9*) was also an auxotroph (Fig. 1D). *TRK1*, a K^+ transporter of the PM that activates Pma1 (*7*), was also identified.

Because the *pma1-007* and *Δtrk1* mutants have an impaired capacity to pump protons out of the cell, they should be sensitive to acidification of the cytosol. To test this hypothesis, we subjected the strains to acid stress by growing them on medium buffered at low pH. Unlike in wild-type cells, pH_i in the *pma1-007* and *Δtrk1* mutants decreased with acidification of the medium (Fig. 2A). To determine whether cytosolic acidification causes derepression of Opi1, we measured transcription of Opi1-dependent genes by reporter assay (*3*) at pH 3, 4, and 5. We found almost complete repression in the *pma1-007* mutant at lowered pH, which was alleviated by deletion of *OPI1* (Fig. 2B and fig. S3). Wild-type cells showed a modest decrease in UAS_{INO} expression that was also dependent on *OPI1*. As expected, derepression of

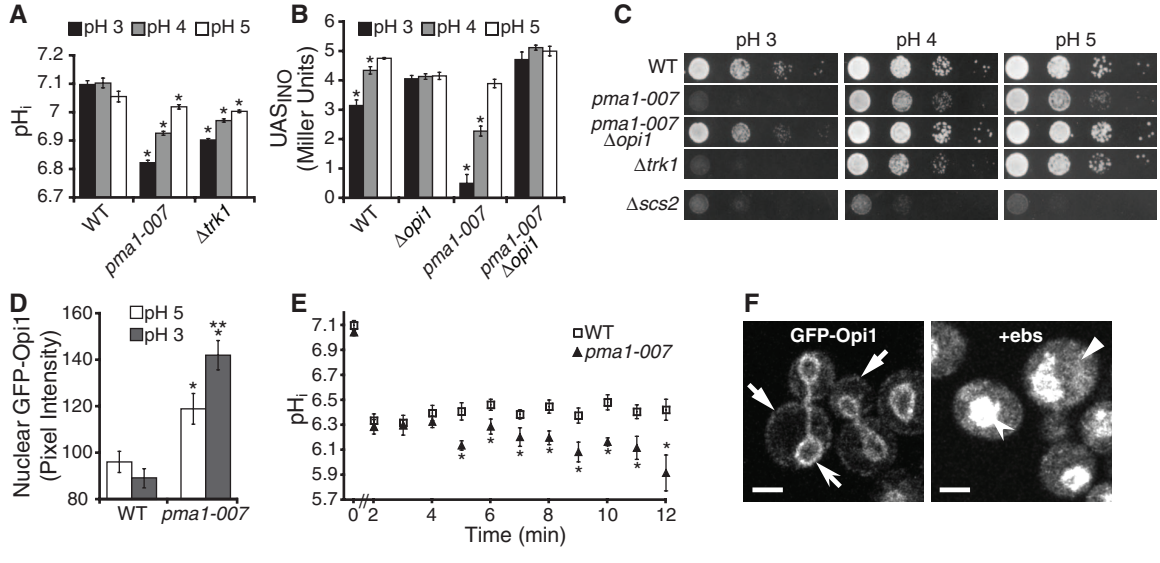

Fig. 2. pH regulates phospholipid metabolism. (**A**) pH_i of mutants grown in medium at pH 3, 4, and 5 compared to the wild type (WT) (*, versus WT at a given pH, $P < 0.001$). (**B**) UAS_{INO} reporter expression measured in different mutants grown at pH 3, 4, and 5 (*, versus pH 5, $P < 0.001$). (**C**) Growth of mutants in the absence of inositol at varying pH at 37°C. (**D**) Nuclear localization of GFP-Opi1 in cells grown at pH 3 and 5 quantified by confocal microscopy (*, versus WT at a given pH, $P < 0.005$; **, versus *pma1-007* at pH 5, $P < 0.01$). (**E**) Effect on pH_i after addition of 100 μM ebselen to WT and *pma1-007* cells grown in medium at pH 5 (*, versus WT at a given time point, $P < 0.05$). (**F**) Effect on the localization of GFP-Opi1 5 min after addition of 100 μM ebselen (+ebs). Arrows indicate ER localizations (straight, cortical; jagged, nuclear envelope); arrowheads indicate cytoplasmic (straight) and nuclear (jagged) localizations. Error bars indicate SEM in (A), (D), and (E) and SD (B). Scale bars, 2 μm.

Downloaded from www.sciencemag.org on August 27, 2010

Opi1 resulted in inositol auxotrophy of *pma1-007* and Δ*trk1* cells at low pH (Fig. 2C and fig. S4). This was in contrast to the Δ*scs2* mutant, which remained an inositol auxotroph at all pH values. Deletion of *OPI1* in the *pma1-007* mutant rescued its inositol auxotrophy at each pH. Opi labeled with green fluorescent protein (GFP-Opi1) accumulated in the nucleus of *pma1-007* cells, particularly at lowered pH (Fig. 2D), consistent with the decrease in UAS_{INO} expression. The drug ebselen, found to inhibit Pma1 in vitro (*10*), caused an immediate drop in pH_i of both wild-type and *pma1-007* cells to ~6.3 (Fig. 2E). Whereas wild-type cells stabilized at pH_i ~ 6.4, pH_i of *pma1-007* cells continued to decrease, indicating that the mutant is more sensitive, likely as a result of reduced gene dosage (*10*, *11*). Within 5 min, ebselen caused GFP-Opi1 to translocate from the ER to the cytosol and nucleus (Fig. 2F). Thus, pH_i regulates the localization and function of Opi1 and is a signal regulating transcription of phospholipid metabolic genes.

We examined whether pH affected the binding of Opi1 to PA. A basic domain in Opi1, Q2, directly binds the predominant pool of yeast PA, located in the PM (*3*). Ebselen caused GFP-Q2 to delocalize from the PM (Fig. 3A). This was also true for Spo20 (Fig. 3B), the other verified PA-binding protein in yeast (*12*). PM delocalization with ebselen was not due to endocytosis (fig. S5A). To control pH_i precisely, we treated yeast with the proton ionophore carbonyl cyanide 3-chlorophenylhydrazone (CCCP) over a range of pH values (*13*) and quantified GFP-Q2 localization to the PM (*5*). GFP-Q2 delocalized as pH decreased from 7.2 to 6.4 (Fig. 3, C and D). In contrast, localization of a probe for phosphatidylserine in the PM, GFP-Lact-C2 (*14*), did not change (fig. S5B). Thus, the binding of proteins to PA in vivo is sensitive to pH_i.

GFP-Q2 was delocalized in a V-ATPase mutant, Δ*vma2*, that had an acidified cytosol (Fig. 3, E and F). GFP-Lact-C2 localization was unaffected in this mutant (fig. S5C). Consistent with

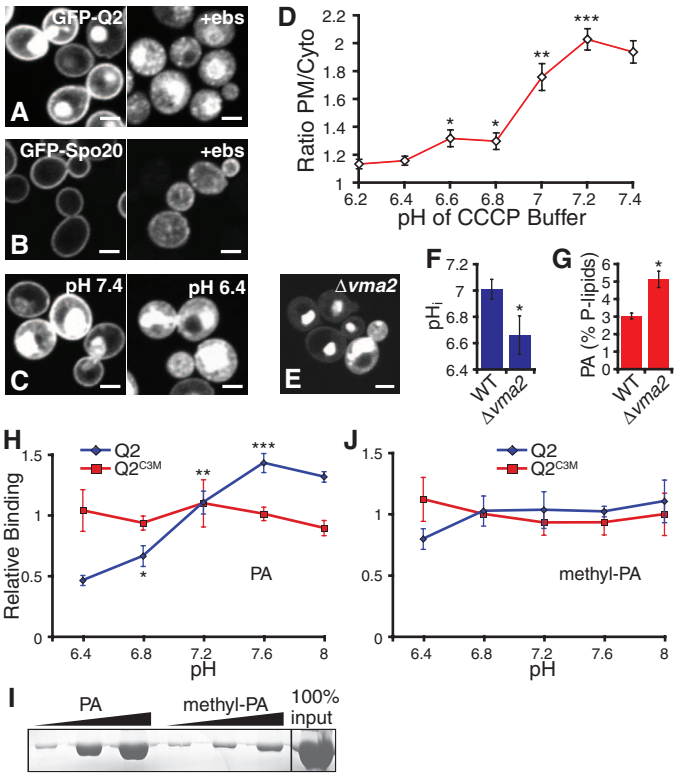

Fig. 3. pH governs the binding of Opi1 to PA through its protonation state. (**A**) Localization of GFP-Q2 after 5 min of ebselen treatment. (**B**) Localization of the PA-binding domain of Spo20 (GFP-Spo20$^{61\text{-}91}$) after 5 min of ebselen treatment. (**C**) Treatment of yeast expressing GFP-Q2 with CCCP buffered at the indicated pH. (**D**) Quantification of PM localization of GFP-Q2 with CCCP treatment (*, versus pH 6.4; **, versus pH 6.8; ***, versus pH 7; $P < 0.005$). (**E**) GFP-Q2 localization in Δ*vma2* cells. (**F**) pH_i measured in WT and Δ*vma2* cells grown in pH 5 medium (*$P < 0.0001$). (**G**) Total PA measured by mass spectrometry in WT and Δ*vma2* cells grown in pH 5 medium (*$P < 0.0001$). (**H**) Binding of Q2 and Q2^{C3M} to liposomes containing 10 mol % PA, 40 mol % phosphatidylethanolamine (PE) over a range of pH values (*, versus pH 6.4; **, versus pH 6.8; ***, versus pH 7.2; $P < 0.05$). (**I**) Binding of Q2 to liposomes (0, 100, 200 μM total lipid) containing 50 mol % PA or methyl-PA at pH 7.2. (**J**) Binding of Q2 and Q2^{C3M} to liposomes containing 20 mol % methyl-PA, 40 mol % PE over a range of pH values. Error bars indicate SD except in (D) (SEM). Scale bars, 2 μm.

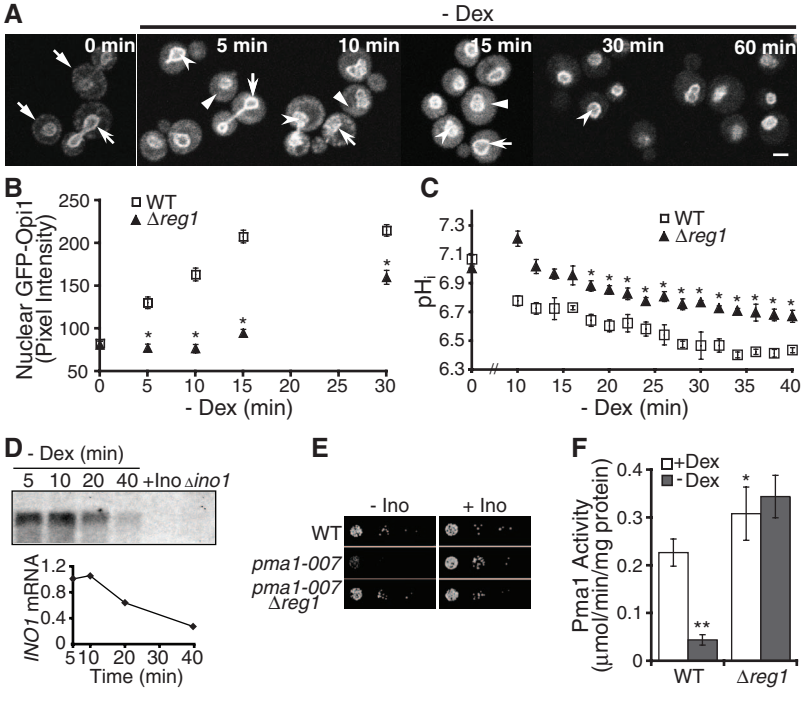

Fig. 4. Nutrient sensing and phospholipid metabolism are co-regulated by pH. (**A**) Localization of GFP-Opi1 in WT cells during glucose starvation. Time after removal from glucose (–Dex) is shown. Arrows and arrowheads as in Fig. 2. (**B**) Quantification of nuclear GFP-Opi1 after glucose starvation in WT and Δ*reg1* cells (*, versus WT at a given time point, $P < 0.0001$). (**C**) Change in pH_i measured in WT and Δ*reg1* cells during glucose starvation (*, versus $t = 0$ for Δ*reg1*, $P < 0.001$). (**D**) *INO1* mRNA levels during glucose starvation measured by Northern blot (+ Ino, cells grown in medium with inositol). (**E**) Growth of mutants at pH 4 in the presence or absence of inositol at 37°C. (**F**) Pma1 specific activity measured in WT and Δ*reg1* cells before and 20 min after glucose starvation (*, versus WT +Dex, $P < 0.05$; **, versus WT +Dex, $P < 0.005$). Scale bar, 2 μm.

Downloaded from www.sciencemag.org on August 27, 2010

an inability of Opi1 to bind PA in Δ*vma2* cells, GFP-Opi1 was translocated to the nucleus in this mutant, which also had decreased UAS_{INO} expression and was an inositol auxotroph (fig. S6). These phenotypes were not due to decreased PA levels, which were instead elevated ~70% in the mutant (Fig. 3G) (*5*). Thus, Opi1 failed to bind PA at lowered pH_i in this mutant.

Next, we bound recombinant Q2 to liposomes containing PA at varying pH (*5*). We found a near-linear increase in binding between pH 6.4 and 7.6 (Fig. 3H and fig. S7D). Three basic amino acids in Q2, $K_{136}K_{137}R_{138}$, are thought to participate in electrostatic interactions with the negatively charged headgroup of PA (*3*). Binding of the triple alanine substitution mutant ($Q2^{C3M}$) (*3*) to PA between pH 6.4 and 7.6 no longer depended on pH (Fig. 3H and fig. S7D). Thus, the direct interaction between Q2 and PA is sensitive to pH.

Unlike other phospholipids, the phosphate headgroup of PA is a monoester and has a second pK_a measured in model membranes to be between 6.6 and 7.9, depending on their phospholipid and protein composition (*15*, *16*). Changes in the ionization state of PA might thus be responsible for the observed pH-dependent binding of Opi1. We tested binding of Q2 to methyl-PA, which bears a methyl-group substitution on the phosphate and lacks the second pK_a (fig. S7A). Binding remained specific (fig. S7C), but was considerably weaker (Fig. 3I) and was pH independent (Fig. 3J and fig. S7D). Thus, Opi1 had higher affinity for deprotonated PA, consistent with the proposed electrostatic/hydrogen bond switch mechanism for the interaction of proteins with PA (*17*).

Because glucose-starved yeast exhibit a rapid drop in pH_i to ~ 6 (*7*) and our screen identified several major regulators of glucose signaling (fig. S8) (*5*), we hypothesized that glucose might be a physiological pH signal. Glucose starvation resulted in translocation of GFP-Opi1 from the ER to the nucleus (Fig. 4, A and B), which correlated with the drop in pH_i (Fig. 4C). *INO1* transcription was also repressed on a similar time scale (Fig. 4D). Translocation of GFP-Opi1 was not dependent on known modulators of PA levels (fig. S9) (*5*), suggesting that glucose acted independently of changes in the concentration of PA. Consistently, PA levels measured in ER microsomes isolated after 20 min of glucose starvation did not change significantly (fig. S10).

Reg1 is the glucose-signaling–specific regulatory subunit for Glc7, yeast's protein phosphatase type 1. Glc7 is implicated in repression of Pma1 (*18*), and Δ*reg1* yeast fail to repress *INO1* and overproduce inositol (*19*), suggesting that Reg1/Glc7 regulates pH_i through Pma1. Deletion of *REG1* rescued the inositol auxotrophy of the *pma1-007* mutant (Fig. 4E). Pma1 activity in the Δ*reg1* mutant was higher and failed to repress upon glucose starvation (Fig. 4F). Deletion of *REG1* attenuated the rapid drop in pH_i in glucose-starved cells (Fig. 4C). Thus, Reg1 repressed Pma1 in response to glucose starvation. GFP-Opi1 translocation was delayed in Δ*reg1* cells (Fig. 4B and fig. S9). In both wild-type and Δ*reg1* cells, translocation coincided with a drop in pH_i below 6.9, consistent with the reduced affinity of Opi1 for protonated PA.

Phosphatidic acid signaling can be dynamically regulated by changes in pH (fig. S11). This involves a change in the protonation state of the phosphate headgroup, making the lipid a pH biosensor. A pH-sensing role for lipids may not be limited to PA because phosphatidylinositol phosphates and ceramide-1-phosphate have pK_a values within the physiological range (*20*, *21*). Given the established roles for these lipids in signaling and the universality of pH regulation in biology, pH-dependent protein-lipid interactions may be important in a wide variety of systems.

References and Notes

1. J. L. Goldstein, R. A. DeBose-Boyd, M. S. Brown, *Cell* **124**, 35 (2006).
2. T. Hoppe *et al.*, *Cell* **102**, 577 (2000).
3. C. J. Loewen *et al.*, *Science* **304**, 1644 (2004).
4. G. M. Carman, S. A. Henry, *J. Biol. Chem.* **282**, 37293 (2007).
5. See supporting material on *Science* Online.
6. P. M. Kane, *Microbiol. Mol. Biol. Rev.* **70**, 177 (2006).
7. G. A. Martínez-Muñoz, P. M. Kane, *J. Biol. Chem.* **283**, 20309 (2008).
8. T. Ferreira, A. B. Mason, C. W. Slayman, *J. Biol. Chem.* **276**, 29613 (2001).
9. Z. Porat, N. Wender, O. Erez, C. Kahana, *Cell. Mol. Life Sci.* **62**, 3106 (2005).
10. G. Chan, D. Hardej, M. Santoro, C. Lau-Cam, B. Billack, *J. Biochem. Mol. Toxicol.* **21**, 252 (2007).
11. G. Giaever *et al.*, *Nat. Genet.* **21**, 278 (1999).
12. H. Nakanishi, P. de los Santos, A. M. Neiman, *Mol. Biol. Cell* **15**, 1802 (2004).
13. R. Orij, J. Postmus, A. Ter Beek, S. Brul, G. J. Smits, *Microbiology* **155**, 268 (2009).
14. T. Yeung *et al.*, *Science* **319**, 210 (2008).
15. A. Bhushan, M. G. McNamee, *Biophys. J.* **64**, 716 (1993).
16. E. E. Kooijman *et al.*, *Biochemistry* **44**, 17007 (2005).
17. E. E. Kooijman *et al.*, *J. Biol. Chem.* **282**, 11356 (2007).
18. T. Williams-Hart, X. Wu, K. Tatchell, *Genetics* **160**, 1423 (2002).
19. L. C. Hancock, R. P. Behta, J. M. Lopes, *Genetics* **173**, 621 (2006).
20. E. E. Kooijman, K. E. King, M. Gangoda, A. Gericke, *Biochemistry* **48**, 9360 (2009).
21. E. E. Kooijman *et al.*, *Biophys. J.* **94**, 4320 (2008).

22. We are grateful to T. Levine for insight and critical reading of the manuscript; C. Boone for access to SGA technologies; M. Davies and L. Conibear for a preliminary inositol screen; and J. Church for discussions. This research was supported by grants from the National Sciences and Engineering Council of Canada (NSERC), the Canadian Institute of Health Research (CIHR), the Michael Smith Foundation for Health Research (MSFHR), the Canada Foundation for Innovation, and the British Columbia Knowledge Development Fund (C.J.R.L. and E.J.); the Intramural Research Program of the National Institute of Diabetes and Digestive and Kidney Diseases (W.A.P.); and the Singapore National Research Foundation under CRP Award 2007-04, the Biomedical Research Council of Singapore (R-183-000-211-305), the National Medical Research Council (R-183-000-224-213), and the SystemsX.ch RTD project LipidX (M.R.W.). J.J.H.S. is the recipient of a NSERC Alexander Graham Bell Canada Graduate Scholarship. C.J.R.L. is a CIHR New Investigator, a MSFHR Scholar, and a Tula Foundation Investigator.

Supporting Online Material

www.sciencemag.org/cgi/content/full/329/5995/1085/DC1
Materials and Methods
SOM Text
Figs. S1 to S11
Tables S1 to S3
References

16 April 2010; accepted 2 July 2010
10.1126/science.1191026

Downloaded from www.sciencemag.org on August 27, 2010

SAMPLE COOLING/FREEZING

Thermo-conductive CoolRacks tubes, plates, and sample holders introduce critical reproducibility and instant organization into benchtop sample cooling and freezing. Precision-engineered and manufactured from novel thermo-adaptive alloy, CoolRacks standardize temperature control and quickly equilibrate all wells to within 0.1°C of the source temperature. The portable and versatile CoolRacks can be easily implemented in any procedure requiring ice, dry ice, liquid nitrogen, water bath, heat block, or any other laboratory temperature source. All samples are kept upright at exactly the same temperature regardless of well position, and racked samples can be moved from ice to water bath en masse, giving a rapid identical temperature shift for all samples. CoolRacks are available in a comprehensive range of formats for use with cryo tubes, microfuge tubes, PCR strips and plates, and many other consumables, and can be easily integrated into any process, diagnostic, or clinical kit.

BioCision

For info: 888-478-2221 | www.biocision.com

WATER PURIFICATION SYSTEM

The PURELAB Pulse Type II EDI (electrodeionization) water purification system, developed to produce consistently high-purity water at economical running costs, uniquely incorporates recirculation of purified water up to the dispense point—guaranteeing optimum purity. The Pulse technology integrates EDI, which combines ion-exchange resins and ion-selective membranes with direct current to efficiently remove ionized impurities from water. It is complemented by pretreatment, reverse osmosis, and a 254 nm ultraviolet lamp to produce Type II pure water that meets and exceeds ASTM D1193, ISO 3696 plus European, United States, and Japanese Pharmacopeia standards. In addition, the PURELAB Pulse can be fitted with a point-of-use biofilter to deliver bacteria levels of less than 1 CFU/10 ml. The PURELAB Pulse has been designed to fit into any laboratory environment and is easy to operate and maintain. It can be wall or bench mounted for convenient access and can be fitted with ELGA's unique wraparound reservoir to save valuable space.

ELGA

For info: 877-315-3542 | www.elgalabwater.com

NIR PHOTOMETRIC LINEARITY REFERENCE SETS

Near-infrared (NIR) traceable photometric linearity reference sets are available to pharmaceutical quality assurance labs and customer support organizations looking to qualify their NIR systems. These reference sets offer operational qualification and performance qualification of the transmittance scale in the NIR using industry standard protocols. The sets are based on easy-to-handle, nonconsumable Certified Reference Materials for qualifying the NIR Transmittance scale. The wavelength range covered is 1,100 to 2,850 nm, with a %T (A) range of 1.5 %T (1.82 A) to 61 %T (0.21 A). Filters are produced in an ISO/IEC 17025 and ISO Guide 34 accredited environment and are certified traceable to National Research Council Canada.

Starna Cells, Inc.

For info: 800-228-4482 | www.starna.com

TRYPSIN-FREE CELL HARVESTING

SplitKits offer a gentle, efficient, contamination-free way to dissociate cells. The kits are the first specifically designed for use in both serum-based and serum-free methodologies. Developed using a vegetable-based component rather than trypsin, SplitKits avoid any risk of contamination with either animal or human viruses or bacteria and are suitable for a wide variety of cell culture systems. The extremely gentle action of the vegetable-based enzyme gives higher cell yields and better cell growth recovery following detachment. In addition, surface epitopes and cell membranes remain unaltered and fully functional, making the kits ideal for use in flow cytometry. Each SplitKit is composed of the enzymatic reagent (SplitCells), AntiSplitCells, and SplitCells buffer to make a fully flexible cell dissociation system that can perform at ambient temperature. Three different formats are available, each optimized for use with specific cell types: SplitKit Strong for strongly adherent and bioreactor-cultured cells, SplitKit Moderate for moderately adherent cells, and SplitKit Mild for mildly adherent cells.

Sera Lab

For info: +44-(0)-1444-250010 | www.seralab.co.uk/splitkits

XUV WAVELENGTH CALIBRATION SOURCE

The McPherson Model 642-1 calibration light source for extreme ultraviolet (EUV) and soft x-ray (XUV) features a six position anode carousel to exchange target materials and permits selecting various emission wavelengths without breaking vacuum. This model is easy to set up and provides laboratories excellent, reliable means for at-wavelength calibration, or metrology of EUV lithography materials as well as multilayer or grazing incidence optical systems for astrophysics and other fundamental research. The Model 642-1 is a Manson type electron impact light source and uses a hot filament to produce electrons subsequently accelerated toward a solid anode target by high voltage. The EUV and XUV output emission spectrum follows the target anode material valence band structure. Dual symmetrical output beams provide sample/reference comparison and device calibration in various test setups. Users can readily exchange anodes in the carousel in order to produce desired wavelengths. Many different anodes are characterized and available as accessories.

McPherson

For info: 800-255-1055 | www.mcphersoninc.com

Electronically submit your new product description or product literature information! Go to **www.sciencemag.org/products/newproducts.dtl** for more information.

Newly offered instrumentation, apparatus, and laboratory materials of interest to researchers in all disciplines in academic, industrial, and governmental organizations are featured in this space. Emphasis is given to purpose, chief characteristics, and availability of products and materials. Endorsement by *Science* or AAAS of any products or materials mentioned is not implied. Additional information may be obtained from the manufacturer or supplier.

Downloaded from www.sciencemag.org on August 27, 2010

Multiply The Power of Science

***Science* Careers**
Classified Advertising

For full advertising details, go to ScienceCareers.org and click For Employers, or call one of our representatives.

Tracy Holmes
Worldwide Associate Director
Science Careers
Phone: +44 (0) 1223 326525

UNITED STATES & CANADA

E-mail: advertise@sciencecareers.org
Fax: 202-289-6742

Tina Burks
Midwest/West Coast/
South Central/Canada
Phone: 202-326-6577

Elizabeth Early
East Coast & Industry
Phone: 202-326-6578

Kate Panganiban
Advertising Operations Manager
Phone: 202-326-6582

Online Job Posting Questions
Phone: 202-326-6577

EUROPE & REST OF WORLD

E-mail: ads@science-int.co.uk
Fax: +44 (0) 1223 326532

Alex Palmer
Phone: +44 (0) 1223 326527

Susanne Kharraz Tavakol
Phone: +44 (0) 1223 326529

Dan Pennington
Phone: +44 (0) 1223 326517

Lisa Patterson
Phone: +44 (0) 1223 326528

JAPAN

ASCA Corporation
Jie Chin
Phone: +81-3-6802-4616
Fax: +81-3-6802-4615
E-mail: careerads@sciencemag.jp

To subscribe to *Science*:
In US call 866 434-2227
In the rest of the world call +1 202 326-6417

All ads submitted for publication must comply with applicable US and non-US laws. *Science* reserves the right to refuse any advertisement at its sole discretion for any reason, including without limitation for offensive language or inappropriate content, and all advertising is subject to publisher approval. *Science* encourages our readers to alert us to any ads that they feel may be discriminatory or offensive.

Science Careers
From the journal *Science* AAAS

POSITIONS OPEN

MCGOWEN POSTDOCTORAL FELLOWSHIP
Department of Neurology, University of Miami Miller School of Medicine

Available October 1, 2010. Initial appointment for one year; can be extended to two years or longer.

A Postdoctoral position is available immediately in the area of central nervous system biomarker and drug discovery in neurodegeneration and addiction. Qualified candidates must have a Ph.D. in Neuroscience (or related field of biology). Experience with molecular biology or the science of biospecimen banking and clinical specimen repositories are highly desired. The successful applicant will be a highly motivated individual with good communication skills, interest in Parkinson's or in other neurodegenerative diseases or addiction biology, and ability to work independently.

To apply, send a cover letter, curriculum vitae with brief statement of research interests, publications, and contact information for recommendations to **e-mail: dmash@med.miami.edu** or to the following address: **Dr. Deborah C. Mash, Department of Neurology, Miller School of Medicine, 1501 NW 9th Avenue, Miami, FL 33136.** Review of applications will begin immediately and will continue until the position is filled. The department is especially interested in candidates who can contribute to the diversity and excellence of the academic community through research, teaching and service. Additional information may be viewed at **website: http://brainbank.med.miami.edu/.**

A **POSTDOCTORAL POSITION** is available for a motivated scientist to investigate the mTOR pathway and inflammatory cytokines in chronic diarrheal diseases including inflammatory bowel disease. The Albany Medical College (AMC) is one of the nation's oldest private medical schools, located in the capital city of New York with easy access to Boston, New York, Montreal and close to a number of research institutions including: Rensselaer Polytechnic Institute (RPI), Ordway Research Institute, State University of New York at Albany, and Wadsworth center New York state department of health. Candidates with a strong background in molecular biology, biochemistry, microbiology, and immunology are encouraged to apply. If you are interested, please contact **Dr. Xinjun Zhu** with curriculum vitae and three letters of references to:

Xinjun Zhu, M.D.
Assistant Professor
Department of Medicine &
Center for Cardiovascular Sciences (MC8)
Albany Medical College
47 New Scotland Avenue
Albany, NY 12208-3479
E-mail: xzhu15@jhmi.edu

AMC supports a diversified, smoke-free environment and is proud to be an Equal Opportunity/Affirmative Action Employer, encouraging women and minorities to apply. In support of a safe, drug-free environment, criminal background checks and drug testing are part of our hiring process.

POSTDOCTORAL POSITION Harvard Medical School Computational Biology and Bioinformatics. Qualifications: (i) Ph.D. in bioinformatics, biostatistics, computer science, or related fields; (ii) familiarity with molecular biology and genomics; (iii) strong programming skills (R, C++, Python); and (iv) proficiency in microarray software Bioconductor, dChip, and GenePattern. Working at the interface of biology, statistics, and computing, the candidate will analyze high throughput gene expression microarray data in cancer genomics. The goal is to develop novel data analysis algorithms and software and to identify genomics signatures in cancer patients and tumor-bearing mice. Please send curriculum vitae, a career statement, and three letters of reference to: **Dr. A.I. Kassis, HMS, Armenise Building, 200 Longwood Avenue, Boston, MA 02115. E-mail: amin_kassis@hms.harvard.edu.** *An Equal Opportunity/Affirmative Action Employer.*

POSITIONS OPEN

PASTEUR FOUNDATION

POSTDOCTORAL FELLOWSHIPS
Institut Pasteur, Paris, France

Come work in Paris at the Institut Pasteur, the world-renowned, private, biomedical research organization. We invite applications from outstanding Fellowship candidates to any of 130 laboratories within our 10 departments. Areas include: developmental and cell biology, epidemiology, immunology, genomics, genetics, microbiology, neuroscience, structural biology, parasitology, mycology and virology. Next deadline: September 17, 2010. Annual package is $70,000 for three years. *U.S. citizenship required.*

E-mail: pasteurus@aol.com. Website: http://www.pasteurfoundation.org.

POSTDOCTORAL RESEARCH POSITIONS
San Diego State University
Heart Institute–SDSU Research Foundation

The San Diego State University Heart Institute is recruiting **POSTDOCTORAL FELLOWS** to work in a dynamic, state-of-the-art cardiovascular cell and molecular biology research setting in the laboratory of the Institute Director **Dr. Chris Glembotski,** studying roles for heart-derived secreted cytokines (cardiomyokines) on cardiac protection and repair. Applicants should have a Ph.D. in a relevant field, demonstrated expertise in basic cell and molecular biology, including methods to examine gain- and loss-of-gene-function in culture and animal models of heart disease, excellent communication skills, a record of peer-reviewed journal publications, and the desire and ability to write and submit competitive research grant applications. Salary is commensurate with experience; excellent benefits. Applicants should submit a cover letter, curriculum vitae, and a description of research experience and professional goals with the application for **Job #100120** at **website: https://jobsfoundation.sdsu.edu** or call **telephone: 619-594-5703.** *Equal Employment Opportunity/Affirmative Action/Title IX Employer.*

POSTDOCTORAL POSITION in HEPATOBILIARY CANCER RESEARCH

A Postdoctoral position is currently available to investigate tumor stromal/cancer cell interactions in cholangiocarcinoma progression. Candidates should be highly motivated and possess a Ph.D. in Cell and Molecular Biology or related fields of study. Demonstrable expertise (as indicated by published first author papers) in mammalian cell culture methods, molecular biology techniques, and in histology and immunohistochemistry methods is required. Strong oral communication and writing skills are also required. Interested persons should apply electronically by submitting a letter of interest, an updated curriculum vitae, copies of recent peer-reviewed publications, and three letters of reference to: **Dr. Alphonse E. Sirica, Professor and Division Chair, Division of Cellular and Molecular Pathogenesis, Department of Pathology, Virginia Commonwealth University School of Medicine, Richmond, VA 23298-0297, E-mail: asirica@mcvh-vcu.edu.** *Virginia Commonwealth University is an Equal Opportunity/Affirmative Action Employer. Women and minority candidates and persons with disabilities are encouraged to apply.*

POSTDOCTORAL SCIENTIST
Cancer Research Southern Research Institute, Birmingham, Alabama

Ph.D. with experience in cancer research and record of publication required. The research will study cyclooxygenase-independent mechanisms for chemopreventive properties of nonsteroidal anti-inflammatory drugs and will focus on cGMP phosphodiesterase as a potential target as described in *Mol. Cancer Ther.* **8:**3331, 2009. Experience in cell-based models, enzymology, and signal transduction is preferred. Must apply at **website: http://www.southernresearch.org. Posting number sr-02319.**

Affirmative Action/Equal Opportunity Employment.

THE POSTDOC EXPERIENCE

TAKING A LONG TERM VIEW

Faced with a shaky economy and an increasingly competitive job market, postdocs are being forced to take a long-term view of their positions. That means ensuring that it provides not only additional research training and publications, but also the necessary connections and experience that will be needed for a future career. It also means staying flexible and frequently reevaluating career plans. By Laura Bonetta.

"You have to be proactive and get the experience you will need for your future career."

Postdoc supervisors and their postdocs don't always see eye to eye when it comes to the factors that contribute to a successful postdoc experience, according to the annual surveys conducted by *Science* Careers, which alternate each year between asking the opinions of postdoc supervisors and the postdocs themselves.

The 3,500 or so current and former postdocs who responded to this year's survey put having a supervisor with adequate funding and opportunities for networking at the top of their list. On the other hand, the postdoc supervisors who responded to last year's survey ranked these factors as 6th and 7th most important, respectively. Supervisors put mentoring, direction and vision, and communication at the top of their list.

"I believe these differences are in large part due to different perspectives," says **Cathee Johnson Phillips,** executive director of the National Postdoctoral Association (NPA). Whereas postdoc supervisors may view the postdoc years mainly as an opportunity to obtain further training and improve research skills, "more and more postdocs are thinking long-term in regard to their career positions," says Phillips.

What does this mean? "You have to be proactive and get the experience you will need for your future career," says **Sarah Gaffen,** associate professor at the University of Pittsburgh. "If you want to be an academic PI, talk to people who are in search committees who can tell you how you are doing."

NETWORKING IS KEY…

Establishing a network of colleagues who can provide guidance and support and help open doors is key to a successful postdoc experience, according to 92 percent of this year's survey respondents.

Former postdoc **Jamie DeWitt** says her postdoc adviser at the U.S. Environmental Protection Agency (EPA) made sure she met his network of colleagues at scientific meetings and asked her to co-author review papers and book chapters with continued »

CREDIT: © ISTOCKPHOTO.COM/PAGADESIGN

Postdocs Rate Factors That Contribute to a Successful Postdoc Experience, Plus Rankings Compared to 2009 PI Survey

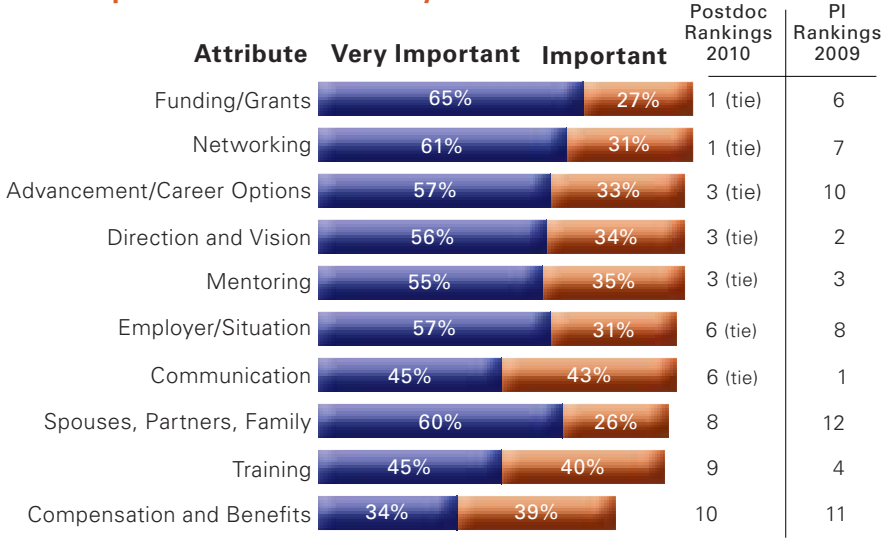

Survey Methodology

This year's survey was launched on March 16, 2010, with an e-mail invitation to about 60,000 current and former postdocs worldwide. Of the 3,475 qualified surveys that were collected 49 percent came from individuals in North America, 29 percent from individuals in Europe, and 22 percent from individuals in Asia Pacific or the rest of the world. Most (79 percent) postdoc positions were held in academic institutions. Life and medical sciences were the most common disciplines, being cited by 62 percent of respondents. A much smaller group of individuals (10 percent) worked in chemistry, while the remaining 28 percent worked in other non–life science disciplines. Most current postdocs (62 percent) were between 31 and 40 years of age. A smaller group (30 percent) was 30 years old or younger, while fewer still (8 percent) were 41 or older.

UPCOMING FEATURES

Faculty 2: Small vs. Large Universities—September 10
Focus on Germany—September 24
Diversity 2 (online only)—October 1

TOP TALENT WANTED IN SINGAPORE

PREMIER PROGRAMMES FOR THE BEST AND FINEST

Did You Know?

- *Singapore is the world's most prolific research location based on output per capita. Singapore tops the world in spending on science and technology, with a budget of US$10 billion*
- *The infrastructure for research in Singapore is cutting-edge and purpose-built. They range from biomedical sciences research complexes to research centres within university campuses*

State-of-the-Art Facilities

Purpose-built Infrastructure

Housing private and public sector research institutions under one roof, Biopolis is a nucleus of state-of-the-art facilities where the community of researchers may embark on the development and testbedding of niche research areas before bringing them to market.

Its sister development, Fusionopolis, serves the same purpose for science and engineering research, co-locating research institutes in the fields of manufacturing technology, high performance computing and communications.

Research Universities

The National University of Singapore (NUS) and the Nanyang Technological University (NTU) are top ranked tertiary institutions and research universities.

Commitment to Education and Research

Furthering its commitment to education and research, Singapore recently established the Singapore University of Technology and Design (SUTD) in collaboration with the Massachusetts Institute of Technology (MIT). The university will focus on design through an integrated multi-disciplinary curriculum. Many of the newly hired SUTD faculty will also spend up to a year at MIT in a specially tailored collaboration and professional development programme.

Programmes for The Best

There is a strong demand for good researchers and scientists in Singapore. Here are some of the most prestigious programmes that offer generous research funding and remuneration, freedom to pursue research directions, and the opportunity to work with some of the most renowned scientists in the world.

NTU Elite Nanyang Assistant Professorship

Key Features

- Hold tenure track appointments and play lead roles in the university's new wave of multi-disciplinary, integrative research

Funding and Remuneration

- Start-up research grants of up to S$1 million
- Attractive remuneration package and other benefits including assistance with accommodation

Eligibility

- Outstanding researchers and scholars
- Under the age of 40 years at the date of application, within 10 years of gaining your PhD and ready for independent leadership of your own research groups

Closing date for application:
October 1, 2010

To apply:
www.contactsingapore.sg/science_ntu

A*STAR Investigatorship (Biomedical Science)

Key Features

- Provides for an independent position for a duration of 3+3 years, with a review at the end of the second year and a possibility of "fast-track" promotion
- Tenable at one of A*STAR's prestigious biomedical research institutes, freedom to select a mentor from A*STAR and harness existing talent, equipment and other resources as you conduct and publish your research independently

Funding and Remuneration

- Attractive remuneration, support for set-up costs, research funding, research staff and access to state-of-the-art scientific equipment and facilities, including the Biopolis Shared Facilities and the Biological Resource Centre
- Each A*STAR Investigator's laboratory will be funded with up to US$500K per annum

Eligibility

- Have obtained your PhD not more than 48 months prior to the application date, and demonstrated a strong ability and creativity in research
- Applicants with MD-PhD should be in your last year of, or have completed your clinical specialty training at the time of application

Applications are accepted throughout the year. The next selection panel will convene in October 2010

To apply:
www.contactsingapore.sg/science_astar

Singapore NRF Fellowship

Key Features

- Complete independence and freedom to pursue your own research direction
- Freedom to choose host organisations, e.g. Singapore-based university, which you think will give you the best environment, in terms of access to relevant equipment and facilities and in building up the team for your research

Funding and Remuneration

- Up to US$2 million over five years, to support projects that exhibit high likelihood of a research breakthrough
- This grant excludes your salary, and will adequately support a research team comprising at least 1 post-doctoral fellow and 2 PhD students, costs of incremental research facilities, consumables and travels for conferences and meetings
- Your salary will be covered over and above the research grant awarded, and will be pegged to that of an Assistant Professor at a local university

Eligibility

- All areas of science and technology: Life Sciences, Natural/Physical Sciences, Engineering (all branches), Computer Science (including Infocomm Technology and Interactive and Digital Media)
- Outstanding scientists and researchers of all nationalities are welcome to apply

Closing date for application:
September 15, 2010

To apply:
www.contactsingapore.sg/science_nrf

For more information on working, investing and living in Singapore, please visit
www.contactsingapore.sg

For career opportunities, please go to
www.JobsAtSingapore.sg

For enquiries, please email
newyork@contactsingapore.sg

Find us on Facebook
www.contactsingapore.sg/facebook/americas

LinkedIn
www.contactsingapore.sg/linkedin

Singapore Translational Research (STaR) Investigator Award

Key Features

- A prestigious award, jointly offered by the Singapore Ministry of Health's National Medical Research Council (NMRC) and the Agency for Science, Technology and Research (A*STAR), to recognise and support investigators with outstanding qualifications in translational and clinical research
- Successful candidates will receive 3- to 5-year support

Funding and Remuneration

- STaR Investigators will be funded to start new research programmes in Singapore in biomedical research. STaR Investigators may, if you wish, spend up to 20% of your time engaging in direct patient care
- Awards include (I) Annual Research Support, (II) Annual Salary Support and (III) Start-up Costs

Eligibility

- Medically qualified doctors (MDs/MBBS) with advanced clinical specialty training or PhDs active in clinical research such as epidemiology and biostatistics
- Possess a medical qualification recognised by the Singapore Medical Council (please refer to www.smc.gov.sg/html/1150880211414.html)
- A physician scientist, clinical investigator, population geneticist, epidemiologist, health services researcher or an investigator engaged in other kinds of population-based biomedical research
- Strong track record of scientific achievement and impact in translational and clinical research
- Commit to a full time appointment in Singapore and your proposed research must be conducted in Singapore

Application window:
November 2010 to end January 2011

To apply:
www.contactsingapore.sg/science_star

Singapore University of Technology and Design (SUTD)

SUTD will matriculate its first intake of students in 2011. The University's programmes will be based on four pillars leading to separate degree programmes in Architecture and Sustainable Design, Engineering Product Development, Engineering Systems and Design, and Information Systems Technology and Design. Design, as an academic discipline, cuts across the curriculum and will be the framework for novel research and educational programmes.

Faculty Members

The qualifications for the faculty position include: an earned doctorate in Architecture, any field in Engineering, or Basic Sciences and Social Sciences, a strong commitment to teaching at the undergraduate and graduate levels, a demonstrated record of or potential for scholarly research, and excellent communication skills.

We invite applications for interdisciplinary faculty appointments at all levels, with many opportunities available in particular at the Assistant and Associate Professor levels. Duties include teaching of graduate and undergraduate students, research, supervision of student research, advising undergraduate student projects, and service to SUTD and the community. Faculty will be expected to develop and sustain a strong research programme. Attractive research grant opportunities are also available.

Founding Head of Pillars in the Following Disciplines (Engineering Product Development, Engineering Systems Design, Information Systems Design, Architecture and Sustainable Design)

For the Founding Head of Pillar, our search criterion is nothing short of the best and most reputable in the field. Shortlisted candidates must minimally have an excellent doctoral qualification and be an international award recipient for academic and research contributions to the relevant specialised field, with publications in renowned and reputable journals recognised by the international research community.

We invite applications with a specialisation in any of the four disciplines as well as the basic sciences.

Successful candidates can look forward to internationally competitive remuneration, and assistance for relocation to Singapore.

To apply:
www.contactsingapore.sg/science_sutd

THE DOT IS HOT

Contact Singapore
contactsingapore.sg

ADVERTISING SUPPLEMENT

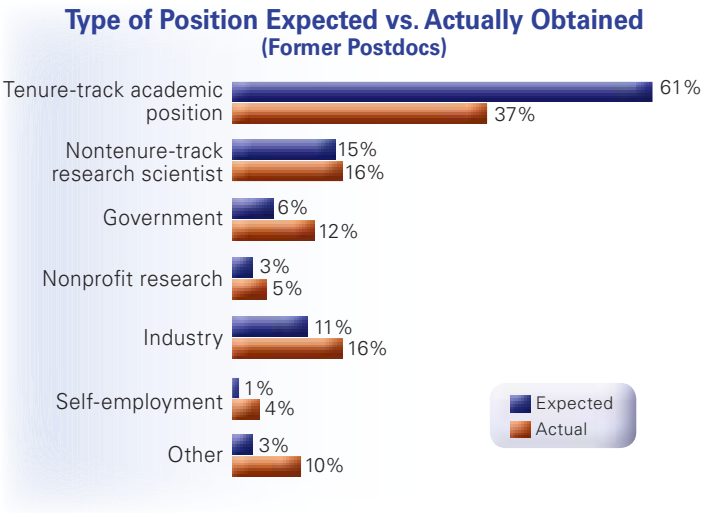

him. "All these things helped to introduce me to the broader scientific community," says DeWitt.

But she also took some initiative networking on her own. "I was involved in the postdoc association at EPA and was a postdoc representative for the Society of Toxicology, so I met a lot of people that way," she says. "I always tell postdocs not to be afraid to walk up to scientists at conferences and say 'I read your paper and wanted to meet you.'"

Being known among her colleagues helped DeWitt obtain her current faculty position at East Carolina University. "I would say that both having published several papers and networking were very important," she says. "The publications helped support what my colleagues were saying about me."

Networking was critical for **Eleni Tzavara** to obtain her current position at the National Institute for Health and Medical Research (INSERM) in Créteil, France. While she was a postdoc at Eli Lilly and Company in Indianapolis, Indiana, Tzavara attended a scientific conference. There, she met a neuroscience department director from INSERM who encouraged her to apply for a faculty position at INSERM. "I still had some time left in my postdoc so I was not looking for a position at that time," recalls Tzavara. "But I decided to apply and had to go through a really tough evaluation process. Once I had an offer it was hard to say no."

…AND SO IS FUNDING

Both DeWitt and Tzavara had productive postdocs in part because the resources were in place at their postdoc labs to hit the ground running. "A postdoc at EPA is very project oriented," she says. "The support system was in place for me to do research in a timely manner so I was able to get papers out quickly." Ninety-two percent of postdocs polled in this year's survey ranked having a supervisor with funding or grants at or near the top of their list for a successful postdoc experience. Tzavara had a similar experience. "The resources in industry are very good and the scientific environment challenging, so I was able to be very productive," she says.

The importance of funding hit home for **Virna Dapic** when she was doing a postdoc at the Moffitt Cancer Center in Tampa, Florida. She saw the impact her PI's struggle to obtain funding had on postdoctoral fellows and graduate students. As a result, she decided that "academic research was not meant for me," she says. "I didn't want to constantly worry about the money and the ability to maintain a research lab."

PLANNING FOR YOUR CAREER

An increased awareness of the need for long-term planning may explain why having "advancement opportunities and career options" jumped from 6th to 3rd place in the list of factors contributing to a successful postdoc experience in this year's survey compared to the one conducted two years ago, which also polled postdocs.

"My advice to postdocs is to use the position to train yourself for the job you want to do and also find out if it is the right job for you," says Gaffen. "But also be realistic."

At the start of her postdoc Gaffen was unsure an academic PI position would be right for her. But after publishing several papers and gaining recognition from her colleagues, she started to think a faculty position might be within her reach. "But I also realized that if I was going to do that job I would have to get the skills I needed for it," says Gaffen.

One thing Gaffen did was take courses in writing papers and grants. Her postdoc adviser also presented her with networking and grant writing opportunities to help her gain the necessary skills. "Success in obtaining a grant, particularly one that you can take with you to a faculty position, is worth a top journal paper to a search committee," says Gaffen.

PLANNING FOR TWO

Postdocs today are not only putting more emphasis on planning their own careers but also taking into account those of their partners. Over half (56 percent) of the survey group indicated that their career choice was limited by their spouse's or partner's career. Furthermore, accommodations made for spouses, partners, and family jumped from 10th to 8th place in the list of factors that postdocs view as contributing to a successful experience in the 2008 and 2010 surveys, respectively.

"We decided we would stay together and always look for positions in the same geographical areas," says **Mariel Vazquez,** continued »

FEATURED PARTICIPANTS

Eli Lilly and Company
www.lilly.com

Moffitt Cancer Center
www.moffitt.org

National Cancer Institute
www.cancer.gov

National Institute for Health and Medical Research
www.inserm.fr

National Postdoctoral Association
www.nationalpostdoc.org

San Francisco State University
www.sfsu.edu

U.K. Research Staff Association
www.vitae.ac.uk/researchers/205761/UKRSA.html

University of Dundee
www.dundee.ac.uk

University of Illinois at Urbana-Champaign
www.illinois.edu

University of Lausanne
www.unil.ch/central/page2192_en.html

University of Pittsburgh
www.pitt.edu

U.S. Environmental Protection Agency
www.epa.gov

Walden University
www.waldenu.edu

Washington University in St. Louis
www.wustl.edu

Yale University
www.yale.edu

Science Careers online @sciencecareers.org
POSTDOCTORAL OPPORTUNITIES

FIMM NCMM MIMS EMBL

Nordic EMBL Partnership for Molecular Medicine

The Nordic EMBL Partnership for Molecular Medicine was established in 2007 as a joint venture between the European Molecular Biology Laboratory (EMBL) and the Universities of Helsinki, Finland, Oslo, Norway and Umeå, Sweden and involves building of national sister institutions in the three countries. The partnership between EMBL, the Institute for Molecular Medicine Finland (FIMM), the Centre for Molecular Medicine Norway (NCMM) and the Laboratory for Molecular Infection Medicine Sweden (MIMS) is dedicated to the growing field of life sciences that investigates the molecular basis of disease and explores molecularly and genetically based treatments. Aiming to combine complementary strengths in the Nordic EMBL Partnership each partner brings in a unique set of expertise, skills and facilities encompassing EMBL's recognized research strengths in the areas of molecular, cellular and developmental biology, bioinformatics and structural biology complemented by Norway's expertise in molecular mechanisms of disease, Sweden's focus on microbial pathogenicity and molecular infection medicine and Finland's strength in human genomics and medical systems biology which equip the partners to tackle some of the most challenging problems of biomedicine. The Partnership provides access to scientific infrastructure, including databases, facilities and instrumentation, as well as to clinical materials and networks and training activities provided by the partners and adopts the EMBL model for international recruitment of young group leaders, staff turnover and scientific reviews.

The Nordic EMBL Partnership is now seeking outstanding international candidates for the positions of

RESEARCH GROUP LEADERS

Successful candidates are expected to initiate new independent research programs with a clear relevance to molecular medicine in areas indicated below.

FIMM: Helsinki, Finland
> Molecular Medicine

Ref. no. F/2010/01

The Institute for Molecular Medicine Finland (FIMM) is a research institute focusing on building a bridge from discovery to medical applications. The research areas of FIMM include human genomics, medical systems biology and translational research. FIMM Technology Centre also develops infrastructures for genomics, bioinformatics, HTS and biobanks. This time, applications are sought in particular in the following fields: biomarkers, biobanks, personalized medicine, human genetics, genetic epidemiology, medical bioinformatics/ systems biology. We are seeking promising young early-stage group leaders. Additional and novel contributions to existing FIMM and Meilahti campus expertise as well as international mobility will be valued. >>> www.fimm.fi

NCMM: Oslo, Norway
> Molecular Medicine – Disease Mechanisms

Ref. no. N/2010/8129

The overall objective of NCMM is to facilitate translation of discoveries in basic medical research into clinical practice. NCMM focuses particularly on disease mechanisms where Norway has clear strengths and will investigate mechanisms of non-communicable diseases, such as cancer, cardiovascular and CNS-related disease and immune disorders. NCMM will develop and adapt technologies for personalized medical applications and will be expected to unravel new diagnostic methods and drug targets. To facilitate translation and collaboration, NCMM plans for all group leaders to have adjunct appointments in university hospital departments. We are seeking outstanding candidates working with mechanisms of disease in relevant areas. >>> www.ncmm.uio.no

MIMS: Umeå, Sweden
> Molecular Infection Medicine

Ref. no. 316-706-10

The aim of MIMS is to strengthen Swedish research and enhance the dynamics in the field of molecular medicine, partly by promoting the career opportunities for young scientists. MIMS is established within the Umeå Centre for Microbial Research (UCMR) that includes researchers in molecular and clinical microbiology, molecular biology, chemistry and physics and is closely connected to the university hospital. Successful candidates should have a record of outstanding research in fields relevant to molecular infection medicine and are expected to initiate and maintain strong research programs synergizing with the UCMR research environment and to take active part in collaborative research opportunities and exchange programs within the Nordic EMBL Partnership for Molecular Medicine. >>> www.mims.umu.se

For further details and more comprehensive job descriptions please visit the websites of the respective institutes.

Applications should include a covering letter summarizing the applicant's career, past research accomplishments and future plans (max 1-2 pages), a CV and a list of publications (with 5 most significant publications indicated), a short research plan (max 5 pages) with a summary of expected translational, medical or public health impact and names of three references. Applications for all positions should be sent electronically following the instructions given by the institutes' websites.

Closing date: 1 October 2010

LAWRENCE POSTDOCTORAL FELLOWSHIP

The Lawrence Livermore National Laboratory (LLNL) has openings available under its Lawrence Fellowship Program. This is a highly desirable, prestigious postdoctoral position with ample resources and freedom to conduct cutting-edge research in a field of the candidate's choice. The duration of the Fellowship is up to three years. Typically two to four openings are available each year. Fellowships are awarded only to candidates with exceptional talent, credentials and a track record of research accomplishments.

Candidates will do original research in one or more aspects of science relevant to the mission and goals of LLNL which include: Physics, Applied Mathematics, Computer Science, Chemistry, Material Science, Engineering, Environmental Science, Atmospheric Science, Geology, Energy, Lasers and Biology. Successful candidates may participate in experimental or theoretical work at LLNL, and will have access to LLNL's extensive computing facilities, specialized laboratory facilities and field equipment. A senior scientist will serve as a mentor to each of the Fellows. The candidates will receive full management and administrative support. The salary is $8,700 per month.

Please refer to our web page **https://fellowship.llnl.gov** for eligibility requirements and instructions on how to apply. When applying and prompted, please mention where you saw this ad. The deadline for application is November 1, 2010. LLNL is operated by the Lawrence Livermore National Security, LLC, for the U.S. Department of Energy, National Nuclear Security Administration. We are proud to be an equal opportunity employer with a commitment to workforce diversity.

Lawrence Livermore National Laboratory

https://jobs.llnl.gov

The California Nanosystems Institute (CNSI) at the University of California-Santa Barbara is pleased to announce the competition for the

ELINGS PRIZE FELLOWSHIPS in EXPERIMENTAL SCIENCE

These prize postdoctoral fellowships provide a salary of $60,000/yr for two years, renewable for a third, along with benefits and research funds. Successful applicants will work with experimental CNSI faculty; applicants should indicate the experimental group(s) with which they would prefer to work. See **www.cnsi.ucsb.edu/fellowships**.

Applicants holding a PhD in science or engineering should prepare a cover letter, curriculum vitae, a one-page research proposal, and arrange for 3 supporting letters and submit via the website **https://fellow.cnsi.ucsb.edu** by **December 1, 2010**.

The University of California is an Equal Opportunity/Affirmative Action Employer.

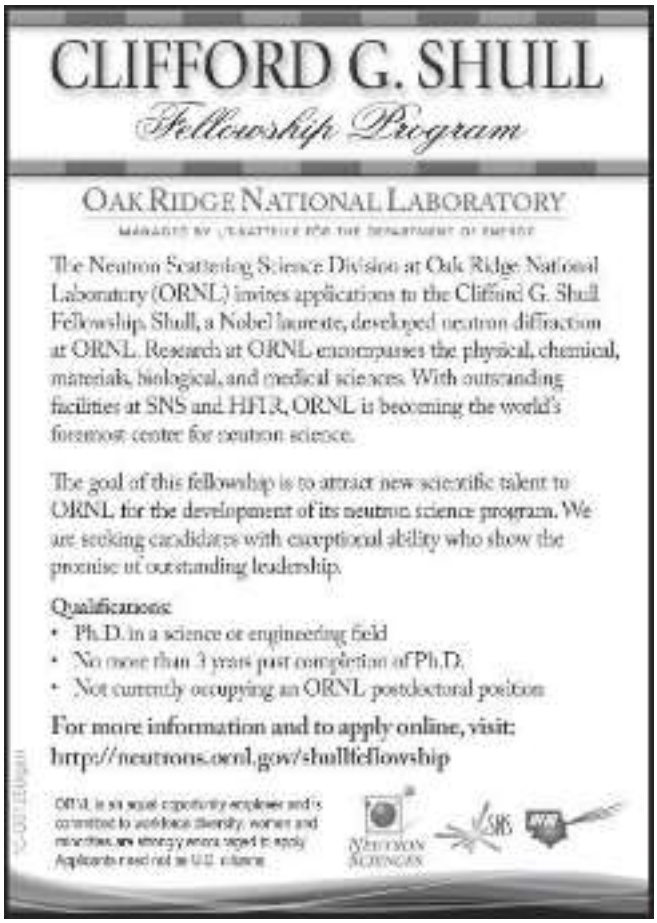

Research in Germany

Alexander von Humboldt Stiftung/Foundation

The Alexander von Humboldt Foundation enables highly-qualified scientists and scholars of all nationalities and fields to conduct extended periods of research in Germany. Fellowships are awarded solely on the basis of the applicant's academic record, the quality and feasibility of the proposed research and the candidate's international publications. The Humboldt Foundation particularly welcomes applications from qualified, female junior researchers.

Humboldt Research Fellowship for Postdoctoral Researchers who have completed a doctoral degree within the past four years.

- Allows for a stay of 6-24 months in Germany; monthly stipend of 2,250 EUR plus additional allowances

Humboldt Research Fellowship for Experienced Researchers who have completed a doctoral degree within the past twelve years.

- Allows for a stay of 6-18 months in Germany; fellowships may be divided into a maximum of three visits lasting three months or longer; monthly stipend of 2,450 EUR plus additional allowances

www.humboldt-foundation.de

Job Vacancy
Research Fellow
Quantification of complex analytes for Laboratory Medicine

Background

The International Bureau of Weights and Measures (BIPM) in Sèvres, France, is an intergovernmental scientific organization whose mandate is to provide the basis for a coherent system of measurements throughout the world, traceable to the International System of Units (SI). It has an international staff of over 70 and an annual budget of about 13 million euros. Further information about the BIPM can be found on the website: **www.bipm.org.**

The Chemistry Department of the BIPM organizes international comparisons related to organic substance purity determination. An extension of this programme is being developed to support the establishment of Reference Measurement Systems in the field of diagnostics and therapeutics.

The closing date is 30 September 2010

Duties

The BIPM has a vacancy for a Research Fellow for the development of analytical methods for the quantification of complex analytes (amino acids, peptides, and small proteins). The successful candidate will undertake projects to develop and improve qualitative and quantitative analytical methods, with a focus on high-performance liquid-chromatography - mass spectrometry (LCMS/MS), to identify impurities and to provide precise and accurate measurements for traceable mass fraction value assignments.

Qualifications

Applicants should have:

- a Ph.D. in a relevant field (chemistry, biochemistry or laboratory medicine);
- experience in LC-MS/MS of complex molecules relevant to therapeutics/ diagnostics;
- a fluent level of spoken and written English;
- the ability to work in a multicultural environment and the ability to maintain good working relations inside and outside the organization.

Previous experience with peptide/protein chemistry (hydrolysis, digestion, modification, labeling and purification) and familiarity with the operation of other relevant analytical instrumentation would be an advantage.

Employment conditions

The BIPM offers a full-time 2-year fixed-term appointment. The BIPM offers remuneration and conditions of employment detailed in its Staff Regulations, Rules and Instructions, which are comparable with those of other international organizations based in France. It manages its own contributory pension scheme and subscribes to a private medical insurance scheme for its staff and their families.

Applications

The BIPM encourages applications from both women and men with relevant qualifications. A full *curriculum vitae* (C.V.) and covering letter should be sent by mail to the Director, BIPM, Pavillon de Breteuil, F-92312 Sèvres Cedex, France, by **30 September 2010**, with a copy by email to: **ldelloro@bipm.org**. The selected applicants may be requested to take a written test and only shortlisted applicants will be invited for an interview. Applications should include the names of two referees who will be asked to comment upon the candidate's suitability for the post.

Requests for additional information may be addressed to Dr Robert Wielgosz, Director of the Chemistry Department: **rwielgosz@bipm.org.**

STONY BROOK

POSTDOCTORAL POSITIONS

The Research Foundation of SUNY at Stony Brook anticipates the following postdoctoral positions being available.

• APPLIED MATHEMATICS AND STATISTICS

Structure, flow, and strength changes induced by CO2 sequestration.
W. Brent Lindquist, WC-R-6426-10-08-S

Computational biology, development, and application for structure-based drug design.
Robert Rizzo, WC-R-6463-10-08-S

• BIOCHEMISTRY AND CELL BIOLOGY

Role of O-flucose in mesoderm/endoderm patterning during mouse development.
Bernadette Holdener, WC-R-6435-10-07-S

Biochemistry of glycoprotiens. William J. Lennarz, WC-R-6450-10-08-S

Developmentally programmed changes in chromatin structure. Aaron Neiman, WC-R-6425-10-08-S

• BIOMEDICAL ENGINEERING

Develop optical imaging devices and molecular probes for clinical applications.
Jonathan Liu, WC-S-6449-10-08-S

Conduct high impact, data driven modeling in LSEC lab. Lilianne Mujica-Parodi, WC-S-6428-10-07-S

Research in bone loss and biology concerning therapeutics for fracture healing.
Yi-Xian Qin, WC-R-6432-10-07-S and WC-R-6433-10-07-S

Research in photoacoustic imaging of biomaterials and small animals.
Balaji Sitharaman, WC-R-6464-10-08-S

Research in biomaterials and animal models in biomedical engineering laboratory.
Balaji Sitharaman, WC-R-6466-10-08-S

• ELECTRICAL AND COMPUTER ENGINEERING

Design 100Gbps data transfer protocols for distributed data centers and cloud computing.
Dantong Yu, WC-R-6395-10-08-F

• GEOSCIENCES

Theoretical minerology and material design. Artem Oganov, WC-R-6472-10-08-S

• MOLECULAR GENETICS AND MICROBIOLOGY

Cell cycle control in yeast. Bruce Futcher, WC-R-6471-10-08-S

Develop novel candidates for human and animal vaccines. Eckard Wimmer, WC-R-6451-10-08-S

• NEUROBIOLOGY AND BEHAVIOR

Electrophysiology of the injured spinal cord. Lorne Mendell, WC-R-6457-10-08-S

Study of electrophysiology of cholinergic circuit related to cognition. Lorna Role, WC-R-6456-10-08-S

• ORAL BIOLOGY AND PATHOLOGY

Study the role of protein kinase in skin epithelia. Soosan Ghazizadeh, WC-R-6438-10-08-S

• PHARMACOLOGY

Breast cancer metastasis and cancer proteomics. Emily Chen, HS-R-6452-10-08-S

Mammalian signal transduction: lipid signaling, diabetes, mitochondria dynamics, cancer, and secretion.
Michael Frohman, HS-R-6475-10-08-S

Structural and functional studies of mitochondria gene expression.
Miguel Garcia-Diaz, WC-R-6447-10-08-S

Structural biology of damaged DNA and its interaction with proteins.
Carlos de los Santos, HS-R-6455-10-08-S

Studies of the solution dynamics of protein kinases by NMR. Markus Seeliger, HS-R-6453-10-08-S

Protein engineering of specific ubiquitin tags. Markus Seeliger, HS-R-6454-10-08-S

• PHYSICS AND ASTRONOMY

Ab initio molecular dynamics simulations under external electrical fields.
Maria Fernandez-Serra, WC-R-6465-10-08-S

To apply online and for information, visit *www.stonybrook.edu/jobs* under category "K" or mail résumés to: Human Resource Services, 390 Administration Building, Stony Brook University, Stony Brook, NY 11794-0751.

Stony Brook University/SUNY is an affirmative action equal, opportunity educator and employer.

"In this job market I am not sure I would advise postdocs to drastically change research topics."
—Julie Belanger

an assistant professor in mathematics at San Francisco State University, where her husband, **Javier Arsuaga,** also holds a faculty position. "This was just a personal decision. It is challenging, but it has always worked out for us." The key, says Arsuaga, "is to both be highly competitive. Then, if an institution really wants one of the two, the chances are higher that they will consider interviewing the other one."

CALLING ALL MENTORS

To plan their careers many postdocs rely on advice from one or several more experienced scientists who are their mentors. More than half (61 percent) of the survey group knew someone they would describe as a mentor.

In most cases (75 percent) the mentor was either the individual's supervisor (52 percent) or Ph.D. (23 percent) adviser. But sometimes the relationship with the supervisor is strained, as it happened to be for **John Antonakis,** currently a professor of organizational behavior at the University of Lausanne in Switzerland.

Having obtained a Ph.D. in leadership management at Walden University in Minnesota, Antonakis did a postdoc at Yale University in Connecticut. "I wanted to supplement my doctoral training," says Antonakis. "The Yale name opens doors." He says he greatly benefited from the environment at Yale and the reputation of the university, but his adviser "did not provide the support and training I needed as a postdoc."

As a result Antonakis collaborated with mentors at other institutions. "They worked with me on publications and helped me get my first faculty position," says Antonakis.

WHEN THINGS DON'T GO AS INITIALLY PLANNED

Even with the best planning, the unpredictability of scientific research and the job market makes it difficult to ensure success. When a postdoc appointment does not lead to an academic position, many people choose to seek additional postdoc positions—a practice that is becoming increasingly common ("The Evolving Postdoctoral Experience," *Science,* 2009, doi:10.1126/science.opms.r0900076).

Three-fifths (60 percent) of the former postdocs polled in this year's survey held only a single postdoc position, while 29 percent held two such positions. Relatively few (11 percent) former postdocs held three or more positions. Forty percent of the survey respondents who held multiple postdocs said they did so due to poor job prospects; this percentage is similar to those reported in postdoc surveys conducted in 2006 and 2008, but 13 percent higher than that in the 2004 study.

Christian Beaulé's initial goal, when he started his postdoc in 2003 at the University of Illinois at Urbana-Champaign, was to stay for a few years and then return to his native country of Canada to a faculty position. But after a second postdoc at Washington University in Saint Louis, Missouri and fewer publications than he had hoped, Beaulé will be returning to Canada for another postdoc. "I will start a third postdoc to get more publications, but also for family and immigration reasons," he says.

And while he continues to seek academic positions, he will be keeping all his options open. "I am looking for academic positions in research but I am also looking at teaching, government, and industry positions," he says.

Although Beaulé had to adjust his expectations, he says, in retrospect, he would not do things differently. "In terms of papers I was not as productive as I had hoped but I am happy with what I did. In terms of science, learning, and professional development, this was a very productive postdoc experience," he says. "My advice to postdocs is to try to have fun but also have an end-goal in mind and try to make sure that the postdoc experience helps you reach that goal. Also, be realistic about your situation and be ready to revise your end-goal if you need to."

HAVING A PLAN B

Beaulé's situation is not unusual. Today more than ever postdocs are seeking career opportunities outside of bench research ("The evolving postdoctoral experience," *Science,* 2009, doi:10.1126/science.opms.r0900076). Sixty-one percent of former postdocs and 57 percent of current ones hoped to get tenure-track academic positions after completing their postdoctoral studies, but only 37 percent of the former postdocs who wanted to work in a tenure-track academic position ended up doing so. (see graph, p. 1094)

Julie Belanger switched research areas when she began her postdoc at the National Cancer Institute at Frederick, Maryland, from polymer chemistry to chemical biology. "In this job market I am not sure I would advise postdocs to drastically change research topics," she says. "I am very diverse and learned a lot about many aspects of chemistry, from nanomaterials to virology, but I feel I am a harder sell. My passion for an academic career comes across in person, but getting an interview has not been easy." On the flip-side, Belanger's diverse skill set and broader experience could serve her well now that she is also looking for government positions at the Food and Drug Administration and Centers for Disease Control and Prevention that are not research related.

Postdoc **David Proctor** has instead turned his sights to a career in science policy. "When I realized that my postdoc research wasn't turning out as I had hoped, I began to get more involved in my local postdoc association," recalls Proctor, who is from the United States, but is doing his postdoc at the University of Dundee, Scotland. "This later led to my involvement in the creation of the U.K. Research Staff Association, the British counterpart of the NPA. Overall this has reinforced my interest in science policy."

There are many considerations that go into choosing a postdoc position, which often need to be weighed against one another. Most postdocs' advice is to visit the prospective lab and spend time speaking with the head of the lab and its members to see if it will be a good fit.

In the end whether a postdoc is successful depends on someone's interests, needs, and aspirations. The key is to make sure that the experience provides the necessary skills, connections, and training for moving on to the next position—whatever that might be.

Laura Bonetta is scientist turned freelance writer based in the Washington D.C. area.

DOI: 10.1126/science.opms.r1000093

CREDIT: NATIONAL CANCER INSTITUTE AT FREDERICK

Focus on GERMANY

Recent funding initiatives, the development of centers of excellence, and increasing international appeal are impacting Germany's research environment.

Make sure your ad appears in this issue to benefit from:

- **Bonus distribution** at worldwide events, including **Biotechnica 2010**, Hannover, Germany
- Special bonus distribution to 5,000 scientists beyond our regular circulation
- Free 8-week online job posting on sciencecareers.org

For details:
Telephone: +44 (0) 1223 326500
E-mail: ads@science-int.co.uk

Science/AAAS Business Office feature

AMERICAN SOCIETY FOR MICROBIOLOGY AND CENTERS FOR DISEASE CONTROL AND PREVENTION

2011 POSTDOCTORAL RESEARCH FELLOWSHIP PROGRAM

Up to ten fellowship positions will be awarded by the American Society for Microbiology for full-time research in infectious diseases, which cause significant public health problems. Fellows will perform research in residence at one of the Centers for Disease Control and Prevention (CDC) locations in Atlanta, GA; Ft. Collins, CO; Anchorage, AK; or San Juan, Puerto Rico.

Eligible fields of study include:
Bacterial and Mycotic Diseases
Viral and Rickettsial Infections
Nosocomial Infections
HIV/AIDS
Vector-borne Infectious Diseases
Sexually Transmitted Diseases
Parasitic Diseases

The fellowship positions are limited to individuals who either earned their doctorate degree (Ph.D., Sc.D., M.D., D.V.M., or D.D.S.) or have completed a primary residency within three years of their proposed start date. Consideration will be given to individuals with more experience if there are compelling reasons for doing so, such as postgraduate subspecialty training or national service. Qualified applicants will receive consideration without regard to race, creed, color, age, sex, or national origin. Diversity among fellows is encouraged. The program provides an annual stipend for two years, health care benefits package up to $3,000 annually, relocation benefits up to $500, and up to $2,000 annually for professional development.

The application deadline is January 15, 2011. The Postdoctoral Research Program is administered by the American Society for Microbiology.

For more information, visit ASM's home page at **http://www.asm.org/postdocs** or e-mail: **Fellowships@asmusa.org**.

The application is available online.

AMERICAN SOCIETY FOR MICROBIOLOGY

CDC

THE UNIVERSITY OF ALABAMA AT BIRMINGHAM

Postdoctoral Positions

The University of Alabama at Birmingham (UAB) is one of the premier research universities in the US with internationally recognized programs in AIDS and bacterial pathogenesis, bone biology and disease, cancer, diabetes and digestive and kidney diseases, free radical biology, immunology, lung disease, neuroscience, trauma and inflammation, and basic and clinical vision science among others. UAB is committed to the development of outstanding postdoctoral scientists and has been consistently ranked in recent years as one of the top locations among US universities for training postdoctoral scholars.

UAB is recruiting candidates for postdoctoral positions in a variety of research areas. UAB faculty are well funded (top 25 in NIH funding), utilize multidisciplinary approaches, and provide excellent research training environments that can lead exceptional candidates to entry level positions in academia, government or the private sector. Full medical coverage (single or family), competitive salaries/stipends, sick leave, vacation, and maternity/paternity leave are offered with every position as well as AD&D, disability and life insurance. Depending on the source of funding, retirement benefits may also be available. Birmingham is a mid-size city centrally located in the southeast near beaches and mountains and enjoys a moderate climate for year round outdoor activities and a cost of living rate lower than most metropolitan areas.

Visit our web site at **www.postdocs.uab.edu**, under Postdoctoral Opportunities to view posted positions. Send your CV and cover letter to the contact name for those positions for which you are qualified and which interest you. **University of Alabama at Birmingham, Office of Postdoctoral Education, 205-975-7020**.

UAB is an Equal Employment Opportunity Employer.

MFPL Max F. Perutz Laboratories

Vienna International Post-Doctoral Training in Molecular Life Sciences

With support from the Austrian Ministry of Science and Research and the City of Vienna, the Max F. Perutz Laboratories offer a unique post-doctoral training programme, the Vienna International Post-Doctoral Training in Molecular Life Sciences (VIPS).

Join the VIPS

Application Deadline 15th of November 2010

www.mfpl.ac.at/vips

Our Mission:
To promote Post-Docs on their way to scientific independence

Our Offer:

- 3-5 years Post-Doctoral training
- Independent research budget
- Travel money
- Mentoring and Coaching
- Career development
- Grant writing support
- Child care

Our profile:
MFPL is part of the Vienna Biocenter Campus, a center for world class research. We offer a broad coverage of research areas, ranging from Biochemistry, Cellular Biology, Immunobiology to Organismal Biology, Bioinformatics, Structural Biology and Neurosciences.

Spend your post-doctoral training in a thriving scientific environment in one of the most liveable cities of the world!

Contact: Gabriele Permoser, e-mail: vips@mfpl.ac.at

BMWF City of Vienna

The Jackson Laboratory

leading the search for tomorrow's cures

DIRECTOR AND CHIEF EXECUTIVE OFFICER

The **Jackson Laboratory** (JAX®) is seeking applications and nominations for the position of **Director and Chief Executive Officer**.

The Jackson Laboratory is an independent, non-profit biomedical research institution and NCI-designated Cancer Center. JAX® has several operating models; a research model which operates as an NIH funded academic institution, a Genetic Resources Science model (GRS) that conducts research and serves as a resource repository for a large number of unique mouse strains, and a production and services model known as the JAX® Mice & Services (JMS), which is the world's premier source of genetically characterized and modified mice. The overall JAX annual operating budget is $182 MM.

The Director of JAX® is the chief executive officer of the Laboratory and appointed by the Board of Trustees. In addition to being an exceptional leader, the candidate must be a highly respected scientist, have strong business acumen, exhibit sensitivity to a unique culture, and have the ability to manage a complex organization. He/she must demonstrate the interpersonal skills that will assure successful relationship building with a variety of external stakeholders, including government figures, donors, and affiliated organizations. The Director/CEO will play the major role in the planning and implementation of a developing Florida initiative intended to advance discoveries needed to drive clinical progress.

Candidates will have an M.D., Ph.D., or both, with a sustained record of peer reviewed funding by NIH, and have national and/or international recognition for their research program.

Korn/Ferry International is assisting The Jackson Laboratory with this important search. Please forward, as soon as possible, nominations of appropriate candidates to:

Warren E. Ross, M.D.
c/o Betsy Messina (betsy.messina@kornferry.com)
Korn/Ferry International
1835 Market Street, Suite 2000
Philadelphia, PA 19103

The Jackson Laboratory is an Equal Opportunity/Affirmative Action Employer and Educator.

COLUMBIA UNIVERSITY MEDICAL CENTER

FACULTY POSITION

Department of Genetics and Development

The Department of Genetics and Development at Columbia University Medical Center is expanding its faculty and seeks outstanding applicants with the ability to develop an independent research program for a tenure-track position at the Assistant Professor level. In special circumstances, applicants at other levels will also be considered. Applicant's research program should use molecular genetic approaches to study, in any model organism, questions relevant to vertebrate physiology and to the molecular bases of human degenerative diseases. Our department spans a broad range of interests including developmental biology, physiology, DNA repair and recombination, cancer and human genetics.

Applicants should include a curriculum vitae and summary of current and proposed research programs, and arrange for three letters of reference to be sent. Completed applications should be submitted via the following Website:

https://academicjobs.columbia.edu/applicants/Central?quickFind=53431

Consideration for completed applications will begin September 30, 2010.

Columbia University is an equal opportunity/affirmative action employer. Women and minorities are encouraged to apply.

UNIVERSITY OF MINNESOTA

Medical School

Department of Pharmacology
(with potential joint appointment in the Institute for Translational Neuroscience)
TENURE/TENURE TRACK POSITION
(Assistant Professor, Associate Professor, Professor)

The Department of Pharmacology at the University of Minnesota invites applications for a tenure/tenure track faculty position (Assistant, Associate or Full Professor). Applicants using molecular, biochemical, cellular, and/or integrative translational approaches to study problems relevant to pharmacological sciences are encouraged to apply. Positions are also available in this joint recruitment with the Institute for Translational Neuroscience, whose interest is in how basic science discoveries may lead to new therapeutic principles of certain neurological disorders (see their website for more details). Qualifications include a Ph.D. in biomedical science, or an M.D. degree, and relevant postdoctoral research experience. Applicants must have a strong record of research accomplishments, as documented by publications in leading peer-reviewed journals. The successful **Assistant Professor** candidate will be expected to develop an innovative, competitive research program supported by extramural funding and to participate in departmental teaching activities. Applicants for **Associate Professor and Professor** positions must demonstrate distinction in published research, evidence of consistent extramural funding, and a commitment to teaching. For additional information about the department and the Institute for Translational Neuroscience, visit: **www.pharmacology.med.umn.edu** and **http://www.itn.umn.edu**.

Interested applicants should apply online at **http://employment.umn.edu/applicants/Central?quickFind=88959** for the **Assistant Professor** position or at **http://employment.umn.edu/applicants/Central?quickFind=88961** for the **Associate Professor or Professor** position, and attach a letter of interest, curriculum vitae, brief statement of research interests, and contact information for three references.

Burnett School of Biomedical Sciences
College of Medicine

Faculty Positions in Four Areas:
Cancer, Cardiovascular and Metabolic Diseases, Infectious Diseases and Neurodegenerative Diseases

University of Central Florida is expanding its Biomedical Research and Education Program into a new 198,000sq.ft. Burnett Biomedical Science building in the new medical campus. We seek outstanding scientists working on molecular, cellular, physiological, biochemical, or pharmacological approaches to study important problems with relevance to cancer, cardiovascular and metabolic diseases, infectious diseases and neurodegenerative diseases. Faculty at Assistant, Associate or Full Professor level will be considered. Successful applicants must hold an earned doctorate in a discipline appropriate to the school and will be expected to establish a well funded research program, contribute to teaching, and actively participate in MS and PhD programs.

Competitive salaries, startup funds, new laboratories, transgenic animal facilities and access to the new multimillion dollar shared core instrumentation facilities will be provided. Medical campus is part of multibillion dollar biomedical cluster that includes the Burnett School of Biomedical Sciences, the Medical School, Sanford-Burnham Medical Research Institute, Veterans Administration Hospital and Nemours Children's Hospital. Burnett School researchers will have access to the extensive core facilities in the adjacent Sanford-Burnham Medical Research Institute.

The University of Central Florida is the nation's third largest university and ranks third in innovation and patents. It is located in Orlando, a dynamic and progressive metropolitan region, a major player in high-tech industry, and adjacent to a top ranked Research park and a great place to live and work.

Review of candidates will begin on November 1, 2010. Please apply specifying your area of interest, a curriculum vitae, a two page summary of research plans and contact information for three or more references to **biomed@mail.ucf.edu** .

University of Central Florida

The University of Central Florida is an equal opportunity, equal access, and affirmative action employer. As a member of the Florida State University System, all application materials and selection procedures are available for public review.

Science Careers online @sciencecareers.org

Cornell University

Tenure Track Faculty Positions at Cornell University in the Weill Institute for Cell and Molecular Biology in Ithaca, NY

- BIOMEDICAL ENGINEERING - CHEMISTRY & CHEMICAL BIOLOGY - PLANT BIOLOGY -

Cornell University has established and endowed the Weill Institute for Cell and Molecular Biology **(http://www.icmb.cornell.edu).** The Institute will consist of 12 faculty members as the core component in a $160M new research building—Weill Hall—designed by renowned architect Richard Meier, and dedicated in October, 2008. The goal of the Institute is to build a vibrant center of scientific excellence in basic biology integrated with existing outstanding programs in chemistry and chemical biology, cell and molecular biology, physics, computational biology, engineering and plant biology. Institute faculty have full academic appointments in basic science departments to which they contribute teaching and service. The Institute, directed by Professor Scott Emr, currently has seven faculty. Searches for three new faculty are being initiated this year.

WEILL INSTITUTE / BIOMEDICAL ENGINEERING – Assistant/Associate Professor - #012010
Applications are invited for a tenure-track faculty position in the Weill Institute and the Department of Biomedical Engineering (BME) **(http://www.bme.cornell.edu).** Depending on experience, the position can be at the Assistant or Associate Professor level. BME is a new department, located in Weill Hall, currently with 14 faculty members. BME was formed to act as an intellectual bridge between engineering and the physical sciences and biology and medicine. Applicants trained in cell/molecular biology and engineering or the physical sciences who are using joint experimental/computational approaches to quantitatively address a fundamental question in molecular or cell biology (e.g. cell cycle, cell signaling, etc.) related to human health are encouraged to apply. Candidates whose research includes the use and development of instrumentation are also encouraged to apply. Questions about the position can be directed to Professor Michael King, the search committee chair, at **mrk93@cornell.edu.**

WEILL INSTITUTE / CHEMISTRY & CHEMICAL BIOLOGY – Assistant/Associate Professor - #022010
A faculty position is available at the Assistant/Associate Professor level in the Weill Institute and the Department of Chemistry and Chemical Biology (CCB) **(http://www.chem.cornell.edu).** CCB currently has 29 faculty working in areas from inorganic catalysis to structural analysis of signaling molecules. Applicants for this position should have a strong background in chemistry and/or chemical biology with research that addresses fundamental questions in molecular cell biology (e.g. cell cycle, signaling, cytoskeleton etc.). Candidates exploiting specialized approaches, for example chemical synthesis, structural biology, novel cellular probes, or high-resolution microscopy, will also be considered. Questions about the position can be directed to Professor Richard Cerione, the search committee chair, at **chemfacsearch@cornell.edu.**

WEILL INSTITUTE / PLANT BIOLOGY – Assistant Professor - #032010
The Department of Plant Biology (PB) **(http://www.plantbio.cornell.edu)** in conjunction with the Weill Institute invites applications at the Assistant Professor level. PB currently has 31 faculty working in plant research areas ranging from genomics, development to the molecular genetics of reproduction and evolution. For this position, applicants should have a strong background in plant biology and genetics with research that addresses fundamental questions in molecular cell biology (e.g. control of cell growth and cell division, cell polarity, cellular architecture and function, cell signaling, etc.). Questions about the position can be directed to Professor June Nasrallah, the search committee chair, at **jbn2@cornell.edu.**

HOW TO APPLY: Applicants should submit a curriculum vitae (highlighting 3-5 publications with title and abstract), a research plan (2-3 pages), and a statement of teaching interests. Personal statements summarizing teaching experience, leadership efforts, and contributions to diversity are encouraged. Three letters of recommendation are also required. The cover letter should describe how the applicant fits the interests of the Weill Institute and relevant Department. All materials, including letters of recommendation, should be submitted electronically to **https://fastbme.icmb.cornell.edu (BME position), http://www.chem.cornell.edu/facsearch (CCB position), or https://fastpb.icmb.cornell.edu (PB position).** The committees will evaluate completed applications received by November 1, 2010, with later applications possibly being considered until the position is filled. Administrative questions can be addressed to **Cathy Williammee, Weill Institute Manager, at icmb_recruiting@cornell.edu.**

About Cornell - The main campus of Cornell University, which overlooks 40-mile-long Cayuga Lake, is located in the Finger Lakes region of Upstate New York, a scenic environment of spectacular lakes, waterfalls, gorges, rolling hills, farmland, vineyards, and state parks. It is an area with outstanding recreational and summer and winter sports opportunities for individuals and families. The Cornell campus itself is one of the most beautiful in the country. Cornell comprises a varied array of academic units from music and literature to astrophysics and veterinary medicine and is a member of the Ivy League. The Ithaca community is culturally diverse with excellent theater, music, sports, and other activities befitting a major university town yet also has the warmth and friendliness of a small community. The area is known for its many bookstores and restaurants, an extensive walking trail system, arboretum, Laboratory of Ornithology, marina, Farmers' Market, a hands-on Sciencenter, and art and science museums. For more information and links to individual attractions, visit **http://www.visitithaca.com/.**

Cornell University, located in Ithaca, New York, is an inclusive, dynamic, and innovative Ivy League university. Its staff, faculty, and students impart an uncommon sense of larger purpose and contribute creative ideas and best practices to further the university's mission of teaching, research and outreach. Cornell is an equal opportunity employer and educator.

Science Careers online @sciencecareers.org

PICTURE YOURSELF AS A AAAS SCIENCE & TECHNOLOGY POLICY FELLOW

Make a Difference.
Help give science a greater voice in Washington, DC! Since 1973, AAAS Fellows have applied their skills to federal decision-making processes that affect people in the U.S. and around the world, while learning first-hand about the government and policymaking.

Join the Network.
Year-long fellowships are available in the U.S. Congress and federal agencies. Applicants must hold a PhD or equivalent doctoral-level degree in any behavioral/ social, biological, computational/ mathematical, earth, medical/health, or physical science, or any engineering discipline. Individuals with a master's degree in engineering and three years of post-degree professional experience also may apply. Federal employees are not eligible and U.S. citizenship is required.

Apply.
The application deadline for the 2011-2012 AAAS Fellowships is 5 December 2010. Fellowships are awarded in the spring and begin in September. Stipends range from $74,000 to $97,000.

Note: Additional fellowships are available through approximately 30 scientific society partners. Individuals are encouraged to apply with AAAS as well as with any scientific societies for which they qualify.

Full details at: **fellowships.aaas.org**

Enhancing Public Policy, Advancing Science Careers

Kwabena Yiadom, PhD

Chemistry, Georgetown University

2004-05 AAAS Fellow at the U.S. Department of Defense, International Technology Programs Office

Now an operational research analyst at the U.S. Department of Defense, Office of the Secretary of Defense

AAAS
ADVANCING SCIENCE, SERVING SOCIETY

Science Careers online @sciencecareers.org

ISTITUTO ITALIANO DI TECNOLOGIA

ISI GENOMICS CENTER OF GENOMIC SCIENCE

Italian Institute of Technology Outstation on Genomic Science at the European School of Molecular Medicine (IIT@SEMM), IFOM-IEO Campus, Milan, Italy

The Italian Institute of Technology (IIT, http://www.iit.it) has recently created an IIT-Network comprising nine outstations at Italian research institutions. The IIT@SEMM outstation is affiliated with the European School of Molecular Medicine (SEMM; http://www.semm.it) at the IFOM-IEO Campus in Milan (http://www.ifom-ieo-campus.it), a vibrant research center dedicated to basic and translational cancer biology, home to state-of-the-art technological services. The focus of IIT@SEMM is on Genomic Science, and in particular Cancer Genomics (http://genomics.iit.it). The program includes a Genomic Unit, a high-throughput phenotype Screening Unit and a Computational Research Unit. The setup of IIT@SEMM is coordinated by Pier Giuseppe Pelicci and Bruno Amati, who may be contacted for informal enquiries (firstname.lastname@ifom-ieo-campus.it). Applications are invited for the following positions within the IIT@SEMM program.

Group Leader, Computational Biology

The candidate will lead an independent research group, with full access to all the technological facilities of both IIT@SEMM and the IFOM-IEO Campus. Priority will be given to scientists developing and using computation tools in Genomics, with or without wet-lab activity. Areas of interest include genome-wide mutational analysis, functional genomics, epigenome analysis, gene regulation (coding, non-coding or small RNAs; regulatory networks), or any other activity pertinent to Cancer Genomics. Applications will be considered at the Junior and Senior levels.

Coordinator, Screening Unit

This is a unique career opportunity for an ambitious candidate interested in the setup, implementation and operation of a state-of-the-art robotic screening platform. The Screening Unit will aim at the identification of relevant gene products through microscopy-based high-throughput phenotypic screens in cells exposed to nucleic acid (cDNA or siRNA) or chemical compound libraries. Barcode-based genetic dropout screens will also be considered. Critical technological challenges in the setup of the unit will include automation and integration of the experimental and analytical processes, robotic transfer and handling of samples, multi-channel automated microscopes, etc. Candidates with the appropriate expertise will be strongly advantaged. Substantial funding is available for the purchase of suitable machinery, the acquisition of computational resources, and the hiring of collaborators. He/she will interact with other scientists of the IFOM-IEO Campus to identify suitable projects and collaborations, and will actively contribute to the interpretation of the results. The pursuit of independent research and fundraising will also be encouraged.

Technician, Genomic Unit

The Genomic Unit is a team deploying solutions to Academic Researchers based on high-throughput technologies, and in particular on Next Generation DNA Sequencing. Tasks will include RNA/DNA quality controls, library preparation using standard molecular biology techniques, as well as processing of experiments using dedicated instruments and software. The applicant must have a solid experience in molecular biology, be highly organized, focused, ready to dedicate full time to sequencing projects, willing to work in a team and in direct contact with scientists in the Campus. The capacity to test and adopt new technological evolutions will be an essential asset. Previous experience on Next Generation Sequencing technologies will be a plus, but is not mandatory.

Junior Developer/Programmer, Computational Research Unit

This Unit is the core computing facility of IIT@SEMM, guaranteeing informatic development, implementation, training and support in Genomic research activities. The candidate will be involved in developing and maintaining a website-based interface between all research groups in the Campus and the elaborated raw data provided by the Unit. Candidates should have excellent Java/J2EE software engineering skills, experience with JDBC, Spring, Struts, Hibernate, XML, SQL and Junit, as well as familiarity with either Netbeans, Eclipse, or IntelliJIDE.

High-throughput sequencing Data Analyst, Computational Research Unit

Candidates must have previous experience with the analysis of high-throughput DNA sequencing data (e.g. ChIP-seq, RNA-seq), a strong background in statistics and familiarity with statistics packages such as R. The ideal candidate will have Programming skills, as well as a solid understanding in Molecular Biology, enabling him/her to productively interact with wet-lab biologists. Tasks will include providing support to scientists in annotating sequencing tracks with known genomic features; aiding the discovery of novel genomic features (e.g. exons, splice sites); transforming sequence tag counts into expression values; performing DNA motif searches, cluster analyses, meta-analyses, etc.

According to IIT policy, position 1 above will be subject to a Senior Researcher contract, position 2 to a Team Leader or Senior Researcher contract depending on seniority, and positions 4 and 5 to Post-doctoral or Team Leader contracts depending on seniority. Internationally competitive salaries will be provided.

Applications including the CV, the names and e-mail addresses of three referees, and a personal statement should be sent as a single Pdf file to ***genomics@iit.it.*** *For positions 1 and 2 above, the statement should focus on future research and/or development plans, as applicable (max. 3 pages). For positions 3-5 it should focus on technological skills and interests (max. 2 pages). Please refer to the position number in the application. Application deadline: October 15, 2010.*

VILLANOVA UNIVERSITY

The Dennis M. Cook Endowed Gregor Mendel Chair in Genetics

We seek a nationally recognized teacher/scholar who will contribute to the Augustinian foundation of Villanova through the development and implementation of an ethical and socially responsible program that includes interaction with and involvement of undergraduate and graduate students in both teaching and research. Research may focus on classical inheritance, functional genomics, gene expression, bioinformatics, evolutionary genetics, or other areas that integrate genes and/or genomic material into the research program. See **http://www.villanova.edu/artsci/biology/jobs/genetics_chair** for more information.

Applicants must apply online at **https://jobs.villanova.edu**. Applications are to include a current and complete curriculum vitae and a cover letter describing a proposed program of teaching, research, and service. Applicants should also provide the names and contact information for four references.

Appointment is expected to be at the Associate Professor or Professor rank, with a starting date of August 2011. Review of applications will begin on **1 December 2010**; the search will remain open until the position is filled. Questions may be addressed to: **Dr. R. Kelman Wieder, Associate Dean for Sciences - Email: Kelman.Wieder@villanova.edu; Ph.: 610-519-4856**.

Villanova is a Catholic university sponsored by the Augustinian order. An AA/EEO Employer, Villanova seeks a diverse faculty committed to scholarship, service, and especially teaching, who understand, respect, and can contribute to the University's mission and values.

SOUTHWESTERN
THE UNIVERSITY OF TEXAS
SOUTHWESTERN MEDICAL CENTER
AT DALLAS

Faculty Positions in Infectious Diseases

The Division of Infectious Diseases in the Department of Internal Medicine at the University of Texas Southwestern (UTSW) Medical Center at Dallas is seeking new faculty members at the Assistant Professor level. Faculty will be expected to develop independent and externally funded independent research programs that focus on understanding the molecular pathogenesis of infectious diseases and/or host defense mechanisms. Preference will be given to applicants performing "cutting-edge" research on medically important pathogens, emerging pathogens, and/or agents of potential biothreat. Excellent opportunities exist for collaborations with faculty members in Infectious Diseases, the Department of Microbiology, and the Department of Immunology at UTSW and with the Regional Center of Excellence (RCE) for Biodefense and Emerging Infectious Diseases. UTSW is an outstanding scientific environment with established strengths in structural biology, biochemistry, molecular biology, genetics, and numerous other areas. Candidates will be expected to contribute to the teaching and research training of Infectious Diseases fellows. The positions offer attractive start-up packages and laboratory space. Candidates should have an M.D. and/or a Ph.D. degree with at least two years of postdoctoral experience and an outstanding publication record.

To apply, submit a C.V., three letters of reference, and a description of research interests to: **Dr. Beth Levine, Chief, Division of Infectious Diseases, UT Southwestern Medical Center, 5323 Harry Hines Blvd, Dallas, TX 75390-9113. E-mail: Cindy.Jozefiak@UTSouthwestern.edu**.

UT Southwestern is an Equal Opportunity/Affirmative Action Employer.

UBC

TENURE TRACK ASSISTANT PROFESSOR POSITION IN ECOLOGY

The Department of Zoology, University of British Columbia, invites applications for a tenure track faculty position in ecology. Applicants must have a PhD and will be expected to develop a strong externally funded research program. They will be expected to contribute to high quality undergraduate and graduate teaching in ecology and animal biology, and to supervise graduate students.

The successful applicant will become a member of the new Biodiversity Research Center, a world-class group of scientists studying ecology, evolution and systematics, and will actively interact with more broadly based members of the Zoology Department. With this position we seek to complement existing strengths in the Department. Desired research areas include but are not limited to population ecology, theoretical ecology, and ecology of terrestrial vertebrates. The appointment will be at the Assistant Professor level and is subject to final budgetary approval. Salary will be commensurate with experience.

Applicants should submit a curriculum vitae, summary of research interests and teaching philosophy, reprints of four key publications, and evidence of teaching effectiveness online at **www.hr.ubc.ca/faculty_relations/careers/**. Applicants should have letters of support from three referees sent to: **Dr. Dolph Schluter, Ecology Search, Department of Zoology, University of British Columbia, 6270 University Blvd., Vancouver, BC, Canada V6T 1Z4 (email ecologysearch@zoology.ubc.ca, Fax 604-822-5780)**. Inquiries may be sent to the same address. Deadline for applications is **October 15, 2010**.

The University of British Columbia is strongly committed to diversity within its community and we strongly encourage applications from underrepresented groups. We encourage all qualified persons to apply: however Canadians and permanent residents of Canada will be given priority.

UNIVERSITY OF MICHIGAN

BIOLOGICAL SCIENCES SCHOLARS PROGRAM

For Junior, Tenure-Track Faculty

The University of Michigan announces recruitment for the Biological Sciences Scholars Program (BSSP) to continue to enhance its investigational strengths in the life sciences research programs.

Now entering its 14th year, this Program has led to the recruitment of outstanding young scientists in the areas of genetics, microbiology, immunology, virology, structural biology, pharmacology, biochemistry, molecular pharmacology, stem cell biology, cancer biology, physiology, cell and developmental biology, and the neurosciences. The Program seeks individuals with PhD, MD, or MD/PhD degrees, at least two years of postdoctoral research experience, and evidence of superlative scientific accomplishment and scholarly promise. Successful candidates will be expected to establish a vigorous, externally-funded research program, and to become leaders in departmental and program activities, including teaching at the medical, graduate, and/or undergraduate levels. Primary college and department affiliation will be determined by the applicant's qualifications and by relevance of the applicant's research program to departmental initiatives and focus. All faculty recruited via the BSSP will be appointed at the Assistant Professor level.

APPLICATION INSTRUCTIONS: Please apply to the Scholars Program through the BSSP website at: (http://www.med.umich.edu/medschool/research/bssp/). A curriculum vitae (including bibliography), a three-page research plan, an NIH biosketch, and three original letters of support should all be submitted through the BSSP website. More information about the Scholars Program, instructions for applicants and those submitting letters of recommendation, and how to contact us is located on the BSSP web site: (http://www.med.umich.edu/medschool/research/bssp/). The deadline for applications is Friday, October 29, 2010.

The University of Michigan is an Affirmative Action/Equal Opportunity Employer.

DISCOVERY RESEARCH SCIENTIST/ TUMOR IMMUNOLOGIST

To view the complete job description and apply online, visit:
http://careers-halozyme.icims.com/jobs/2775/job

Halozyme Therapeutics, Inc. is looking for a highly motivated and committed investigator to participate in our continued work on cancer therapeutics discovery. Located in San Diego, California, Halozyme is focused on the discovery and development of biotherapeutics for cancer and other diseases, with particular emphasis on targets in the extracellular matrix.

Position Summary:
In this position, the Tumor Immunology Scientist will be a bench scientist investigating the regulation of immune activation, and anti-tumor immune-cell activity in cancer animal models. The successful applicant will be expected to develop and validate animal models and *in vitro* immunobiology studies to support the *in vivo* models; design, execute and interpret experimental results; and work collaboratively with other laboratory team members to advance multiple projects. The individual will also be part of a multidisciplinary team including clinical research and external research organizations. The position requires a PhD and at least 3 years of postdoctoral experience. The ability to independently design and carry out experiments is essential, as well as the motivation and ability to publish in peer-reviewed journals.

For more information on Halozyme and our open positions, please visit our website at:

www.halozyme.com

EOE.

Halozyme

Matrix Therapies For Life

The University of Texas at Austin

Cancer Molecular Biology Position

The Institute for Cellular and Molecular Biology

The Institute for Cellular and Molecular Biology, Alan Lambowitz, Director, invites applications for a tenure-track/tenured position in cancer molecular biology. Academic appointments at the level of Assistant, Associate, or Full Professor will be in the section of Molecular Genetics and Microbiology in the College of Natural Sciences. Candidates should have an outstanding record of research productivity and a research plan that utilizes molecular and biochemical approaches to address important problems in cancer biology. Areas of particular interest include but are not limited to DNA damage responses, genome instability, post-translational regulatory mechanisms, chromatin, and small regulatory RNAs.

Building on a strong existing faculty, the Institute has recruited more than 50 new faculty members over the past ten years. In addition to its highly interactive and interdisciplinary research environment, the Institute provides administrative and financial support for the Graduate Programs in Cell and Molecular Biology, Microbiology, and Biochemistry, and state-of-the art core facilities including DNA sequencing, mass spectrometry, electron and confocal microscopy, DNA microarrays, robotics, mouse genetic engineering and Next-Gen sequencing. An MD-PhD program with the UT Medical Branch and the new Dell Pediatrics Research Institute enhance the environment for basic Biomedical Research.

Austin is located in the Texas hill country and is widely recognized as one of America's most beautiful and livable cities.

Please send a single PDF file containing your curriculum vitae, summary of research interests and names of three references before November 1, 2010 to: **mgm_search@biosci.utexas.edu.** References may also send their letters directly to the same email address.

Homepages • http://www.icmb.utexas.edu • http://www.biosci.utexas.edu/MGM •

The University of Texas at Austin is an Equal Opportunity Employer.
Qualified women and minorities are encouraged to apply; a background check will be conducted on applicant selected.

Nontraditional Careers:
Opportunities Away From the Bench
Webinar

Want to learn more about exciting and rewarding careers outside of academic/industrial research? View a roundtable discussion that looks at the various career options open to scientists across different sectors and strategies you can use to pursue a nonresearch career.

Now Available
On Demand
www.sciencecareers.org/webinar

Participating Experts:

Dr. Lori Conlan
Director of Postdoc Services,
Office of Intramural Training and Education
National Institutes of Health

Pearl Freier
President
Cambridge BioPartners

Dr. Marion Müller
Director, DFG Office North America
Deutsche Forschungsgemeinschaft
(German Research Foundation)

Richard Weibl
Director, Center for Careers in Science and Technology
American Association for the Advancement of Science

Produced by the
Science/AAAS Business Office.

Science Careers
From the journal *Science* AAAS

THE UNIVERSITY OF CALIFORNIA AT BERKELEY

Department of Molecular and Cell Biology, Helen Wills Neuroscience Institute and Center for Computational Biology

The Department of Molecular and Cell Biology (MCB), the Helen Wills Neuroscience Institute (HWNI) and the center for Computational Biology (CCB) are seeking applications for four faculty positions in the areas listed below. We seek candidates with Ph.D. and/or M.D. degrees who have a strong interest in undergraduate and graduate teaching and demonstrated excellence, originality and productivity in research.

Biomedical Sciences (MCB): We seek candidates interested in molecular and cellular mechanisms of disease processes. Areas of research could include cancer, human genetics, aging, molecular physiology, animal models of human disease, infectious and neurodegenerative diseases, or any other area of biomedical science. This position is open at the Assistant Professor level (tenure-track).

Molecular, Cellular or Developmental Neuroscience (MCB/HWNI): We seek candidates in any area of molecular, cellular, and developmental neurobiology, with a particular emphasis on molecular genetic approaches to understanding neural circuit function, development, or regeneration. Approaches could include (but are not limited to) human genetics, use of genetic model organisms, genomics, behavioral analysis, optical imaging, and/or computational modeling. This position is open at the Assistant Professor level (tenure-track)

Human Genome Variation (MCB/CCB): We seek candidates whose research focuses on an understanding of genome and epigenome variation of humans as it relates to phenotype, particularly disease predisposition, using both computational and laboratory approaches. This position is open at the Assistant Professor level (tenure-track).

Stem Cell Biology (MCB): We seek candidates whose research focuses on any aspect of stem cell biology, including (but not limited to) the use of stem cells to develop models of human biology or disease, molecular mechanisms of transcriptional regulation in pluripotent and differentiating stem cells, the regulation of stem cell renewal and differentiation during development, and the biology of cancer stem cells. This position is open at any level (tenured or tenure-track).

Applications and letters of reference should be submitted online through **http://mcb.berkeley.edu**. Applications should include a *curriculum vitae*; a list of publications; copies of three significant publications; a brief description of research accomplishments; and a statement of research objectives and teaching interests. In addition, junior applicants applying for a non-tenured position should arrange to have three letters of reference submitted online. Potential reviewers should be referred to the Statement of Confidentiality found at: **http://apo.chance.berkeley.edu/evalltr.html**. The deadline for applications is **November 15, 2010**.

We are interested in candidates who will contribute to diversity and equal opportunity in higher education through their teaching, research, and service. We are also committed to addressing the family needs of faculty.

The University of California is an Affirmative Action/Equal Opportunity Employer.

---

ucc

Coláiste na hOllscoile Corcaigh, Éire
University College Cork, Ireland

PROFESSOR / HEAD OF SCHOOL OF LIFE SCIENCES

A JOINT APPOINTMENT BETWEEN THE COLLEGE OF MEDICINE AND HEALTH AND THE COLLEGE OF SCIENCE, ENGINEERING AND FOOD SCIENCE

Applications are invited for the post of Professor / Head of School of Life Sciences, a joint appointment in the College of Science, Engineering and Food Science (SEFS) and the College of Medicine and Health (M&H) at University College Cork.

The School of Life Sciences incorporates the Departments of Anatomy, Biochemistry, Microbiology, Pharmacology & Therapeutics, and Physiology, and comprises 58 academic staff, 14 administrative and 25 technical staff, 50 researchers/post-docs, 272 postgraduate FTEs (including 195 PhD students) and 1028 undergraduate FTEs.

As part of its activities in SEFS, the School hosts four BSc programmes (Biochemistry, Microbiolgy, Neuroscience and Physiology), plays a major role in two interdisciplinary BSc programmes (Biomedical Science and Genetics), and provides support teaching programmes in food science. In M&H the school plays an integral role in the delivery of all of the professional programmes including Medicine, Pharmacy, Dentistry, Nursing, and Therapies.

The School's research activities incorporate the BioSciences Institute, and life sciences disciplines continue to attract significant national and international funding through competition. In addition, the School has recently secured multi-million euro funding under the government's Programme for Research in Third Level Institutions (PRLTI) Cycle 5 for laboratory based biomedical and molecular bioscience research, and translational research, to allow further development of its research profile.

An academic leader of international standing is now sought to take up the position of Professor of Life Sciences and Head of School of Life Sciences to ensure that the School operates as an internationally recognised centre of excellence in research-led teaching and learning, and research and innovation, and to provide the leadership and vision to develop the strategic direction of the life sciences at University College Cork.

The ideal candidate will have a doctorate or appropriate professional qualification, a significant internationally-recognised record of research and publication in a relevant discipline, and a track record of leadership in an academic environment. S/he will have experience of leading innovative research programmes, with evidence of significant success in winning competitive funding, and a high-quality publication record. The appointee will also be expected to play a leadership role in curriculum development in life sciences, and to demonstrate evidence of achievement of excellence in research-led teaching and learning in life sciences (at both undergraduate and postgraduate levels). In addition, the appointee will have a strong track record in academic administration.

Appointment as Professor will be permanent and the term of office of Head of School will be an initial term of three years (internal appointment), or five years (external appointment), with the possibility of extension in office, subject to the Rules of the Colleges.

The salary scale (new entrants) for this permanent post is €113,604 - €145,953 per annum.

For informal discussion, please contact Professor Patrick Fitzpatrick, Head of College of Science, Engineering and Food Science, Telephone +353 (0)21 490 3075, Email headofcollege@sefs.ucc.ie, or Professor Geraldine McCarthy, Head of College of Medicine and Health, Telephone +353 (0)21 490 1554, Email g.mccarthy@ucc.ie

Closing date: 12.00 noon on 8th October, 2010

Application forms must be completed and are available, together with full details, from http://www.ucc.ie/en/hr/vacancies/academic/ or from the Department of Human Resources, University College Cork, Cork, Ireland. Email: recruitment@per.ucc.ie / Tel: + 353 21 4903603 Fax: + 353 21 4271568

For further information see www.ucc.ie/hr/vacancies

UCC IS AN EQUAL OPPORTUNITIES EMPLOYER

University College Cork – National University of Ireland, Cork

Science Careers online @sciencecareers.org

POSTDOCTORAL OPPORTUNITIES

POSTDOCTORAL SCIENTIST

The Department of Biochemistry at George Washington University (GW) seeks a highly motivated and creative individual to advance his/her career in cancer biology. The position will study the contribution of signaling components in DNA damage response and cell cycle progression in breast cancer cells, as well as gain novel insights about functional interactions between coregulatory proteins and histones in normal and cancer cells. The laboratory is interested in signaling-dependent posttranslational modifications, protein-DNA interactions, transcriptional controls, and secreted proteins.

Qualifications: Ph.D. in biochemistry, molecular biology, or cell biology. Prior experience in the needed laboratory methods and clear career goals are highly desired. Excellent scientific writing ability and strong oral communication skills are a must. Individuals with prior research publications as well as strong laboratory skills are highly desired.

To apply for this position visit our **website: http://www.gwu.jobs** and search for **posting number 0601920**. *GW is an Equal Opportunity Employer/Affirmative Action Employer.*

POSTDOCTORAL OPENING: Los Alamos National Laboratory (LANL), Los Alamos, New Mexico. We have an immediate opening for a Postdoctoral **RESEARCH ASSOCIATE** in integrated measurement and computational analysis of cellular variability in RNA expression. Single molecule fluorescence techniques will be used to measure cell-to-cell fluctuations of RNA levels (under advisement of **Dr. James Werner**) and theoretical models will be developed to test quantitative hypotheses and design subsequent experiments (led by **Dr. Brian Munsky**). Experience with fluorescence microscopy is desired, but talented experimental scientists with other research backgrounds are invited to apply. Experience in quantitative modeling and programming is desired. Strong communications skills are required. To apply, please send curriculum vitae, including a list of three references, to **Dr. James Werner** (**e-mail jwerner@lanl.gov**). Information about the LANL postdoctoral program, including salary guidelines, can be found at **website: http://www.lanl.gov/science/postdocs/index.shtml.** A Ph.D. completed within the past five years is required for this position.

POSTDOCTORAL RESEARCHER position available to study the genetics of pain, analgesia, and treatment side effects in animal models. The federally funded project has recently determined regions of the mouse genome containing candidate genes for several pain phenotypes. Determining the responsible candidate genes remains to be done via expression analysis, behavioral pharmacology, knockout mouse testing, and other methods. Highly motivated candidates with a neuroscience of pain background and experience with related methods should send research interests, curriculum vitae, and contact information of references to **William R. Lariviere,** Ph.D., **e-mail: lariwr@upmc.edu,** Anesthesiology, University of Pittsburgh School of Medicine.

POSTDOCTORAL POSITIONS
Available at Sloan-Kettering Institute

Seeking research scientists with postdoctoral experience to join a laboratory in order to study the molecular pathogenesis of multiple myeloma and utilize mouse models to develop new therapeutic approaches. Applicants must have a thorough knowledge of plasma cell biology and expertise using genetically modified mice to study cancer pathogenesis. Send a description of your research interests, curriculum vitae, and the names and telephone numbers of three references to: **Dr. Stephen D. Nimer, Memorial Sloan-Kettering Cancer Center, 1275 York Avenue, Box 575, New York, NY 10065.**

The Memorial Sloan-Kettering Cancer Center is an Affirmative Action/Equal Opportunity Employer.

POSITIONS OPEN

VSP UCAR Visiting Scientist Programs

Exciting research opportunities in atmospheric and related science. **POSTDOCTORAL** and **EXPERIENCED SCIENTISTS** sought for positions across the United States. *The University Corporation for Atmospheric Research values and encourages diversity in the workplace.*

Website: http://www.vsp.ucar.edu.

PHYSIOLOGIST
University of Wyoming

The Department of Zoology and Physiology at the University of Wyoming invites applications for a full-time tenure-track **FACULTY POSITION** in Animal Physiology to start August 2011. The position is endowed by **Hank Gardner,** M.D., and **Marilyn Fiske** and is at the **ASSISTANT PROFESSOR** rank, although applications from individuals at the **ASSOCIATE** level, with an outstanding record of research accomplishments, will also be considered. We are seeking candidates with a Ph.D. in the biological sciences, or equivalent, and strong evidence of productivity. Physiologists using comparative models are especially encouraged to apply. The successful candidate will be expected to develop an externally funded research program and contribute to Departmental teaching in human medical/clinical and animal physiology. A compelling start-up package and excellent microscopy, analytical, and animal core facilities are associated with this position.

Interested applicants should electronically send curriculum vitae, a statement of research and teaching interests, three publications, and three letters of recommendation as PDF files to **e-mail: zprequest@uwyo.edu** for the attention of The Gardner-Fiske Search Committee. **Website: http://uwyo.edu/Zoology.** Review of applications will begin on September 30, 2010. *The University of Wyoming is a Carnegie Foundation Research/Doctoral Extensive Institution, and is committed to increasing the diversity of its faculty, staff and students. Women, minorities, and people with disabilities are encouraged to apply. The University of Wyoming is an Equal Opportunity/Affirmative Action Employer.*

The University of Rochester Department of Chemistry invites applications in the area of Inorganic Chemistry, broadly defined. This search is primarily for candidates at the **JUNIOR** level, but exceptional **SENIOR CANDIDATES** can also be considered. Candidates are expected to establish an outstanding program of original research, and be effective teachers at the graduate and undergraduate levels. Application materials are to be submitted online at **website: https://www2.chem.rochester.edu/facultyapp/.** Materials submitted are to include curriculum vitae indicating graduate and postdoctoral advisors, a statement of research plans, and a statement of teaching interests. Junior candidates will be instructed how to arrange for three letters of recommendation to be submitted electronically. The Department will solicit letters for senior candidates. Review of completed applications will begin on October 4, 2010. *The University of Rochester has a strong commitment to diversity and actively encourages applications from candidates from groups underrepresented in higher education. The University is an Equal Opportunity Employer.*

ASSISTANT PROFESSOR
Physical Geography/Aquatic Sciences
Department of Watershed Sciences
Utah State University

The Department of Watershed Sciences (**website: http://www.cnr.usu.edu/wats**) at Utah State University is resuming its search for a nine-month (50 percent research, 40 percent teaching, and 10 percent service), tenure-track position with expertise in physical geography/aquatic sciences. See **website: https://jobs.usu.edu** (requisition ID **052010**) for a complete position description and application instructions. Review of applications will start 27 September 2010.

POSITIONS OPEN

GLOBAL CHANGE ECOLOGIST
ASSOCIATE or FULL PROFESSOR
Plant Community Ecology
Colorado State University

Colorado State University is recruiting a Global Change Ecologist with empirical research expertise in Plant Community Ecology at the rank of Associate or Full Professor (with tenure). Outstanding Assistant Professors qualified for immediate rank advancement will be considered. We seek a broadly trained individual with an established research program that integrates across levels of organization to provide a mechanistic understanding of community and ecosystem responses to global environmental change. The successful candidate will use innovative tools and approaches that span multiple hierarchical levels, potentially ranging from genes to ecosystems. We are particularly interested in candidates who have a proven track record of collaboration and team leadership, strong quantitative skills, and research interests that cross traditional disciplinary boundaries. The successful candidate should have primary research interests in grassland systems with clear linkages to global change issues. Success in extramural funding of research and an exceptional publication record in high-quality scientific outlets are expected. The successful candidate will be expected to contribute to undergraduate and/or graduate teaching.

To apply and view a complete position description, please visit **website: http://warnercnr.colostate.edu/employment-opportunities.html** and apply by 5:00 p.m. October 1, 2010, for full consideration. Applications will be accepted until position is filled.

CSU is an Equal Opportunity/Affirmative Action Employer. Colorado State University conducts background checks on all final candidates.

CELL BIOLOGIST. The Biology Department of Franklin & Marshall College (F&M, **website: http://www.fandm.edu/biology**) invites applications for a tenure-track **ASSISTANT PROFESSOR** position in cell biology, beginning fall 2011. Special consideration will be given to candidates with expertise in microbiology, immunology, or virology. Candidates should have the Ph.D. and demonstrated strengths in teaching and research.

The teaching load is 3/2 and includes: (1) lecture and laboratory sections of a team-taught course in sophomore-level cell biology, (2) an advanced laboratory elective in the candidate's area of expertise, and (3) participation in the College's general education curriculum. Successful candidates will have opportunities to participate in our interdisciplinary programs including Biochemistry and Molecular Biology, Bioinformatics, Animal Behavior, Neuroscience, and Public Health.

F&M has a tradition of excellence in faculty and student collaborative research in the sciences. In 2007, the Biology Department moved into a 100,000 square feet state-of-the-art interdisciplinary teaching and research facility. In 2008, F&M received a Howard Hughes Medical Institute award to launch a bioinformatics program.

Applicants should arrange to have letters sent from three referees, and should submit a letter of application, curriculum vitae, copies of graduate and undergraduate transcripts, teaching evaluations, and a statement that explains plans for actively engaging undergraduates through teaching and research and describes goals for developing as a teacher and scholar. Electronic applications will not be accepted. Priority will be given to complete applications received by October 8, 2010. Applications should be sent to: **Dr. Daniel Ardia, Search Committee Chair, Department of Biology, Franklin & Marshall College, P.O. Box 3003, Lancaster PA 17604. Telephone: 717-291-4118. Fax: 717-358-4548. E-mail: janice.kaufman@fandm.edu.** *Franklin & Marshall College is a highly selective liberal arts college with a demonstrated commitment to cultural pluralism. Equal Opportunity Employer.*

Download your free copy today.

ScienceCareers.org/booklets

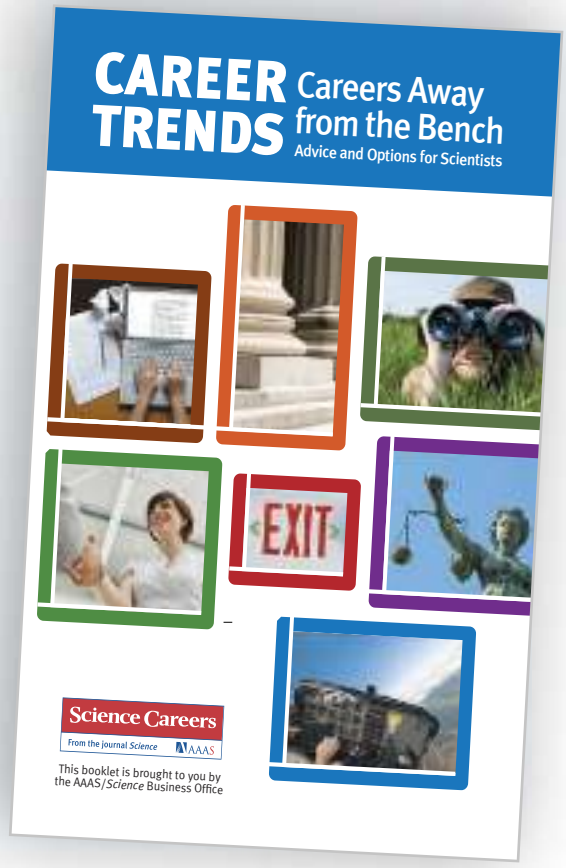

From technology specialists to patent attorneys to policy advisers, learn more about the types of careers that scientists can pursue and the skills needed in order to succeed in nonresearch careers.

Science Careers
From the journal *Science* AAAS

UNIVERSITY OF CALIFORNIA
UCRIVERSIDE

The University of California, Riverside School of Medicine

seeks to recruit **three** faculty members at the **tenured Associate to Full Professor** level. Successful applicants will be appointed in the Division of Biomedical Sciences, joining a small group of exceptional faculty members who have directed a successful M.D. program in collaboration with UCLA for the past 33 years. The newly-approved School of Medicine will evolve from the current Division and is slated to open in August of 2012. Successful candidates will be expected to bring and maintain a vigorous, well-funded research program and provide research leadership through group development and collaboration with existing faculty, both within and outside of the Medical School. Areas of research within the Division include integrative immunology (vaccine development, neuro-immune, endocrine-immune, host-pathogen interactions), glial-neuronal interactions, cancer biology, cardiovascular disease, and diseases of ion transport. Particular strengths on the campus include genetics, epigenetics, genomics/bioinformatics, microRNAs, vector biology, bioengineering and nanotechnology, and synthetic and analytical chemistry. UCR has several vivaria, including a new one ready for occupancy, and excellent core facilities in genomics, microscopy, and stem cell biology, the latter supporting an emerging focus on campus. Substantial initial complement and research space in a brand new medical research building with a BSL-3 facility is available. The Division of Biomedical Sciences sponsors an innovative Ph.D. program that integrates the core medical curriculum with biomedical graduate training and research. Successful candidates would be expected to teach in the medical curriculum and actively participate in the Biomedical Sciences Ph.D. program.

Position 1: Role of inflammation in the onset or progression of disease, including its role in cancer, metabolic syndrome, and cardiovascular disease, as well as autoimmune and infectious diseases.
Position 2: Molecular mechanisms of CNS neurological disease, including genetic and environmental, causes, and immune- or glial-neuronal interactions in neurodevelopment and neurodegeneration.

For both of these positions, the ideal candidate would utilize one or more mammalian disease models that contribute to investigation of molecular and cellular mechanisms.

Position 3: Population-based health outcomes/effectiveness research, including population-based assessment of health and wellness, assessment of health interventions and health disparity, and access research. We are particularly interested in those individuals experienced in comparable effectiveness research who could analyze site and type of practice variability in the inland Southern California area. Approaches to quantify behaviors, services and tools that could lead to superior patient outcomes and lowered cost of care are also desirable.

All applicants must hold a Ph.D., M.D., or equivalent degree and qualify for appointment at the tenured Associate Professor level. For all three positions, research programs that are particularly applicable to the mission of the medical school are highly encouraged:- *to improve the health of the people of California and, especially, to serve Inland Southern California by training a diverse workforce of physicians and by developing innovative research and health care delivery programs that will improve the health of the medically underserved in the region and become models to be emulated throughout the state and nation.* Applications will be reviewed beginning **October 1, 2010** and the position will remain open until filled. Applicants should send a curriculum vitae, a statement of research accomplishments and goals, and the names of three individuals who will be asked to provide letters of reference once a short list is developed to **Faculty Search Committee Chair (state position 1, 2 or 3), Division of Biomedical Sciences, University of California, Riverside, CA 92521**.

UC Riverside is an Equal Opportunity/Affirmative Action Employer.

POSITIONS OPEN

BIOGERONTOLOGY
University of Michigan

The University of Michigan Geriatrics Center is seeking to hire a tenure-track **FACULTY MEMBER** to conduct Biogerontology research. The ideal candidate would be working on a fundamental problem in the cellular and molecular biology of aging, using a mixture of genetic, bioinformatics, and biochemical methods, and committed to establishing a reputation as a leader in aging research. Successful candidates will be housed in newly constructed Biogerontology laboratory space, and will receive a primary appointment in a basic science or research-oriented clinical department as appropriate. Minimum qualifications are a Ph.D., MD, or equivalent, several years of highly productive postdoctoral research, and a clear interest in problems relevant to biogerontology. The Geriatrics Center provides a superb environment for research on aging, including NIA support for its Nathan Shock Center, Claude Pepper Center, and Aging Training programs. Substantial start-up funding will be available.

Applicants should submit curriculum vitae, a one- to two-page description of research interests, a synopsis of current and previous research support, and contact information for three to five references to: **Rich Miller, 3001 BSRB, Box 2200, 109 Zina Pitcher Place, Ann Arbor, MI 48109-2200.**

The University of Michigan is an Equal Opportunity Employer committed to maintaining diversity in its hiring programs.

FELLOWSHIP PROGRAM in AIDS Vaccine Research and Development
International AIDS Vaccine Initiative (IAVI)

International AIDS Vaccine Initiative (IAVI) is a global not-for-profit organization born in 1996 that has an international mandate to ensure the development of a safe, effective, accessible preventive AIDS vaccine for use worldwide through an integrated program of research and development (R&D), policy research, and global advocacy. Organized as the first modern biomedical product development partnership (PDP), IAVI has been acknowledged for revolutionizing the way vaccines and medicines are produced for the world's poor.

IAVI's newly created two year, **POSTDOCTORAL** Fellowship Program in AIDS Vaccine Research & Development is a premier program that provides a unique opportunity for talented young postdoctoral candidates to train alongside some of the leading scientists in the vaccine field today, as well as to contribute to the history-making effort to develop an HIV vaccine. Selected via a competitive application process, IAVI Fellows will receive a salaried position of two to three years, contingent on satisfactory performance, and placement in one or more of the laboratories in IAVI's global network. The program places special emphasis on training scientist from places where the HIV epidemic is most severe as further preparation for careers in their home countries. Under special consideration, the program allows for a possible extension to three years.

For a detailed description of the application process and attributes of this fellowship, please access at **website: http://www.iavi.org/about-IAVI/careers/Pages/Careers.aspx.** Click on career search and apply to Fellowship **ID 1408**.

FACULTY POSITION
Institute of Molecular and Cellular Biology
National Taiwan University

The institute is seeking an outstanding scientist to fill a full-time faculty position available on August 1, 2011. The level of appointment is open. The research area should be related to Molecular and Cellular Biology. Candidates must have a Ph.D. degree (a postdoctoral experience is preferred). Applicants should submit curriculum vitae, a brief research and teaching statement, and three recommendation letters by November 30, 2010 to: **Faculty Search Committee, Institute of Molecular and Cellular Biology, National Taiwan University, Number 1, Section 4, Roosevelt Road, Taipei, Taiwan 10617. E-mail: ntuclsimcb@ntu.edu.tw. Website: http://cell.lifescience.ntu.edu.tw/english/index.htm.**

POSITIONS OPEN

ASSISTANT PROFESSOR POSITION
(Job code # 08-25-06-3215-20188)
University of Illinois at Chicago

The Department of Biological Sciences at the University of Illinois at Chicago (UIC) invites applications for an Assistant Professor level position. This tenure-track faculty position starts August 16, 2011. Final authorization of the position is subject to availability of state funding. Located in the heart of Chicago, UIC is one of the nations leading research universities. Numerous opportunities exist for collaborative research in biological sciences across disciplines at UIC and with colleagues and institutions throughout the Chicago region.

A successful candidate will establish a vigorous, externally-funded research program, and teach effectively in the Department's undergraduate biochemistry and graduate molecular biology training programs. Research programs applying a biochemical approach to cellular pathways, development, microbial physiology, or protein structure/function will be favored. The successful candidate will join an interdisciplinary scientific community on the UIC campus and the Chicago area, as a member of a diverse department investigating a broad range of areas of biology, supported by excellent facilities and resources.

Candidates must have a Ph.D., significant postdoctoral experience, and a demonstrated record of research accomplishments. For fullest consideration, please submit your curriculum vitae, research and teaching statement, and three reference letters to **website: http://www.uic.edu/depts/bios/search.shtml** before October 1, 2010.

UIC is an Affirmative Action/Equal Opportunity Employer.

ASSISTANT PROFESSOR, Environmental Stress–Tenure-track. The Department of Zoology at Oklahoma State University (**website: http://zoology.okstate.edu**) invites applications for an Assistant Professor in environmental stress. Areas of research emphasis could include, but are not limited to, natural and anthropogenic stressors, environmental physiology, toxicology, and global change. Applicants should have a Ph.D., postdoctoral experience, teaching experience, and success in obtaining extramural funding. Responsibilities include establishing an extramurally funded research program, mentoring M.S. and Ph.D. students, and teaching at the undergraduate and graduate level. To apply please (1) send a single PDF file composed of a cover letter, curriculum vitae, and separate statements of research interests and teaching philosophy; (2) send three publications; and (3) arrange to have three letters of recommendation sent in support. All of the items should be sent to the search committee chair, **Dr. Jason Belden**, at **e-mail: zoologysearch@okstate.edu.** Application review will begin 8 October 2010, with employment beginning 1 January 2011. Filling of this position is contingent upon availability of funding.

Oklahoma State University is an Affirmative Action/Equal Employment Opportunity/E-Verify Employer committed to diversity. OSU-Stillwater is a tobacco-free campus.

ASSISTANT PROFESSOR of CHEMISTRY

The Department of Chemistry of the University of Chicago invites applications from outstanding individuals for the position Assistant Professor of Chemistry. This search is in the areas broadly defined as inorganic, organic, and physical chemistry. Applicants must apply online to the University of Chicago Academic Career page at **website: http://tinyurl.com/36pmntk.** Applicants must upload a cover letter, curriculum vitae with a list of publications, and a succinct outline of research plans. The cover letter should be addressed to the **Inorganic Search Committee, Organic Search Committee,** or **Physical Search Committee,** depending on the discipline of interest. The successful candidate must have a Ph.D. in Chemistry or related field. In addition, three reference letters will be required. Review of completed applications will begin October 1, 2010. To ensure full consideration, all material should be submitted by that date.

The University of Chicago is an Affirmative Action/Equal Opportunity Employer.

Your career is our cause.

Get help from the experts.

www.sciencecareers.org

- Job Postings
- Job Alerts
- Resume/CV Database
- Career Advice
- Career Forum

Science Careers
From the journal *Science* AAAS

We deliver customized job alerts.

Science Careers
From the journal *Science* AAAS
www.ScienceCareers.org

MARKETPLACE

Knockout Mice
Deltagen, Inc.
Inventory of over 900 lines of knockout mice with targeted gene deletions available to be licensed for research and drug development. Visit www.deltagen.com to do a BLAST search of our inventory or to download the list of available KO mouse lines.
• GPCRs • Secreted proteins • Transporters
• Kinases • Ion Channels • Others
www.deltagen.com (650) 345-7602

Widely Recognized Original & Guaranteed
KlenTaq1
8¢/u Truncated Taq DNA Polymerase Withstand 99°C
US Pat #5,436,149
Call: **Ab Peptides**
Fax: 314•968•8988
e-mail: abpeps@msn.com
1•800•383•3362
www.abpeps.com